QUANTITATIVE MODELING OF OXYGEN PRECIPITATION IN SILICON

Yi Yang

A DISSERTATION

in

Mechanical Engineering and Applied Mechanics

Presented to the Faculties of the University of Pennsylvania

in

Partial Fulfillment of the Requirements for the

Degree of Doctor of Philosophy

2017

Supervisor of Dissertation

_____

Talid R. Sinno, Professor of Chemical and Biomolecular Engineering

Graduate Group Chairperson

_____

Kevin T. Turner, Professor of Mechanical Engineering and Applied Mechanics

Dissertation Committee

John L. Bassani, Richard H. and S. L. Gabel Professor of Mechanical Engineering and Applied Mechanics

Howard H. Hu, Professor of Mechanical Engineering and Applied Mechanics

Talid R. Sinno, Professor of Chemical and Biomolecular Engineering

Acknowledgement

As I started to write a thank you note to everyone who has influenced me in my time at Penn, I quickly realized I would have to include over a hundred names! To have crossed paths with so many extraordinary people, leaves me with more wonderful memories than I can count.

First of all, I would like to greatly thank my advisor Professor Talid R. Sinno for all his support, guidance and motivation. Professor Sinno's stupendous passion for research and his constant demand for high quality work have inspired and pushed me to go beyond my limit every day to improve my research skills. We together have spent countless weekends and stayed up until 3AM in numerous mornings over the phone or in the office, making breakthroughs and progresses in research. To be honest, I don't think I have ever or will ever meet anyone like Professor Sinno, who is willing to provide this level of support for his students and devote himself to academic pursuits. Moreover, I feel very lucky to be able to get to know Professor Sinno better on the personal level over the past few years as I found we shared a lot of things in common such as the enthusiastic personality, the craving for spicy food and the similar athletic experience in collegiate cycling racings. I would also like to thank the members of my thesis committee, Professor John L. Bassani and Howard H. Hu for their valuable comments, advice and support. I thank Professor Bassani for providing me with his immense knowledge in continuum mechanics and his sense of humor that made everyone's life in the Department of Mechanical Engineering and Applied Mechanics (MEAM) so enjoyable. I thank Professor Hu for his tremendous patience and guidance in finite element methods. When I was his TA, Professor Hu was always smiling and teaching me by precept and by example. A special word of thanks goes to Professor Pedro Ponte Castañeda, my academic advisor when I was a Master's student at Penn, for making my introduction into this PhD program so easy and for his help in his renowned Continuum Mechanics (MEAM 530) as I struggled to get familiar with the tensor algebra.

I greatly acknowledge Siltronic AG for the financial support and inputs on many issues. I want to acknowledge Dr. Andreas Sattler at Siltronic for all the valuable discussions, insights and the computational resources provided by him. I want to acknowledge Dr. Gudrun Kissinger and Dr. Eric Dornberger for the abundant experimental data they provided. I want to acknowledge Professor Jan Vanhellemont for inspiring us to investigate the "Vanhellemont Mechanism" which is a very important subject of my research project, may he rest in peace.

Interestingly I was told by a lot of people many times that perhaps another thing Professor Sinno and I have in common is that we both made a life-long friend from Germany. To me, this precious friend is Peter Johannes Käshammer (aka Mr. PJK). I still remember the first day when I met Peter in 2011, I told him about the only German words I know and my favorite music is Trance, we both laughed so hard and became best friends with each other immediately. Our friendship were not only strengthened by the over 10,000 hours we spent together (in Peter's own word, he "has spent more time with Yi Yang than his wife at Penn") on doing research and training ourselves to be mentally stronger, but also by so many priceless memories we had in the dining halls or near the food trucks at Penn or in the bars or grocery stores in Philly's center city and so on. We were such good friends that even though while I was bombarding Peter's ears at lunch time every day with my Chinese Food/History Lessons and we did support different soccer teams, we never had a fight in the bar. All joking aside I want to say Peter is indeed one of my best friends.

Another person who has provided me with great support during my PhD study is Daniel P. Kaiser (aka Mr. DPK). Danny is one of the kindest persons I met who always took pleasure to help people around him. Without his guidance in parallel computing and molecular dynamics, I will never be able to finish my thesis. I also appreciate every wonderful discussion we had for research or for his sharing the stories of his cat during our countless car rides together from Towne building to the center city.

One of the most important reasons why I am determined to pursue my PhD at Penn is the home-like atmosphere provided by my colleagues: Claire Yungchi Chuang, Ian Jenkins, Yichen

Lu, Abdullah Alateeqi, Alex Nieves, Matthew Flamm and Xiao Liu, by the MEAM departmental staff: Maryeileen Banford Griffith and Susan Waddington-Pilder as well as the entire MEAM PhD Community. Among them, five people must be mentioned specifically: Tianxiang (Tyson) Su, Qiwei Shi, Xin Wang, Jinzhou Yuan and Xinzhou Liu who are not only my friends but also my teachers. In addition to their guidance in solid/fluid mechanics and mathematics, they all have supported me in various aspects of my life. To name a few, both Tianxiang and Xin have graciously lent their apartments to me for free at some point; Qiwei has provided me with thousands of tips for living in Philly and invited me to play saxophone on his wedding. It was a great honor! Jinzhou and Xinzhou were always encouraging me to study even during my most difficult time at Penn.

Due to the interdisciplinary nature of my research project and Professor Sinno's primary position in the Department of Chemical and Biomolecular Engineering (CBE), I was fortunate to make a lot of friends in CBE and to be invited to many CBE-only events such as the Transport Process Midterm Exam Happy Hours and the "annual fun trip" to Atlantic City with Huikuan Chao, Cory Silva and Amit Shavit.

Outside the circle of my PhD community, there are also tons of people I would like to thank. Derek Zichuan Tang, one of my best friends in US, I thank him for helping me to quickly adjust to life in US. Many thanks to my first year roommate and mentor, Aftab Iman, who will knock on my door every night to ask about my well-being. Many thanks to Chenyang (Ray) Lei. As "one of the most handsome party animals at Penn", Ray never said no to any of my invitations to nightclubs or my home parties. Many thanks to the entire Penn Cycling team for all of the intense RPM training we have done together at 6:30 am, for the memorable races we participated over the weekends and for the great teamwork environment they provided. Great thanks to my personal strength coach Caleb Powers for all of the weight lifting trainings and outdoor boot camps. Caleb is definitely one of the hardest working person I have seen. Even in winter at 20°F, he always showed up on time in the outdoor training field at 6:00AM and waited for me there to get it started. Thanks to my triathlon coach Todd Lippin at Breakaway Bikes who has to endure with my amateur

skills during those long distance rides. Thanks to Huan Zhu, Evan Galipeau, Jacob Levinson, Zhiran Xu, Rang Zhang, Hisanori Fujiwara, Ayako Suzue, Alice Mi, Chang Liu, Jason Gui, Ryan Ye, Weizhao Qi, Yang Luo, Siyong Liang, Yayang Tian, Si Stephani Chen, Kun Peng, Yaoxian Li, Yupeng Lu and Jiayi Zheng for all of the great time and their close friendship!

Pursuing a PhD is a very enjoyable yet challenging experience, I have encountered a lot of obstacles not just in the academic world but in my daily life. My parents, however, are always there to provide me with a warm harbor where I can lick my wounds to rejuvenate quickly and charge myself with power to face and overcome those challenges directly. Without their strongest support, I will not be able to graduate.

Finally, I would like to express my deepest love and gratitude to my wife, Lin Yang, who undoubtedly reigns supreme. I met her during the darkest days in my life, and from that point on, she has been continuously bringing me love, light, hope and a whole different meaning of life. She is the one single reason why our journey has been so magical. Being with her, knowing her and loving her is the best thing that ever happened to me. Thank you, Lin.

ABSTRACT

QUANTITATIVE MODELING OF OXYGEN PRECIPITATION IN SILICON

Yi Yang

Talid R. Sinno

The vast majority of modern microelectronic devices are fabricated on single-crystal silicon wafers, which are produced predominantly by the Czochralski (CZ) melt-growth process. Important metrics that ultimately influence the quality of the silicon wafers include the concentration of impurities and the distribution of lattice defects (collectively known as microdefects). This thesis provides a multiscale quantitative modeling framework for describing physics of microdefects formation in silicon crystals, with particular emphasis on oxide precipitates.

Among the most prevalent microdefects found in silicon crystals are nanoscale voids and oxide precipitates. Oxide precipitates, in particular, are critically important because they provide gettering sites for highly detrimental metallic atoms introduced during wafer processing and also enhance the mechanical strength of large-diameter wafers during high-temperature annealing. On the other hand, like any other crystalline defect species, they are undesirable in the surface region of the wafer where microelectronic devices are fabricated. Although much progress has been made with regards to oxide precipitate prediction and optimization, it has been surprisingly difficult to generate a robust, quantitative model that can accurately predict the distribution and density of precipitates over a wide range of crystal growth and wafer annealing conditions.

In the first part of this thesis, a process scale model for oxide precipitation is presented. The model combines continuum mass transport balances, continuum thermodynamic and mechanical principles, and information from detailed atomic-scale simulations to describe the complex physics of coupled vacancy aggregation and oxide precipitation in silicon crystals. Results

for various processing situations are shown and comparisons are made to experimental data demonstrating the predictive capability of the model.

In the second part of this thesis, atomistic simulations are performed to study the stress field and strain energy of oblate spheroidal precipitates in silicon crystals as a function of precipitate shape and size. Although the stress field of a precipitate in silicon crystals may be studied within a continuum mechanics framework, atomic scale modeling does not require the idealized mechanical properties (and precipitate shapes) assumed in continuum models and therefore provides additional valuable insight. The atomistic simulations are based on a Tersoff empirical potential framework for silicon, germanium and oxygen. Stress distributions and stress energies are computed for coherent germanium precipitates and for incoherent, amorphous silicon dioxide precipitates in a crystalline silicon matrix. The impacts of precipitate size and shape are considered in detail, and for the case of oxide precipitates, special emphasis is placed on the role of interfacial relaxation. Whenever possible, the atomistic simulation results are compared with analytical solutions.

TABLE OF CONTENTS

LIST OF TABLES

All of the reprinted tables are republished with permission of publishers of the Ref.20,21, from Ref.20,21; permission conveyed through Copyright Clearance Center, Inc.

LIST OF FIGURES

1. Introduction

Microelectronic devices such as laptops, smartphones, televisions and tablet PCs are essential components in modern society. Most of the microelectronic devices are fabricated on single-crystal silicon wafers. In 2014 the global production of microelectronics is a $1.45 trillion industry[1] supplied by the silicon wafer market that worth over $7.9 billion[2]. The crystalline quality of wafers is crucial to microelectronic device yield and performance. Thus, one of the most important goals in crystal growth and wafer manufacturing is to continue to engineer optimal microstructure (namely the distribution of defects) in wafers to achieve desired qualities. Precise control of defects requires a comprehensive understanding of the formation and transport physics of defects in silicon. Although defect formation and evolution during wafer manufacturing have been studied extensively for decades, there remains a need for predictive modeling to replace costly trial-and-error experimentation. The goal of this thesis is to develop a computational framework to quantitatively study the physics of defects in silicon and connect them to the operating conditions of manufacturing processes. In particular, the thesis focuses on the complex oxide precipitation process, which plays a multifaceted role in establishing wafer quality.

1.1. Manufacturing Stages of CZ Silicon Wafers

The starting point of the manufacturing stages is the Czochralski (CZ) melt-growth process[3] During the CZ process, polycrystalline silicon in the quartz crucible is first heated up (Figure 1.1(a)) to above its melting point (about 1415 ˚C). Then a seed crystal is introduced into the melt and slowly pulled out while it is rotating (Figure 1.1(b, c and d)). The slow pulling process ensures the melted material solidify into a single crystalline ingot (Figure 1.1(e)). In industry the CZ process is performed in state-of-the-art facilities and it requires the highest standard of precision and absolute cleanness[3]. Usually the industrial CZ process lasts for days. The ingot is then cut into

thin wafers and the wafers are subsequently received a series of mechanical, thermal and chemical treatments (some are plotted in Figure 1.2) to achieve the desired quality.

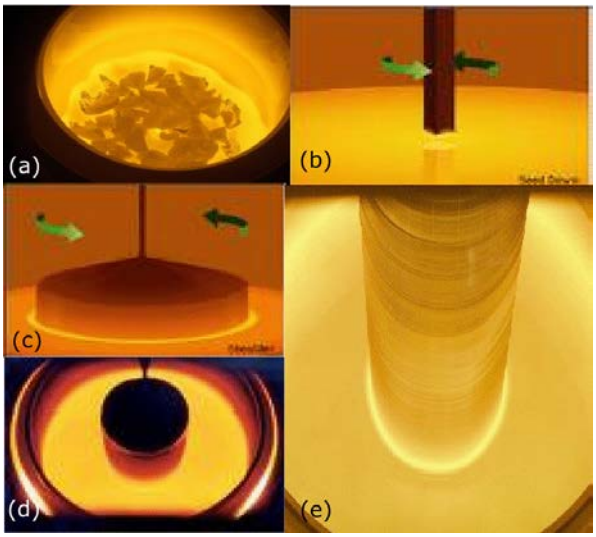

Figure 1.1: Various stages of Czochralski crystal growth: (a) meltdown; (b) seed dip; (c) top; (d) shoulder; and (e) body.[3] (Copyright © 2012, IEEE)

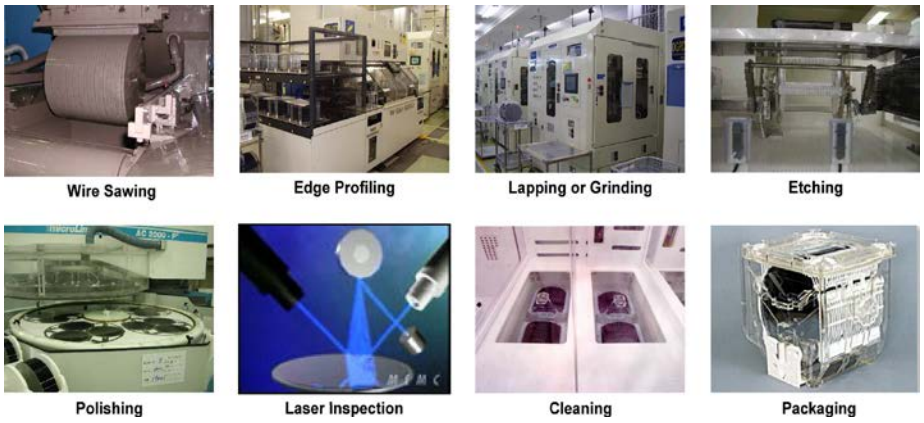

Figure 1.2: Principal Manufacturing Stages of CZ Silicon wafers.[3] (Copyright © 2012, IEEE)

1.2. Microdefects in CZ Silicon Wafers

Important metrics that ultimately influence the quality of the silicon wafers includes the distribution of lattice defects and impurities (collectively known as microdefects), which are shown schematically in Figure.1.3. The basic lattice defect is the intrinsic point defect and can be classified into two types: a vacancy (a lattice site with a missing atom) and a self-interstitial (a lattice atom located in an off-lattice position). Thermodynamics predicts a finite equilibrium concentration of the point defects at finite temperature. Under certain conditions point defect populations may become supersaturated where they tend to aggregate and form clusters such as voids and interstitial precipitates (Figure 1.3(a)).Impurities can also be categorized into two types: unavoidable defects such as carbon atoms that are unintentionally introduced to the crystal during the manufacturing processes and intentional dopants such as boron and hydrogen atoms that are intentionally incorporated into the crystal to modify the material properties (electrical and mechanical properties etc.) of the wafer ((Figure 1.3(b))).

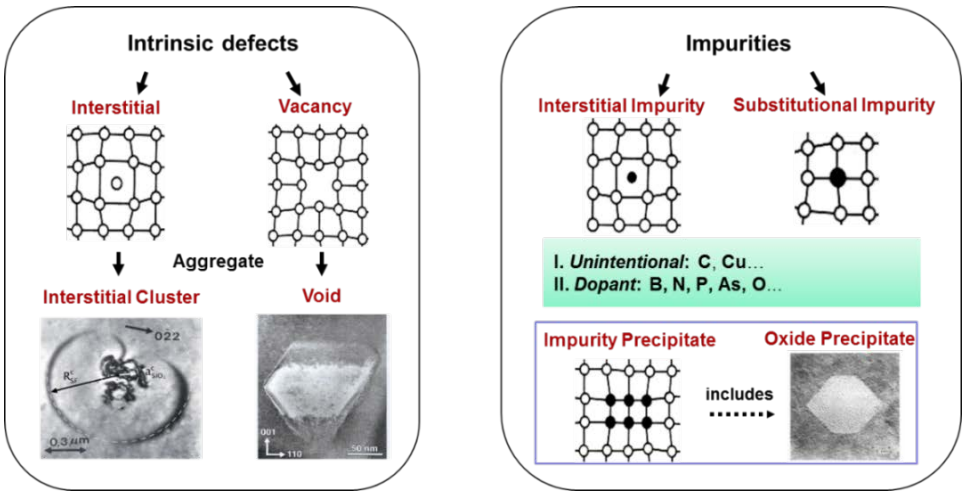

(a) (b)

Figure 1.3: Schematic of microdefects (a) intrinsic defects and their clusters (b) impurities and impurity precipitates.[4-6] Reprinted with permission.

Among the most prevalent microdefects found in silicon crystals are nanoscale voids[7-10] and oxide precipitates[11-15]. Oxide precipitates, in particular, are critically important because they can provide gettering sites[11,15] for highly detrimental metallic atoms introduced during wafer processing and enhance mechanical strength of large-diameter wafers[9]. On the other hand, like other crystalline defects, they are undesirable in the surface region of the wafer where the microelectronic devices are fabricated[13]. An example ideal oxide precipitate distribution is shown in Figure 1.4 (reproduced from Ref. 15 with permission). Here, the precipitate density away from the surface is high enough to ensure reliable internal gettering, while near the surface of the wafer a defect-free layer or a *denuded zone* (DZ) is present for device fabrication.

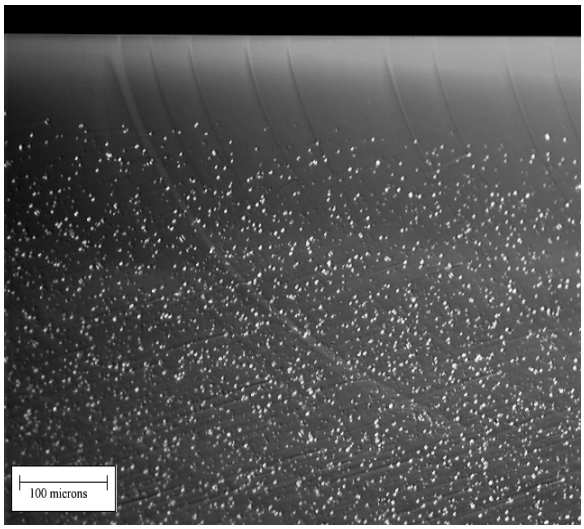

Figure 1.4: An example of a silicon wafer with an ideal distribution of oxygen precipitates for internal gettering purpose.[15] Reprinted with permission.

DZs are usually created by one of the following two methods. The first one is the so-called "High-Low-High" conventional anneal[14]. In this treatment, oxygen is first out-diffused during an anneal at high temperature ($T > 1000\ ^{\circ}C$) by two mechanisms: (1) evaporation of oxygen atoms from the wafer surface[16] and (2) the formation of a thin oxide layer on the wafer surface which serves as a sink for oxygen atoms[17]. As shown schematically in Figure 1.5(a), oxygen out-diffusion creates an oxygen depth profile within the wafer. Next, the high temperature anneal is followed by a low temperature anneal ($600-750\ ^{\circ}C$), during which the supersturated oxygen atoms nucleate small oxide precipitates. Finally, another high temperature anneal ($1000-1100\ ^{\circ}C$) is performed to grow these oxide precipitate nuclei into stable gettering sites. In the 'conventional anneal', a DZ structure is formed to due to lower oxygen concentration near the wafer surface[18] (Figure 1.5(b)).

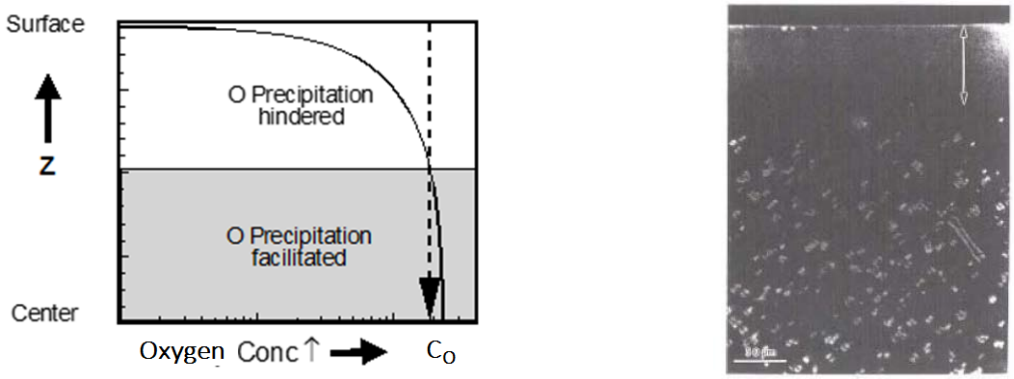

(a) (b)

Figure 1.5: (a) Schematic of the oxygen distribution after conventional anneal. (b) A wafer cross-section created by conventional anneal showing a sharp denuded zone near the wafer surface.[18] Reprinted with permission.

The second approach for creating DZ configurations in silicon wafers is via the application of rapid thermal annealing (RTA)[15,19]. It is now well established that oxide precipitation depends strongly on the presence of single vacancies, which lower the thermodynamic cost of forming

compressively stressed precipitates[20,21]. And it has been demonstrated that manipulation of vacancy populations by RTA of wafers can be used to precisely tailor the distribution of oxide precipitates in order to create a DZ near the wafer surface while producing a high precipitate density elsewhere. Typically in this treatment, the wafer is heated rapidly from room temperature to a holding temperature, T_{RTA}, ($1150-1250\ ^{\circ}C$) for several seconds. During the hold at T_{RTA}, Frenkel pair formation (*Lattice*$\rightarrow$ *Silicon Interstitial* + *Vacancy*) forms equal amounts of silicon interstitial (I) and vacancy (V). Several seconds later, both defect species independently achieve equilibrium by recombination and diffusion to and from the wafer surface. The wafer is then allowed to cool at a controlled rate during which the equilibrium concentrations drop exponentially. The resulting I and V supersaturations can be released either by I-V recombination, or by outdiffusion to the wafer surface. The highly mobile I species outdiffuse far more rapidly than the vacancies leading to a vacancy-depth profile such as the one shown in Figure 1.6(a). During the cooling process, the driving force for oxygen precipitation is insignificant until the supersaturation of interstitial oxygen, C_{Oi}/C_{Oi}^{eq}, also becomes large enough and then proceeds rapidly if a sufficient number of vacancies are available to reduce the resulting stress. In subsequent nucleation-growth thermal treatments, e.g. a standard "low-high" nucleation-growth anneal such as a 4-hour anneal at 800 °C followed by a 16-hour anneal at 1000 °C, regions of the wafer that have a residual vacancies exhibit rapid formation of oxide precipitate nuclei. In this way, a DZ is formed as the one shown in Figure 1.6(b)[15].

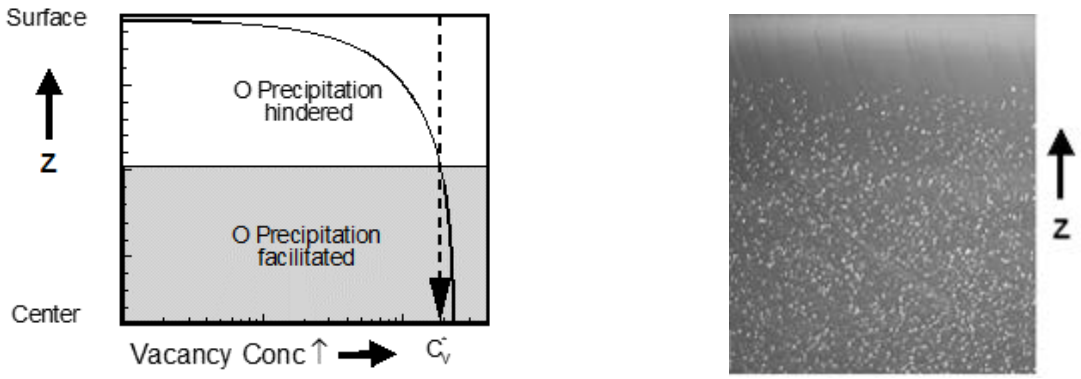

(a) (b)

Figure 1.6: (a) Schematic of the vacancy distribution after RTA. (b) A wafer cross-section created by RTA showing a sharp denuded zone near the wafer surface.[15] Reprinted with permission.

Given the importance of oxygen precipitation, the modeling and quantitative prediction of oxygen precipitation in silicon has had a long history, and numerous models[14,15,20-32] have been proposed to simulate the CZ crystal growth and the subsequent wafer high-temperature processing. However robust and comprehensive predictive capability is still elusive. The primary reason for this relative lack of predictive success is simply that oxide precipitation in silicon is surprisingly complex. The first complexity comes from the fact that, as shown in Figure 1.7, oxide precipitates observed experimentally come in various morphologies[18] (e.g., needles, plates, and polyhedral) that appear to depend strongly on processing conditions such as anneal temperatures.

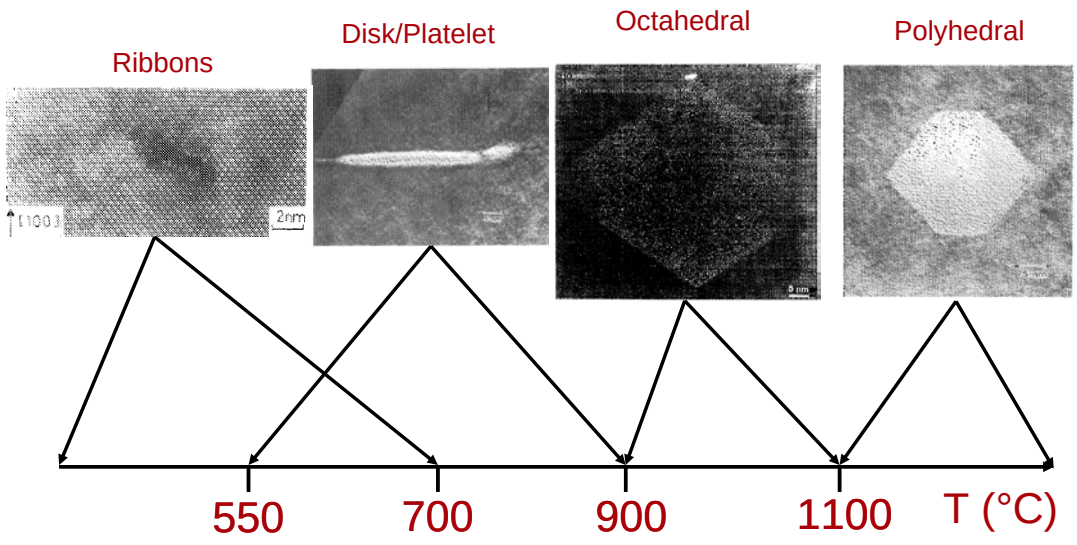

Figure 1.7: Oxide precipitate morphology as a function of temperature. Progression is from low-dimensional, high surface area, structures at low temperature, to more compact structures at high annealing temperature.[18] Reprinted with permission.

The second complexity associated with the description of oxygen precipitation arises because the precipitation process generates high internal (compressive) stresses that must somehow be released; the stress is generated because the volume per silicon atom in the oxide phase (at any composition) is larger than that in the silicon matrix phase. Well documented stress relief mechanisms associated with oxygen precipitation include interaction with intrinsic point defects present in the surrounding crystal matrix, i.e., vacancy absorption[15] from and/or self-interstitial emission[23] to the matrix, and morphological evolution in which the equilibrium precipitate shape evolves to reduce stress energy, usually at the cost of increasing the precipitate-matrix interface area[31]. A much less well-studied stress relaxation mechanism more recently described by Vanhellemont et al.,[25,32] has also been proposed, whereby the precipitate absorbs silicon atoms from the surrounding matrix in order to generate additional free volume in the matrix. In much of the literature[14,15,20-32], oxide precipitates are usually assumed to be comprised of amorphous SiO_2.

However the latter mechanism leads to a change in the composition of the precipitate as silicon atoms are incorporated (the oxide now represented by the sub-oxide, SiO_x, may have composition anywhere between SiO_2 and SiO) and suggests that the assumption that oxide precipitates are comprised of SiO_2 may not hold for all operating conditions.

1.3. Modeling Approach

The overall strategy for building a simulator for predicting defect phenomena is illustrated in Figure 1.8 to demonstrate the general features of our modeling approach.

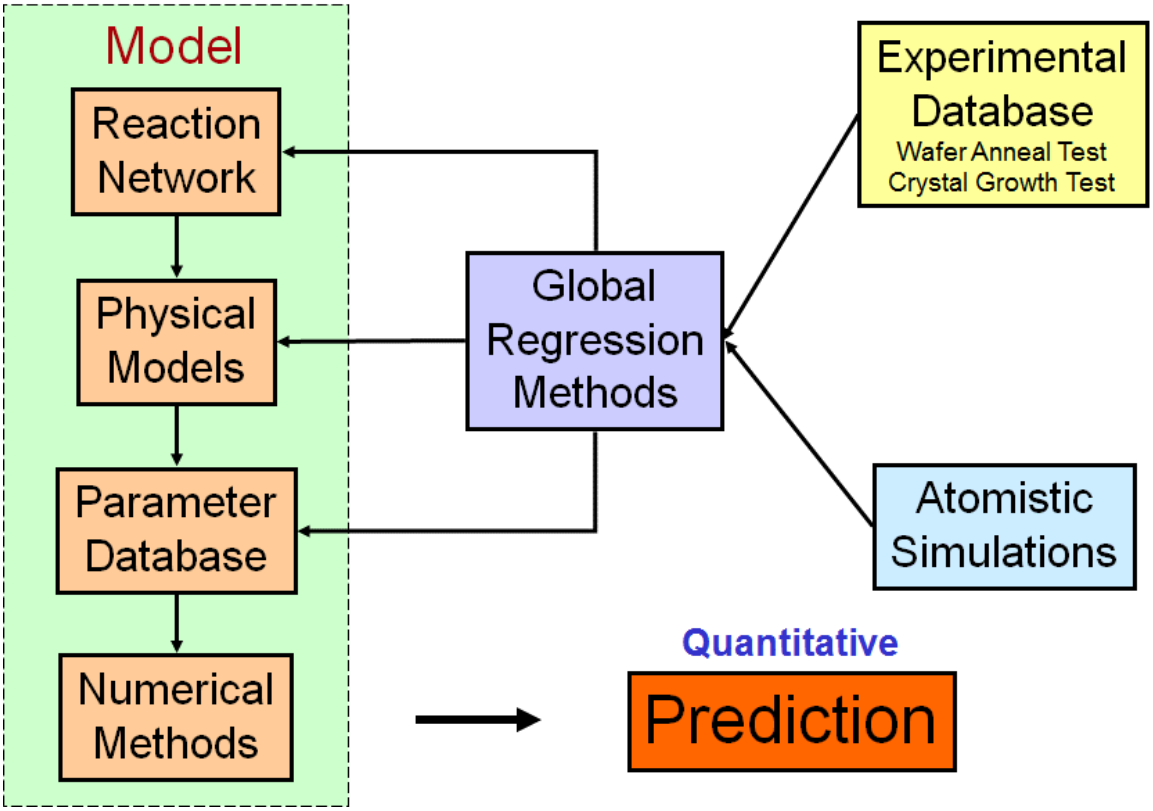

Figure 1.8: Overall strategy for building a comprehensive simulator for studying and predicting defect phenomena.

Experimental measurements are obtained during crystal growth and subsequent wafer annealing (yellow box). In order to analyze the experimental data, a process scale model (green box) is needed for describing the physics of defects (such as diffusion, convection and reaction of defects) happening in the experiments. The process model includes reaction network and physical model that contain parameters not measurable by experiments for all defect species. The resulting system

of equations is then solved numerically with different model parameters (such as point defect diffusivities, cluster binding energies, kinetic constants, etc). The average deviation between results generated by process model and the experimental data is measured by an objective function. A global regression (purple box) is performed in order to find the best parameter set that corresponds to the minimum objective function. Our continuum modeling effort for simulating coupled vacancy aggregation and oxide precipitation in silicon crystals is based on an extension of an existing code (Comprehensive Aggregation Simulator for Silicon Processing, or CASSP) used to model vacancy aggregation in silicon crystals. As shown in Figure 1.9, in addition to general balance equations and reaction network for all monomer and cluster species, two model components must be developed specifically for oxide precipitates. The first one is a set of explicit expressions for the growth and dissolution rates of oblate spheroidal oxide clusters, respectively (upper left purple box). The second component consists of specific free energy expressions for oxide precipitates as a function of temperature and size (lower purple box). These free energy expressions are used as inputs for specifying growth and dissolution rate. A detailed analysis of these expressions will be presented in Chapter 3.

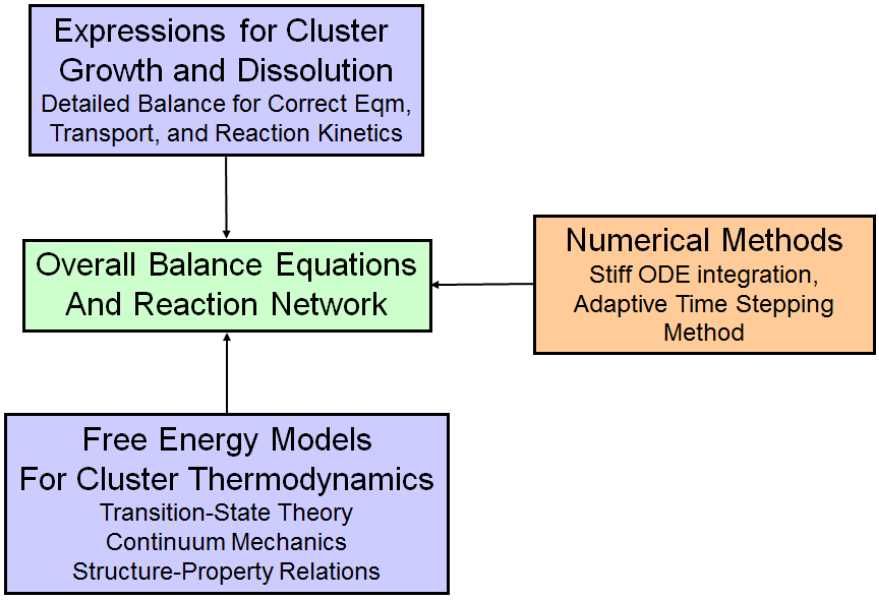

Figure 1.9: Components in CASSP: (1) Generic balance equations for all monomer and cluster species, and reaction network (2) Expressions for cluster dissolution and growth, (3) Free energy models for clusters. Numerical methods are then applied to solve the resulting system of non-linear partial differential equations.

1.4. Thesis Objectives

The primary objective of this thesis is to develop and apply a process scale modeling framework for predicting the distribution of oxide precipitates in silicon crystals as a function of processing conditions during crystal growth and wafer thermal processing. The model combines continuum thermodynamic and mechanical principles with information from detailed atomic-scale simulations. Chapter 2 provides a literature review of theoretical and experimental studies aimed at the characterization of the Si/SiO_2 interface, which is the primary regression parameter in our oxide precipitation modeling. Chapter 3 is devoted to the description of continuum model for oxide precipitation and includes details of the various physical elements in the model. Chapter 4 presents the regression analysis of the model to experimental data, along with a detailed mechanistic analysis. In Chapter 5, atomistic simulations are described to investigate the stress field and strain energy of oblate spheroidal clusters in a crystalline silicon matrix as a function of cluster shape and size. A Tersoff-based empirical potential[33-38] is used for describing the properties of pure Si[35,36], Ge[33] and Si-Ge system[33] and O[34,37,38]. Comparisons are made between the atomistic simulation predictions and analytical solutions from elasticity theory for coherent germanium precipitates and incoherent, amorphous silicon dioxide precipitates in a crystalline silicon matrix. Finally, conclusions are presented in Chapter 6.

2. Literature Analysis of c-Si/a-SiO_2 Surface Energy

As discussed in Chapter 1, the crystalline Si/amorphous SiO_2 (c-Si/a-SiO_2 or Si/SiO_2 for compactness) surface energy function is the key regression parameter in our oxide precipitation model. Si/SiO_2 surface values obtained from various literature sources are summarized in this Chapter in order to establish meaningful interpretations of the surface energy obtained by regression. The data sources can be divided into three groups: (1) direct experimental measurements of the interface energy, (2) atomistic calculation, and (3) model fitting to oxide precipitate data. These are described separately in the following sections.

2.1. Direct Experimental Measurements

Wafer bonding experiments represent the primary source for measurement of the Si/SiO_2 interface energy[39-44]. In general, wafer bonding experiments can be divided into 2 types: (1) classical wafer bonding process (without plasma treatment), and (2) plasma-activated wafer bonding (PAWB) process. As will be discussed briefly later in this section, the plasma treatment increases the number of hydroxyl groups, and enhances water diffusivity and content on the wafer surface by creating porous oxide. It therefore assists the following reaction and enhances wafer bonding:

$$Si-OH+HO-Si \rightarrow Si-O-Si+H_2O \tag{2.1}$$

For both types of experiments, (100) wafers are used and the surface energies are measured directly by using the crack opening method[45] or pulling test[42]; see Figure 2.1.

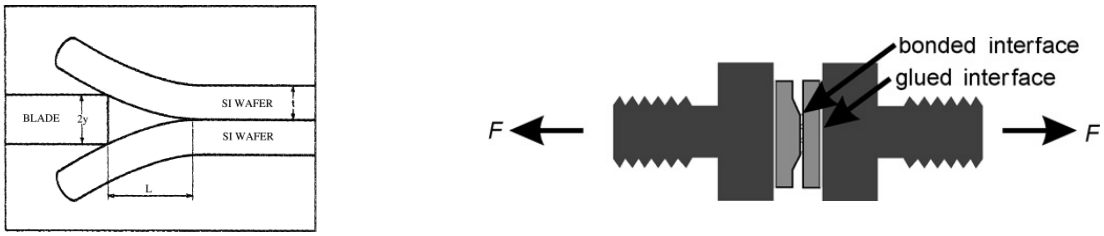

(a) (b)

Figure 2.1: Schematic diagram of the (a) crack opening method (b) pulling test.[45,42] Reprinted with permission.

As reported by Suni et al.[43], Dragoi et al.[39], Schjolberg et al.[42], Plach et al.[40,41] and Goesele et al.[44], there is a general trend that the interface energies increase from ~0.1 to ~2.8 J/m^2 as the temperature or anneal/storage time increases. For example, Suni et al.[43] find that the Si/SiO_2 interface energy (Figure 2.2) increases as annealing temperature increases, while Dragoi et al.[39] present evidence (Figure 2.3) that the energy increases as annealing time increases. The values range from ~0.1 J/m^2 to ~2.6 J/m^2.

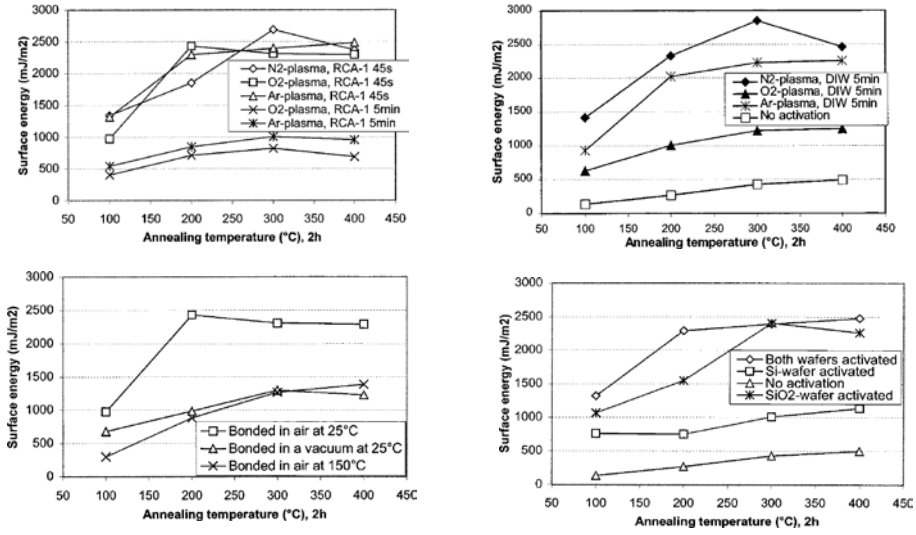

Figure 2.2: Measured Si/SiO_2 surface energies as a function of annealing temperature.[43] Reprinted with permission.

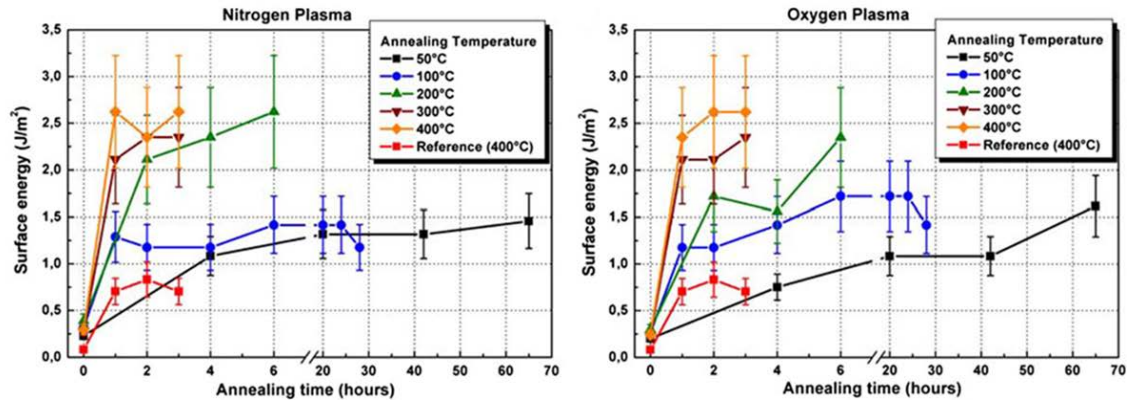

Figure 2.3: Surface energy versus time for various annealing temperatures.[39] Reprinted with permission.

Schjolberg-Henrisken et al. [42] measure the Si/SiO_2 interface energy by using both the crack opening method and the pulling test. Without thermal annealing, the interface energy of two bonded wafers is measured as 0.11 J/m^2 by using the crack opening test method. After the wafers are annealed for 2h at 400ºC in vacuum, the interface energy is measured as 1.5 J/m^2 if the crack opening method is used or 0.98J/m^2 if the pulling test is used. Plach et al.[40,41] obtain the surface energy as a function of annealing temperature, storage time at room temperature, and annealing time at 50 ºC or 300 ºC (Figure 2.4, 2.5 and 2.6).

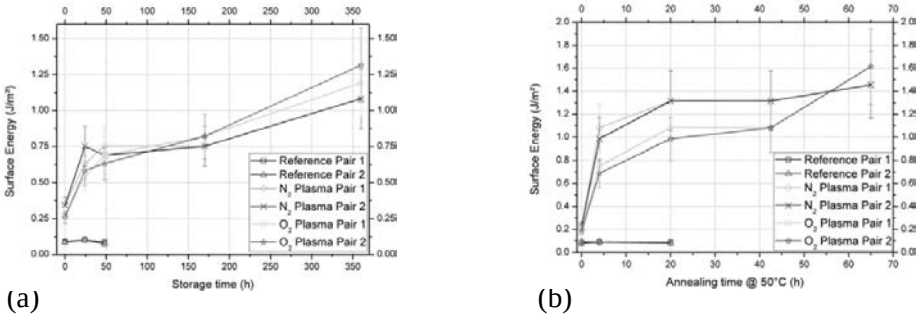

Figure 2.4: Interface energy as a function of (a) storage time at room temperature (b) annealing time at 50 ºC.[40,41] Reprinted with permission.

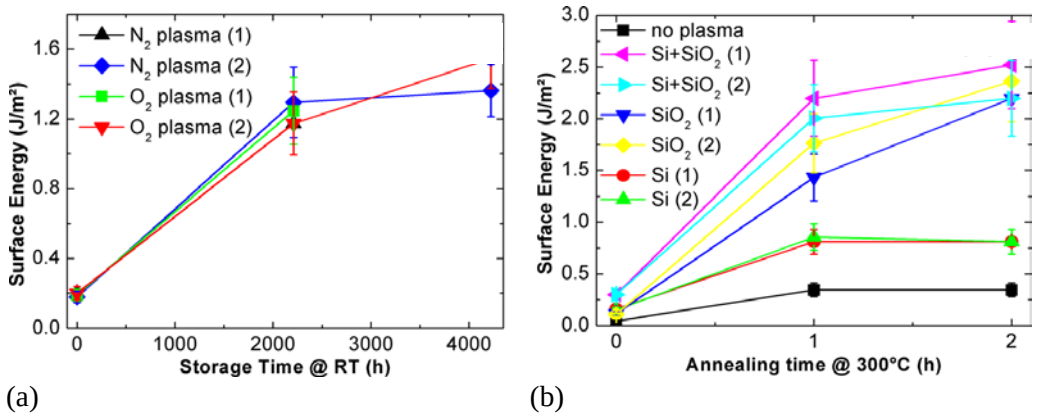

(a) (b)

Figure 2.5: Interface energy as a function of (a) storage time at room temperature (b) annealing time at 300 ºC.[41] Reprinted with permission.

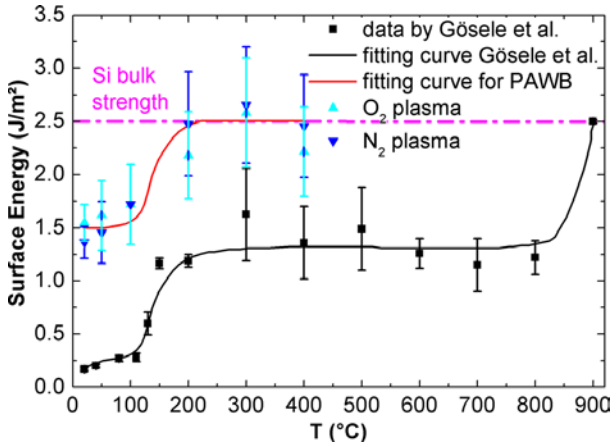

Figure 2.6: Interface energy as a function of process temperature during PAWB (light blue deltas and dark blue gradients and during plasma-free process (black squares).[40,41] Reprinted with permission.

As shown in Figure 2.7, Plach et al.[41] summarize the model for both the classical process[44] and PAWB process to try to explain the 4 mechanisms (stages 1-4 on Figure 2.7) behind the trends in the experimental data shown above.

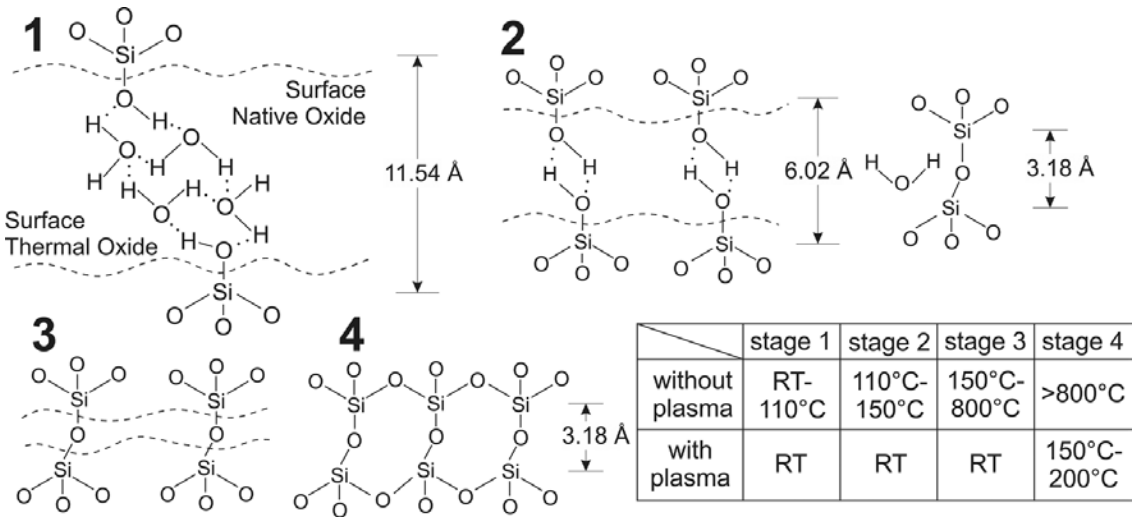

	stage 1	stage 2	stage 3	stage 4
without plasma	RT-110°C	110°C-150°C	150°C-800°C	>800°C
with plasma	RT	RT	RT	150°C-200°C

Figure 2.7: Schematic drawings of the four different stages that occur during wafer bonding.[41] Reprinted with permission.

Stage 1: the wafers are held together via van der Waals type hydrogen bonds after water is introduced at the interface, explaining the relatively low energy (~0.1 J/m^2).

Stage 2: the interface energy suddenly increases due to the formation of Si-O-Si bonds when the reaction in eq. (2.1) occurs. The reaction product, water, either is being removed by thermal annealing above 100 ºC in the classical process, or is diffusing out or being stored in the subsurface regions in the PAWB process.

Stage 3: after the water is removed from the interface, the surface energy is limited by the Si-O-Si bond strength and the surface gap or roughness (shown by the dashed line in Figure 2.7/Stage 3) and reaches a stable value ~1.5J/m^2.

Stage 4: the surface gap is closed by either the viscous flow of the oxide in the classical process or the growth of the oxide in the PAWB process, and correspondingly the surface energy increases to ~2.5 J/m^2. A summary is given in Table 2.1.

Source	Si/SiO_2 Surface Energy (J/m^2)
Stengl et al. (1999)	0.1-2.5
Suni et al. (2001)	0.1-2.8
Dragoi et al. (2005)	0.1-2.6
Schjolberg et al.(2008)	0.11, 0.98 or 1.5
Plach et al. (2008) and (2013)	0.1-2.5

Table 2.1: Experimental measurements of the Si/SiO2 interface energy.

2.2. Atomistic Simulations

Atomistic calculations of the Si/SiO_2 interface energy include (1) Monte Carlo (MC) bond-switch algorithms using Keating potentials, (2) density functional theory (DFT), and (3) molecular dynamics (MD) using empirical potentials.

2.2.1. Monte Carlo Simulations

MC simulations are used to study the properties of planar interfaces. These calculations demonstrate that the surface energy is a function of the orientation of the c-Si and all use Keating-like valence force models[46] of the form

$$E = \sum_{i \in bonds} \frac{1}{2} k_i^b \left(b_i - b_{i0}\right)^2 + \sum_{j \in angles} \frac{1}{2} \left(\cos\theta_j - \cos\theta_{j0}\right)^2 + U \qquad (2.2)$$

where b_{i0} is the equilibrium bond length, θ_{j0} is the equilibrium bond angle, k_i^b and k_j^θ are the "spring constants" and *U* is the chemical energy cost for the formation of suboxides. The Wooten, Waire, and Winer (WWW) algorithm[47] is used to build the amorphous SiO_2 structure. This procedure ensures the random structure of the amorphous SiO_2 while maintaining the 4-fold coordination throughout.

Tersoff et al.[46] studied (001)-oriented Si/a-SiO_2 interface using 10 layers of Si and SiO_2 periodically repeated in the interface-normal direction. The WWW algorithm was used to create the a-SiO_2 structure. The interface energy was calculated as 0.1089 J/m^2. Hadjisavvas et al.[48] calculated the surface energy for the planar interface with 6 different Si orientations using MC simulations with a Keating-like valence force model supplemented by the WWW construction method. The surface energies as function of the Si orientations are summarized in Table 2.2. In addition to the study of planar surfaces, they also calculated the interface energy of the "curved,

more or less spherical" interface created by the nanocrystalline (nc) Si embedded in a-SiO_2. The values are summarized in Table 2.3.

Si Orientation	Si/SiO_2 Surface Energy (J/m^2)
100	0.7370
121	0.8171
110	0.8972
111	0.8972
210	1.7143
221	1.5381

Table 2.2: Interface energy vs. Si orientations.[48]

Si structure	Si/SiO_2 Surface Energy (J/m^2)
Faceted Si Cluster (diameter ~3nm)	1.2177
Faceted Si Cluster (diameter ~5nm)	0.8331
Spherical Si Cluster (diameter ~3nm)	1.1696
Spherical Si Cluster (diameter ~5nm)	1.0574

Table 2.3: Surface energy vs. nanocrystalline Si/a-SiO_2 structures.[48]

Kong et al.[49] used MC simulations with the WWW algorithm with 20 layers of Si and SiO_2 periodically repeated in a 7×7 cell. 3 possible Si ionization states (Si^{+1}, Si^{+2} and Si^{+3}) and 4 different Si orientations (001, 110, 111 and 112) were considered. The results are summarized in Table 2.4.

Si Orientation and Component	Si/SiO_2 Interface Energy (J/m^2)
001 (Si^{+1} :Si^{+2}: Si^{+3} = 0:1:0)	0.9933
001 (Si^{+1} :Si^{+2}: Si^{+3} = 1:1:1)	1.2497
110 (Si^{+1} :Si^{+2}: Si^{+3} = 1:0:0)	1.2016
110 (Si^{+1} :Si^{+2}: Si^{+3} = 0:0:1)	1.6663
111 (Si^{+1} :Si^{+2}: Si^{+3} = 1:0:0)	0.8812
111 (Si^{+1} :Si^{+2}: Si^{+3} = 0:0:1)	1.0574
111 (Si^{+1} :Si^{+2}: Si^{+3} = 1:1:1)	1.8745
112 (Si^{+1} :Si^{+2}: Si^{+3} =0:1:2)	0.9933

Table 2.4: Surface energy vs. Si orientations and components.[49]

2.2.2. Density Functional Theory

To calculate the interface energy, Kroll et al.[50] construct quasi-spherical Si clusters consisting of 17, 29, 47, 71 or 99 atoms embedded in a-SiO_2 with diameters from 0.8 to 1.6 nm by using a combination of network construction followed by DFT. The WWW algorithm is used to construct the random topology of the SiO_2 network. DFT in the local density approximation (LDA) is used to perform further ionic relaxations and for the assessment of electronic properties. All calculations have also been repeated within the more accurate generalized gradient method (GGA). The result is 1.5 J/m^2.

2.2.3. Molecular Dynamics Simulations

Djurabekova and Nordlund[51] perform MD simulations of Si/SiO_2 at 3 different temperatures (1100K, 1400K and 1600K). They construct quasi-spherical Si clusters in an a-SiO_2 matrix and consider 6 different Si/SiO_2 interface structures (labeled 1 to 6 in Table 2.5) with different amounts of under and over-coordinated atoms, as well different numbers of suboxide atoms at the interface. The WWW algorithm with Keating-like potential is used in order to construct a defect-free amorphous SiO_2 structure. The potentials developed by Watanabe et al.[52] and Ohta et al.[53] were used to calculate energies. These potentials are derived based on the classical Stillinger-Weber potential.

Finally, Chuang et al.[34] (our group) construct quasi-spherical Si clusters embedded in amorphous SiO_2, using a similar approach to that described by Djurabekova and Nordlund[51] to calculate the Si/SiO_2 surface energy. Tersoff-based potentials developed by Munetoh et al.[54] (MT) and Lee et al.[55] (LT) are used and the amorphous SiO_2 is constructed by quenching the melted β-cristobalite SiO_2 from 5000K to 0K instead of using the WWW algorithm. The results are 1.1 J/m^2 for LT and 1.5 J/m^2 for MT.

Temperatures (K)	Si/SiO_2 Surface Energy (J/m^2)
1100 (structure 1)	1.3939
1100 (structure 2)	1.5060
1400 (structure 3)	1.2177
1400 (structure 4)	1.3298
1600 (structure 5)	1.1536
1600 (structure 6)	1.2337

Table 2.5: Si/SiO_2 surface energy as a function of annealing temperatures and structures.[51]

2.3. Model Fitting to Experimental Data

Approaches in which model fitting to oxide precipitate data is used for Si/SiO_2 interface energy calculation can be divided into 2 groups: (1) models that employ homogeneous nucleation theory and (2) models that employ rate equations.

2.3.1. Models Employing Steady State Nucleation Theory

Inoue et al.[22] and Voronkov et al.[29] both fit their calculated nucleation rate of oxide precipitate to nucleation rate data assuming that a closed system equilibrium oxide precipitate size distribution is already established and that the supersaturation of monomers is constant. Inoue et al.[22] first provide an expression of the Gibbs free energy [eq. (2.3)] of a oxide precipitate as a function of the latent heat of fusion and interfacial energy (the strain energy is ignored in their expression) then calculate the critical size (r_C) by setting $dG/dr = 0$.

$$G = G_{\text{lat\_heat}} + + G_{\text{int}}. \tag{2.3}$$

Next, the equilibrium concentration of clusters of critical radius r_C is calculated as

$$C^{eq}\left(r_C\right) = \rho \exp(-G\left(r_c\right)/k_B T) \tag{2.4}$$

and the nucleation rate is calculated as

$$J = ZgC^{eq}\left(r_C\right), \tag{2.5}$$

where g is the frequency of oxygen attachment for oxide precipitate of critical size and Z is the Zeldovich factor. Here eq. (2.5) is used to match experimental data of nucleation rates (Figure 2.8). The interface energy is calculated as 0.38 J/m^2 and Z is calculated as 0.2 in order to obtain a good fit.

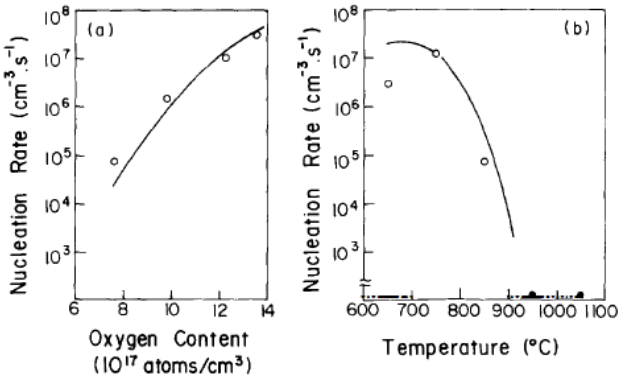

(a) (b)

Figure 2.8: The measured (circles) and calculated (solid curves) nucleation rate as function of (a) the oxygen concentration and (b) temperature.[22] Reprinted with permission.

Voronkov et al.[29] calculate the steady state nucleation rate of oxide precipitate as a function of the free energy at 800 ºC by using a similar approach described by Inoue et al[22]. In their model, however, the free energy expression includes the supersaturation of vacancies and oxygen, the strain energy, and the interfacial energy. The experimental data of nucleation rate (shown in Figure 2.9) for fitting the surface energy is produced in a RTA-treated wafer by a two-step annealing (800 ºC for 2 to 16h plus 1000 ºC for 16h) at three given oxygen concentrations: 8×10^{17}cm^{-3} (High C), 7×10^{17}cm^{-3} (Medium C) and 6×10^{17}cm^{-3} (Low C). The surface energy is calculated as 0.89 J/m^2.

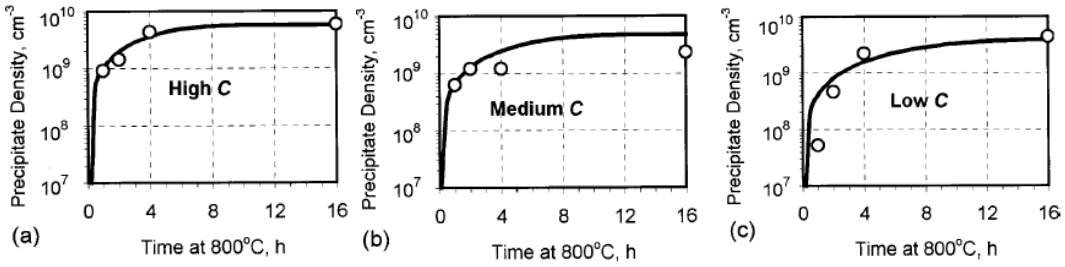

Figure 2.9: Comparison between the experimental data (circles) and the calculation results (solid curves).[56] Reprinted from Ref.56 with the permission of AIP Publishing.

Senkader et al.[27] obtain the interface energy by fitting a calculated oxide precipitate aspect ratio to experimental measurements of the oxide precipitate aspect ratio. The free energy of the oxide precipitate as a function of the supersaturation of monomers, the strain energy, and the interfacial energy (the latter two are functions of aspect ratio β of the oxide precipitate) is given by:

$$G = G_{super} + G_{strain}(\beta) + G_{\text{int}}(\beta). \tag{2.6}$$

Assuming the vacancy and interstitial concentrations are at equilibrium ($G_{super} = 0$), then the aspect ratio (the only unknown) can be obtained by the minimization of the free energy with respect to the aspect ratio. Finally, along with eq. (2.6), five measured aspect ratios of oxide precipitates (shown in Table 2.6) at 700 ºC and 800 ºC and different oxygen concentrations in the wafers, are used to perform the model regression. The surface energy is calculated as 0.67 J/m^2 if oxide precipitates are assumed to be comprised of SiO and 1.68 J/m^2 if oxide precipitates are assumed to be SiO_2.

Temp (ºC)	700	700	700	800	800
C_O (10^{17} cm^{-3})	8.36	5.26	3.01	8.06	6.01
β (10^{-3})	23.3	24.6	22.2	8.57	7.89
β_{SiO}^{calc} (10^{-3})	23.5	19.3	16.5	11.2	8.9
$\beta_{SiO_2}^{calc}$ (10^{-3})	29.0	20.6	16.6	11.6	8.46

Table 2.6: Calculated aspect ratio vs. experimental data of the aspect ratio of oxide precipitates.[27]

Vanhellemont et al.[20,21] derived a similar free energy expression [eq.(2.7)] for oxide precipitates to the Senkader one[27] by using a homogeneous nucleation model and then calculating the critical radius (r_c) by setting $dG/dr = 0$. They link the interface energy and critical radius by

$$\sigma = \frac{2V_{SiO_2}}{xr_C kT_{OI}} \frac{T_S^{OI}}{T_S^{OI} - T}, \tag{2.7}$$

where V_{SiO_2} is the molecular volume of SiO_2, T_S^{OI} is the temperature at which the total amount of interstitial O would be soluble, k is the Boltzmann constant and kT_{OI} (=1.52 eV) is the solubility energy. The interface energy and the experimental data used to calculate it are summarized in Tables 2.7 and 2.8. Note that the interface energy obtained by using the data in Table 2.7 is larger than 3.4J/m^2 and the strain is assumed to be completely released.

corresponding interface energy σ is also represented with $\sigma = \rho k T_{OI}/\Omega_{OX}$ and $\rho = 0.125$ nm, $T_{OI} = 16241$ K.

	Ω_{ox}/Ω_{Si} [a]	K[a] (10^9 Pa)	p[b] (10^9 Pa)	α	σ (erg cm^{-2})
a-SiO_2					
Low p	2.25	37	0–3	0.57–0.63	310
High p	1.87	37	0–3	0.38–0.44	374
Coesite	1.64	100	2.5–8	0.23–0.31	427
Stishovite	1.14	···	>8	<0.07	621

Table 2.7: The experimental data used as input in eq. (2.7) for computing the surface energy.[21]

Reprinted from Ref.21 with the permission of AIP Publishing.

Anneal temperature (K)	Anneal time (h)	Interstitial oxygen content ($\times 10^{17}$ cm^{-3})	Solubility temperature T_s (K)	$(T_s/T_s - T)$	Critical platelike precipitate thickness h_c (nm)	Critical radius $r_c = \frac{3}{2} h_c$ (nm)
973 (Ref.2)	700	2.88	1394	3.31	3.7	5.5
1073 (Ref.2)	200	7.71	1475	3.67	3.6	5.4
1173 (Ref.2)	64	9.59	1511	4.47	5	7.5
1373 (Ref.3)	1	8.63	1506	11.3	11	16.5

Table 2.8: The experimental data used as input in eq. (2.7) for computing the surface energy.[20]

Reprinted from Ref.20 with the permission of AIP Publishing.

2.3.2. Models Employing Rate Equations

A much more rigorous approach that employs rate equations for oxide precipitate evolution is presented in this section. To obtain the interface energy, Schrems et al.[23] assume oxide precipitates are spheres and can release stress by interstitial emission. They use the following experimental data for the fitting: (1) Interstitial O concentration vs. depth after 2 different "HI-LO-HI" anneals for an initial O concentration of 9.5×10^{17} cm^{-3} and (2) denuded zone depth vs. initial O concentration for 3 different denudation times (Figure 2.10). A temperature-dependent surface energy is obtained: 0.235 J/m^2 (750 ºC), 0.169 J/m^2 (1000 ºC) and 0.150 J/m^2 (1050 ºC); see Figure 2.11.

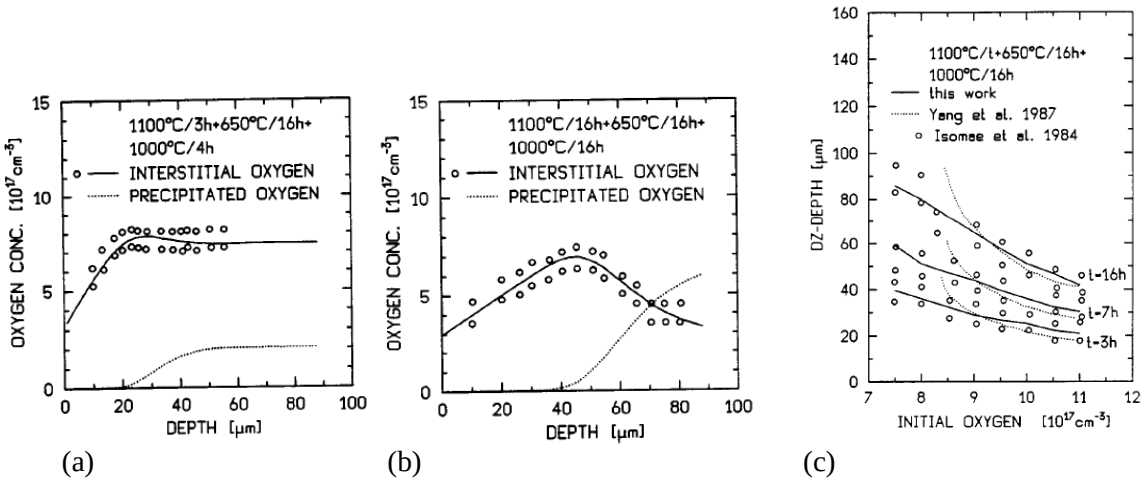

Figure 2.10: Interstitial oxygen vs. depth after (a) anneal 1 (b) anneal 2. (c) Denuded zone depth from wafer surface vs. initial oxygen concentration for 3 different denudation times.[23] Reprinted with permission.

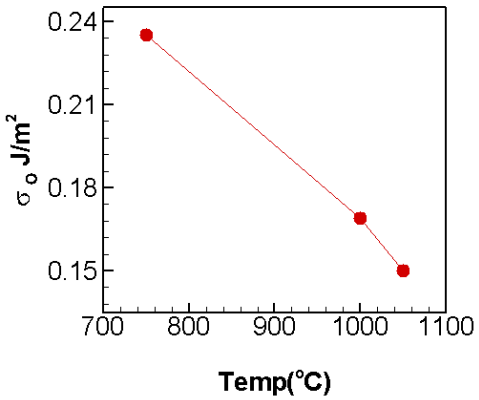

Figure 2.11: Temperature dependent surface energy from reference[23].

Esfandyari et al.[26] used the same model framework as Schrems et al.[23] to fit their model to experimental data. Similarly, the following experimental data is used for the fitting: (1) Interstitial O concentration vs. depth from the wafer surface after 2 different HI-LO-HI anneals (anneals "1" and "2") for an initial oxygen concentration of 9.5×10^{17} cm^{-3} [Figure 2.12 (a, b)]; (2) The interstitial and precipitated O concentration as a function of initial O concentration after anneal 1 [Figure 2.12 (c)], and (3) denuded zone depth vs. initial O concentration for 3 different denudation time [Figure 2.13]. By fitting to the above data, a size-dependent surface energy is obtained (eq. (2.8)). The function is plotted Figure 2.14:

$$\sigma = 0.427\left[1+\left(\frac{0.85}{n}\right)^{1/3}+\left(\frac{0.65}{n}\right)^{2/3}\right]. \qquad (2.8)$$

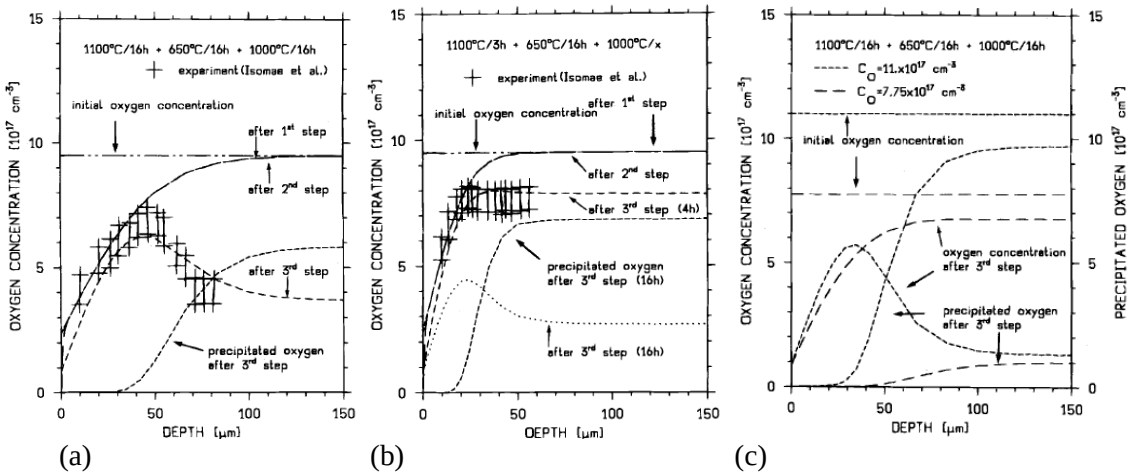

Figure 2.12: Interstitial oxygen concentration vs. depth for (a) anneal 1 (b) anneal 2; interstitial and precipitated oxygen concentration as a function of initial oxygen concentration after anneal.[26] Reprinted with permission.

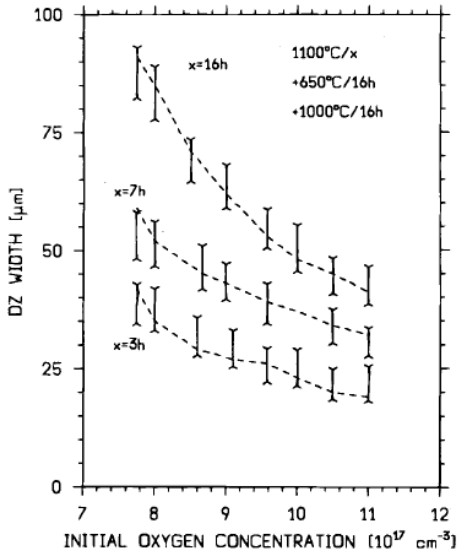

Figure 2.13: Denuded zone depth from wafer surface vs. initial oxygen concentration for 3 different denudation time.[26] Reprinted with permission.

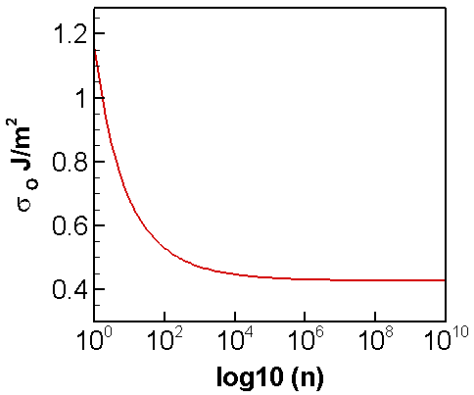

Figure 2.14: Cluster size dependent surface energy (plotted against the log cluster size.[26]

Ko and Kwack[28] used three sets of surface energies in order to capture the experimental data for the one-step, two-step and three-step wafer anneals and crystal growth. First, they obtained a constant interface energy, 0.373 J/m^2, to capture the experimental data at 1100 ºC for crystal growth (data not shown in the paper). Secondly, they obtained a temperature-dependent interface energy by using experimental data from one-step and two-step wafer treatments. For one-step anneals, an empirical expression fitted by using the experimental data oxide precipitate densities[57] at different temperatures is used in their model regression:

$$N = 6\times10^{-3}\exp\left(3\text{eV}/k_BT\right). \tag{2.9}$$

For two-step anneals, the experimental data of oxygen loss (Figure 2.15) as a function of initial oxygen concentration after annealing for 800 ºC 2h +1050 ºC 16 h. The interface energy is tabulated in Table 2.9.

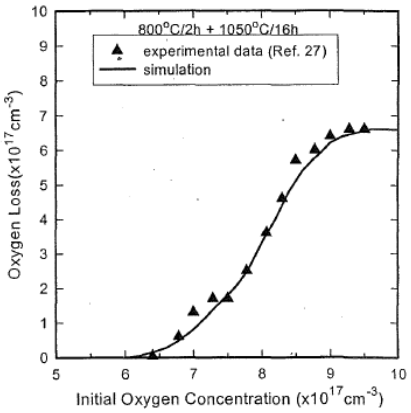

Figure 2.15: Oxygen loss as a function of initial oxygen concentration.[28] Reprinted from Ref.28 with the permission of AIP Publishing.

Temp (ºC)	650	700	800	850	900	950	1000	1050	1100
σ (J/m^2)	0.25	0.278	0.280	0.310	0.325	0.347	0.372	0.400	0.400

Table 2.9: Temperature dependent surface energy for one-step and two-step anneal.[28]

For the three-step anneals, the interstitial O concentration as a function of the depth from the wafer surface are obtained after two different types of anneals, 1100 ºC (3h) +650 ºC (6h) +1000 ºC (4h) [Figure 2.16(a)] and 1100 ºC (16h) +650 ºC (16h) +1000 ºC (16h) [Figure 2.16(b)] are used for the model regression. However, the surface energy at 650 ºC, 1000 ºC, and 1100 ºC have to be modified from 0.25 J/m^2 to 0.343 J/m^2, from 0.400 J/m^2 to 0.398 J/m^2 and from 0.400 J/m^2 to 0.395 J/m^2, respectively to capture this set of data.

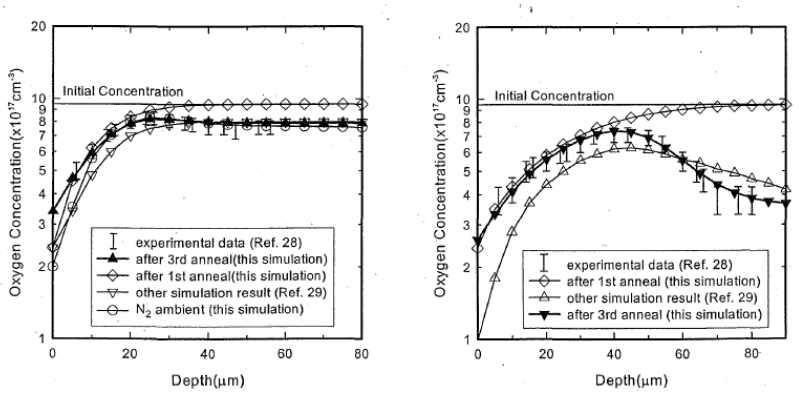

(a) (b)

Figure 2.16: O concentration as a function of depth for two different anneals: (a) 1100 ºC (3h) +650 ºC (6h) +1000 ºC (4h) and (b) 1100 ºC (16h) +650 ºC (16h) +1000 ºC (16h).[28] Reprinted from Ref.28 with the permission of AIP Publishing.

Falster et al.[14,58] use rate equations to perform regression of interface energy assuming oxide precipitates are spherical and that the strain energy is completely released. A large set of wafer anneals are considered (Figure 2.17).

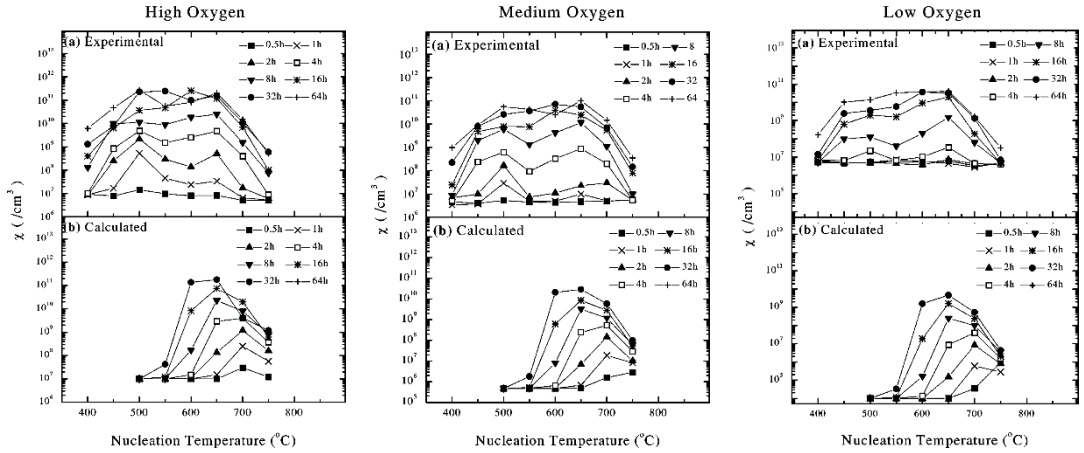

(a) (b) (c)

Figure 2.17: Measured and calculated oxide precipitate densities for 3 initial O concentrations: (a) 8×10^{17} cm^{-3} (b) 7×10^{17} cm^{-3} (c) 6.1×10^{17} cm^{-3}.[14] Reprinted from Ref.14 with the permission of AIP Publishing.

The obtained temperature dependent interface energy is shown in Figure 2.28:

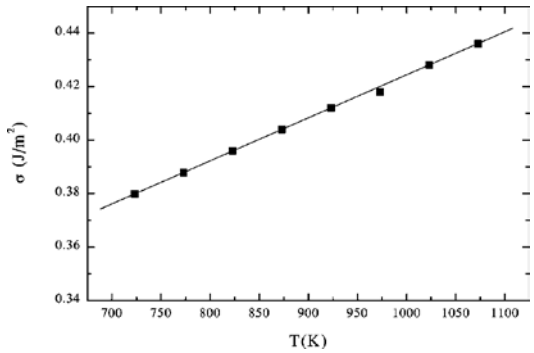

Figure 2.18: The temperature dependent surface energy.[58] Reprinted from Ref.58 with the permission of AIP Publishing.

Wang[30] obtained a temperature dependent interface energy by fitting their model to crystal growth data[30] and the experimental data of both Kelton et al.[14,58] [Figure 2.19 (a-c) and Figure 2.20] and from RTA experiments [Figure 2.21 (a-b)]. The fitted surface energy is given by:

$$\sigma = 0.51 + 3\times10^{-4}(T - 873K) \tag{2.10}$$

In addition to surface energy, the ramp rate is also part of the fitting parameters.

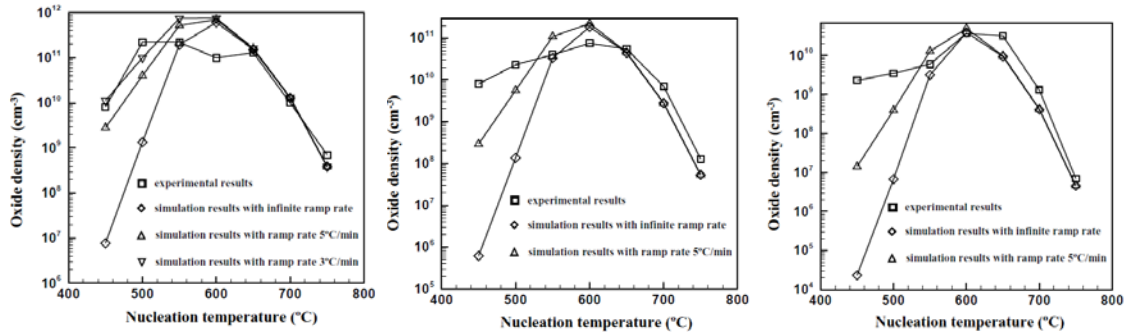

Figure 2.19: Measured (squares) and calculated oxide precipitate densities (gradient, delta and diamonds) as a function of anneal conditions, using 3 different initial O concentrations: (a) 8×10^{17} cm^{-3} (b) 7×10^{17} cm^{-3} (c) 6×10^{17} cm^{-3} for conventional anneals.[30] Reprinted with permission.

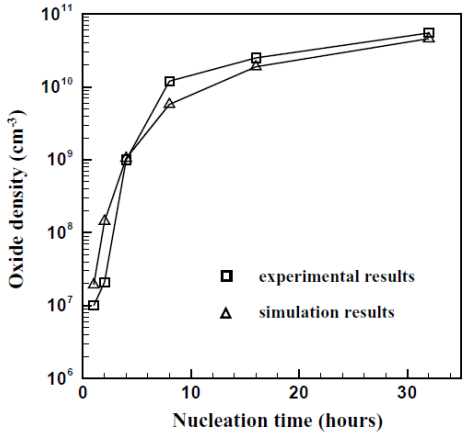

Figure 2.20: Logarithmic oxide precipitate density as a function of nucleation time at 650 °*C* for $C_O = 7\times10^{17}$ cm^{-3}.[30] Reprinted with permission.

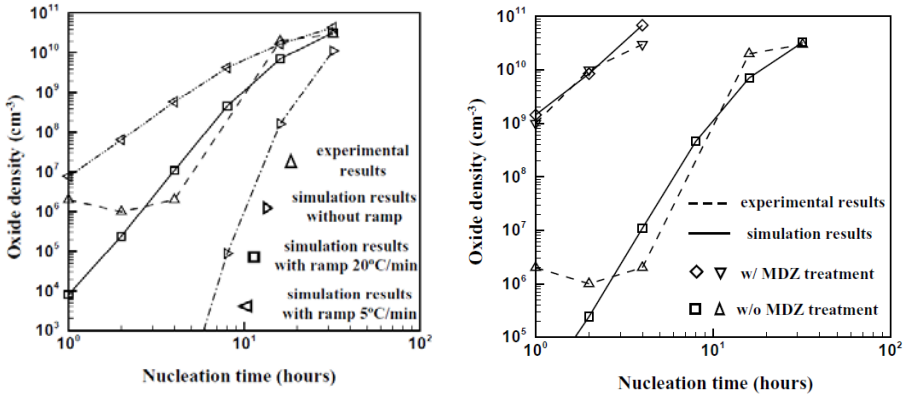

Figure 2.21: Oxide precipitate density as a function of nucleation time for RTA experiments.[30] Reprinted with permission.

Note that for RTA experiments, the Wang model does not consider the dependence of the oxide precipitates on initial RTA temperatures or the dependence of the oxide precipitates on nucleation temperatures.

Dunham et al.[59] use a set of simplified rate equations to obtain a temperature dependent interface energy. They fit their model to measurements of O consumption in three anneals performed by two different groups[60].

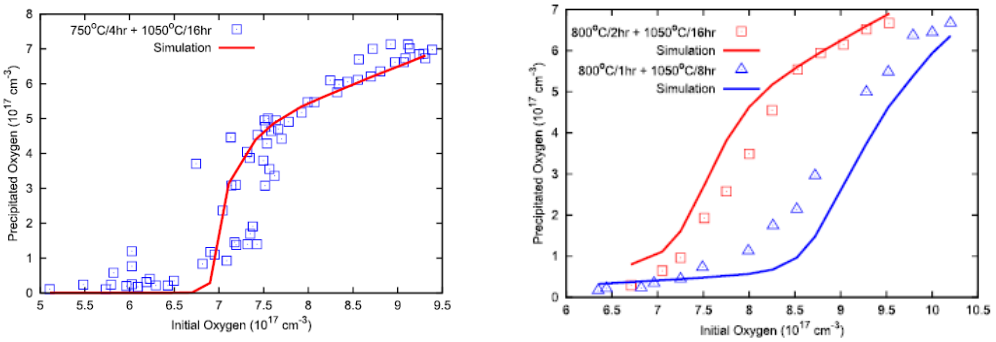

(a) (b)

Figure 2.22: O consumption as function of initial O concentration (a) Swaroop et al.[60] and (b) Chiou and Shive.[61] Reprinted from Ref.59 with the permission of AIP Publishing.

The resulting temperature-dependent interface energy is shown in Figure 2.23:

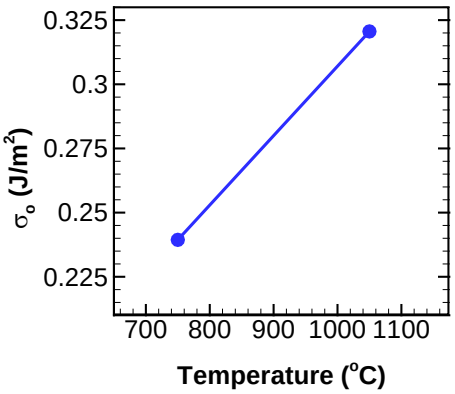

Figure 2.23: Temperature-dependent interface energy from reference[59].

Senkader et al[62]. used the same model framework as Schrems et al.[23] to fit their model to experimental data. In their model the primary fitting parameter is the additional free energy barrier for the oxide precipitate clustering event. The Si/SiO_2 interface energy is assumed to be 0.31 J/m^2. The following experimental data is used for the fitting: (1) The precipitated O concentration as a function of initial O concentration after (i) a two-step anneal [Figure 2.24 (a)], (ii) a HI-LO-HI anneal [Figure 2.24 (b)], (iii) a two-step anneal without RTA [Figure 2.24 (c)], (iv) a RTA anneal followed by (iii) [Figure 2.24 (c)], (v) a complementary metal oxide semiconductor (CMOS) type anneal [Figure 2.25]; (2) The precipitated O concentration as a function of thermal annealing time during a CMOS type anneal [Figure 2.26].

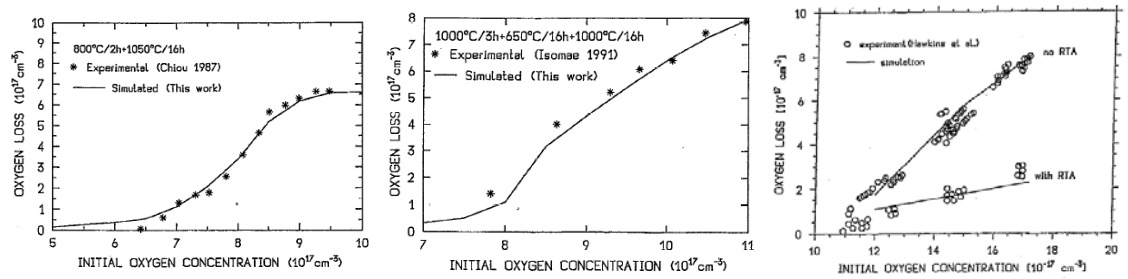

(a) (b) (c)

Figure 2.24: Interstitial and precipitated oxygen concentration as a function of initial oxygen concentration after: (a) anneal (i) (b) anneal (ii) (c) anneal (iii): (950 ºC (1h)+1200 ºC (13h), no RTA) and anneal (iv): (1200 ºC (2s)+950 ºC (1h)+1200 ºC (13h)).[62] Reprinted from Ref.[62] with the permission of AIP Publishing.

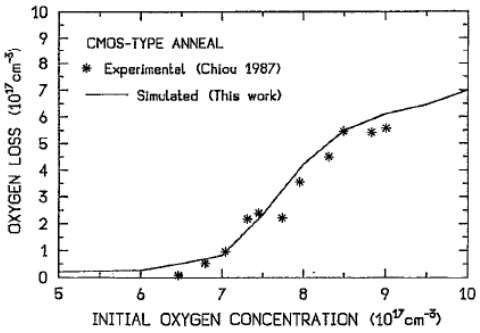

Figure 2.25: Interstitial and precipitated oxygen concentration as a function of initial oxygen concentration after a CMOS anneal that consists of 925 ºC (5h), 800 ºC (45min), 1150 ºC (20h) and 925 ºC (14h).[62] Reprinted from Ref.[62] with the permission of AIP Publishing.

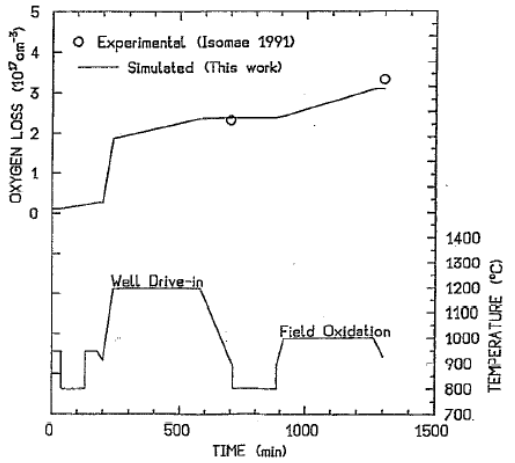

Figure 2.26: Major thermal steps of the CMOS type anneal and the precipitated O concentration as a function of annealing time for an initial oxygen concentration of 9.5×10^{17} cm^{-3}.[62] Reprinted from Ref.[62] with the permission of AIP Publishing.

A summary of interface energies is shown in Table 2.10 on the following page. Overall, the direct measurements show the widest range but seem to suggest that fully 'healed' interfaces are high in energy (~2.5 J/m^2), although it is not necessarily clear that these interfaces correspond to oxide precipitate-matrix interfaces formed by bulk oxygen precipitation. Interestingly, it is the plasma-treated cases that generally provide values near the upper end of the range – most of the cases without this treatment tend to lead to values in the range 1-1.5 J/m^2. It may therefore be the case that the plasma treatment somehow alters the interface in a way that does not correspond to spontaneous oxide precipitation in the Si bulk.

Atomistic simulations suggest values in the range 0.8-1.5 J/m^2. Much of the scatter in this data is likely to be the result of a combination of two factors: (1) error in the potential models used to compute the energy, and (2) insufficient annealing of the interface. It is interesting to note that the atomistic simulation results are quite consistent with the direct experimental measurements for the non-plasma treated cases.

Finally, the oxide precipitate model fitting literature appears to provide interface energies that are generally lower: 0.2-0.7 J/m^2, although several studies provide outlier values. Note that the oxide precipitate model fitting estimates generally implicitly include any entropic effects and therefore should be interpreted as effective free energies. Whether this is also the case for the direct experimental measurements is more difficult to assess because it depends on whether the pulling/cracking process was performed under reversible conditions (not likely). Overall, there is a suggestion that the oxide precipitate models prefer interface energy values that are significantly lower than those obtained by either atomistic simulations or direct measurement.

Source	Si/a-SiO_2 Surface Energy (J/m^2)
Stengl et al. (1999)	0.1-2.5
Suni et al. (2001)	0.1-2.8
Dragoi et al. (2005)	0.1-2.6
Schjolberg et al. (2008)	0.11, 0.98, 1.5
Plach et al. (2008) and (2013)	0.1-2.5
Kroll et al. (DFT) (2007)	1.5
Tersoff et al. (MC) (2001)	0.11
Hadjisavvas et al. (MC) (2006)	0.74-1.71
Kong et al.(MC) (2008)	0.8-1.87
Djurabekova and Nordlund (MD) (2008)	1.15-1.51
Chuang et al. (MD) (2013)	1.1, 1.5
Inoue et al. (1981)	0.38
Vanhellemont et al. (1987)	0.31-0.62
Schrems et al. (1993)	0.15-0.23
Senkader et al. (1993)	0.31
Vanhellemont et al. (1996)	3.4-6
Senkader et al. (1996)	1.68
Esfandyari et al. (1996)	0.427
Ko and Kwack et al. (1998)	0.25-0.40
Voronkov et al. (2002)	0.89
Kelton et al. (2000)	0.37-0.43
Wang (2002)	0.46-0.66
Dunham et al. (2013)	0.24-0.32

Table 2.10: Summary of Si/SiO_2 interface energy. Blue – direct experimental measurements; green – atomistic simulation; orange – model fitting.

3. Continuum Modeling of Oxide Precipitation in CZ Silicon

In this chapter we present a continuum model for simulating coupled oxide precipitation and vacancy aggregation in both wafer thermal annealing and crystal growth environments. First, in Section 3.1, the model is introduced in the context of previously developed modeling approaches. Next, the important components of the model are presented: (1) the kinetic model (rate equation system) and the morphology model (oblate spheroid model) are outlined in detail in Section 3.2; (2) the principles of detailed balance and quasi-equilibrium, which underpin the governing equations are discussed in Section 3.3; (3) the thermodynamic model (free energy model) is outlined in detail in Section 3.4. In addition, in Section 3.5, the brief descriptions of the models for voids and single point defects are given. Finally key numerical methods for solving the resulting equation systems are presented in Section 3.6.

3.1. Overview: Key Physical Elements in the Model and Experimental Data for Model Regression

Common modeling approaches (that are using the Si/SiO_2 interface energy as the primary fitting parameter) for oxide precipitation can be categorized into 2 groups: (I) models that employ homogeneous nucleation theory [20-22,27,29] and (II) models that employ rate equations[14,23,26,28,30,31,58,59]. Typically in a category (I) model, a steady-state nucleation rate of oxide precipitates, i.e. the number of new precipitates being formed per unit time[5], is calculated and fitted to the experimental data. This involves with the calculation of the Gibbs formation free energy (G) of an oxide precipitate as a function of its size (n) and locating the size (n_C) at which the free energy was a maximum by setting $dG/dn = 0$. Once these are obtained, the nucleation rate (usually an

exponential function of the Gibbs free energy at size n_C) can be calculated. Category (I) models can only calculate the transient nucleation rate at a constant temperature and supersaturation of monomer so it cannot simulate any processes. Category (II) models, however, are able to simulate the evolution of oxide precipitates by solving a set of rate equations that describe the cluster aggregation and dissolution. Our model falls into this category. In order to fully define these rate equations, several key physical elements need to be specified. As shown in Table 3.1, these elements are summarized in column 2 to 5 for each model and shaded based on their levels of sophistication (darker color means more sophisticated): (1) the growth of a oxide precipitate (for all models) is assumed to be diffusion-limited i.e. the growth is controlled only by the rate at which the reactants (precipitates/monomers) diffuse together; (2) the morphology a oxide precipitate can be: (a) just a sphere[5,12,15,17,46,47], (b) either a sphere or a plate[19] and (c) an oblate spheroid[20]; (3) the mechanism for stress relaxation can be: (a) none[5,46] (the stress is always assumed to be fully relaxed), (b) just interstitial emission[12,15,17,47] and (c) interstitial emission and shape change[19,20]; (4) the Si/SiO_2 interface energy can be: (a) a constant[12,20], (b) a temperature dependent function[5,17,19,46,47] and (c) a size dependent function[15]. Additionally the experimental data for parametrizing and validating the model are summarized in column 6, some models[5,12,15,46,47] consider conventional anneal only, some models[20] consider both conventional anneal and RTA and some[17,19] consider conventional anneal, RTA and crystal growth. As shown in the last row of Table 3.1, our model contains diffusion-limited transport, oblate spheroid morphology, stress relaxation through both point defect interaction and shape change and a size dependent Si/SiO_2 interface energy. Note that temperature-dependent interface energy is not included in our model because there is no clear evidence for this. Finally the experimental data considered in our model includes conventional anneal, RTA and crystal growth.

<table>
<tr><th rowspan="2">Models</th><th colspan="4">Key Physical Elements</th><th rowspan="2">Experiments Considered</th></tr>
<tr><th>Kinetics</th><th>Oxide Morphology</th><th>Stress Relaxation</th><th>Interface Energy</th></tr>
<tr><td>Schrems</td><td rowspan="8">Diffusion-limited Transport</td><td rowspan="4">Sphere</td><td>Interstitial emission</td><td>Constant</td><td rowspan="4">Conventional anneal

No Crystal Growth Data</td></tr>
<tr><td>Esfandyari</td><td>Interstitial emission</td><td>Size dependent function</td></tr>
<tr><td>Dunham</td><td>Interstitial emission</td><td rowspan="2">Temp. dependent function</td></tr>
<tr><td>Falster</td><td>None</td></tr>
<tr><td>Sueoka</td><td>Oblate spheroid</td><td rowspan="2">Interstitial emission & Shape change</td><td>Constant</td><td>Conventional and RTA

No crystal growth data</td></tr>
<tr><td>Wang</td><td>Sphere or plate</td><td>Temp. dependent function</td><td rowspan="3">Conventional and RTA

Crystal Growth Data</td></tr>
<tr><td>Ko and Kwack</td><td>Sphere</td><td>Interstitial emission</td><td>(3 sets of) Temp dependent function</td></tr>
<tr><td>This work</td><td>Oblate Spheroid</td><td>Interstitial emission & Shape change</td><td>Size dependent function</td></tr>
</table>

Table 3.1: Key physical elements and experimental data considered in our model and in previous modeling approaches that employed rate equations.[14,23,26,28,30,31,58,59]

3.2. Kinetic Model for Oxide Precipitation

3.2.1. Cluster Aggregation and Dissolution

All clusters (size≥2) are assumed to be immobile and can grow/dissolve only by monomer association/dissociation. Defining $g(n)$ as the growth rate and $d(n)$ as the dissolution rate of a cluster of size *n*, the aggregation/dissolution process can be represented as:

$$\cdots \leftrightarrow n-1 \underset{d(n)}{\overset{g(n-1)}{\leftrightarrow}} n \underset{d(n+1)}{\overset{g(n)}{\leftrightarrow}} (n+1) \leftrightarrow \cdots \tag{3.1}$$

The well-known master equations are used to describe the above process:

$$\left(\frac{\partial}{\partial t} + v\frac{\partial}{\partial z}\right) C(n) = J(n) - J(n+1) \qquad (n = 2,3,...n_{\max} - 1), \tag{3.2}$$

where *v* denotes the crystal pull rate ($v = 0$ during wafer annealing), $C(n)$ denotes the concentration of a cluster that contains *n* atoms and $J(n)$ denotes the net flux between clusters of size *n* and *n*+1, i.e.,

$$J(n) = g(n)C(n) - d(n+1)C(n+1). \tag{3.3}$$

However *n* ranges from 2 to about 10^{10} hence billions of coupled rate equations have to be solved, which is practically impossible. Nevertheless when *n* is large enough ($n \geq 30$) discrete master equations can be transformed into continuous Fokker-Planck type equations[63]:

$$\left(\frac{\partial}{\partial t}+V\frac{\partial}{\partial z}\right)f\left(n\right)=-\frac{\partial I(n)}{\partial n}, \tag{3.4}$$

where

$$I\left(n\right)=-B\left(n\right)\frac{\partial f\left(n\right)}{\partial n}+A\left(n\right)f\left(n\right), \tag{3.5}$$

$$A\left(n\right)=g\left(n\right)-d\left(n\right)-\frac{\partial B\left(n\right)}{\partial n}, \tag{3.6}$$

$$B\left(n\right)=\frac{g\left(n\right)+d\left(n\right)}{2}, \tag{3.7}$$

and $f(n)$ denotes the continuous form of the cluster concentration. In this way the number of equations is greatly reduced (from billions to several hundred).

3.2.2. Oblate Spheroid Model for an Oxide Precipitate

As shown in Figure 3.1, our model generalizes oxide precipitate morphologies observed in experiments[18] to that of oblate spheroids, which considers a gradual transition between spherical and plate-like precipitates[24,31].

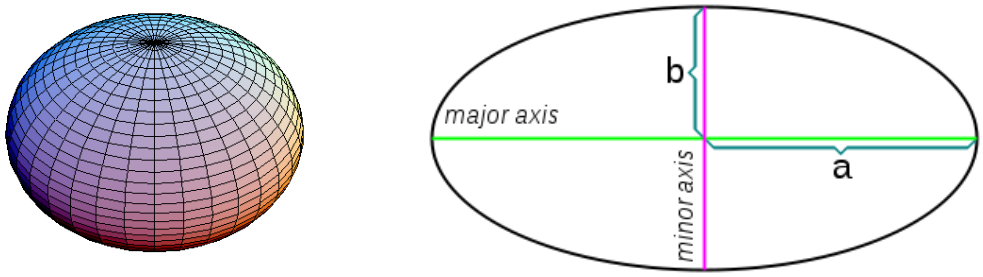

Figure 3.1: Oblate Spheroid geometry for modeling oxide precipitate shapes.

Assuming that oxide precipitates are grown under diffusion-limited conditions, local oxygen monomer concentration profiles can be obtained by solving a steady state diffusion problem around an oblate spheroidal cluster. The governing equation is given by

$$D\nabla^2 C = 0\,, \tag{3.8}$$

where C and D are the concentration and diffusivity of the monomer, respectively. In the oblate spheroidal coordinates (ξ,η,ϕ) eq. (3.8) becomes:

$$\frac{D}{\left(\xi^2+\eta^2\right)}\left[\frac{\partial}{\partial\xi}\left(\xi^2+1\right)\frac{\partial C}{\partial\xi}+\frac{\partial}{\partial\eta}\left(1-\eta^2\right)\frac{\partial C}{\partial\eta}+\frac{\xi^2+\eta^2}{\left(\xi^2+1\right)\left(1-\eta^2\right)}\frac{\partial C}{\partial\phi^2}\right]=0\,. \tag{3.9}$$

The boundary conditions are:

$$C\left(|\mathbf{r}| = \infty\right) = C_1, \tag{3.10}$$

$$C\left(\mathbf{r} = \mathbf{r}^{\mathbf{i}}\right) = 0, \tag{3.11}$$

where $\mathbf{r}$ is the position vector measured from the center of the cluster, $\mathbf{r}^{\mathbf{i}}$ defines the cluster/matrix interface and C_1 is the monomer concentration in the bulk.

The concentration profile is obtained by solving eqs.(3.9)-(3.11):

$$C = C_1 \frac{\operatorname{arccot} \xi}{\operatorname{arccot} \xi^i} + C_1 . \tag{3.12}$$

The growth rate is calculated by integrating the arrival flux of monomers over the capture surface area of the cluster (assumed to be the surface area of the spheroid)[24]:

$$\begin{aligned} g(n) &= \int \frac{\partial C}{\partial \xi}\left(\mathbf{r} = \mathbf{r}^{\mathbf{i}}\right) dA \\ &= 4\pi R_P \frac{\sqrt{1-\beta^2}}{\cos^{-1}(\beta)} \beta^{-1/3} D C_1 \end{aligned} . \tag{3.13}$$

The dissolution rate is given by:

$$d(n) = 4\pi R_P \frac{\sqrt{1-\beta^2}}{\cos^{-1}(\beta)} \beta^{-1/3} D C^{GT}(n) . \tag{3.14}$$

Here C^{GT} is the Gibbs-Thomson concentration around a cluster of size *n*:

$$C^{GT}\left(n\right)=C_1^{eq}\exp\left(\frac{\partial G^f(n)/\partial n}{k_BT}\right), \tag{3.15}$$

where C_1^{eq} is the solubility limit of the monomer and G^f is the formation free energy of a cluster of size *n*. A thorough derivation of eq.(3.14)-(3.15) will be provided in the next section.

3.3. Principles of Detailed Balance and Quasi-equilibrium

The equilibrium condition for a distribution of clusters and monomers is defined by the condition that the net flux at each point between adjacent cluster sizes is zero[64]. This condition is an expression of detailed balance in a materially closed system: the only way to achieve $dC(n)/dt = 0$ for all *n* in a closed system is by requiring[64] $J(n) = 0$. Therefore, at equilibrium, the following relationship holds:

$$\frac{g(n)}{d(n+1)} = \frac{C^{eq}(n+1)}{C^{eq}(n)}, \tag{3.16}$$

where $C^{eq}(n)$ is the equilibrium concentration of clusters of size *n* in a materially closed system. Next the nature of this general equilibrium in closed systems is discussed briefly. The total free energy of a closed lattice containing a fixed number of monomers (or any other types of particles), N_{tot}, is given by[65]:

$$G = G_0 + \sum_i^{N_{\max}} X_i G^f(i) - kT \sum_i^{N_{\max}} \left\{ X_i \ln i + \frac{N_s}{i} \ln(\frac{N_s}{i}) - \left[\frac{N_s}{i} - X_i \right] \ln \left[\frac{N_s}{i} - X_i \right] - X_i \ln X_i \right\}, \tag{3.17}$$

subject to the constraint that the total number of monomers is conserved so that

$$\sum_i^{N_{\max}} i X_i = N_{tot}, \tag{3.18}$$

where G_0 is a reference free energy, defined here as the free energy of a perfect lattice with the same total number of lattice sites, N_S . X_i is the number of clusters containing *i* monomers and $N_{\max}$ is the maximum possible cluster size considered in the system. The second term on the right-hand side of eq.(3.17) represents the total internal free energy of formation for all clusters in the system, which includes enthalpy, and cluster vibrational and internal configurational entropy, i.e.

$$G^f(i) = \left\langle E^f(i) \right\rangle - T\left\langle S^f_{vib}(i) \right\rangle - TS_{conf}(i), \tag{3.19}$$

where the angular brackets reflect the fact that each cluster can assume an ensemble of micro-configurations[66]. The last summation in eq.(3.17) represents the translational (or mixing) entropy of the system, and reflects the number of ways that an ensemble of clusters of different sizes can be arranged within the lattice. It is important to distinguish this translational entropy from the internal configurational entropy of each cluster; the latter is defined here as the number of configurations that a cluster can attain *per lattice site*[66]. In other words, the translational entropy is the mixing entropy contribution that arises from assuming each cluster size to be a distinguishable, non-degenerate entity. The sum of this translational entropy plus all the cluster internal configurational entropies is the total system configurational entropy.

At equilibrium, the total free energy of a materially closed system is minimized subject to the constraint that the total number of monomers is fixed. An optimization problem can be formulated by defining an augmented free energy function as [67]:

$$\hat{G} = G_0 + \sum_i^{N_{\max}} X_i G^f(i) + \lambda\left(\sum_i^{N_{\max}} iX_i - N_{tot}\right)$$
$$- kT\sum_i^{N_{\max}}\left\{X_i \ln i + \frac{N_s}{i}\ln\frac{N_s}{i} - \left[\frac{N_s}{i} - X_i\right]\ln\left[\frac{N_s}{i} - X_i\right] - X_i \ln X_i\right\}, \qquad (3.20)$$

where the last term represents the vacancy number constraint and λ is a Lagrange multiplier. At equilibrium, the derivatives of the augmented free energy with respect to the number of each cluster size are equal to zero and are given by

$$\frac{\partial \hat{G}}{\partial X_i} = G^f(i) - k_B T \ln\frac{N_s - iX_i}{X_i} + i\lambda = 0 \qquad \left(i = 1, 2, \ldots, N_{\max}\right). \qquad (3.21)$$

The set of equations represented by eq.(3.21) provide relationships between system size, cluster size distribution, and cluster formation free energies. In other words, under the most general conditions, the formation free energy (and equilibrium concentration) of a given cluster size is a function of the monomer concentration as well as the concentrations of all other cluster sizes. Unfortunately, using eq.(3.21) to compute the formation free energies as a system of clusters evolves in time is too computationally intensive because the Master/Fokker-Planck equations governing the cluster size distribution must be solved simultaneously with eq.(3.21) at each time step. On the other hand, in most cases of interest for defect dynamics in silicon, the system is dilute and the entropic interaction between clusters can be neglected without significant error. This dilute system approximation is formally invoked by assuming that $iX_i << N_s$ in the second term of eq. (3.21) and therefore

$$G^f(i) = k_B T \ln\frac{N_s}{X_i} - i\lambda\,. \qquad (3.22)$$

Applying eq. (3.22) to the case of monomers i.e. $i = 1$,

$$\lambda = -G^f(1) - kT \ln \frac{X_1}{N_s} = -G^f(1) - kT \ln \frac{C(1)}{\rho}, \tag{3.23}$$

and combining this result with the general form of eq. (3.22) gives

$$G^f(n) = k_B T \ln \frac{\rho}{C^{eq}(n)} + n(G^f(1) + kT \ln \frac{C(1)}{\rho}), \tag{3.24}$$

where ρ is the concentration of lattice sites. After rearranging,

$$C^{eq}(n) = \rho \times \exp\left(-\frac{\psi(n)}{kT}\right), \tag{3.25}$$

where

$$\psi(n) = -nkT \log(C(1) / C^{eq}(1)) + G^f(n), \tag{3.26}$$

and $C(1)$ and $C^{eq}(1)$ represent the actual bulk monomer concentration and solubility of the monomer, respectively. The first term in eq. (3.26) arises from the change in mixing entropy associated with the formation of a cluster of size *n* from *n* monomers, in a closed system that is infinitely dilute in all other clusters. The second term, $G^f(n)$, represents the internal free energy of formation of a cluster as defined already in eq. (3.19).

Rearranging eq.(3.26) by using eq.(3.25), the concentration of cluster of size *n* in equilibrium with a solution of monomers is given by

$$C^{eq}(n) = \rho\left(\frac{C(1)}{C^{eq}(1)}\right)^{n} \exp\left(-\frac{G^{f}(n)}{kT}\right). \tag{3.27}$$

Therefore, the detailed balance condition in eq. (3.16) can be rewritten as

$$\frac{g(n)}{d(n+1)} = \frac{C^{eq}(n+1)}{C^{eq}(n)} = \left(\frac{C(1)}{C^{eq}(1)}\right)\exp\left(-\frac{G^{f}(n+1)-G^{f}(n)}{kT}\right). \tag{3.28}$$

Note that the entire discussion above was based on the assumption that equilibrium conditions prevail and that $J_n = 0$ for all *n*. Clearly, this does not necessarily hold for systems that are far away from equilibrium. In order to apply the formalism presented here to any system (whether at steady-state or not) it is necessary to make a quasi-equilibrium assumption, whereby clusters are assumed to respond instantaneously to their surroundings.

One way to think about quasi-equilibrium is to consider the monomer concentration as an external system driving force – i.e. the system (which consists of a distribution of clusters of various sizes) acts to equilibrate with respect to a given imposed monomer concentration. Thus, in a steady-state setting in which the monomer concentration is spatially variable, the cluster size distribution everywhere is equilibrated with respect to the local "imposed" monomer concentration. Under transient conditions, the cluster size distribution evolves in time in response to local changes in the imposed monomer concentration changes. A transient system is said to be in quasi-equilibrium if it responds rapidly to changes in the monomer concentration and is able to achieve equilibrium with respect to the instantaneous monomer concentration for all time. Quasi-equilibrium is

analogous to the commonly applied quasi-steady state assumption. In the following, quasi-equilibrium is assumed to always be valid and eq.(3.28) is used to ensure that the forward and backward rates satisfy detailed balance.

3.4. Free Energy Model for Oxygen Precipitates

Throughout Chapter 3, oxide precipitates are always assumed to be comprised of amorphous SiO_2. Accordingly, the oxide precipitation process is schematically represented here by

$$P_n + Si + 2O + 2\gamma_V V \leftrightarrow P_{n+1} + stress\,, \tag{3.29}$$

in which a precipitate, *P*, containing *n* oxygen atoms grows by "oxidizing" one matrix silicon atom with two oxygen atoms to create a unit of SiO_2 and then partially relaxing the resulting stress by absorbing at the matrix-precipitate interface γ_V vacancies per oxygen atom ($2\gamma_V$ in total). Note that the process of vacancy absorption is thermodynamically equivalent to emitting a silicon interstitial at the precipitate-matrix interface. The equivalency arises because of the process of interstitial-vacancy (IV) recombination in the bulk matrix, $I + V \rightarrow Si$. Although we do not consider the kinetics of point defect recombination in the present work, self-interstitial emission and vacancy absorption are equivalent in practice only if recombination is fast relative to the oxide precipitation process. In the remainder of this thesis, we consider vacancy absorption as the only point-defect mediated stress relief mechanism.

The overall function for describing the free energy of an oxide precipitate is given by:

$$G = G^c + G^s + G^i\,. \tag{3.30}$$

The following definitions apply: the chemical energy (G^c) is given by

$$G^c = -nk_BT \ln\frac{C_O}{C_O^{eq}} - n\gamma_V k_BT \ln\frac{C_V}{C_V^{eq}}\,, \tag{3.31}$$

where the first two terms represent the difference between the chemical potential of oxygen atoms and vacancies in the matrix and oxide phases, respectively. These two terms also indicate that removal of oxygen atoms/vacancies (or addition of self-interstitials) from the matrix to the oxide precipitate results in a change of mixing entropy. In other words, if C_O (or C_V) is above equilibrium, the system tends to reduce the C_O (or C_V) to reduce the system free energy and it would be energetically favorable to bring oxygen atoms/vacancies into precipitate from the matrix.

The strain energy (G^s) can be calculated by[68]:

$$\frac{1}{2}\Delta V^2 \frac{K^*\varphi(\beta)}{K^*+\varphi(\beta)}V_p, \tag{3.32}$$

$$\Delta V = \frac{V_{SiO_2} - (V_{Si} + 2\gamma_V V_{Si})}{V_{Si} + 2\gamma_V V_{Si}}, \tag{3.33}$$

$$\varphi(\beta) = \frac{K\left[(S_{1111}+S_{1122}-1)(1-S_{3333})+2S_{1133}S_{3311}\right]}{(S_{1111}+S_{1122}-1)\left(S_{3333}-\frac{2}{3}\right)+2(S_{3333}-S_{1133}-S_{3311}-1)/3-2S_{1133}S_{3311}}, \tag{3.34}$$

where V_p is the volume of the precipitate, V_{Si} and V_{SiO_2} is the volume of a Si and SiO_2 on a per Si atom basis respectively, K^* is the bulk modulus of the oxide precipitate, β is the aspect ratio of the oblate spheroidal oxide precipitate, K is the bulk modulus of the silicon matrix and S_{ijlm} is the Eshelby tensor[69-71] for a spheroidal precipitate in a cubic symmetric silicon matrix. A more thorough derivation of eqs.(3.32)-(3.34) will be provided in Chapter 5.

The interface energy (G^i) is given by:

$$G^i = \pi R_P^2 \left(2 + \frac{\beta^2}{\sqrt{1-\beta^2}} \ln\left(\frac{1+\sqrt{1-\beta^2}}{1-\sqrt{1-\beta^2}} \right) \right) \beta^{-2/3} \left(\frac{1+e_C}{1+Xe_C} \right)^2 \sigma_O . \quad (3.35)$$

Here e_C is the constrained strain and X is given by:

$$X = 1 + \frac{4\mu}{3K}, \quad (3.36)$$

where μ is the shear modulus of Si . σ_O (the primary fitting parameter in this model) is the Si/SiO_2 interface energy per area.

Finally, the complete expression of the free energy (*eV*) is given as

$$\begin{aligned} G(n, \gamma_V, \beta) = & -nk_B T \ln \frac{C_O}{C_O^{eq}} - n\gamma_V k_B T \ln \frac{C_V}{C_V^{eq}} + \frac{1}{2}\Delta V^2 \frac{K^{*Z}C(\beta)}{K^{*Z}C(\beta)} V_P \\ & + \pi R_P^2 \left(2 + \frac{\beta^2}{\sqrt{1-\beta^2}} \ln\left(\frac{1+\sqrt{1-\beta^2}}{1-\sqrt{1-\beta^2}} \right) \right) \beta^{-2/3} \left(\frac{1+e_C}{1+Xe_C} \right)^2 \sigma_O \end{aligned} . \quad (3.37)$$

A *Generalized Equilibrium Model* (GEM) is used in our model assuming oxide precipitates always maintain thermodynamic equilibrium with their environments (monomer concentrations and temperatures). In this way the optimal vacancy fraction, γ_V, and aspect ratio, β, of oxide precipitate of each size are determined via 2D minimization of the free energy.

The minimization is achieved by solving:

$$\begin{matrix} \frac{\partial G(n,\gamma_V,\beta)}{\partial \gamma_V} = 0 \\ \frac{\partial G(n,\gamma_V,\beta)}{\partial \beta} = 0 \end{matrix} . \tag{3.38}$$

The constraints for the minimization is:

$$\begin{matrix} 0 \le \gamma_V \le 0.625 \\ 0 \le \beta < 1 \end{matrix} . \tag{3.39}$$

3.5. Brief Description of the Models for Voids and Single Point Defects

The void model is based on the existing model framework taken from the PhD thesis of Frewen[72]. The rate equations in the void model are the same as eqs.(3.2)-(3.7) discussed in Section 3.2.1. However in Frewen's model[72] a reaction-limited kinetic model (RLA) is used for to perform the parametric studies for void physics. The RLA assumes that there exists an additional free energy barrier for the clustering event as shown below.

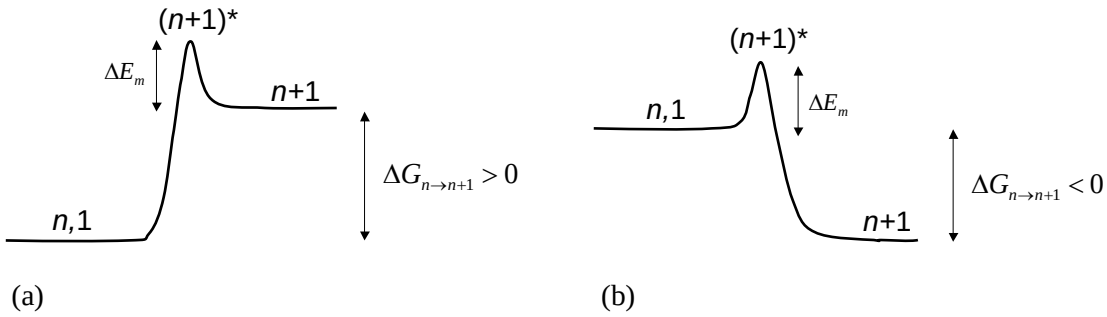

Figure 3.2: RLA Model: free energy profiles for void growth. (a) Increase in free energy, (b) decrease in free energy. ΔE_m represents the energy barrier for diffusion.

The free energy (eV) of a void as a function of T is given by[72]:

$$G(n,T) = (-2.01\times10^{-7}T^2 - 2.23\times10^{-4}T + 2.78 + 2.224\times shift\_fac)n^{2/3} \quad , \qquad (3.40)$$

where $shift\_fac$ (a fitting parameter) is a shift in the surface energy of a void[72].

In our model a diffusion-limited aggregation framework is used, which does not assume the existence of the free energy barrier. Consequently parameters in Frewen model such as the *shift_fac* for the void, equilibrium concentrations and diffusivities of vacancies and interstitials cannot be used directly and a parameter fitting similar to the one discussed in Frewen thesis[72] was performed to find the optimal parameters. The fitting is done by our colleague Andreas Sattler at Siltronic.

All monomer species, interstitial oxygen (O), vacancy (V) and interstitial silicon (I), are assumed to be diffusively mobile. Currently the reactions considered in the model include cluster aggregation/dissolution as described by eq. (3.1) for all monomers species and Frenkel pair formation/recombination for vacancies and interstitials:

$$V + I \leftrightarrow Si\,, \tag{3.41}$$

Consequently the governing equations for O, V and I are given by:

$$\left(\frac{\partial}{\partial t}+v\frac{\partial}{\partial z}\right)C_O = \quad D_O\frac{\partial^2 C_O}{\partial z^2}+\left(\frac{\partial}{\partial t}+v\frac{\partial}{\partial z}\right)\left[\int_2^{30} nC_O(n)\,dn+\int_{31}^{n_O^{\max}} nf_O(n)\,dn\right], \tag{3.42}$$

$$\begin{aligned}\left(\frac{\partial}{\partial t}+v\frac{\partial}{\partial z}\right)C_V = {} & D_V\frac{\partial^2 C_V}{\partial z^2}-k_{IV}(C_I C_V - C_I^{eq}C_V^{eq}) \\ & +\left(\frac{\partial}{\partial t}+v\frac{\partial}{\partial z}\right)\left[\int_2^{30} nC_V(n)\,dn+\int_{31}^{n_O^{\max}} nf_V(n)\,dn\right] \\ & +\left(\frac{\partial}{\partial t}+v\frac{\partial}{\partial z}\right)\left[\int_2^{30} n\gamma_V(n)C_O(n)\,dn+\int_{31}^{n_O^{\max}} n\gamma_V(n)\,f_O(n)\,dn\right]\end{aligned}, \tag{3.43}$$

$$\left(\frac{\partial}{\partial t}+v\frac{\partial}{\partial z}\right)C_I = D_I\frac{\partial^2 C_I}{\partial z^2}-k_{IV}(C_I C_V - C_I^{eq}C_V^{eq})\,. \tag{3.44}$$

Here v denotes the crystal pull rate ($v = 0$ during wafer anneal), C_X and C_X^{eq} denote the concentration and solubility of the species of X(X=O, I or V) respectively, D_X denotes the diffusivity of the species of X (X=O, I or V) . $C_X(n)$ and $f_X(n)$ X(X=O,V) denote the discrete form and the continuous form of concentration of a cluster species that contains *n* oxygen or vacancy atoms, respectively. $n_X^{\max}$ X (X=O,V) denotes the maximum cluster size included in the model. k_{IV} is the rate coefficient for recombination of interstitials and vacancies given by $k_{IV} = \Lambda_{IV}\left(D_V + D_I\right)$. Note that the last two terms in eq.(3.42) represent the sink/source terms due to the aggregation/dissolution of oxide precipitates. The last four terms eq.(3.43) represent the sink/source term due to aggregation/dissolution of voids and vacancy absorption/emission caused by oxide precipitation. The model can be expanded by considering complexes formation which will not be discussed in this thesis.

The boundary conditions for single point defects are specified as the following. For crystal growth, at the crystal melt/solid interface interstitial oxygen concentration is set to be a constant. On the crystal top, no-flux condition is applied. For wafer anneal in an inert ambient, on the wafer surface, concentrations of vacancies and interstitials are assumed to be at their equilibrium and interstitial oxygen concentration is assumed to be a constant. At the center of the wafer, no-flux condition is applied due to axial symmetry.

3.6. Key Numerical Methods

Sections 3.2 to 3.5 provide the full equation system and they can be solve numerically in our model. Details of key numerical methods are provided in this section. A schematic representation of the numerical integration scheme is shown in Figure 3.3. The monomer and cluster equations are integrated separately and sequentially, rather than using a fully implicit approach (rightmost panel in Figure 3.3). The sequential solution scheme is an operator-splitting approach[73] because equations are grouped according to whether they represent diffusing (monomers) or non-diffusing (cluster) species.

The primary reason for not using the fully implicit approach is that it requires the calculation of a large Jacobian matrix in which the derivative of every equation must be evaluated with respect to every species. The challenges related to this Jacobian matrix are two-fold: the matrix is large and ill-conditioned and is therefore computationally expensive to factor multiple times at each time step. More critically, the evaluation of the various derivatives, which must be carried out numerically due to the complexity of the equations, can severely limit the convergence behavior of the Newton method used to solve the equations. Once again, the difficulty in evaluating accurate derivatives stems from the large range of concentrations across all species.

First the equation systems are discretized in time and space by using finite difference scheme. Based on eqs. (3.1) to (3.3), the balance equations for clusters are now represented by:

$$\left(\frac{\partial}{\partial t}+V\frac{\partial}{\partial z}\right)C_X\left(n\right)=J\left(n\right)-J\left(n+1\right), \tag{3.45}$$

where X represents the species index, t is the time, z is the position, $C_X\left(n\right)$ is the cluster concentration of size n, and $J\left(n\right)$ is the net flux function between cluster sizes n-1 and n given by:

$$J(n) = g_X(n-1)C_X(n-1) - d_X(n)C_X(n). \tag{3.46}$$

All of the coupling between the cluster and monomer equations is contained within the growth and dissolution rates, $g\left(C_X(1), n\right)$ and $d\left(C_X(1), n\right)$. In other words, the growth and dissolution rates are complex functions of the monomer concentrations. Note that, as is well-established in Section 3.2.1, the Master equations for larger cluster sizes are usually replaced by a single Fokker-Planck equation (FPE) in which the size becomes a continuous independent variable. The Fokker-Planck equations are discretized by using CC70 method[74] (more details of the derivation can be found in Frewen's thesis[72]) However, the FPE does not generate any additional dependencies between equations, and all the numerical issues can be described on the basis of the Master equations, so the FPE is not considered explicitly here. The monomer equations are schematically represented by

$$\left(\frac{\partial}{\partial t} + V\frac{\partial}{\partial z}\right)C_X(1) = \nabla\cdot\left(D_X\nabla C_X(1)\right) + R(C_X(1), C_X(n)), \tag{3.47}$$

where *R* represents a set of reaction and aggregation processes between monomers and various cluster species, $C_X(n)$.

The integration scheme is shown Figure 3.3. The schematic represents the operations required to advance the simulation from the (previous) time point, t_n to the (current) time t_{n+1}. The primary difference between this integration scheme and previous schemes developed by Mori[73] is that the cluster and monomer equations are now both embedded within a single Newton loop. In the first iteration of this outer loop (which is denoted as 'Step 4' in Figure 3.3), the growth and

dissolution rates are computed using the monomer concentration at the previous time point, $C_X^{t_n}(1)$. The cluster fluxes are then represented by

$$J(n) = g_X\left(C_X^{t_n}(1), n-1\right)\cdot C_X(n-1) - d_X\left(C_X^{t_n}(1), n\right)\cdot C_X(n), \tag{3.48}$$

and the Master equations by

$$\left(\frac{\partial}{\partial t} + V\frac{\partial}{\partial z}\right)C_X(n) = J\left(C_X^{t_n}(1), n\right) - J\left(C_X^{t_n}(1), n+1\right) \tag{3.49}$$

The expressions above emphasize the fact that the cluster equations are explicit in the monomer concentrations. In this context, the monomer concentration at the previous time point should be regarded as an initial guess for the monomer concentration at the new time.

All of the coupling next eq. (3.49) is integrated forward from time t_n to t_{n+1}, using the Implicit Euler method, i.e. the cluster concentrations on the right-hand side of the equation are evaluated at time t_{n+1}. Note that the cluster system of equations is linear in the cluster concentrations – no Newton iterations are required for this step. This step then provides cluster concentrations at the current time point, i.e. $C_X^{t_{n+1}}(n)$ so that

$$J(n) = g_X^{t_{n+1}}\left(C_X^{t_{n+1}}(1), n-1\right)\cdot C_X^{t_{n+1}}(n-1) - d_X^{t_{n+1}}\left(C_X^{t_{n+1}}(1), n\right)\cdot C_X^{t_{n+1}}(n), \tag{3.50}$$

and

$$\left(\frac{\partial}{\partial t}+V\frac{\partial}{\partial z}\right)C_X(n)=J^{t_{n+1}}\left(C_X^{t_{n+1}}(1),n\right)-J^{t_{n+1}}\left(C_X^{t_{n+1}}(1),n+1\right), \tag{3.51}$$

where the fact that the growth/dissolution rates and cluster fluxes are now fully implicit with respect to both cluster and monomer concentrations is denoted by the notation $g_X^{t_{n+1}}$, $d_X^{t_{n+1}}$ and $J^{t_{n+1}}$.

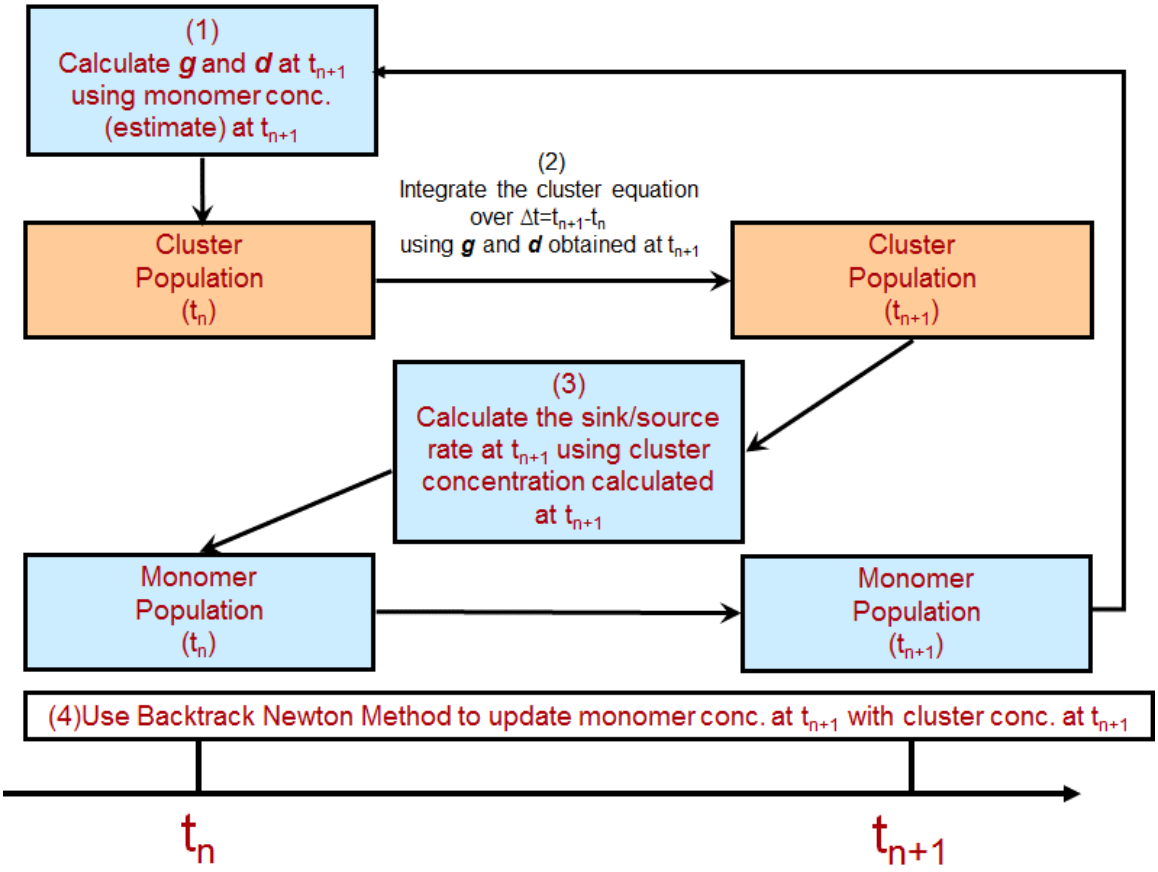

Figure 3.3: Schematic illustration of semi-implicit operator splitting approach for time integration of monomer and cluster equations.

In Step 3 in Figure 3.3, the consumption/source term of monomers come from the cluster evolution is computed using the expression

$$B = \sum_{2}^{n_{match}} n\left(\frac{\partial}{\partial t} + V\frac{\partial}{\partial z}\right)C_X(n) + \ldots \\ \sum_{j=n_{match}+1}^{n_{max}} \left\{\frac{1}{2}(n_{j+1} - n_j)\left[n_{j+1}\left(\frac{\partial}{\partial t} + V\frac{\partial}{\partial z}\right)f_X(n_{j+1}) + n_j\left(\frac{\partial}{\partial t} + V\frac{\partial}{\partial z}\right)f_X(n_j)\right]\right\}, \quad (3.52)$$

where $C_X(n)$ represents discrete clusters, n_j is the continuous cluster size variable used in the Fokker-Planck equation, and $f_X(n_j)$ represents the Fokker-Planck concentrations.

The overall form of the monomer balance equations will now be given by

$$\left(\frac{\partial}{\partial t} + V\frac{\partial}{\partial z}\right)C_X(1) = A^{t_{n+1}}(C_X^{t_{n+1}}(1)) + B^{t_{n+1}}(C_X^{t_{n+1}}(1)), \quad (3.53)$$

where A represents non-cluster related processes and B is defined by eq.(3.52). Note that the apparent implicitness of B with respect to the monomer concentrations is only valid upon convergence of the entire procedure; up to that point, only approximations for the correct monomer concentration at the current time are available.

As mentioned above, the preceding three steps are iterated within a Newton loop until convergence. The Newton loop only updates the monomer concentrations directly. The cluster problem can be considered to be a sub-function that must be evaluated in order to fully evaluate the terms in the monomer equation. To make this more apparent, we denote the Newton loop by

$$\underline{\underline{J}} \cdot \underline{\delta C}(1) = -\underline{R}, \quad (3.54)$$

where R is the residual defined for eq.(3.53), J is the Jacobian matrix corresponding to derivatives of R with respect to the monomer concentrations, and $\delta C(1)$ is the update vector of all monomer of all species. The required evaluation of J is the chief drawback of the integration scheme. Because $B^{t_{n+1}}$ (see eq. (3.52)XXX) is a very complicated, nonlinear function of the monomer concentration, the Jacobian matrix elements are evaluated numerically. The accuracy of the numerical derivatives is an important constraint on the stability of the scheme. Upon convergence of the Newton loop, the method becomes essentially fully implicit with respect to both monomer and cluster concentrations.

An adaptive time-stepping approach is employed to increase efficiency. During the simulations, the time step is adjusted on the error analysis using a method discussed in Wang[30] thesis. In this method, the time step is adjusted by performing two time integrations. The first is with the existing step, while the second is based on two half-steps. The solution norms are then compared and the new time step is given by the expression

$$\Delta t_{new} = \Delta t_{old} \times \min\left[\left(\frac{\varepsilon}{\left\|C_X(2*0.5\Delta t) - C_X(\Delta t)\right\|}\right)^{1/2}, \delta\right], \tag{3.55}$$

where ε is a user specified tolerance and eq. (3.55) controls the error as generated by the Euler method but restricts the maximum time step increase to a factor of δ (user defined) for stability reasons.

4. Regression and Mechanistic Analysis Using the Oxide Precipitation Model

4.1. Experimental Data for Parametrizing and Validating Oxide Precipitation Model

In this section a benchmark for establishing the prediction capability of our continuum oxide precipitation based on a subset of the available experimental data is carefully defined. This includes (1) 7 crystal growth performed by Erich Dornberger[75] in which the void precipitate distribution is known while the as-grown oxide precipitate distribution is not precisely known but can be bounded by subsequent wafer treatments and (2) a total of 13 wafer anneal experiments performed by Gudrun Kissinger[76], in which the final oxide precipitate density was measured for each case.

The 7 crystal growth experiments are denoted as 6A, 6C, 6E, 8A, 8B, 8D and 8E based on the nomenclature used in the Ph.D thesis of Dornberger[75]. No visible oxide precipitates (those that are larger than detect limit[77,78] 20~40nm) should be observed at the end of each simulation. The physics behind this is that voids and oxide precipitates compete with each other for absorbing vacancies in order to grow. Since the vacancy aggregation temperature (or nucleation temperature) is higher than the oxygen-vacancy binding temperature, as the temperature decreases during crystal growth, voids always win the competition and suppress oxide precipitates formation.

A schematic representing the 13 wafer annealing experiments is shown in Figure 4.1. Specifically, wafers are subjected to an initial RTA temperature between 1100-1250 °C for 30s after which the temperature is rapidly decreased to 500 °C at a rate of 75 K/s. Subsequently, the temperature is ramped-up at a rate of 100 K /min, a nucleation anneal is applied at a temperature between 650-1000 °C for 4 to 16 hours, followed by a stabilization anneal at 780 °C for 0 or 3 hours. Finally, the oxide precipitate density is measured after a 16 hour growth anneal at 1000 °C.

RTA temperatures, nucleation temperatures, and stabilization temperatures as well as the final oxide precipitate densities and initial oxygen concentrations from the 13 benchmark experimental data are summarized in Table 4.1. Note that experiments 7-13 are similar to the so-called "conventional anneals" performed by Kelton et al.[14] because of the low RTA temperature. Throughout this section, it is assumed that no clusters of any kind are initially present and that the wafer thickness is 0.725 mm.

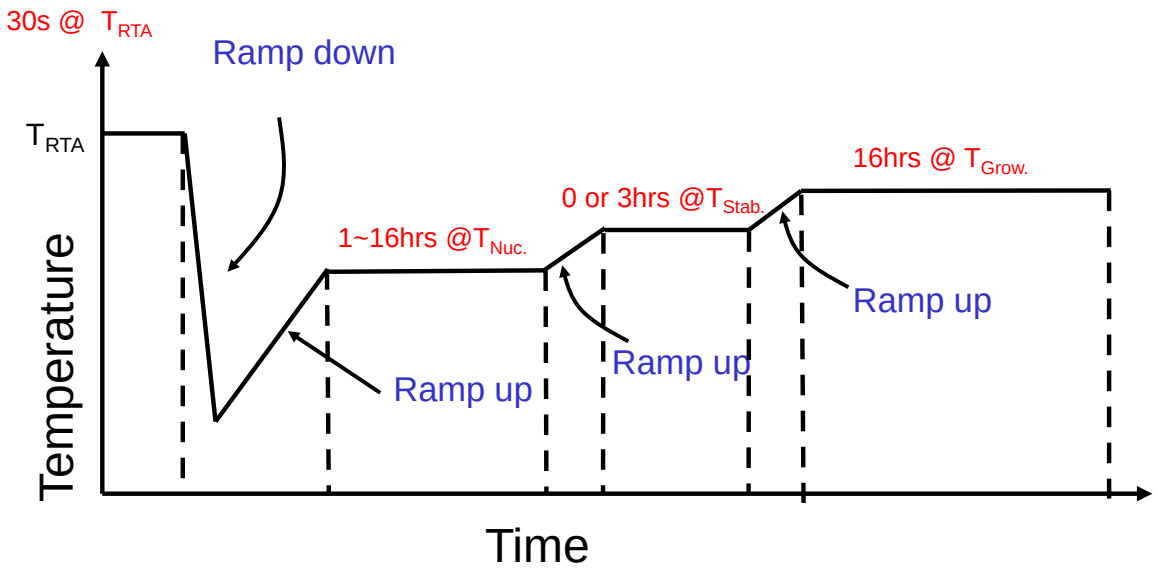

Figure 4.1: Schematic representation of an example of RTA process for simulations.[76]

Experiment	T_{RTA} (ºC)	$T_{nucl.}$ (ºC)	$T_{stabl.}$ (ºC)	Oxide Dens. (cm^{-3})	Init. Oxygen Conc. (cm^{-3})
1	1200	800 (8h)	NA	7.57e9	6.44e17
2	1175	700 (8h)	NA	4.34e8	6.41e17
3	1200	1000 (8h)	NA	8.18e7	6.44e17
4	1250	800 (8h)	NA	1.97e11	6.53e17
5	1250	1000 (8h)	NA	4.50e10	6.53e17
6	1100	800 (8h)	NA	1.00e7	6.4e17
7	1100	700 (8h)	NA	3.58e7	6.4e17
8	1100	700 (16h)	NA	1.18e9	6.65e17
9	1100	700 (8h)	780 (3h)	5.57e8	6.40e17
10	1100	700 (16h)	780 (3h)	4.00e10	6.44e17
11	1100	650 (4h)	780 (3h)	5.17e8	6.40e17
12	1100	650 (8h)	780 (3h)	1.37e10	6.41e17
13	1100	650 (16h)	780 (3h)	5.87e10	6.44e17

Table 4.1: Oxide precipitate densities and initial oxygen concentrations of the 13-experiment benchmark dataset selected from Kissinger's database.[76]

4.2. Summary of Known Model Parameters

In this section known model parameters is summarized. The equilibrium concentration (cm^{-3}) of single interstitial O in silicon crystal as a function of temperature (T) is taken from the work of Mikkelsen[79]:

$$C_O^{eq} = 7.28\times10^{22}\exp\left(\frac{-1.52eV}{kT}\right), \tag{4.1}$$

Implicit in eq.(4.1) is a reference state for the oxygen because unlike the case for native point defects, oxygen atoms in silicon must come from an external source such as the dissolved silica crucible in the melt during CZ crystal growth[75] or the oxide layer form on the wafer surface[17] during wafer annealing. The diffusivity (cm^2/s) of single interstitial O at $T \geq 700\ ^\circ C$ is given by[79]

$$D_O = 0.13\times\exp\left(\frac{-2.53eV}{kT}\right), \tag{4.2}$$

while the oxygen diffusivity at $T < 700\ ^\circ C$ is given by[80]

$$D_O = 7.33\times10^{-7}\exp\left(\frac{-1.52eV}{kT}\right). \tag{4.3}$$

The shift($shift\_fac$) in the vacancy cluster energies, equilibrium concentrations and diffusivities of V and I as a function of temperature, were fitted to the crystal growth data of Dornberger[75] by Andreas Sattler at Siltronic.

$$shift\_fac = 0.06\ J/m^2, \tag{4.4}$$

$$C_V^{eq} = 4.97\times10^{22}\exp(8.29)\exp\left(\frac{-3.86eV}{kT}\right), \tag{4.5}$$

$$C_I^{eq} = 2.97\times10^{23}\exp(8.47)\exp\left(-\frac{4.23eV}{kT}\right), \tag{4.6}$$

$$D_V = 0.00021\times\exp\left(-\frac{0.30eV}{kT}\right), \tag{4.7}$$

$$D_I = 0.223\times\exp\left(-\frac{0.72eV}{kT}\right). \tag{4.8}$$

The bulk modulus (K^*) of the oxide precipitate is chosen to be 34.7 GPa[81], the shear modulus (μ) of silicon matrix is chosen to be 64.1 GPa[30]and the bulk modulus (K) of the silicon matrix is chosen to be 97.8 GPa[82].

4.3. Data-Driven Approach for Si-SiO_2 Interface Energy

The primary fitting parameter in our model is Si/SiO_2 interface energy (σ_O). If a constant σ_O is used, the best result (Figure 4.2) is obtained when σ_O =1.02 J/m^2. However it fails to capture the dependence of oxide precipitate density on RTA temperature and nucleation anneal time.

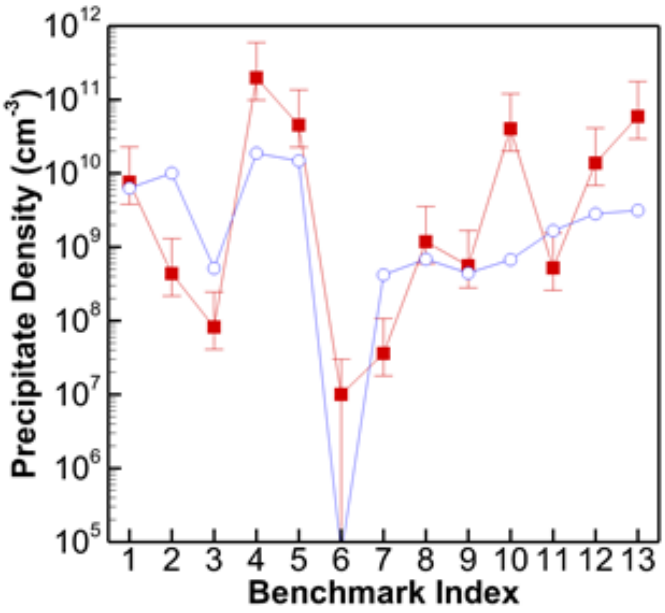

Figure 4.2: Constant interface energy (1.02 J/m^2): final oxide density for 13 different benchmark experiments. Red squares – experiment (with error bars), open blue circles – simulation.

The fact that the constant interface energy does not work indicates some physics associated with it might be missing. First of all when the size is small (n<20) a precipitate is not a continuum entity anymore. Thus the surface area of it cannot be described by a closed form expression and the continuum model for stress is not valid either. In this way a more complex model for interface energy that depends on the precipitate size is required to absorb corrections of this discreetness of small precipitates. Secondly, our interface energy function is also motivated by the atomistic simulation data of formation energies of small oxygen cluster from DFT calculation provided by

Kissinger and Dabrowksi (henceforth referred to as KD)[83,84]. Shown in Figure 4.3 (a) is a plot of the formation energies ($E_{KD}^{f}(n)$) for various oxygen-vacancy complexes as a function of the number of oxygen atoms and vacancies. These formation energies are referenced to a formation energy of 1.51 eV[79] for the isolated interstitial oxygen atom in an otherwise perfect silicon lattice. If we interpret these formation energies (or free energies) in terms of the continuum quantities defined in eq.(3.37), then we can obtain an effective interface energy (σ_O^{eff}) for each oxygen-vacancy cluster. The vacancy fraction, γ_V, is defined directly by the identity of the species e.g. $\gamma_V = 0.5$ for O_2V species. Assume all clusters to be spherical ($\beta = 1$) and both oxygen and vacancy concentrations are at equilibrium, the effective interface energy can be calculated by using the following expression:

$$E_{KD}^{f}(n) = \frac{1}{2}\Delta V^2 \frac{K^{*\,Z}C(\beta=1)}{K^{*+\,Z}C(\beta=1)} V_P + \pi R_P^2 \left(\frac{1+e_c}{1+Xe_c}\right)^2 \sigma_O^{eff}. \qquad (4.9)$$

The effective interface energies (σ_O^{eff}) for each of these species are then plotted in Figure 4.3 (b). Within our model framework, it seems that σ_O^{eff} not only depends on the size of an oxide precipitate but also depends on the vacancy content in the oxide precipitate.

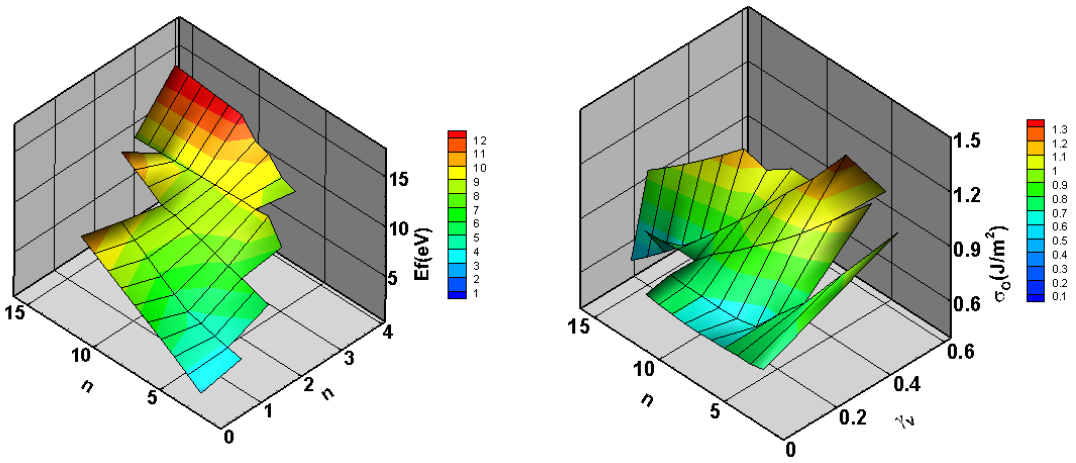

(a) (b)

Figure 4.3: Based on the formation energy data shown in (a), effective interface energy shown in (b) for small clusters (O_nV_m) is computed by using the continuum expression of oxide precipitate free energy expression.

Motivated by Figure 4.3, the interface energy model used to fit the above experimental data is defined according to the following function:

$$\sigma_O = v_1 + \left(v_4 + \frac{v_5\gamma_V}{0.5}\right)\exp\left(\frac{-5n}{v_2(1+2\gamma_V v_3)}\right) + \left(v_6 + \frac{v_7\gamma_V}{0.5}\right)\exp\left(\frac{-5(n-2)}{v_8 - 2}\right), \qquad (4.10)$$

where n is the cluster size, γ_V is the number of vacancies incorporated into the oxide precipitate per oxygen atom, and v_1 is the limiting interface energy per unit area for large clusters. The third term, with fitting parameters, v_2, v_3, v_4, and v_5, represents another decaying function that is applied to larger clusters. The second term, which includes the fitting parameters, v_6, v_7, and v_8, represents a "lip" function that is applied for small clusters. These 8 parameters fully define the interface energy function. The optimal parameter set of Si/SiO_2 interface energy was obtained from

the global regression (using the global optimization packages Dakota[85], DE[86] and PaGMO[87]) performed by Andreas Sattler at Siltronic.

4.4. Optimization-Based Model Fitting

The goal of the global regression is to find a combination of the 8 parameters ($v_1, v_2, v_3 ... v_8$) that: (1) produce no visible oxide precipitates (precipitates that are smaller than detection limit[77,78] 20~40 nm) after crystal growth and (2) minimize the difference between the predicted and experimental oxide precipitate densities for the 13 benchmark experiments. The deviation between model and experiment is quantified according to the objective functions:

$$\varepsilon_X^{oxide} = 100 \cdot \left| \frac{C_{simX} - C_{\exp X}}{C_{simX} + C_{\exp X}} \right|^6, \text{ X=(1,2,3...13)} \tag{4.11}$$

and

$$ObjF = \sum_{X=1}^{13} \varepsilon_X^{oxide} / 13, \tag{4.12}$$

where $C_{\exp X}$ is the measured oxide precipitate density listed in Table 4.1 for benchmark experiment X (X=1,2,3,…,13), C_{simX} is the simulated oxide precipitate density for experiment X (X=1,2,3,…,13).

Shown in Figure 4.4 is the evolution of the total objective function, *ObjF*, as a function of the number of iterations during the global optimization. The plot exhibits 3 approximately 'rectangular regions', with almost flat minimum values, after about 100000 iterations.

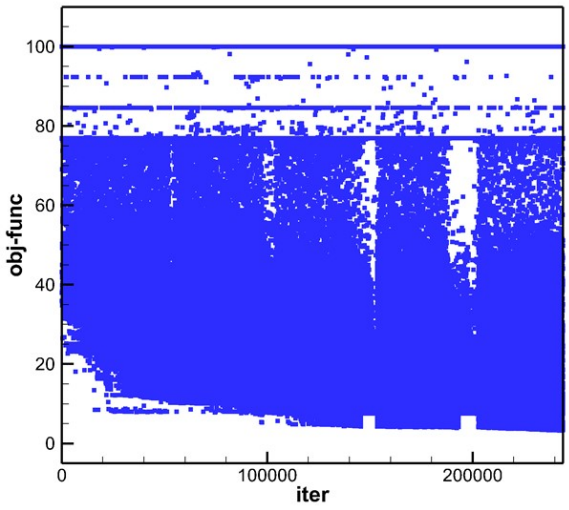

Figure 4.4: Total objective function as a function of the number of iterations in global optimization.

Based on the results shown in Figure 4.4, we proceeded to search for candidate good fit parameter set that corresponds to relatively low objective function value, while resulting in an oxygen-vacancy binding temperature that is lower than the vacancy aggregation one. In order to find such candidates, a systematic approach was used to explore the regression results. Shown in Figures 4.5 and 4.6 are 1D slices of the objective function with respect to each of the eight fitting parameters (as defined above). The slices in Figure 4.5 include objective function values up to 100, while those in Figure 4.6 are focused on values below 25. The latter cut-off was selected based on the fact that this is the objective function value at which many parameter combinations are no longer sampled. In other words, above this value many of the 1D slices show that any parameter value may be accessed, while below the accessible ranges are much tighter.

As seen in Figure 4.6, all slices appear to exhibit local minima with respect to different parameter that correspond to objective function values below about 10. In order to better define these local minima, the slices are shown again in Figure 4.7 on an expanded scale. At this scale it is now possible to find regions of good fit (i.e. below objective function values of 10) that might

be satisfactory. First of all there exists a single region for all 8 parameters for which the objective function is less than 5 – all points in this region correspond to a single local minimum. The lowest objective function in this region is about 3.27, corresponding to an average deviation of about a factor of 3.6 per objective function element (i.e., the oxide precipitate density for each of the benchmark experiments). The parameter set that corresponds to this objective function value is referred to as the "BP" parameter set. The lowest objective function value at which all parameter slices show a local minimum that is distinct from the BP point is about 7.4-7.5, corresponding to an average deviation of about a factor of 4.7 per objective function element. It is in this local minimum that we find a distinct parameter set that we refer here to as "P1". Another distinct parameter set that corresponds to a local minimum value 8.7, an average deviation of about a factor of 5 per objective function element, is defined as "P2".

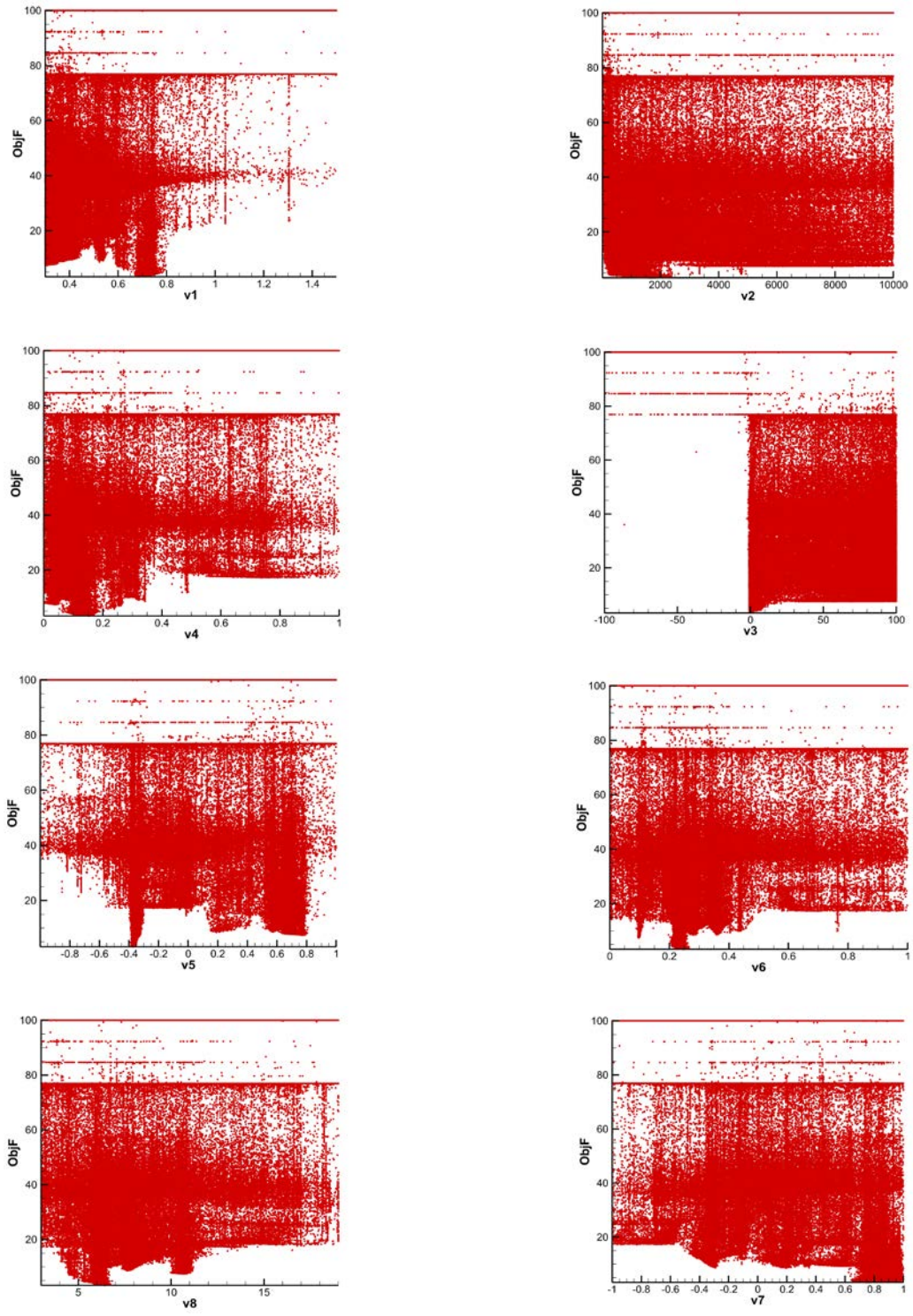

Figure 4.5: Objective function slices (*ObjF*<100) plotted against the 8 fitting parameters.

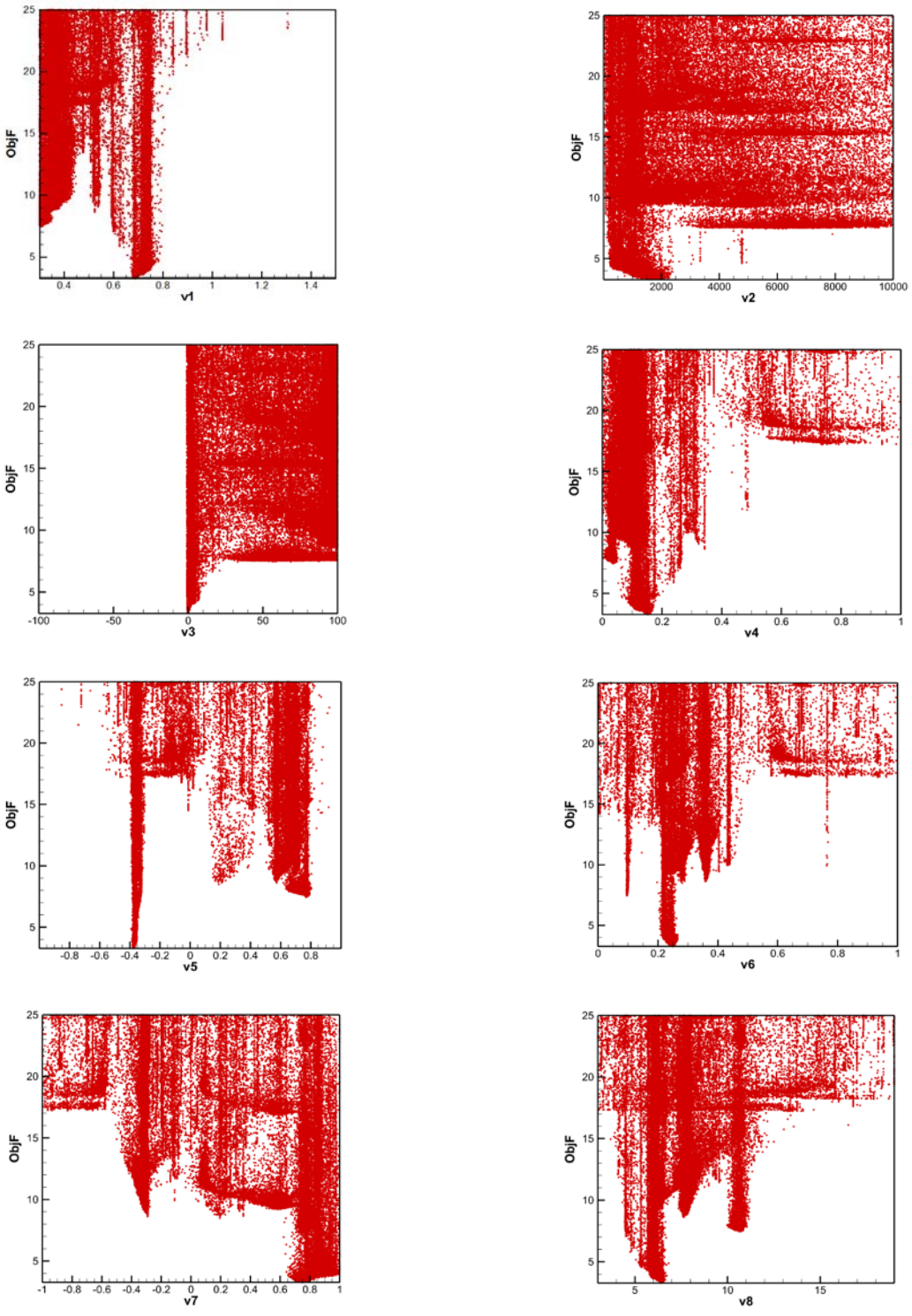

Figure 4.6: Objective function (*ObjF*<25) slices plotted against the 8 fitting parameters.

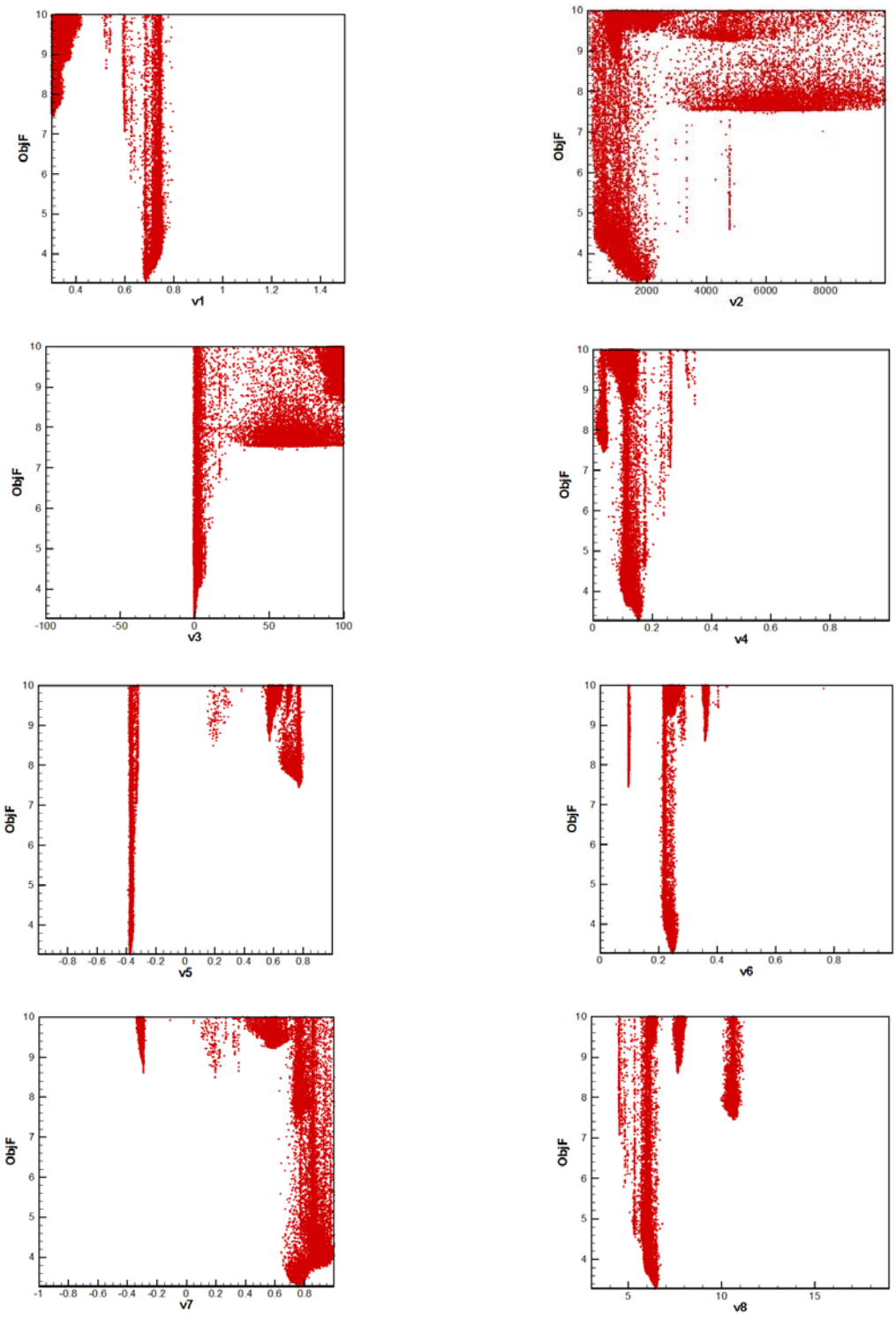

Figure 4.7: Objective function (*ObjF*<10) slices plotted against the 8 fitting parameters.

The parameter set that corresponds to the lowest objective function value in "P1" parameter basin (*ObjF* = 7.54) is analyzed in Figure 4.8. Figure 4.8 (b) shows that the measured oxide precipitate densities from experiments (red squares) and the predicted oxide precipitate densities from the simulations using the best-fit interface energy parameters (blue circles) are in overall good agreement across the benchmark experiments. Note that the experimental data itself is subject to uncertainty (assumed here to be approximately a factor of two as shown by the error bars). This parameter set will be used in our mechanistic analysis in Section 4.5.

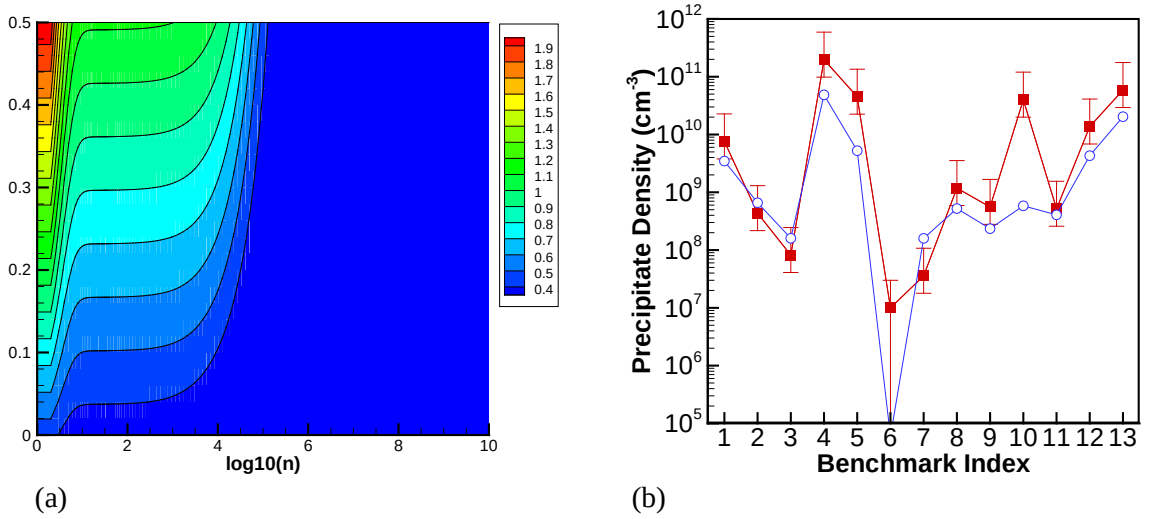

Figure 4.8: P1 Parameter Set (a) 2D contour plot of the interface energy as a function of vacancy fraction and log scale cluster size. (b) Final oxide density for 13 different benchmark experiments. Red squares – experiment (with error bars), open blue circles – simulation.

v_1	v_2	v_3	v_4	v_5	v_6	v_7	v_8	v_9
0.301	7217.286	41.17262	0.041837	0.771268	0.097191	0.771437	10.5972	7.541061

Table 4.2: Details of the optimal interface energy parameter used in our model.

As shown in Figure 4.8(b), P1 parameter set is able to capture most of the important experimental features of the Kissinger data including the dependence of oxide precipitates on RTA temperatures (T_{RTA}), nucleation temperatures ($T_{nucl.}$) and durations of nucleation anneal ($t_{nucl.}$). There are only 2 simulation data points (index 6 and 10) that are lower than the experimental data points – moreover, benchmark experiment 6 corresponds to a sub-threshold oxide precipitate density (the threshold is about $1\times10^{7}\,cm^{-3}$) for which the specific oxide precipitate density is not considered in the objective function.

The P1 parameter is also consistent with crystal growth oxide-void competition. An example is shown in Figure 4.9, the predicted oxide precipitate density is now very low (less than 1×10^{3} cm^{-3}) at the detect limit (20-40 nm) but quite substantial for small sizes. The simulated void density (2.07×10^{3} cm^{-3}), however, is within the experimental data range[75]: 1.01×10^{6} to 2.09×10^{6} cm^{-3}.

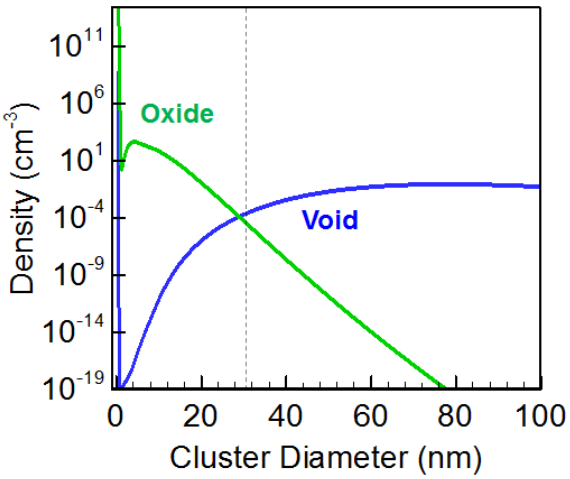

Figure 4.9: Density of oxide precipitates (green) and voids (blue) as a function cluster diameter for Dornberger crystal 8A.[75]

Next other distinct local minima (BP and P2 set) were also probed. The lowest objective function value for P2 set is about 8.75. The corresponding benchmark results are shown in Figure 4.10. The overall agreement is quite good, however, as shown in Figure 4.11, the P2 parameter set is not consistent with crystal growth in that it predicts an oxide precipitate nucleation and growth process that consumes vacancies in advance of the onset of vacancy aggregation, leading to high oxide precipitate and low void distributions. In other words, P2 parameter set corresponds to 'overly aggressive' oxide precipitate growth physics.

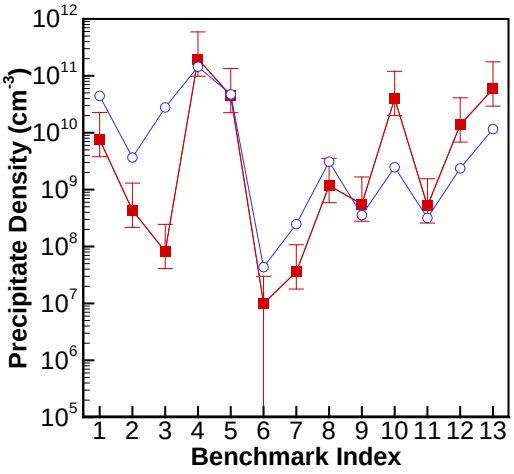

Figure 4.10: Final oxide precipitate density for 13 different benchmark experiments. Red squares – experimental data (with error bars), open blue circles – simulation results.

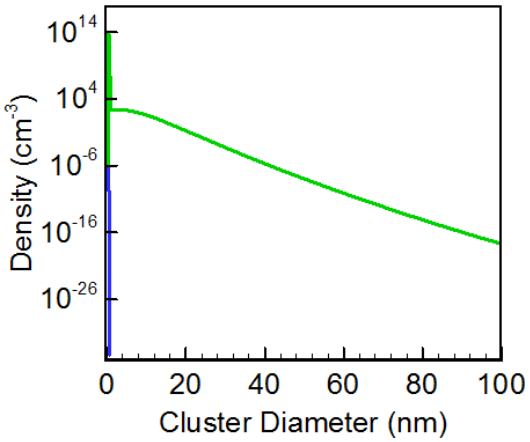

Figure 4.11: Density of oxide precipitates (green) and voids (blue) as a function cluster diameter for Dornberger crystal 8A.[75]

Finally the benchmark results generated by a BP parameter (*ObjF* = 3.27) are shown in Figure 4.12.

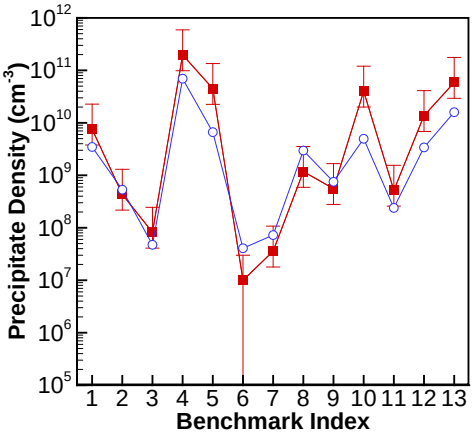

Figure 4.12: Final precipitate density for the 13 benchmark experiments. Red squares – experimental data (with error bars – see text), open blue circles – simulation results.

While the overall agreement is good, this parameter set again is not consistent with crystal growth data, i.e., predicts an early onset of vacancy trapping by oxygen and inhibits void formation as shown in Figure 4.13.

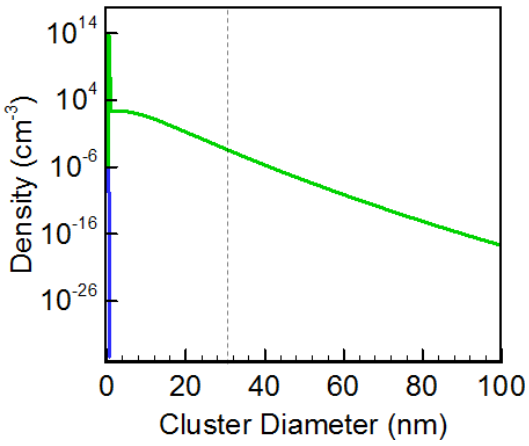

Figure 4.13: Density of oxide precipitates (green) and voids (blue) as a function cluster diameter for Dornberger crystal 8A.[75]

4.5. Mechanistic Analysis of Oxide Precipitate Evolution

As shown in Table 4.1, oxide precipitate density turns out to be very sensitive to wafer annealing conditions such as RTA temperatures. This sensitivity can be explained by studying the evolutions of the oxide precipitate size distribution during the simulations of 13 benchmark experiments. In particular we aim to provide mechanisms that explains how the size distribution is coupled to the wafer annealing conditions. Shown in Figure 4.14 is a snap shot of an oxide precipitate size distribution (blue curve with symbols) and critical size (green vertical line) during a simulation, which is the main tool for our analysis. The basic idea behind our analysis is that precipitates are smaller than critical size will dissolve, those that are larger than critical size will grow.

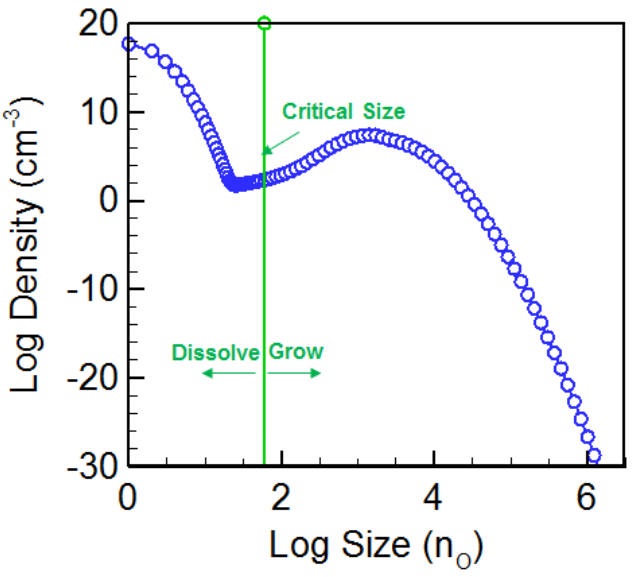

Figure 4.14: A snap shot of an oxide precipitate size distribution (blue curve with symbols) and critical size (green vertical line) during a wafer anneal simulation.

The critical size is determined by calculating the oxide precipitate free energy (eq.(3.37) which is a function of temperature, monomer concentration and monomer equilibrium concentration for all oxide precipitate sizes, at a given time and locating the size at which the free energy was a maximum; examples free energy curves at various times during the benchmark 1 case are shown in the Figure 4.15 below.

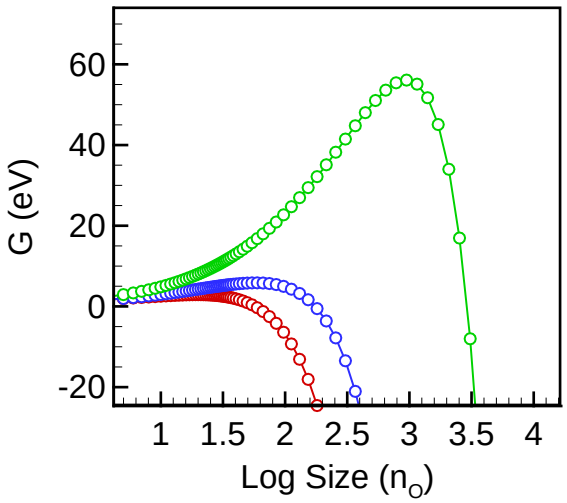

Figure 4.15: Free energy curves based on eq. (3.37) at various times during the annealing process (benchmark 1). Blue – t=220s, red – t=10220s, green – t=39140s.

During the simulations the location of the peak of the free energy is largely dictated by vacancy and interstitial oxygen concentrations. Thus monomer evolutions are also plotted to assist our analysis. Once the critical size (n_{crit}) is found, the stable cluster (clusters that are at and larger than the critical size) density can be calculated by the integral of the size distribution from the critical size to the maximum size:

$$C^{Stable} = \int_{n_{crit}}^{n_{\max}} C(n)dn. \tag{4.13}$$

where n_{max} is the maximum cluster size (chosen as 1×10^{10}) considered in the integration.

Both critical size and size distribution are evolving with time and small changes in positions of critical sizes with respect to the density size distributions might lead to very different stable cluster density. Therefore a proper prediction of position of critical size with respect to size distribution is necessary to reproduce the experimental data. In the following sections we will use this idea to analyze the impacts of RTA temperature, nucleation anneal duration and nucleation temperatures on oxide precipitate density.

4.5.1. Impact of RTA Temperature on Oxide Precipitate Density (Benchmark 1 vs. Benchmark 4)

In this section oxide precipitate evolutions for two different RTA experiments $T_{RTA} = 1200\ ^{\circ}C$ and $T_{RTA} = 1250\ ^{\circ}C$ (benchmark 1 and benchmark 4) are compared and analyzed in detail in order to determine where the large differences in oxide precipitate evolution become apparent, and in particular why the oxide precipitate density is so sensitive on T_{RTA}. Shown in Figure 4.17 is a sequence of snap shots of the oxide precipitate size distributions (curves with symbols) and the current values of the critical sizes (vertical lines) from two simulations (red-$T_{RTA} = 1200\ ^{\circ}C$ and blue-$T_{RTA} = 1250\ ^{\circ}C$). These snap shots are taken at 10 different time points (marked by symbols a, b, c, d, e, f ,g, h, i and j on Figure 4.16). Note that the multiple panels in Figure 4.17 are split into small groups (separated by text and other figures) for convenience and clearer discussion.

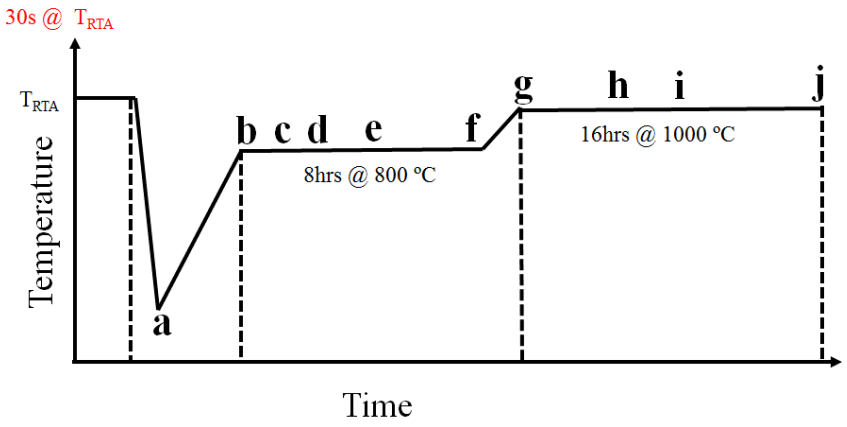

Figure 4.16: Schematic representation of processes: red lines-$T_{RTA} = 1200\ ^{\circ}C$; blue lines-$T_{RTA} = 1250\ ^{\circ}C$. The time points at which the snap shots are taken are marked by a, b, c…to j.

In addition stable oxide precipitate density (Figure 4.18) and monomer concentration (Figure 4.19 and 4.20) evolutions are also plotted as a function of time for both cases to assist the analysis.

The first two snapshots in Figure 4.17 show the system at time points a and b.

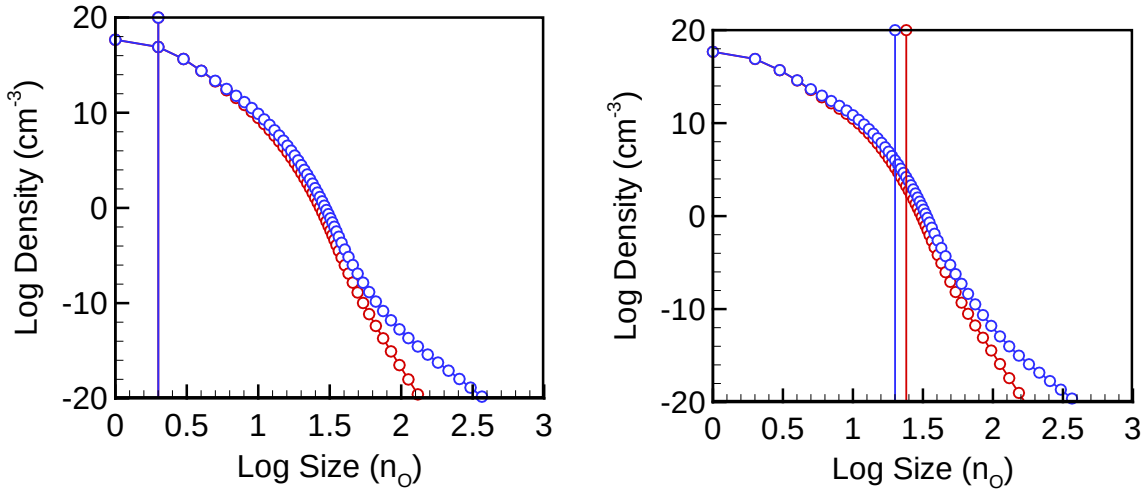

Figure 4.17: Oxide precipitate size distribution (curves with symbols) and critical size (vertical line) at (a) t=40s (bottom of ramp-down from T_{RTA}), (b) t=220s (top of ramp-up to nucleation anneal). Red lines- $T_{RTA} = 1200\ ^{\circ}C$; blue lines- $T_{RTA} = 1250\ ^{\circ}C$.

At this early stage oxide precipitate size distributions are limited to small clusters. By the time the ramp down from the initial RTA temperature is complete (Figure 4.17(a)), the critical sizes for both cases are *n*=2 (the lowest possible value), reflecting a large supersaturation of both vacancies and oxygen monomers that are confirmed in Figures 4.19 and 4.20. During the subsequent ramp-up, the critical sizes increase for both cases as the vacancy supersaturation decreases. By the time the first ramp up is complete (Figure 4.17(b)), a small difference in critical sizes (*n*=24 for $T_{RTA} = 1200\ ^{\circ}C$ case and *n*=20 for $T_{RTA} = 1250\ ^{\circ}C$ case) is created. The smaller critical size in the $T_{RTA} = 1250\ ^{\circ}C$ case is a result of higher vacancy supersaturation. This higher

supersaturation is created due to the fact that a factor of 3 higher initial (equilibrium) vacancy concentration is generated by the higher temperature at the very beginning of the anneal. The small difference in critical sizes between 2 cases, however, leads to about two order-of-magnitude difference in the stable density at time point b (as shown in Figure 4.18), which is a direct consequence of large relative concentration of clusters of different sizes (Figure 4.17(b)). Note that the relative concentration (or the shape of the size distribution) is determined mainly by the interface energy model. As shown in Figure 4.18, while a difference between the two cases is already apparent following the first ramp-up to the top to nucleation anneal at point b, the nucleation anneal leads to further divergence between the two cases. Consequently snapshots taken after time point b during the nucleation anneal at 800 °C are shown next in Figure 4.17 (c-f) to analyze the divergence. Up to t=2220s (point c), the critical size stays at *n*=24 for $T_{RTA} = 1200\ ^{\circ}C$ case and *n*=20 for $T_{RTA} = 1250\ ^{\circ}C$ case because the vacancy and oxygen monomer concentrations are almost constant. Shortly after this point, the vacancy concentration in the $T_{RTA} = 1250\ ^{\circ}C$ case suddenly drops rapidly due to the fact that the oxide precipitate population is now sufficiently large to consume a substantial amount of the vacancies. The result is a strong undersaturation of the vacancy population and thus the critical size in the $T_{RTA} = 1250\ ^{\circ}C$ case start increasing. By t=5220s (point d), the critical size has increased to 32. By t=10220s (point e), the critical size in the $T_{RTA} = 1250\ ^{\circ}C$ has already increased to 60. In contrast, however, a weak supersaturation persists in the $T_{RTA} = 1200\ ^{\circ}C$ case and the critical size stays at n=24 until the later stage of the nucleation anneal when its oxide precipitates also become sufficient enough to consume more vacancies. By t = 29020s (point f), the critical size for both case has reached n=60.

Also can be observed in Figure 4.17(c-f) is that the difference in critical size evolution start changing the oxide precipitate distributions qualitatively. Note that although the critical size

increases more rapidly in the $T_{RTA} = 1250\ ^{\circ}C$ yet it is slow enough to maintain a high stable cluster density throughout the nucleation anneal and keep its advantage over the $T_{RTA} = 1200\ ^{\circ}C$ case.

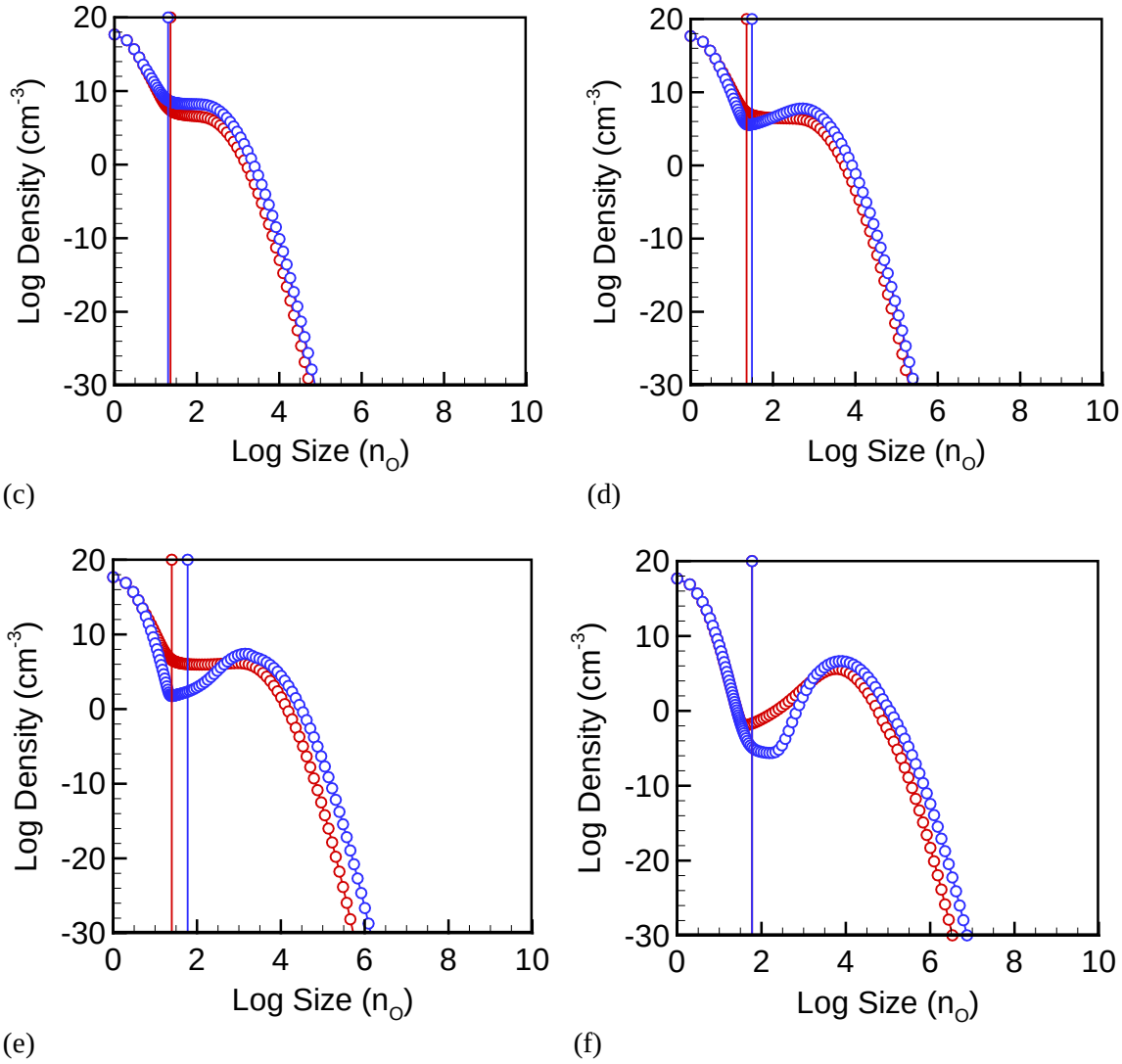

Figure 4.17: Oxide precipitate size distribution and critical size (vertical line) at various points during the nucleation anneal (c) t=2220s, (d) t=5220s, (e) t=10220s, and (f) t=29020s. Red lines- $T_{RTA} = 1200\ ^{\circ}C$; blue lines- $T_{RTA} = 1250\ ^{\circ}C$.

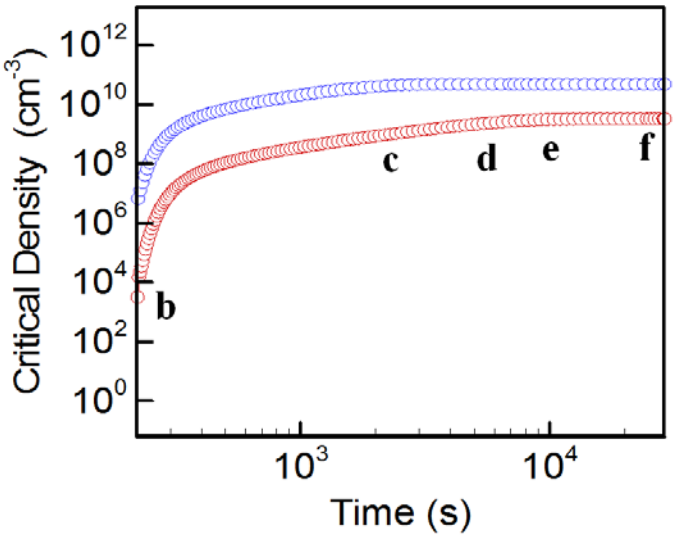

Figure 4.18: Concentration of stable oxide precipitate clusters (those at or above the critical size) as a function of time for (a) red lines-$T_{RTA} = 1200\ ^{\circ}C$ and (b) blue lines-$T_{RTA} = 1250\ ^{\circ}C$.

We now consider the evolution of the oxide precipitate population and critical sizes during the final growth anneal at 1000 °C; snapshots are shown in Figure 4.17(g-j). The divergence between 2 cases continues: the first snapshot at t=29140s (point g), which corresponds to the top of the ramp-up to the growth anneal, shows a clear difference between the two cases. For both case the overall oxide precipitate distribution have already separate into two distinct portions right at the critical size. From this point onwards, the supercritical portion of the distribution grows steadily towards larger sizes, while the subcritical portion achieves a steady-state profile at t=49140 (point h). The $T_{RTA} = 1250\ ^{\circ}C$ case, in which the critical cluster size is always larger, become qualitatively different after 59140s (point i). As the critical size continues to evolve towards larger values the subcritical distribution does not dissolve, leading to a "flatter" oxide precipitate distribution with only a weak peak at large size (as shown Figure 4.17 (j)).

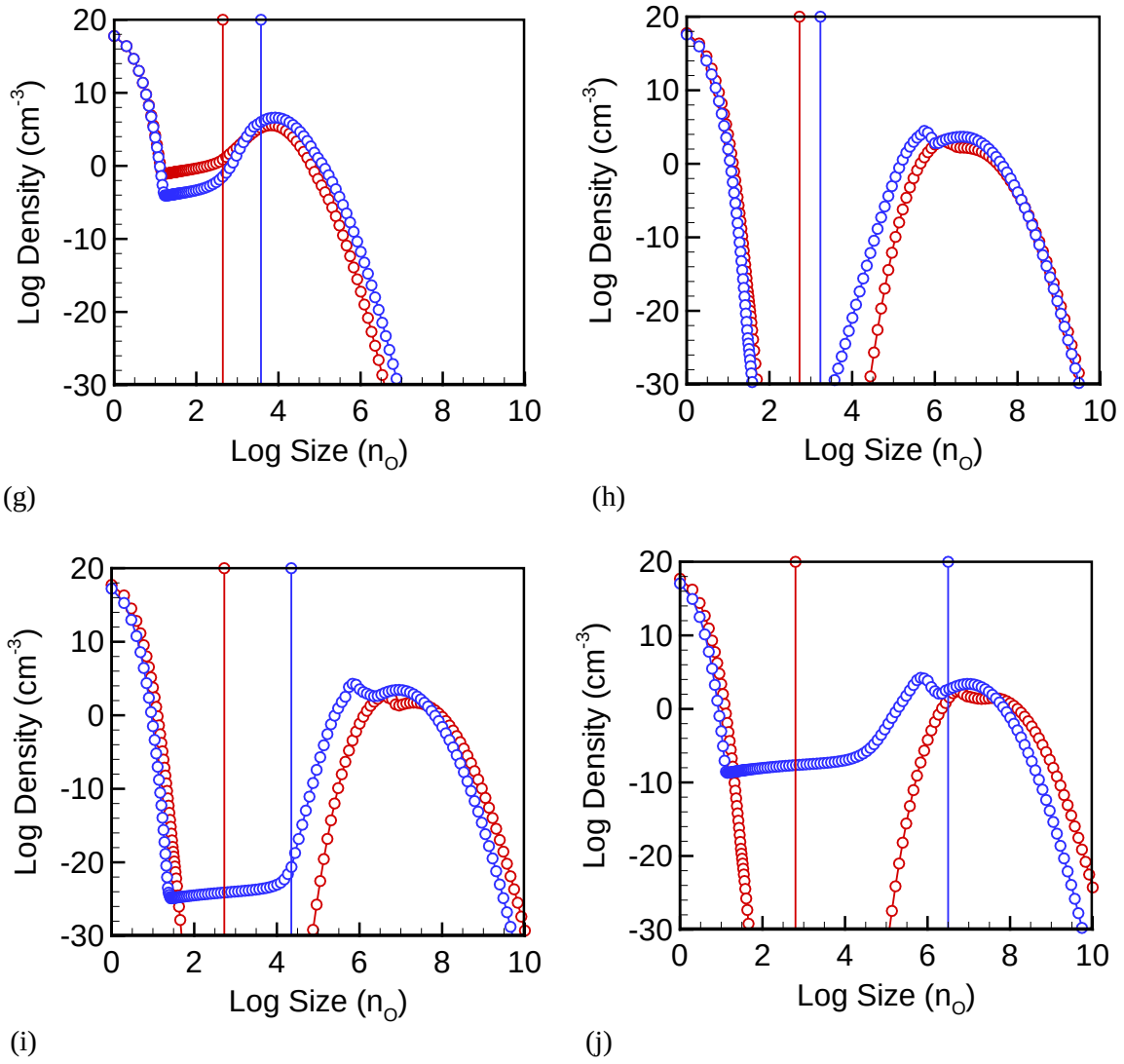

Figure 4.17: Oxide precipitate size distribution and critical size (vertical line) at various points during the nucleation anneal (g) t=29140s, (h) t=49140s, (i) t=59140s, and (j) Final time point. Red lines- $T_{RTA} = 1200\ ^{\circ}C$; blue lines- $T_{RTA} = 1250\ ^{\circ}C$.

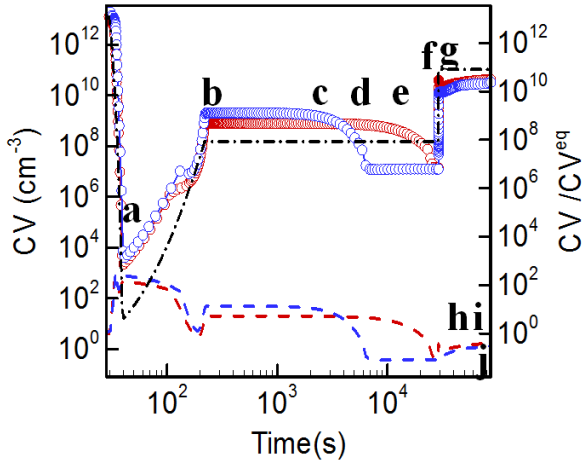

Figure 4.19: Vacancy concentration (left: symbols) and supersaturation (right: dashed lines) as a function of time for (a) $T_{RTA} = 1200\ ^{\circ}C$ (red) and (b) $T_{RTA} = 1250\ ^{\circ}C$ (blue). Dashdot black line shows the equilibrium vacancy concentration.

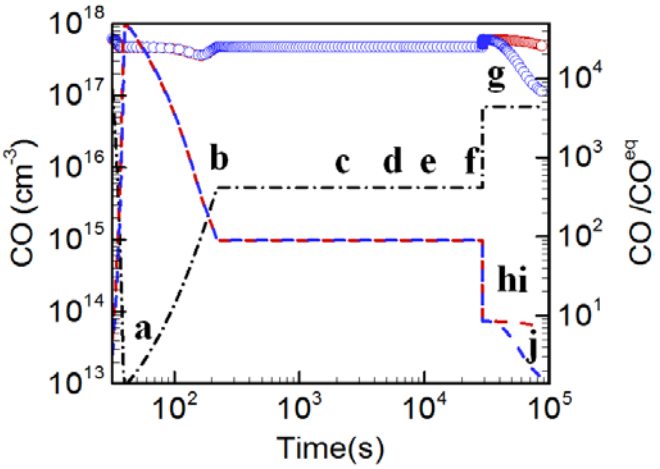

Figure 4.20: Interstitial oxygen concentration (left: symbols) and supersaturation (right: dashed lines) as a function of time for (a) $T_{RTA} = 1200\ ^{\circ}C$ (red) and (b) $T_{RTA} = 1250\ ^{\circ}C$ (blue). Dashed black line shows the oxygen solubility limit.

4.5.2. Impact of Duration of Nucleation Anneal on Oxide Precipitate Density (Benchmark 11 vs. Benchmark 13)

In this section the issue of strongly increasing oxide precipitate density with increasing duration of nucleation anneal (benchmark 11 and benchmark 13 case) will be studied. Our aim is to solve the puzzle of the two order-of-magnitude increase in oxide density when the duration of nucleation anneal is increased from 4h to 16h: is it due to an increase in nucleation rate during nucleation anneal or is it due to a milder dissolution after nucleation anneal? Once again we compare the oxide precipitate size distribution and the critical size evolution for both situations in an attempt to determine what the important factors are. In this analysis, however, snap shots of oxide precipitate size distributions and critical sizes from two simulations (red-$t_{nucl.} = 4h$ and blue-$t_{nucl.} = 16h$) are not analyzed at the same time points but at the same "end points" with respect to its own process. They are marked by a1 and a2 (end point of the nucleation anneal), b1 and b2 (end point of the stabilization anneal) and c1 and c2 (end point of the growth anneal) in Figure 4.21.

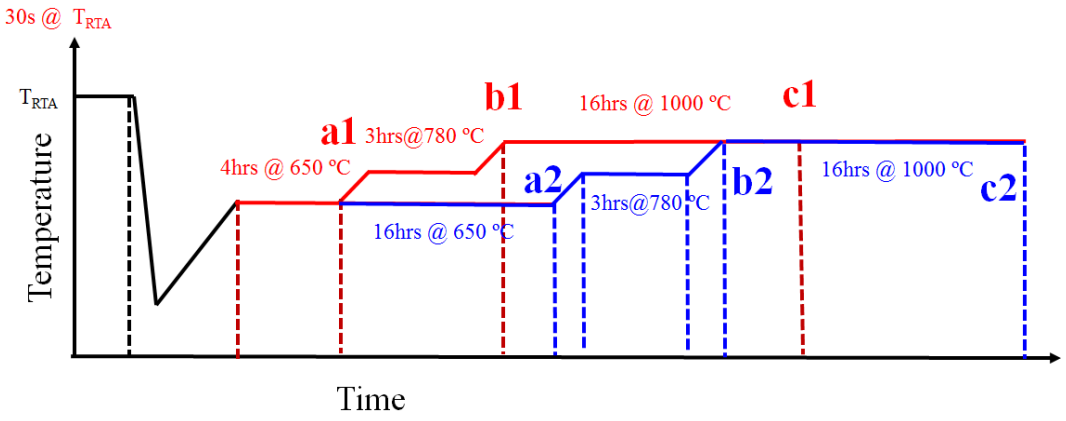

Figure 4.21: Schematic representation of processes: red lines-$t_{nucl.} = 4h$; blue lines-$t_{nucl.} = 16h$. The time points at which the snap shots are taken are marked by a1, a2, b1, b2, c1 and c2.

Obviously the evolutions for the two cases are exactly the same up to the time point a1 (t=14528s). After point a1, temperature in the $t_{nucl.} = 4h$ case increases to the stabilization temperature while temperature in the $t_{nucl.} = 16h$ stays at $T_{nucl.} = 650\ ^{\circ}C$ for another 12 hours until point a2 (t=57806s). In Figure 4.22(a), snapshots at a1 point (t=14528s) for $t_{nucl.} = 4h$ case and at a2 point t=57806s for $t_{nucl.} = 16h$ case are compared. The effect of longer $t_{nucl.}$ during nucleation anneal is straightforward: as can be seen in the plot of stable cluster density evolution (Figure 4.23), 4 times longer $t_{nucl.}$ creates about a factor of 4 more oxide precipitates at time point a2 and leads to more vacancy consumption (or lower vacancy superasaturation). Accordingly the critical size increases and more larger oxide precipitates are formed. The end result is a "flatter" size distribution at point a2.

Next as anneal proceeds to the end of the stabilization anneal, the vacancy supersaturation decreases more and the critical size "swap" through a relatively larger portion of the distribution making a substantial amount precipitates to dissolve at the end of the stabilization anneal (at point b1 in the $t_{nucl.} = 4h$ and point b2 in the $t_{nucl.} = 16h$ case). This dissolution is confirmed in Figure 4.23 as both cases exhibit a sudden and steep decline in the density of stable clusters. Interestingly, compared to the $t_{nucl.} = 4h$ case (the critical size increases from 20 to 46), the $t_{nucl.} = 16h$ case exhibits a larger increase in the critical size (from 40 to 277) but a much smaller stable cluster density drop from the end of the nucleation anneal (a2 point) to the end of the stabilization anneal (b2 point). Again the magnitude of the drop in stable density as the critical size increases is a direct consequence of the relative concentration of clusters of different sizes, which is governed by the Si/SiO_2 interface energy. Returning to the question posed at the beginning of this section, it is clear that the two orders of magnitude difference is created due to the dissolution of the already formed precipitates in the $t_{nucl.} = 16h$ case instead of the increase in nucleation rate.

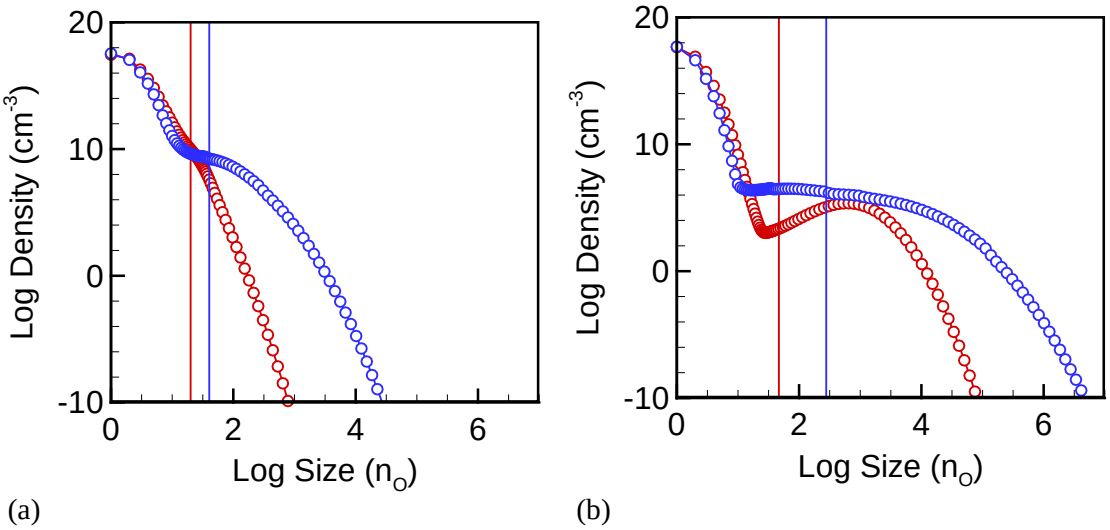

Figure 4.22: Oxide precipitate size distribution and critical size (vertical line) at (a) red-a1 point t=14528s and blue-a2 point t=57806s; (b) red-b1 point t=25406s and blue-b2 point t=68606s.

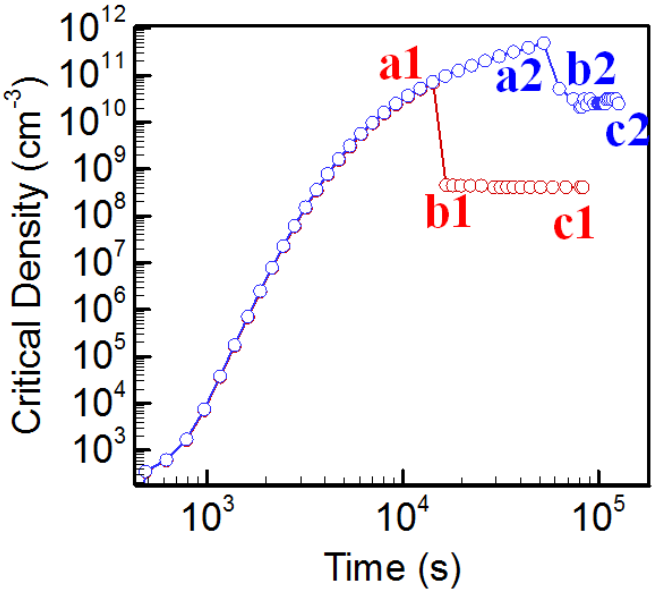

Figure 4.23: Density of clusters with size at or greater than the critical size as a function of time. Red- $t_{nucl.} = 4h$, blue - $t_{nucl.} = 16h$.

Finally as shown in Figure 4.24 at the end of each process (at point c1 or at 83138s for $t_{nucl.} = 4h$ case and at point c2 or at t=126338s for $t_{nucl.} = 16h$ case), the $t_{nucl.} = 16h$ case now has a much larger critical size than the case. Recall that the increase in the critical size at later times (during the growth anneal) is due to the consumption of oxygen monomers.

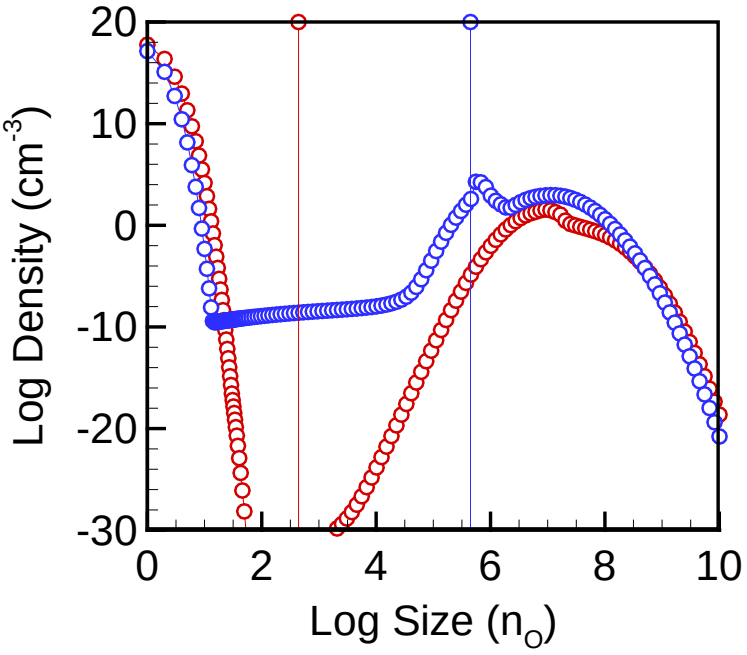

Figure 4.24: Oxide precipitate size distribution and critical size (vertical line) at end of process: Red lines-at t=86138s for case $t_{nucl.} = 4h$; blue lines- at t=126338s for case $t_{nucl.} = 16h$.

4.5.3. Impact of Nucleation Anneal Temperature on Oxide Precipitate Density (Benchmark 1 vs. Benchmark 3)

In this section we study the issue of the reducing oxide precipitate density when the nucleation temperature ($T_{nucl.}$) is increased from 800°C (benchmark 1) to 1000 °C (benchmark 3) for the $T_{RTA} = 1200\ ^{\circ}C$ case. The comparative analysis of the oxide precipitate size distribution and the critical size evolution is repeated here. Shown in Figure 4.26 are snap shots of oxide precipitate size distributions and critical sizes from two simulations (red-$T_{nucl.} = 800\ ^{\circ}C$ and blue-$T_{nucl.} = 1000\ ^{\circ}C$) at 5 different time points (marked by symbols a, b, c, d and e on Figure 4.25). To assist the analysis, evolution of the stable oxide precipitate density (Figure 4.27) and the monomer concentration (Figures 4.28 and 4.29) as a function of time for both cases are also plotted.

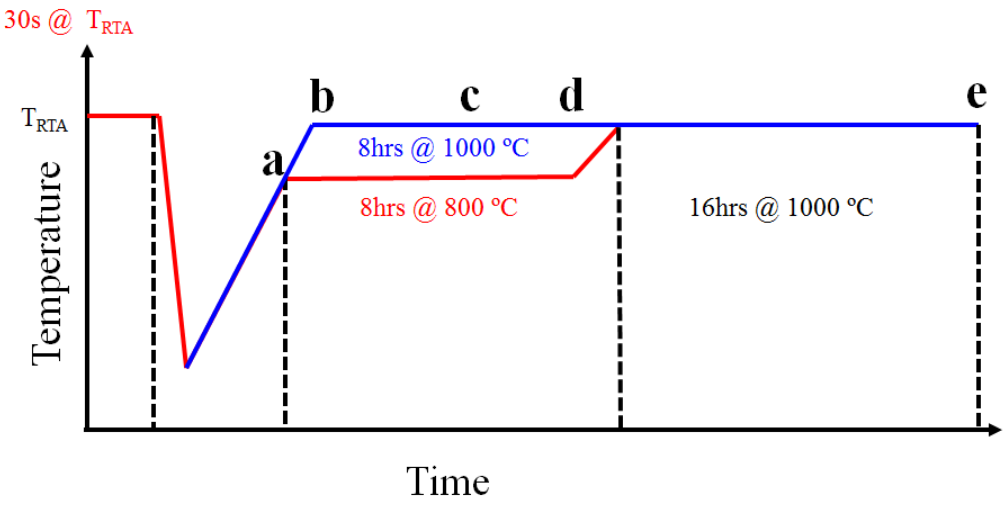

Figure 4.25: Schematic representation of processes: red lines-$T_{nucl.} = 800\ ^{\circ}C$; blue lines-$T_{nucl.} = 1000\ ^{\circ}C$. The time points at which the snap shots are taken are marked by a, b, c, d and e.

Obviously the evolutions for the two cases are identical up to the time point a (t~220s) at which the temperatures for the 2 cases start deviating. The first two snapshots in Figure 4.26 show the distributions at the time points a and b. At t=220s (a), the critical size for both cases is at the same value (n=24) and the distributions are identical. After this time point, as the temperature continues to increase above 800 ℃ in the $T_{nucl.} = 1000\ ^{\circ}C$ case, the higher temperature is causing the supercritical part of the distribution to evolve more rapidly. Thus, as shown in Figure 4.28, a large amount of vacancies are consumed by oxide precipitates and the vacancy supersaturation decreases very quickly. The decrease in the supersaturation then leads to an increase in critical size. By t=340s (b), however, the critical size in the $T_{nucl.} = 1000\ ^{\circ}C$ case has already increased to n=60 (still at n=24 for the $T_{nucl.} = 800\ ^{\circ}C$ case). In fact the early "burst" in the growth of precipitates in the $T_{nucl.} = 1000\ ^{\circ}C$ case consumes almost all of the accessible vacancies (those that are above C_V^{eq}) and prohibits the system from forming new precipitates in the later stage of the anneal. This is confirmed in Figure 4.27(a) as the stable precipitate density profile (blue line) becomes flat after time point b. In contrast, oxide precipitates in the $T_{nucl.} = 800\ ^{\circ}C$ case consumes vacancies more slowly and allows new precipitates to form continuously- the red line in Figure 4.27(a) is still increasing after time point b.

The divergence between two cases continues at t=10220s (c) during nucleation anneal, where it is now observed that the $T_{nucl.} = 1000\ ^{\circ}C$ case has already exhibited a clear "separated" distribution between super- and sub-critical clusters. Simultaneously, the critical size in the $T_{nucl.} = 1000\ ^{\circ}C$ case has continued to increase to about n=258 while in the $T_{nucl.} = 800\ ^{\circ}C$ case stays at n=24. After this point, a substantial amount of oxide precipitates in the $T_{nucl.} = 800\ ^{\circ}C$ case become large enough and start consuming more vacancies. Consequently the vacancy supersaturation also decreases and leads to an increase in critical size. By t=29020s (d), the

nucleation hold has been reached and the critical size is now n=60 for $T_{nucl.} = 800\ ^{\circ}C$ case but still n=258 for $T_{nucl.} = 1000\ ^{\circ}C$ case. As shown in Figure 4.27(b), the trend in the stable cluster density evolution for both cases also continues and establishes a large difference between two cases at the end of the nucleation anneal.

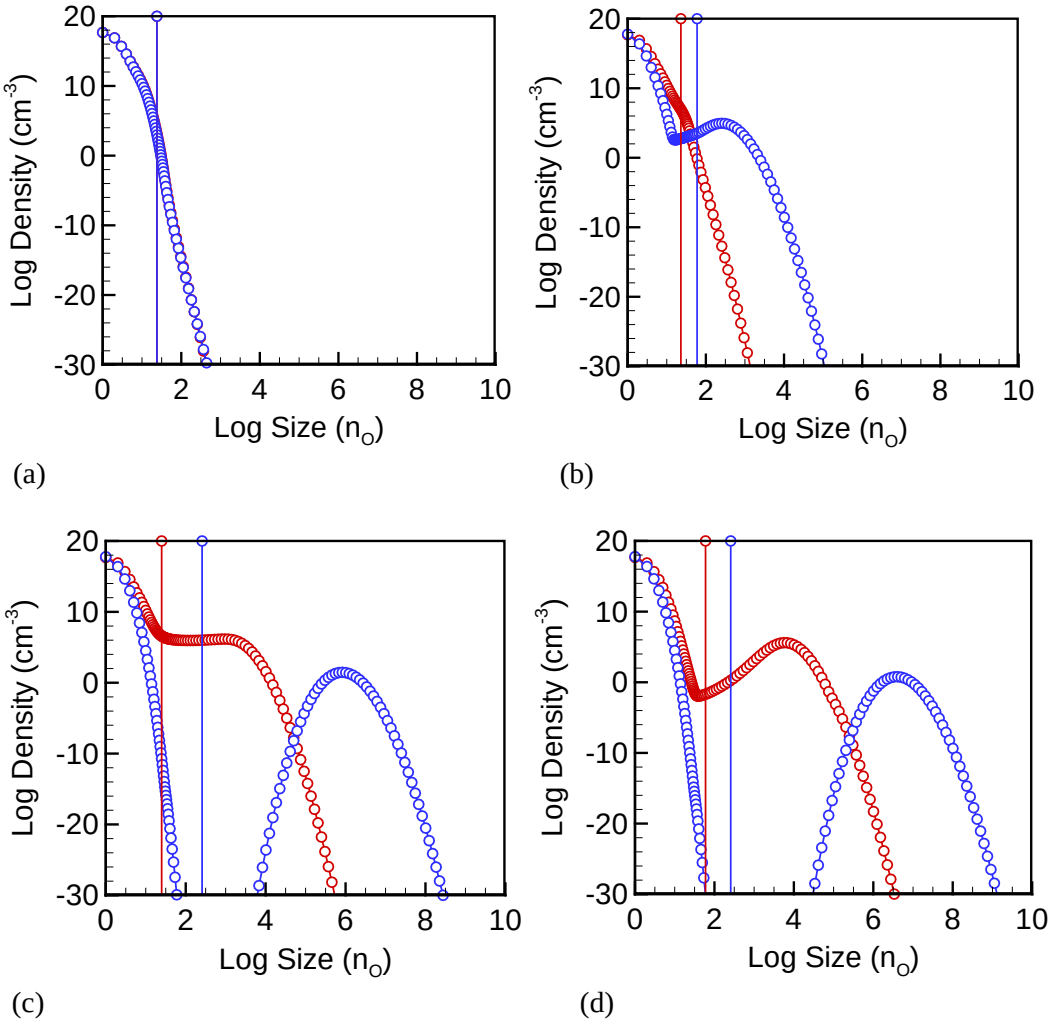

Figure 4.26: Oxide precipitate size distribution and critical size (vertical line) at (a) t=220s, (b) t=340, (c) t=10220s, and (d) t=29020s. Red lines-$T_{nucl.} = 800\ ^{\circ}C$; blue lines-$T_{nucl.} = 1000\ ^{\circ}C$.

The final size distributions of the two cases are shown in Figure 4.26(e), which is a snapshot at the end of the anneal. The $T_{nucl.} = 1000\ ^{\circ}C$ case exhibits larger oxide precipitates but a much smaller density. Note that the critical sizes at the end of the process are reversed: the $T_{nucl.} = 800\ ^{\circ}C$ case now has a larger critical size than the $T_{nucl.} = 1000\ ^{\circ}C$ case. Again recall that this increase in the critical size at later times (during the growth anneal) for the $T_{nucl.} = 800\ ^{\circ}C$ case is due to its strong consumption of oxygen monomers (Figure 4.29).

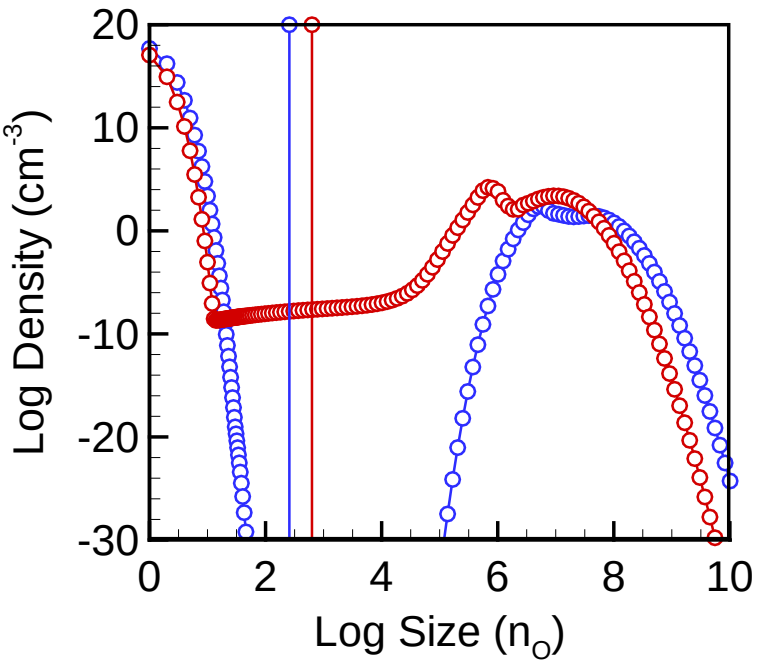

Figure 4.26(e): Oxide precipitate size distribution and critical size (vertical line) at the end of process (t=86738s). Red lines-$T_{nucl.} = 800\ ^{\circ}C$; blue lines-$T_{nucl.} = 1000\ ^{\circ}C$.

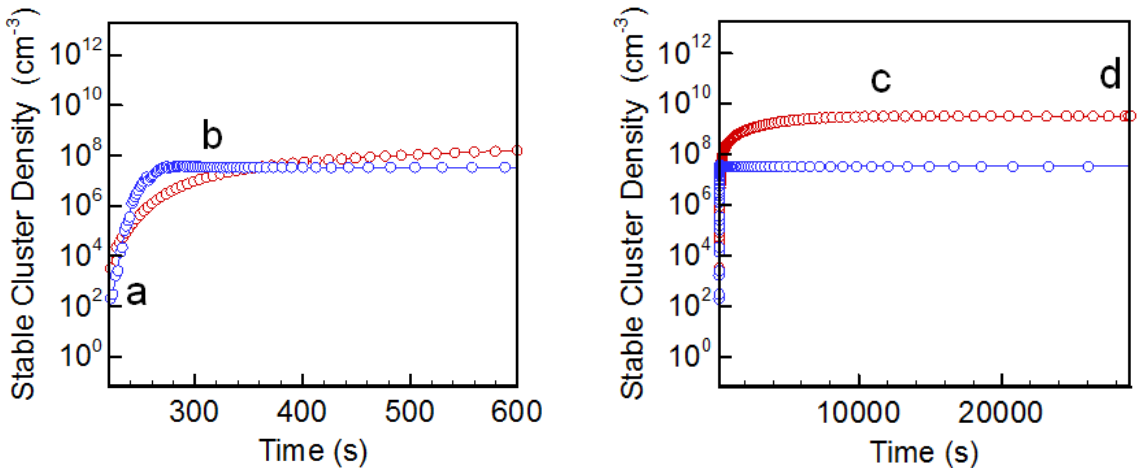

Figure 4.27: Density of stable oxide precipitate clusters (those at or above the critical size) at (a) early stage and (b) later stage of the anneal as a function of time for the $T_{nucl.} = 800\ ^{\circ}C$ (red line) and $T_{nucl.} = 1000\ ^{\circ}C$ (blue line) case.

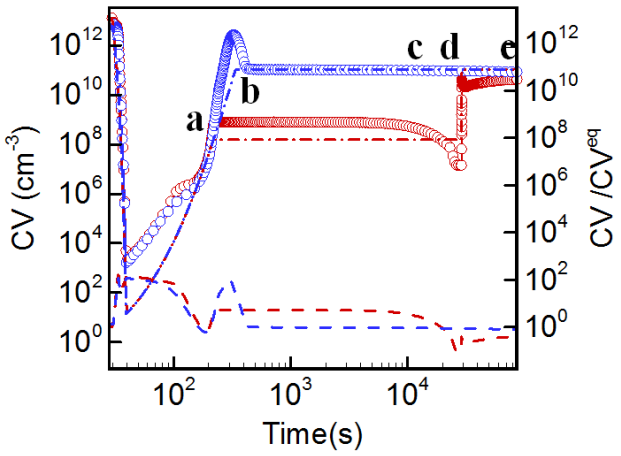

Figure 4.28: Vacancy concentration (left: symbols), equilibrium concentration (left: dashed dot lines) and supersaturation (right: dashed lines) as a function of time for red-$T_{nucl.} = 800\ ^{\circ}C$ and blue-$T_{nucl.} = 1000\ ^{\circ}C$ case.

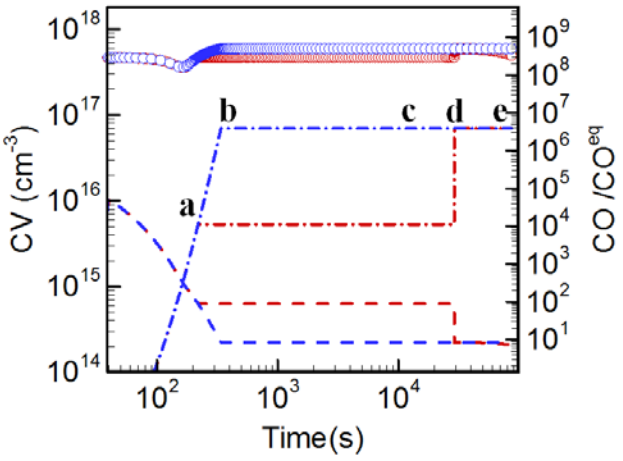

Figure 4.29: Interstitial oxygen concentration (left: symbols), equilibrium concentration (left: dashed dot lines) and supersaturation (right: dashed lines) as a function of time for red-$T_{nucl.} = 800\ ^{\circ}C$ and blue-$T_{nucl.} = 1000\ ^{\circ}C$ case.

5. Detailed Study of the Stress and Strain Energy of Oblate Spheroidal Precipitates in Silicon Crystals

In general, precipitates in a given crystalline material can be categorized into two broad types[88]: (1) coherent precipitates for which there exists a definite relationship between the precipitate structure and the matrix structure so that the lattices match exactly at the interface and (2) incoherent precipitates for which there are no continuity conditions to be satisfied across the matrix/precipitate interface. To better illustrate this point, a coherent and incoherent cluster are plotted schematically in Figure 5.1. For example, germanium precipitates (Si_{1-x} Ge_x precipitates) within a crystalline silicon (Si) bulk phase are usually coherent[89-94], while large amorphous oxide precipitates (SiO_2 precipitates) in Si crystals are usually incoherent due to their disordered structures[13,95]. In this chapter, the study is focused on coherent Ge precipitates while preliminary results for incoherent SiO_2 precipitates are discussed at the end.

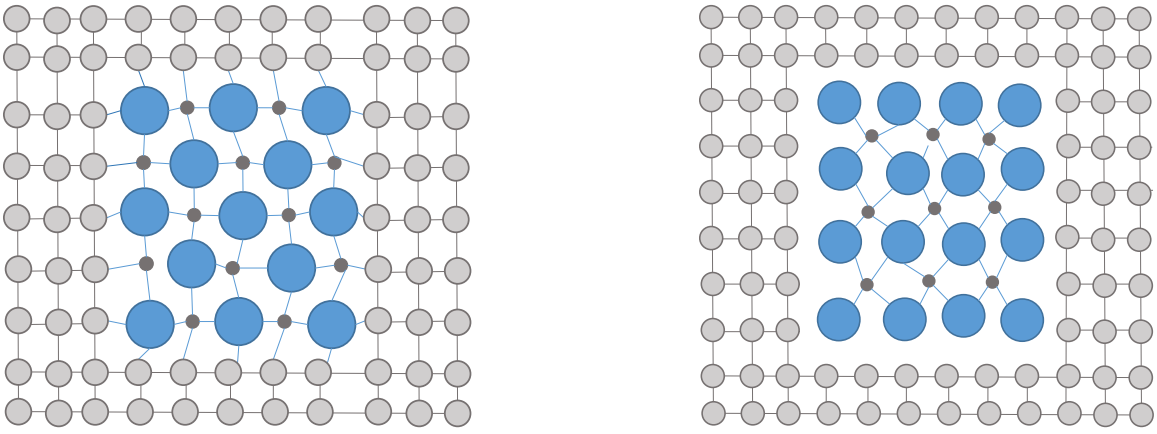

(a) (b)

Figure 5.1: (a) a coherent cluster that has a definite relationship with the crystal structure of the matrix and (b) an incoherent cluster that has no relationship with the structure of the matrix.

5.1. Elasticity Solution for Anisotropic Inhomogeneties in Anisotropic Matrices

By definition[96] a finite sub-domain in a given material is called an *inclusion* if the sub-domain and the material share the same elastic constants. In contrast, the sub-domain is referred to as an *inhomogeneity* if its elastic constants[96] are different from that of the surrounding material. Following these definitions, Ge precipitates and SiO_2 precipitates in Si crystals are both considered as anisotropic inhomogeneities embedded in anisotropic matrices. The elasticity solutions for the stress fields associated with these precipitates are discussed in the following subsections.

5.1.1. Analytical Expression for the Stress Field Associated with an Oblate Spheroidal Inhomogeneity

The analytical expression for the elastic stress inside an oblate spheroidal inhomogeneity in an anisotropic matrix can be obtained by using the theory of Lee and Johnson[68,97], which is derived under the general framework of the equivalent inclusion method[69-71,96]. Within this framework[69-71,96] a precipitate undergoes a uniform stress–free transformation strain, $\boldsymbol{\varepsilon}^T$, in the absence of a surrounding matrix. The presence of the surrounding matrix then produces a constrained strain, $\boldsymbol{\varepsilon}^C$, inside the precipitate. As a result, the precipitate and the matrix both deform and generate an elastic stress field. The elastic strain, $\boldsymbol{\varepsilon}^E$, that produces this elastic stress field satisfies

$$\boldsymbol{\varepsilon}^{\mathbf{C}} = \boldsymbol{\varepsilon}^{\mathbf{T}} + \boldsymbol{\varepsilon}^{\mathbf{E}}, \tag{5.1}$$

where $\boldsymbol{\varepsilon}^T$ is the transformation strain and $\boldsymbol{\varepsilon}^C$ is the constrained strain.

When a precipitate is an inclusion and both the inclusion and the matrix are isotropic, Eshelby[53] has shown that the transformation strain $\boldsymbol{\varepsilon}^T$ and constrained strain $\boldsymbol{\varepsilon}^C$ inside the precipitate satisfy

$$\varepsilon_{ij}^C = S_{ijkl}\varepsilon_{mn}^T, \tag{5.2}$$

where S_{ijkl} is referred to as the Eshelby tensor[68]. The above equation implies that if the transformation strain inside an inclusion is uniform then the constrained strain inside the inclusion is also uniform. Asaro and Barnett[98] later proved that eq.(5.2) is also valid for an anisotropic spheroidal inclusion embedded in an anisotropic matrix. They showed that the Eshelby tensor S_{ijmn} for a oblate spheroidal inclusion in cubic symmetric matrix may be computed according to[98]:

$$S_{ijmn} = w_{ijkl}c_{klmn}, \tag{5.3}$$

$$w_{ijkl} = \frac{abc}{8}\int_0^{2\pi} d\theta \int_0^{\pi} \frac{\sin\varphi\left(Z_i Z_l M_{jk}^{-1} + Z_j Z_l M_{lk}^{-1}\right)}{\left[\sin^2\varphi\left(a^2\cos^2\theta + b^2\sin^2\theta\right) + c^2\cos^2\varphi\right]^{\frac{2}{3}}} d\varphi, \tag{5.4}$$

$$\mathbf{Z} = \left[\sin\varphi\cos\theta, \sin\varphi\sin\theta, \cos\varphi\right], \tag{5.5}$$

$$M_{ik} = c_{ijkl}Z_j Z_l. \tag{5.6}$$

Here eqs.(5.3)-(5.6) are solved in a Cartesian coordinate system in which the coordinate axis is represented by x_1, x_2, x_3 and φ is the angle between the unit vector $\boldsymbol{Z}$ and the axis x_3. The c_{klmn} are the elastic constants of the matrix.

After the Eshelby tensor is evaluated, the next step is to extend the expression of stress for an inclusion to an inhomogeneity. To begin with, the elastic stress σ_{ij} inside an inclusion can be obtained by:

$$\sigma_{ij} = c_{ijkl}\varepsilon_{kl}^{E} = c_{ijkl}\left(\varepsilon_{kl}^{C} - \varepsilon_{kl}^{T}\right), \tag{5.7}$$

where the transformation strain ε_{kl}^{T} and constrained strain ε_{kl}^{C} satisfy eq. (5.2) and c_{klmn} are the elastic constants of the precipitate.

In the case of an inhomogeneity (denoted by *), the interior elastic stress can be calculated by the following formula that is similar to eq.(5.7):

$$\sigma_{ij}^{*} = c_{ijkl}^{*}\varepsilon_{kl}^{E*} = c_{ijkl}^{*}\left(\varepsilon_{kl}^{C*} - \varepsilon_{kl}^{T*}\right), \tag{5.8}$$

where σ_{ij}^{*} is the elastic stress , c_{ijkl}^{*} denotes the elastic constants and ε_{kl}^{T*} represents the transformation strain. However, unlike the case of inclusions, the relationship between ε_{kl}^{C*} and ε_{kl}^{T*} for an inhomogeneity is generally unknown, which makes eq.(5.8) unsolvable. To resolve this issue, the inhomogeneity is replaced by a so-called equivalent inclusion[69-71,96] that has the same elastic constants as the matrix and suffers the same constrained strain as well as elastic stress as those of the inhomogeneity such that:

$$\varepsilon_{kl}^{C} = \varepsilon_{kl}^{C*}, \tag{5.9}$$

$$\sigma_{ij} = \sigma_{ij}^{*}. \tag{5.10}$$

So

$$\sigma_{ij} = c_{ijkl}\left(\varepsilon_{kl}^{C} - \varepsilon_{kl}^{T}\right) = c_{ijkl}^{*}\left(\varepsilon_{kl}^{C} - \varepsilon_{kl}^{T*}\right), \tag{5.11}$$

where ε_{kl}^{C} is the constrained strain, σ_{ij} is the elastic stress , c_{ijkl}^{*} and c_{ijkl} are the elastic constants of the inhomogeneity and the equivalent inclusion respectively, ε_{kl}^{T*} is the transformation strain of the inhomogeneity, and ε_{kl}^{T} is the so-called equivalent transformation strain of the equivalent inclusion. Note that ε_{kl}^{T} and ε_{kl}^{C} satisfy eq.(5.2), which bypasses the difficulty of finding the relationship between ε_{kl}^{C*} and ε_{kl}^{T*}.

After eq. (5.2) is applied, eq. (5.11) contains 6 equations and 18 unknowns (6 unknown components of σ_{ij}, 6 unknown components of ε_{kl}^{T} and 6 unknown components of ε_{kl}^{T*}), which is still unsolvable. In the following cases, however, it can be shown that either the number of equations can be increased or the number of unknowns can be reduced by considering additional physics of the precipitate.

Case 1: when a precipitate is incoherent, the shear stress on the interface between the matrix and the precipitate can always be quickly eliminated by interface sliding[99] so the stress inside an incoherent precipitate is always hydrostatic[68,96,97]. Denote the unknown magnitude of this hydrostatic stress by *P*, then eq.(5.11) can be reduced to 3 equations with 4 unknowns (*P*, ε_{11}^{C}, ε_{22}^{C} and ε_{33}^{C}) as:

$$\sigma_{ij} = P\delta_{ij} = c_{ijkl}\left(\varepsilon_{kl}^{C} - \varepsilon_{kl}^{T}\right), \tag{5.12}$$

where δ_{ij} is the Kronecker delta function. To solve for σ_{ij}, Mura[96] further suggests that one more equation can be added by specifying:

$$\varepsilon_{kk}^{T} = \Theta, \tag{5.13}$$

where Θ is the dilatation of the precipitate. Finally, eq.(5.11) can be solved and the stress σ_{ij} is obtained:

$$\sigma_{ij} = P\delta_{ij} = \frac{3K\Theta\left(S_{1111} + S_{1122} - 1\right)\left(S_{3333} - 1\right) - \left(2S_{1133}S_{3311}\right)}{\left(S_{1111} + S_{1122} - 1\right) + 2\left(S_{3333} - S_{3311} - S_{3311} - 1\right)}, \tag{5.14}$$

where K is the bulk modulus of the matrix. Note that eq.(5.14) is consistent with the fact that the stress is constant inside the precipitate.

Case 2: when a precipitate is coherent, the theory of Lee and Johnson[68,97] suggests that the actual transformation strain ε_{kl}^{T*} instead of the dilatation ε_{kk}^{T} in eq.(5.11) is specified by the lattice mismatch between the matrix and precipitate such that:

$$\varepsilon_{ij}^{T*} = \Theta\delta_{ij}, \tag{5.15}$$

where δ_{ij} is the Kronecker delta function and Θ is the lattice mismatch between the matrix and the precipitate. At this point, eq.(5.11) contains 6 equations with 6 unknowns (6 unknown components of ε_{kl}^{T}) .

$$c_{ijkl}\left(\varepsilon_{kl}^{C} - \varepsilon_{kl}^{T}\right) = c_{ijkl}^{*}\left(\varepsilon_{kl}^{C} - \Theta\delta_{kl}\right) \tag{5.16}$$

Once ε_{kl}^{T} is solved, ε_{kl}^{C} can be calculated by solving eq. (5.2), and then the stress σ_{ij} can be obtained by evaluating eq. (5.11) . The complete expression for σ_{ij} , however, contains several hundred terms; see Appendix A.

The calculation of the stress field outside an anisotropic precipitate is a much more complicated task even for 2D problems[100,101]. The closed-form solution for 3D anisotropic inhomogeneities in anisotropic matrices has not been documented in the literature. Additional complexities and ambiguities are added to the problem if there exists an interphase zone[102-106] just outside the matrix/precipitate interface. The elastic constants in the interphase zone are usually different from those of the matrix or the precipitate and may not vary smoothly in the region. The detailed mechanical description of the interphase zone depends strongly on the microstructure of the system, which is outside of the perspective of continuum mechanics. Atomistic simulations, however, can provide additional insights for specific types of inhomogeneity/matrix systems.

5.1.2. Analytical Expression for the Strain Energy

The analytical expression of the elastic stain energy per unit volume of an anisotropic inhomogeneity in an anisotropic matrix is calculated as follows[69-71,96]:

$$\omega = -\frac{1}{2}\left(\varepsilon_{kl}^{C} - \varepsilon_{kl}^{T*}\right) c_{ijkl}^{*} \varepsilon_{ij}^{T*}, \tag{5.17}$$

where c_{ijkl}^{*} and ε_{kl}^{T*} denote the elastic constants of and transformation strain of the inhomogeneity respectively, and ε_{kl}^{C} denotes the constrained strain of the equivalent inclusion.

When the precipitate is incoherent, the closed form expression for ω^{incoh} is obtained by substituting eq.(5.11) and eq.(5.14) into eq.(5.17)[68,97]

$$\omega^{incoh} = -\frac{1}{2} P \delta_{ij} \varepsilon_{ij}^{T*} \left(\frac{\Delta V}{\varepsilon_{ii}^{T*}}\right)^2 = -\frac{1}{2} P \varepsilon_{ii}^{T*} \left(\frac{\Delta V}{\varepsilon_{ii}^{T*}}\right)^2 = -\frac{1}{2}\left(\Delta V\right)^2 \frac{P}{\varepsilon_{ii}^{T*}}, \tag{5.18}$$

where ΔV is the dilatation of a precipitate and ε_{ii}^{T*} is given by

$$\varepsilon_{ii}^{T*} = \frac{3K\Theta\left(S_{1111} + S_{1122} - 1\right) S_{3333} + \frac{2}{3}\left(S_{3333} - S_{1111} - S_{1122} - S_{1133} - S_{3311}\right) - 2S_{1133}S_{3311}}{\left(S_{1111} + S_{1122} - 1\right) + 2\left(S_{3333} - S_{3311} - S_{3311} - 1\right)}. \tag{5.19}$$

Rearranging eq.(5.18) by using eq.(5.19), the strain energy per unit volume (as given by eqs.(3.32)-(3.34) in Chapter 3) is obtained:

$$\omega^{incoh} = \frac{1}{2}\Delta V^2 \frac{K^* \varphi(\beta)}{K^* + \varphi(\beta)}, \tag{5.20}$$

where $\varphi(\beta)$ is a function of aspect ratio given by

$$\varphi(\beta) = \frac{K\left[(S_{1111} + S_{1122} - 1)(1 - S_{3333}) + 2S_{1133}S_{3311}\right]}{(S_{1111} + S_{1122} - 1)\left(S_{3333} - \frac{2}{3}\right) + 2(S_{3333} - S_{1133} - S_{3311} - 1)/3 - 2S_{1133}S_{3311}}, \tag{5.21}$$

and K is the bulk modulus of the matrix phase.

The strain energy per unit volume for a coherent precipitate, ω^{coh}, is also a function of aspect ratio β and can be obtained in a similar manner as shown above by substituting and into eq,(5.17). The lengthy expression for ω^{coh} is presented in Appendix B. Note that ω^{coh} decreases as β decreases and vanishes when β approaches zero[68,97]. While ω^{coh} also depends on the aspect ratio, the differences are: (1) when the precipitate is softer than the matrix, decreases as aspect ratio decreases; when the precipitate is harder than the matrix, increases as aspect ratio decreases and (2) only a limited amount of reduction in can be achieved as the aspect ratio varies [97,107].

5.2. Atomistic Measurement of the Elastic State of Oblate Spheroidal Precipitates in a Silicon Matrix

In this section, the stress field and strain energy associated with oblate spheroidal precipitates are measured using atomistic simulations in LAMMPS[108]. The simulation results are compared with the analytical solutions described in the previous section. A Tersoff-based empirical potential[33-38] is used for describing the properties of Si[35,36], Ge[33] and O[34,37,38].

5.2.1. Atomic-Level Study of Germanium (Ge) Precipitates

(1). *Simulation Procedure*

A perfect Si lattice with 941,192 Si atoms is replicated in 9 identical 26.17 nm × 26.17 nm × 26.17 nm cubic simulation boxes. At the center of each box a spheroidal region that contains the same number of Si atoms (19,030 atoms) but with a distinct aspect ratio (β) is defined. On the surfaces of the simulation box, periodic boundary conditions are applied and no applied forces are imposed. Next, all of the Si atoms in the spheroidal region are replaced by Ge atoms and consequently a coherent Ge precipitate in the Si lattice is created. The lattice parameters of the undeformed Si and Ge are initially both equal to the values obtained at zero temperature. Due to the fact that the lattice constant of Ge is about 4.2% larger than that of Si, the precipitate is under a large compressive stress, which makes the system energetically unfavorable. To release the stress, molecular statics (conjugate gradient energy minimization) is performed within the LAMMPS simulation package[108] with a convergence criterion that the energy change between two minimization steps be less than 1×10^{-12} eV. The final configurations are shown in Figure 5.2.

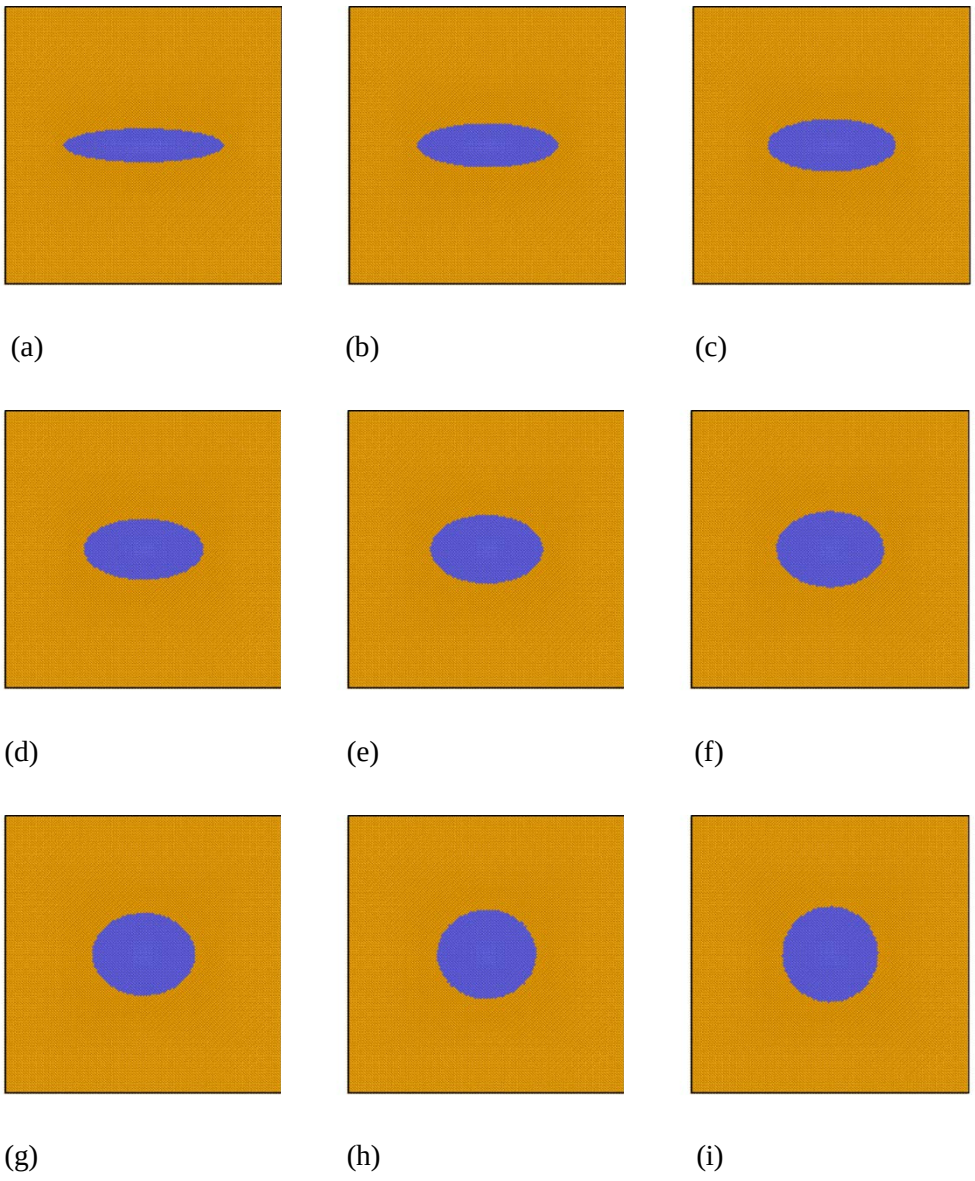

Figure 5.2: Final configurations of Ge precipitate (blue) in crystalline Si matrix (orange) for: (a) $\beta = 0.2$, (b) $\beta = 0.3$, (c) $\beta = 0.4$, (d) $\beta = 0.5$, (e) $\beta = 0.6$, (f) $\beta = 0.7$, (g) $\beta = 0.8$, (h) $\beta = 0.9$ and (i) $\beta = 1.0$.

(2) *Stress Measurement*

According to Thompson et al.[109] and Zimmerman et al.[110], the elastic stress can be calculated by averaging the per-atom virial stress over a well-defined sub-volume of material. The calculation procedure is as follows. First, the system is divided into spheroidal shells (with 500 atoms in each shell) extending outwards from the center of the precipitate. As shown schematically in Figure 5.3, the shells are labeled by index i , where smaller i means the shell is closer to the center of the precipitate. Next, in each shell i, the Voronoi volume, V_{Voro}^{j}, for each atom *j* is computed by using the Voro++ package[111] and summed. The virial stress for each atom, $\phi^{i,j}$, obtained from LAMMPS, is also summed. The average elastic stress in shell *i* is then computed as:

$$\overline{\sigma_{kk}^{i}} = \frac{1}{\sum_{j}(V_{Voro}^{j})}\sum_{j}(\phi_{kk}^{i,j}) . \tag{5.22}$$

The hydrostatic pressure within each shell i then can be calculated according to:

$$p^{i} = \frac{\overline{\sigma_{11}^{i}} + \overline{\sigma_{22}^{i}} + \overline{\sigma_{33}^{i}}}{3} . \tag{5.23}$$

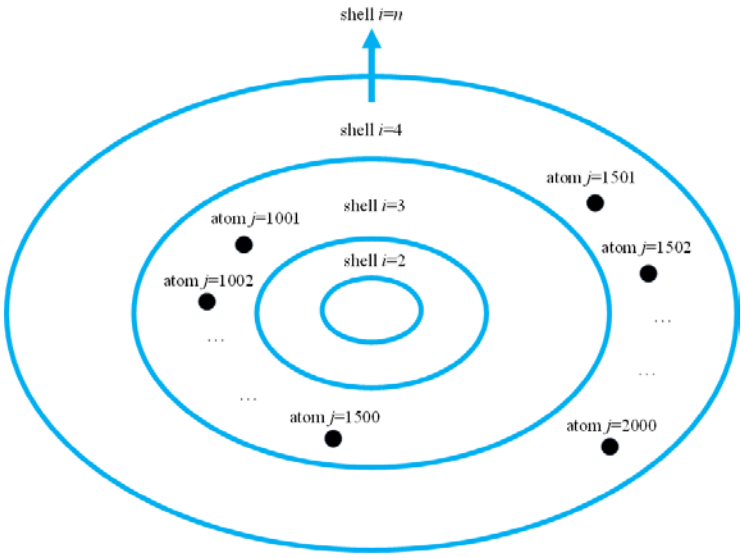

Figure 5.3: Schematic of the shells (labeled by *i*) and atoms (labeled by *j*) in the system. Some atoms are omitted (represented by "…") in the figure for clarity.

(3) *Elastic Constants*

It is convenient to write the stiffness tensor, c_{ijkl}, in eq.(5.11) in Voigt notation $C_{\alpha\beta}$. For cubic symmetric materials such as Si and Ge, the only non-zero components of $C_{\alpha\beta}$ are C_{11}, C_{12} and C_{44}. In order to compare the analytical solution with the simulation predictions in a self-consistent way, C_{11}, C_{12} and C_{44} used in the analytical expressions are specified based on the calculation performed by Kelires et al.[112] using the Tersoff potential[33]. In Table 5.1, both the calculated data[112] and the experimental data[82,113] of C_{11}, C_{12} and C_{44} for Si[82] and Ge[113] are provided.

Data Source	(GPa)	(GPa)	(GPa)
Si (Experiment)[82]	165.7	63.9	79.6
Si (Kelires)[112]	150.0	80.0	70.0
Ge (Experiment)[92]	129.0	48.0	67.0
Ge (Kelires)[93]	137.0	45.0	67.3

Table 5.1: Calculated data[112] and experimental data[82,92] of elastic constants for Si and Ge.

(4) *Pressure Profile*

The elasticity solution of the hydrostatic pressure for the embedded Ge-Si matrix system is obtained by substituting the Kelires[112] parameters from Table 5.1 into eq.(5.11). The stress field associated with each precipitate displayed in Figure 5.2 is first investigated separately. For the convenience of discussion, we define a parameter, *r*, as the distance measured from the center of the spheroid to the outer surface of the spheroidal shell and choose the direction of *r* such that it is aligned with the semi-major axis of the spheroid.

As shown below in Figure 5.4, the hydrostatic pressures as a function of *r* obtained from the simulation and analytical solution are plotted against each other. First, it is observed that the value of the simulated hydrostatic pressure is negative inside the precipitate, which is consistent with the fact that the lattice parameter of Ge is about 4.2% larger than that of Si. Secondly, the simulation reproduces the key prediction made by the elasticity theory, that is, a uniform transformation strain inside a precipitate leads to a uniform constrained strain (and stress) inside the precipitate. This is made possible by using a large enough number of atoms in the simulation system so that the precipitate can be considered as a continuum entity and the transformation strain of the precipitate can be considered as a constant. Thirdly, the simulation is in line with elasticity

theory that predicts that the hydrostatic pressure would decay rapidly outside the precipitate and become essentially zero in the region that is far away from the Ge-Si interface. Here it is assumed that the stress field just outside an isotropic inhomogeneity in an isotropic matrix[56-58,96,114] is qualitatively the same as the one for an anisotropic inhomogeneity in an anisotropic matrix. Note that for aspect ratios, β, below 0.2, very large simulation cells are required to fully contain the elastic field. Therefore the aspect ratios considered in this work were limited to be above 0.2.

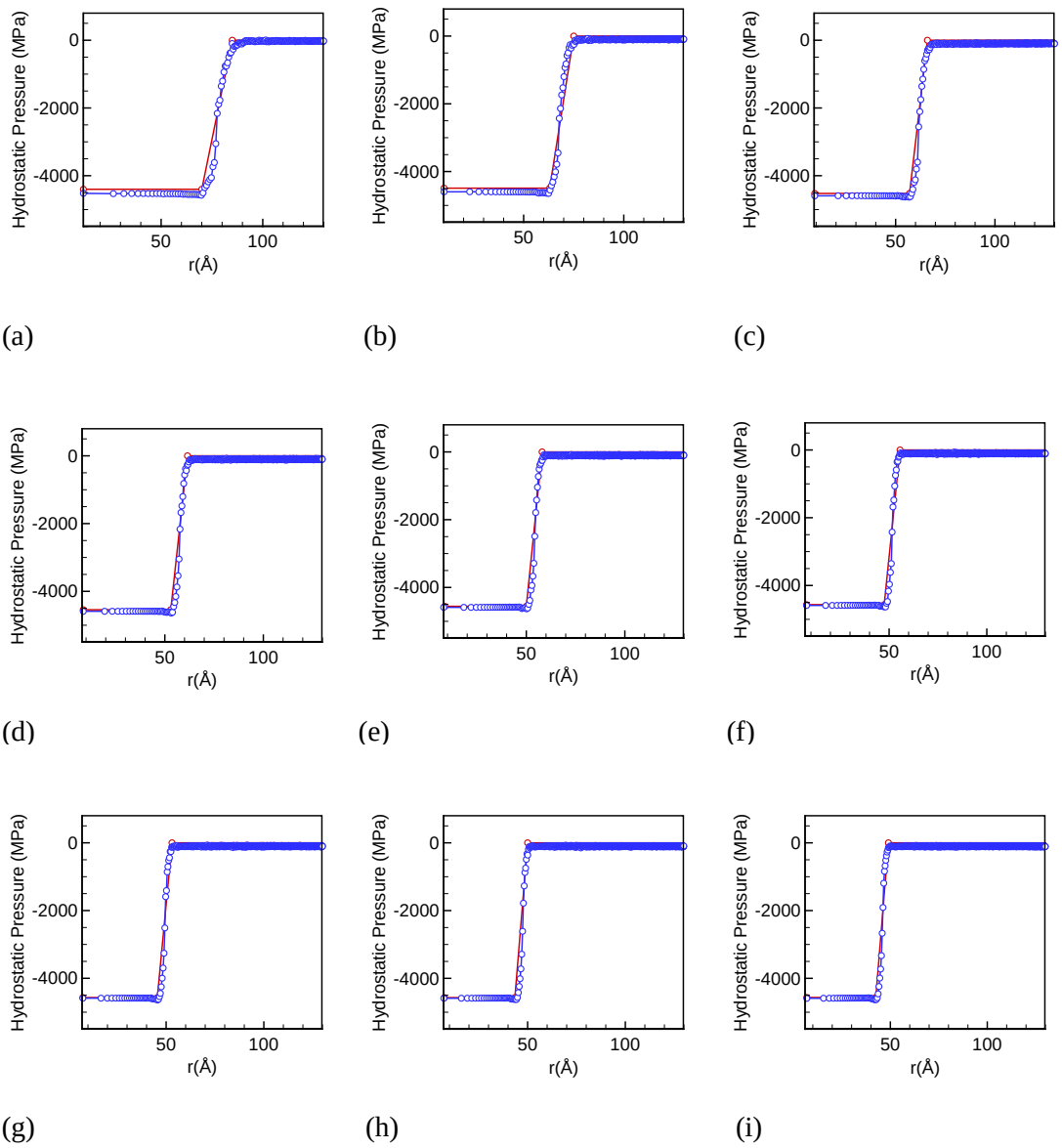

Figure 5.4: Hydrostatic pressure as a function of the distance from the precipitate center. Blue lines-atomistic simulation and red lines-continuum mechanics theory for (a) $\beta = 0.2$, (b) $\beta = 0.3$, (c) $\beta = 0.4$, (d) $\beta = 0.5$, (e) $\beta = 0.6$, (f) $\beta = 0.7$, (g) $\beta = 0.8$, (h) $\beta = 0.9$ and (i) $\beta = 1.0$.

(5) *Elastic State of the Precipitate as a Function of Shape*

The dependence of the interior hydrostatic pressure and the strain energy associated with a Ge precipitate on the precipitate shapes are studied in this subsection. In the range of $0.2 \le \beta \le 1.0$ both the atomistic simulation and the elasticity model predict that there is only a very limited reduction in stress as β decreases. The magnitude of hydrostatic pressure inside the precipitate stays constant at about 4500 MPa. When is β below 0.2, analytical elasticity theory predicts that the shape will start to have larger impact on the stresses, but as mentioned above computational limitations make further investigation of this parameter range difficult. For $0.2 \le \beta \le 1.0$, however, the consistency between the simulation and analytical solution supports the conclusions discussed by Nabarro[115], Christian[106] and Mura[96]: in the absence of other stress relaxation mechanisms such as interstitial emission at the matrix/precipitate interface, the only effective way to release the stress of a coherent precipitate is to first distort the precipitate at the matrix/precipitate interface so that it "breaks away" from the matrix and becomes incoherent, allowing the precipitate to freely deform to a flat plate so that the displacement and traction associated with the precipitate becomes very small, which will then lead to low stresses and low strain energies[96]. In another words, the coherency between the precipitate and the matrix can inhibit stress relaxation. According to Christian[106], the "break away" requires a high enough temperature such that the atoms can move rapidly to reajust their positions or recrystalize at the matrix/precipitate interface. As mentioned above, both the undeformed Ge and Si were initially created at zero temperature. Thus during the energy minimization process, the "break away" is very unlikely to happen. In addition, the low temperature results in very low interstitial emission probability to create space for expansion at the preipitate/matrix interface. As a result, the stresses in the system are not released effetively even after the coherent Ge preciptate is changed to a plate.

Second, as discovered by Lee and Johnson[97], the strain energy of a coherent precipitate softer than the matrix can only decreae by a small amount as the precipitate evolves from a sphere

to a plate. Although Lee and Johnson[97] did not discuss much about the physics behind their results, the following order-of-magnitude estimation that links the pressure and the strain energy may provide more insights. From eq.(5.17) and Appendix B, it can be shown that the strain energy $\omega^{coh}(\beta)$ for a coherent precipitate satisfies:

$$\omega^{coh}(\beta) \sim p^{*}(\beta)\varepsilon^{T*}, \tag{5.24}$$

where the transformation strain ε^{T*} is a constant (lattice misfit) and the hydrostatic pressure p^{*} is a function of aspect ratio β. Consequently, when a coherent precipitate has very limited capabilities to release its stress (pressure) by changing its shape, only a limited reduction in strain energy can be achieved as the precipitate changes its shape. From Table 5.1, the data shows that the elastic constants of Ge are indeed smaller than those of Si. Therefore the findings of Lee and Johnson[97] mentioned above are observed in our system, as expected.

Next, quantitative measures of the strain energy are used to verify the above qualitative discussion. Note that unlike the stress profile that can be obtained directly in LAMMPS, the simulated strain energy needs to be extracted as follows because LAMMPS can only generate the total energy of the system. First, we calculate the formation energy (E^{f}) of the precipitate:

$$E^{f}(\beta) = E_{sys} - N_{Si}E_{Si}^{Pure} - N_{Ge}E_{Ge}^{Pure}, \tag{5.25}$$

where E_{sys} is the energy of the overall simulation system that contains the Ge precipitate, and N_{Si} and N_{Ge} represent the number of Si atoms and Ge atoms in the overall system, respectively. The

energies, E_{Si}^{Pure} and E_{Ge}^{Pure} are, respectively the per-atom energy of Si atoms (-4.63 eV/atom) in the pure Si crystal and per-atom energy of Ge atoms (-3.85 eV/atom) in the pure Ge crystal.

According to classical nucleation theory[107,116,117], the precipitate formation energy can be written in the following form:

$$E^f(\beta) = A\sigma_O + V\omega, \tag{5.26}$$

and

$$\omega = \left(E^f(\beta) - A\sigma_O\right)/V \tag{5.27}$$

where A and V are the surface area and volume of the precipitate, respectively, σ_O and ω are the surface energy per unit area and the strain energy per unit volume, respectively.

To compute A and V of the deformed precipitate, the elastic strain of the precipitate must be obtained first. We assume that the actual strain of the precipitate in the simulation system is the same as the analytical solution calculated from eq.(5.16) and Appendix A, and also assume that σ_O is independent of the aspect ratio, β. The strain energy of the precipitate from the simulation as a function of aspect ratio is computed using σ_O =1.11 meV/ (0.017 J/m^2), as calculated by Beck et al.[118]. As expected, the value of ω based on the simulation results is almost a constant at about 1.83×10^3 eV/ (2.93×10^3 J/m^3), the relative deviation with respect to the analytical solution is below 5%. In addition to the uncertainties in σ_O, the difference between the simulation and analytical solution may come from the fact the precipitates created in the simulation are not perfect spheroids, thus: (1) the surface area or volume may not evolve smoothly as the aspect ratio changes and (2) the actual strain/stress in the simulation system may not be exactly the same as the ones obtain by

the continuum mechanics theory, in which a perfect shape and misfit is imposed. Nevertheless, the general good agreement between the simulation and continuum mechanics model verifies that a coherent precipitate will not release its strain energy effectively by changing its shape as discussed above.

5.2.2. Atomistic-Level Study of Amorphous SiO_2 Precipitate

Although in general the analytical expressions for the stress and strain energy associated with an incoherent precipitate are relatively simpler compared to those for a coherent precipitate, the disordered nature of an incoherent amorphous SiO_2 precipitate creates a few obstacles for atomistic simulation studies. Most significantly, unlike the case for a coherent crystalline Ge precipitate that can be easily created by replacing lattice Si atoms, an amorphous SiO_2 precipitate has to be created separately by a separate process, inserted to the Si matrix, and then relaxed because the positions of its atoms cannot be predetermined in the matrix. In addition, a crystalline Ge precipitate always evolves from an initial configuration that has a well-defined matrix/precipitate interface while the amorphous SiO_2 precipitate always evolves from a disordered configuration that corresponds to a distorted matrix/precipitate interface, which makes the stress relaxation process for the SiO_2 precipitate more complex. As a result, it is generally challenging to optimize the SiO_2 precipitate-matrix interface and generate a realistic configuration. A detailed description of the simulation used to relax amorphous SiO_2 precipitates in bulk crystalline Si is presented below.

(1) *Simulation Procedure*

As mentioned in Section 5.1.1, one important feature of an incoherent precipitate is that its stress is always hydrostatic[68,96,97]. Also a pure dilatational transformation strain is usually assumed in the literature[69-71,96]. Therefore, in our atomistic simulation system we create a SiO_2 precipitate in Si matrix such that the transformation strain and the compressive stress applied to the precipitate are purely dilatational. We have chosen the value of the transformation strain to be 1.5% so that the materials in our system can exhibit linear elasticity behaviors. The specific steps for constructing the Si-SiO_2 simulation system are discussed in the following.

The first step is to create an amorphous SiO_2 precipitate using the approach described in details by Chuang et al.[34] As shown schematically in Figure 5.5, a bulk (periodic) amorphous SiO_2 phase is created by cooling a melted 5.82 nm × 5.82 nm × 5.82 nm bulk β-cristobalite SiO_2 from 5000K to 0K at a rate of 1×10^{12} K/s. Then, a spherical precipitate is cut out of the bulk SiO_2. In order to create a SiO_2 precipitate that undergoes a 1.5% transformation strain in Si matrix, we need to create a spherical hole with R_{Si} = 20 Å in a cubic pure Si simulation box, and insert a SiO_2 precipitate of which radius is 1.5% larger (R_{SiO_2} = 20.3 Å) than R_{Si} . The SiO_2 precipitate tends to relax and return to its original size in the hole and consequently the Si matrix will produce a compressive stress on the precipitate. Continuum mechanics theory predicts that the radius of the precipitate will be compressed from R_{SiO_2} = 20.3 Å to R_{SiO_2} = 20.1 Å .

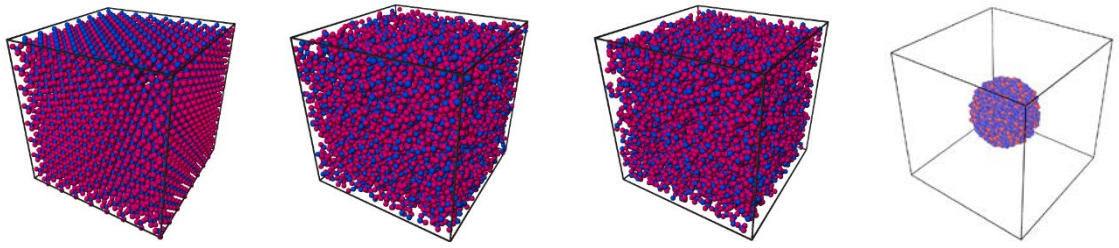

(a) (b) (c) (d)

Figure 5.5: Schematic of the brief procedures to create an amorphous SiO_2 precipitate (a) build a β-cristobalite SiO_2 lattice (b) melt the β-cristobalite SiO_2 at 5000K (c) quench the bulk SiO_2 to 0K and (d) cut a spherical precipitate out of the bulk SiO_2.

To properly insert the SiO_2 precipitate to the hole, the radius of the precipitate needs to be compressed to be $R_{SiO_2} = R_{Si} - \Delta R$ so that a small gap of ΔR [34,51] is formed initially between the SiO_2 phase and the Si phase, in order to avoid the unphysical situation in which the positions of

two atoms are overlapping or nearly overlapping at the matrix/precipitate interface. After the initial configuration is set up, a molecular statics simulation (using the Hessian-free truncated Newton algorithm) is performed in LAMMPS[108] to minimize the energy with a convergence criterion that the energy change between two minimization steps be less than 1×10^{-14} eV. During the simulation, periodic boundary conditions are applied and no applied forces are imposed on the box.

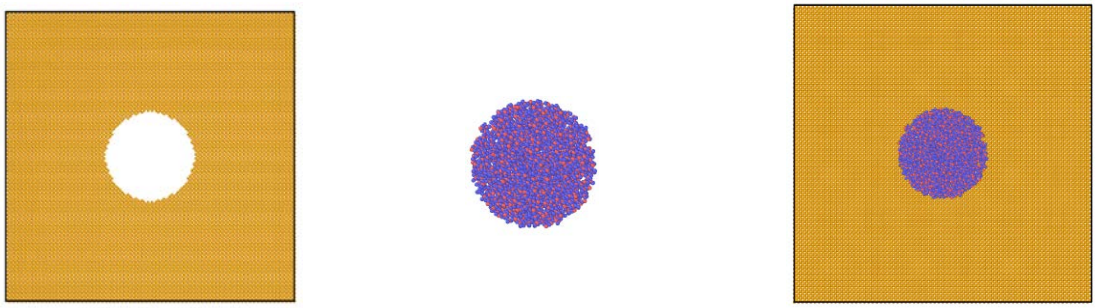

(a) (b) (c)

Figure 5.6: Schematics of (a) an unstrained hole in a Si box, (b) an unstrained precipitate, (c) a compressed precipitate inserted to the hole.

(4) *Pressure Profile*

In this section the hydrostatic pressure as a function of r (where r is defined as the distance measured from the center of the precipitate) are studied. To present the results, the system is divided into spheroidal shells (with 500 atoms in each shell unless otherwise noted) extending outward from the center of the precipitate and the average pressure of atoms in each cell is plotted.

Since there is no external force applied on the simulation box, based on continuum mechanics theory[69-71,96], the pressure far away from the precipitate should decay to a value near zero. The size of the simulation box should be large enough so that the boundary of the system will not "feel" the precipitate. As a result, a convergence study on the simulation box size (L_{box}) is first performed. The same SiO_2 precipitate (containing 783 Si atoms and 1575 O atoms) is

placed in three different sizes of the Si boxes respectively: box (a) 8.15 nm × 8.15 nm × 8.15 nm (contains 27666 atoms in total), box (b) 9.77 nm × 9.77 nm × 9.77 nm (contains 47305 atoms in total) and box (c) 11.95 nm × 11.95 nm × 11.95 nm (contains 85836 atoms in total), then the pressure profiles are plotted in Figure 5.7. As shown on the plot, the three pressure profiles appear to be qualitatively the same, yet it is clear in box (a) the boundary can still "feel" the precipitate. To eliminate the boundary effect, L_{box} needs to be increased to 11.95 nm. Therefore, box (c) is selected for further studies.

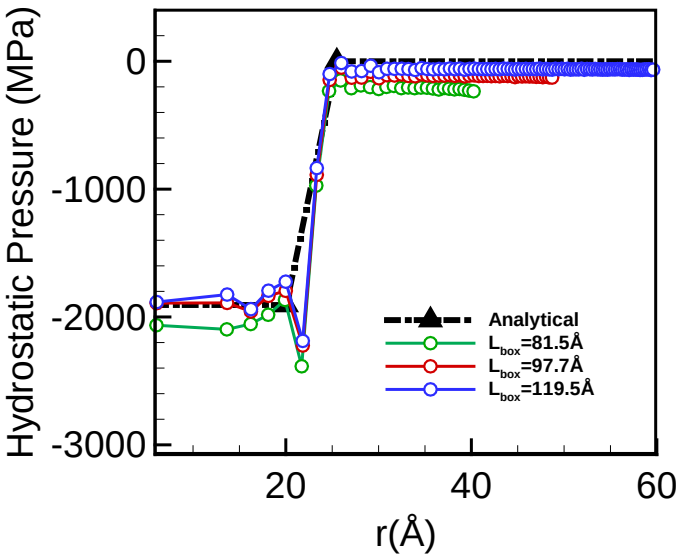

Figure 5.7: Hydrostatic pressure as a function of the distance from the precipitate center. Analytical solution-black line and simulation results from box (a)-green line, from box (b)-red lines and from box (c)-blue line.

From Figure 5.7, we can also observe that, in contrast to the smooth pressure profile within a crystalline Ge precipitate, the pressure profile within an amorphous SiO_2 precipitate exhibits more fluctuations. To reduce statistical uncertainty and to analyze the trend behind these

fluctuations, the simulations were repeated with SiO_2 precipitates cut from 4 different locations of the bulk SiO_2 and the pressures averaged over the 5 configurations are studied below.

First the system is divided into spheroidal shells with 1000 atoms and the average pressure of atoms in each shell is calculated as presented in Figure 5.8 (1)-(5). Next these pressures are averaged over the 5 configurations and it can be seen from Figure 5.8 (6), the fluctuations observed in Figure 5.7 are reduced and the agreement improves with respect to the analytical solution.

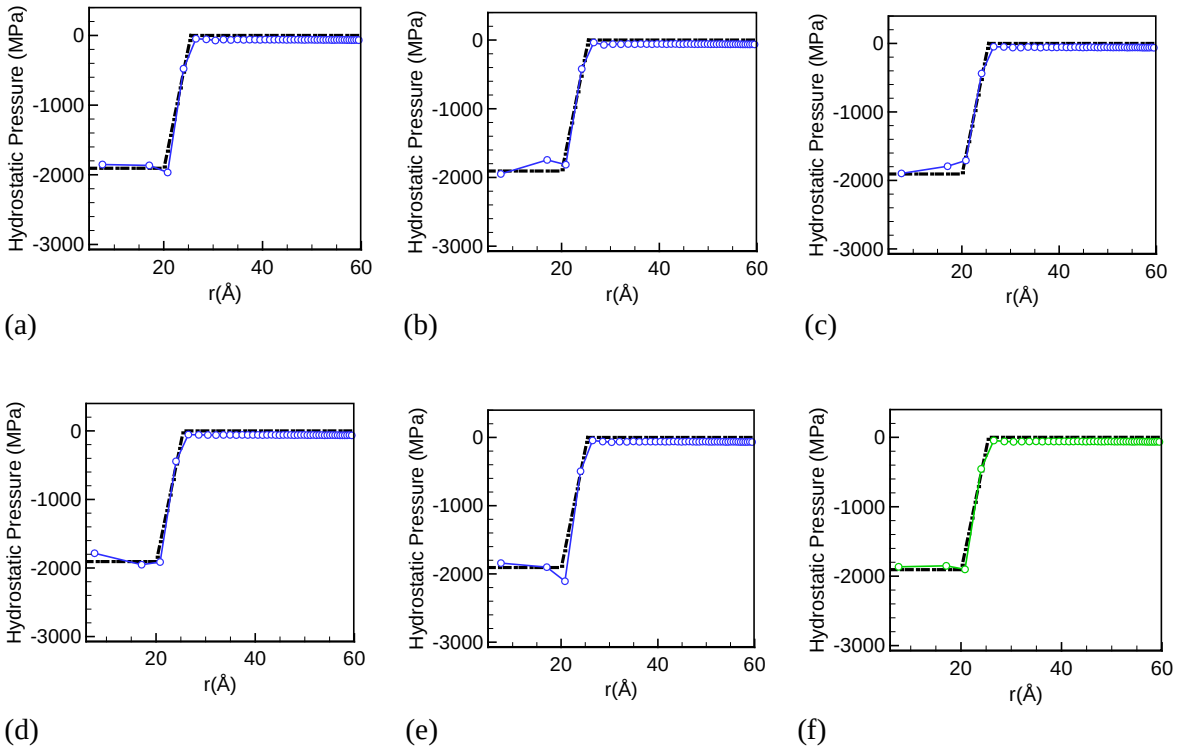

Figure 5.8: Hydrostatic pressure as a function of the distance from the precipitate center. Here (a), (b), (c), (d) and (e) represent the pressure profiles for 5 different SiO_2 configurations while (f) represents the pressure profile averaged over the 5 configurations. Black lines-continuum mechanics theory, blue lines-atomistic simulation results for 5 different SiO_2 configurations and green line-averaged pressure.

Another notable feature in Figure 5.8(f) is that within the region of one lattice parameter (5.432Å) away from the matrix/precipitate interface ($15\text{Å}<r<20\text{Å}$), a jump can be found in the pressure profile. This 'jump' can be seen more clearly in Figure 5.9 in which smaller shells containing only 500 atoms were used to discretize the system. In fact, on top of the statistical fluctuations, an observable jump in the pressure profile is expected when the difference in elastic constants of the precipitate and the matrix becomes large enough. Sometimes this behavior can even be observed near a more structured interface between a coherent isotropic crystalline precipitate and an isotropic crystalline matrix[119]. From a continuum perspective, the jump arises naturally due to the fact that (1) the Eshelby tensor as a function of position, $\bar{\mathbf{r}}$, is discontinuous[96] over the matrix/precipitate interface, and (2) the Eshelby tensor just outside the interface (the so-called exterior-point Eshelby tensor) will not be converged[114,120] to the Eshelby tensor just inside the interface (the so-called interior-point Eshelby tensor), when the position, $\bar{\mathbf{r}}$, moves onto the interface as a limiting case. From a microscopic perspective, it is understandable that whenever two different types of materials, A and B, are joined together by force, a difference in the atomic bonding will be created across the A/B interface. The changes in both interatomic distances as well as configurations will result in the stress per atom near the interface being larger[107] than that in the interior of material A or B. Thus, a jump in the stress that is localized in the vicinity[107] of the interface occurs. In principle, this localized stress can be reduced by a continuous readjustment of atoms position, i.e., the interfacial relaxation near the precipitate boundary. Part of the jump shown in Figure 5.9 might also be reduced by more effective interfacial relaxation during the simulation. In this regard, a thermal anneal might be helpful to facilitate relaxation that may smooth the stress profile.

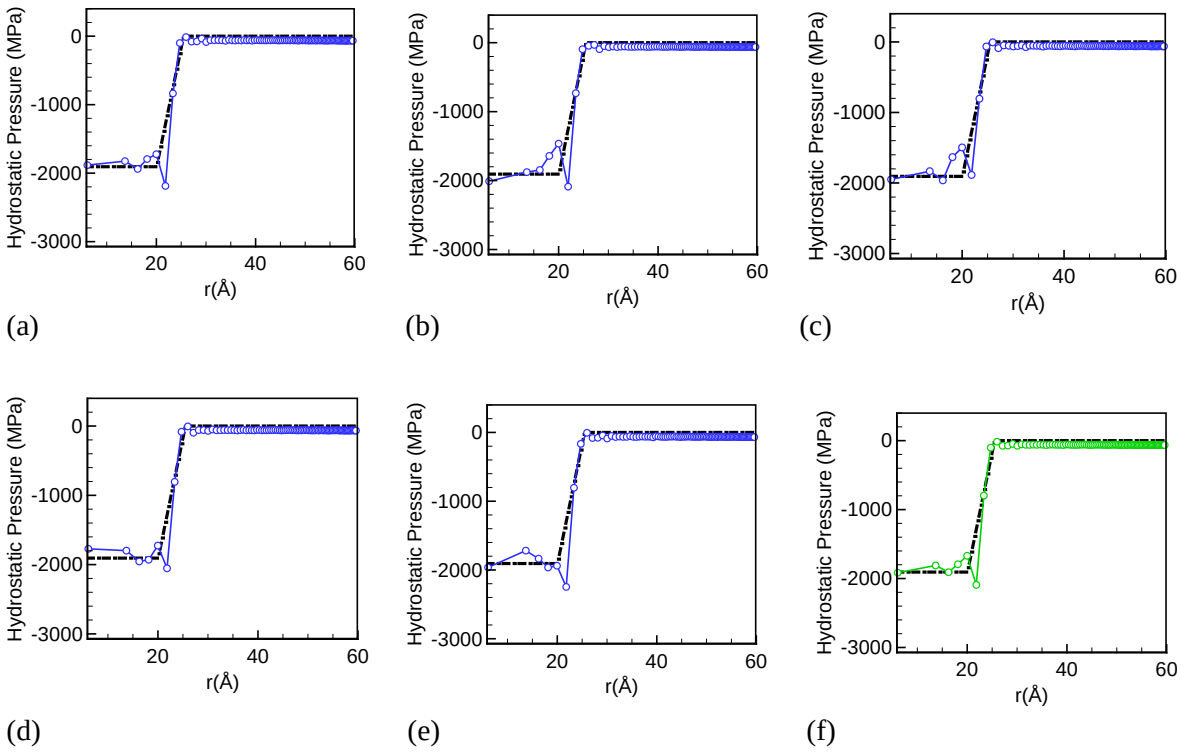

Figure 5.9: Hydrostatic pressure as a function of the distance from the precipitate center. Here (a), (b), (c), (d) and (e) represent the pressure profiles for 5 different SiO_2 configurations while (f) represents the pressure profile averaged over the 5 configurations. Black lines-continuum mechanics theory, blue lines-atomistic simulation results for 5 different SiO_2 configurations and green line-averaged pressure.

In addition to the factors mentioned above, there are some other uncertainties that can also result in the discrepancy between the simulation result and the analytical solution, they are: (1) the configuration in the simulation is not a perfect sphere, in particular, the matrix/precipitate interface is not a smooth spherical surface (2) due to the relative small size (less than 4 nm in diameter) of the precipitate, the applicability of the strict assumptions of elastically homogenous material (made in the elasticity theory) to the amorphous SiO_2 precipitate may not be valid. As a result, possible future studies should consider larger SiO_2 precipitates in larger simulation boxes so that the

elasticity property of the system can be more in line with the continuum mechanics theory assumptions. Also cycles of different alternating high-low thermal anneals may be applied to the system to allow the matrix/precipitate to fully relax.

6. Summary and Outlook

Robust quantitative prediction of oxide precipitation in crystalline silicon poses multiple challenges. From a physics point of view, the major complexities associated with oxide precipitation arises from the fact that the precipitation process generates high internal (compressive) stresses that must be released. Well-documented stress relief mechanisms associated with oxygen precipitation include interaction with intrinsic point defects present in the surrounding crystal matrix, i.e., vacancy absorption as discussed above[15] and/or the equivalent process of self-interstitial emission[23], and morphological evolution in which the equilibrium precipitate shape evolves to reduce the strain energy. The morphological evolution accounts for the fact that larger oxide precipitates observed experimentally usually come in various morphologies (e.g., needles, plates, and polyhedrons) that appear to depend strongly on processing conditions.

In this thesis, a continuum rate equation modeling framework was developed and implemented in our Comprehensive Aggregation Simulator for Silicon Processing (CASSP) code to simulate coupled oxide precipitation and vacancy aggregation in silicon crystals. The model accounts for: (1) diffusion-limited mass transport of point defects and oxygen to simulate precipitate aggregation and dissolution, (2) stress relaxation via matrix vacancy absorption and (3) variable oblate spheroid precipitate morphology. These phenomena collectively require the specification of multiple, difficult-to-measure parameters. Some of these parameters, such as the oxide precipitate-silicon matrix interface energy (which is the principal regression parameter of the overall modeling framework described in this thesis), are intrinsically multiscale in nature and outstanding ambiguities remain in their characterization.

From a numerical method point of view, the major mathematical task associated with the model during a computer simulation is to solve a large system of highly non-linear, coupled, time-dependent partial differential equations (PDEs) to determine the concentrations of point defects and clusters at various positions and times. As a result, several innovative algorithms were designed

and implemented to bypass the difficulties. First, in order to specify the growth and dissolution rates of oxide precipitates in the system of PDEs, the most energetically favorable morphologies and extent of vacancy absorption of oxide precipitates needs to be determined by performing 2D global optimizations of intricate free energy functions at each simulation step. We have identified that the speed and robustness of the global optimization are the key factors that determine the efficiency and convergence property of the model. Consequently we designed a numerical scheme such that the optimizations are collectively performed once before the simulation (instead of at each simulation step). The optimal parameters for specifying the morphology and vacancy absorption are pre-calculated and tabulated as function of processing conditions. Second, the strong coupling of oxide precipitate evolution and vacancies for stress relaxation produces substantial numerical instabilities, especially when oxide formation became significant relative to the vacancy concentration, leading to ill-conditioned systems of equations. To ensure stability, we have extended the partially explicit operator-splitting[73] scheme (in which the point defect and cluster equations are integrated separately and sequentially) to a semi-implicit time integration scheme. In our new approach the point defects and cluster equations are now both embedded within a single iterative solution method, upon convergence, the scheme becomes essentially fully implicit with respect to both point defects and cluster concentrations.

Using the simulation methodology described above, validated by a large database of oxide precipitate measurements, we studied the physics of oxide precipitation in detail and shed light on several features that are commonly observed in wafer thermal annealing processes although not entirely understood. First, and perhaps most significantly, we found that oxide precipitation during a rapid thermal annealing (RTA) process is largely governed by a complex interplay between the dynamics of the precipitate size distribution and the precipitate critical size. Both of these quantities are in turn complex functions of a number of physical parameters and point defect distributions. In particular, we have found that the anomalously high sensitivity of the final oxide precipitate density with respect to RTA temperatures is created by a subtle dependence of the initial size distribution

on the initial vacancy concentrations. At the early stage of a wafer anneal with higher RTA temperature, more vacancies and a higher vacancy supersaturation are generated. As a result, the nucleation barriers (and in particular the strain energy contribution) and critical sizes for small nuclei are reduced significantly. Consequently, compared to an anneal with lower RTA temperature, a larger number of stable precipitates can grow. The difference in the initial size distributions for different anneals is then magnified by the subsequent nucleation and growth anneal. As a result, a big divergence in the final oxide densities is found for relatively small differences in the initial RTA temperature.

We have also found that the strong nonlinear dependence of the final oxide precipitate density on nucleation anneal duration is mainly established during the temperature ramp-up process right after the 'nucleation step' of the anneal. It was observed that when the temperature is increased, the critical size increases rapidly and 'sweeps through' the size distribution, causing a substantial dissolution of already-formed oxide precipitates. This dissolution is a nonlinear function of the nucleation anneal duration—at the end of longer nucleation anneals, a greater number of larger (and more stable) precipitates, which can survive the subsequent dissolution during the ramp-up phase, are formed. Therefore a higher final precipitate density is produced during longer nucleation steps.

Finally, we have found that the inverse dependence of final oxide precipitate density on nucleation anneal temperature is created by a subtle relationship between the nucleation rate and the vacancy absorption rate of oxide precipitates. Indeed, a higher temperature during the nucleation anneal generally leads to a faster nucleation of the oxide precipitate and intuitively should also lead to a higher final density. Yet to keep up with this high nucleation rate, vacancies are also consumed more rapidly (to reduce the nucleation barrier) at the early stage leaving fewer vacancies for the remainder of the process. Consequently, the oxide precipitation is counter-intuitively suppressed at the later stages of the anneal. By contrast, a lower temperature during the nucleation anneal leads a lower nucleation rate but steadier vacancy consumption rate, the oxide

precipitates are therefore able to grow continuously and eventually a higher final density is generated.

These findings collectively explain many of the well-known, yet difficult to predict, features of oxide precipitation during rapid thermal annealing processes. We believe that the modeling framework developed in this thesis is sufficiently predictive to be useful in the design and optimization of rapid thermal annealing processes. Yet, as always, there is room for further developments and improvements. Some possible future studies regarding the continuum modeling of oxide precipitation are briefly described here:

1. In the present study, only those stress relaxation mechanisms that are compositionally conservative were considered in the continuum model and only SiO_2 was considered as the precipitate composition. Several experimental studies[121-126] suggest that the composition of oxide precipitates may take the form of SiO_x, where x can vary from 1 to 2. The still-ongoing debate of this large variation in the precipitate composition suggests it may be worthwhile to study the oxide precipitation by considering a free energy description of oxide precipitates that includes the compositional relaxation mechanism proposed by Vanhellemont et al.[25,32] and investigate its influence on the agreement between the model predictions and experimental data.

2. While the parametric regressions performed to date have been quite successful, assumptions of specific forms of the surface energy function impose unnecessary structure onto the regressed function. A surface energy function based on a more general form, such as a B-spline function (discussed in more detail in Appendix C), with a controllable number of degrees-of-freedom may be used in the future to provide a maximally flexible regression model with as few parameters as possible.

3. Although only the vacancy emission process was considered in this thesis, there are situations in which self-interstitial emission may be preferable. Although, it is often the case that self-interstitial emission and vacancy adsorption can be treated as interchangeable processes through the reversible processes of point defect recombination and Frenkel pair formation, more

generalized models that include both point defect-mediated relaxation processes could provide additional model fidelity.

4. The oblate spheroid geometry assumed in this thesis does not capture the needle-like precipitate shapes observed under some conditions. Additional morphological flexibility may be incorporated into future models to capture a wider range of annealing conditions.

Appendix A

The expression of the elastic stress (σ_{ij}) for a coherent anisotropic inhomogeneity (without shear stress) in an anisotropic matrix is given below. In the expression, ε denotes the lattice mismatch between the inhomogeneity and the matrix, S_{ijkl} represents the Eshelby tensor and C_{ij}^{*} and C_{ij} denote the elastic constants of the inhomogeneity and matrix in Voigt notation respectively.

σ_{11} = -(ε×(C11* + 2×C12*)×(3×C11×C12² + C11³×S1111 + 2×C12³×S1111 + C11³×S2222 + 2×C12³×S2222 + C11³×S3333 + 2×C12³×S3333 - C11³ - 2×C12³ - 3×C11×C12²×S1111 + 2×C12²×C11*×S1111 - 2×C12²×C12*×S1111 + C11²×C11*×S1122 - C11²×C12*×S1122 + C11²×C11*×S1133 - C11²×C12*×S1133 - 3×C11×C12²×S2222 - C12²×C11*×S2211 + C12²×C12*×S2211 - C11²×C11*×S2222 + C11²×C12*×S2222 + C12²×C11*×S2222 - C12²×C12*×S2222 - C12²×C11*×S2233 + C12²×C12*×S2233 - 3×C11×C12²×S3333 - C12²×C11*×S3311 + C12²×C12*×S3311 - C12²×C11*×S3322 + C12²×C12*×S3322 - C11²×C11*×S3333 + C11²×C12*×S3333 + C12²×C11*×S3333 - C12²×C12*×S3333 - C11³×S1111×S2222 + C11³×S1122×S2211 - 2×C12³×S1111×S2222 + 2×C12³×S1122×S2211 - C11³×S1111×S3333 + C11³×S1133×S3311 - 2×C12³×S1111×S3333 + 2×C12³×S1133×S3311 - C11³×S2222×S3333 + C11³×S2233×S3322 - 2×C12³×S2222×S3333 + 2×C12³×S2233×S3322 - 2×C11×C12×C11*×S1111 + 2×C11×C12×C12*×S1111 - C11×C12×C11*×S1122 + C11×C12×C12*×S1122 - C11×C12×C11*×S1133 + C11×C12×C12*×S1133 + C11×C12×C11*×S2211 - C11×C12×C12*×S2211 + C11×C12×C11*×S2233 - C11×C12×C12*×S2233 + C11×C12×C11*×S3311 - C11×C12×C12*×S3311 + C11×C12×C11*×S3322 - C11×C12×C12*×S3322 + 3×C11×C12²×S1111×S2222 - 3×C11×C12²×S1122×S2211 + C11²×C11*×S1111×S2222 - C11²×C11*×S1122×S2211 - C12×C11*²×S1111×S2222 + C12×C11*²×S1122×S2211 - C11²×C12*×S1111×S2222 + C11²×C12*×S1122×S2211 - 3×C12²×C11*×S1111×S2222 + 3×C12²×C11*×S1122×S2211 - C12×C12*²×S1111×S2222 + C12×C12*²×S1122×S2211 + 3×C12²×C12*×S1111×S2222 - 3×C12²×C12*×S1122×S2211 + C12×C11*²×S1111×S2233 - C12×C11*²×S1133×S2211 + C12²×C11*×S1111×S2233 - C12²×C11*×S1133×S2211 + C12×C12*²×S1111×S2233 -

$C_{12}\times C_{12}^{*2}\times S_{1133}\times S_{2211} - C_{12}^{2}\times C_{12}^{*}\times S_{1111}\times S_{2233} + C_{12}^{2}\times C_{12}^{*}\times S_{1133}\times S_{2211} - C_{11}\times C_{11}^{*2}\times S_{1122}\times S_{2233} +$

$C_{11}\times C_{11}^{*2}\times S_{1133}\times S_{2222} + C_{11}^{2}\times C_{11}^{*}\times S_{1122}\times S_{2233} - C_{11}^{2}\times C_{11}^{*}\times S_{1133}\times S_{2222} - C_{11}\times C_{12}^{*2}\times S_{1122}\times S_{2233} +$

$C_{11}\times C_{12}^{*2}\times S_{1133}\times S_{2222} - C_{11}^{2}\times C_{12}^{*}\times S_{1122}\times S_{2233} + C_{11}^{2}\times C_{12}^{*}\times S_{1133}\times S_{2222} + 3\times C_{11}\times C_{12}^{2}\times S_{1111}\times S_{3333} -$

$3\times C_{11}\times C_{12}^{2}\times S_{1133}\times S_{3311} + C_{12}\times C_{11}^{*2}\times S_{1111}\times S_{3322} - C_{12}\times C_{11}^{*2}\times S_{1122}\times S_{3311} + C_{12}^{2}\times C_{11}^{*}\times S_{1111}\times S_{3322} -$

$C_{12}^{2}\times C_{11}^{*}\times S_{1122}\times S_{3311} + C_{12}\times C_{12}^{*2}\times S_{1111}\times S_{3322} - C_{12}\times C_{12}^{*2}\times S_{1122}\times S_{3311} - C_{12}^{2}\times C_{12}^{*}\times S_{1111}\times S_{3322} +$

$C_{12}^{2}\times C_{12}^{*}\times S_{1122}\times S_{3311} + C_{11}^{2}\times C_{11}^{*}\times S_{1111}\times S_{3333} - C_{11}^{2}\times C_{11}^{*}\times S_{1133}\times S_{3311} - C_{12}\times C_{11}^{*2}\times S_{1111}\times S_{3333} +$

$C_{12}\times C_{11}^{*2}\times S_{1133}\times S_{3311} - C_{11}^{2}\times C_{12}^{*}\times S_{1111}\times S_{3333} + C_{11}^{2}\times C_{12}^{*}\times S_{1133}\times S_{3311} - 3\times C_{12}^{2}\times C_{11}^{*}\times S_{1111}\times S_{3333}$

$+ 3\times C_{12}^{2}\times C_{11}^{*}\times S_{1133}\times S_{3311} - C_{12}\times C_{12}^{*2}\times S_{1111}\times S_{3333} + C_{12}\times C_{12}^{*2}\times S_{1133}\times S_{3311} +$

$3\times C_{12}^{2}\times C_{12}^{*}\times S_{1111}\times S_{3333} - 3\times C_{12}^{2}\times C_{12}^{*}\times S_{1133}\times S_{3311} + C_{11}\times C_{11}^{*2}\times S_{1122}\times S_{3333} -$

$C_{11}\times C_{11}^{*2}\times S_{1133}\times S_{3322} - C_{11}^{2}\times C_{11}^{*}\times S_{1122}\times S_{3333} + C_{11}^{2}\times C_{11}^{*}\times S_{1133}\times S_{3322} + C_{11}\times C_{12}^{*2}\times S_{1122}\times S_{3333} -$

$C_{11}\times C_{12}^{*2}\times S_{1133}\times S_{3322} + C_{11}^{2}\times C_{12}^{*}\times S_{1122}\times S_{3333} - C_{11}^{2}\times C_{12}^{*}\times S_{1133}\times S_{3322} + 3\times C_{11}\times C_{12}^{2}\times S_{2222}\times S_{3333} -$

$3\times C_{11}\times C_{12}^{2}\times S_{2233}\times S_{3322} - C_{12}\times C_{11}^{*2}\times S_{2211}\times S_{3322} + C_{12}\times C_{11}^{*2}\times S_{2222}\times S_{3311} - C_{12}^{2}\times C_{11}^{*}\times S_{2211}\times S_{3322} +$

$C_{12}^{2}\times C_{11}^{*}\times S_{2222}\times S_{3311} - C_{12}\times C_{12}^{*2}\times S_{2211}\times S_{3322} + C_{12}\times C_{12}^{*2}\times S_{2222}\times S_{3311} + C_{12}^{2}\times C_{12}^{*}\times S_{2211}\times S_{3322} -$

$C_{12}^{2}\times C_{12}^{*}\times S_{2222}\times S_{3311} + C_{12}\times C_{11}^{*2}\times S_{2211}\times S_{3333} - C_{12}\times C_{11}^{*2}\times S_{2233}\times S_{3311} + C_{12}^{2}\times C_{11}^{*}\times S_{2211}\times S_{3333} -$

$C_{12}^{2}\times C_{11}^{*}\times S_{2233}\times S_{3311} + C_{12}\times C_{12}^{*2}\times S_{2211}\times S_{3333} - C_{12}\times C_{12}^{*2}\times S_{2233}\times S_{3311} - C_{12}^{2}\times C_{12}^{*}\times S_{2211}\times S_{3333} +$

$C_{12}^{2}\times C_{12}^{*}\times S_{2233}\times S_{3311} - C_{11}\times C_{11}^{*2}\times S_{2222}\times S_{3333} + C_{11}\times C_{11}^{*2}\times S_{2233}\times S_{3322} + 2\times C_{11}^{2}\times C_{11}^{*}\times S_{2222}\times S_{3333}$

$- 2\times C_{11}^{2}\times C_{11}^{*}\times S_{2233}\times S_{3322} - C_{11}\times C_{12}^{*2}\times S_{2222}\times S_{3333} + C_{11}\times C_{12}^{*2}\times S_{2233}\times S_{3322} -$

$2\times C_{11}^{2}\times C_{12}^{*}\times S_{2222}\times S_{3333} + 2\times C_{11}^{2}\times C_{12}^{*}\times S_{2233}\times S_{3322} - 2\times C_{12}^{2}\times C_{11}^{*}\times S_{2222}\times S_{3333} +$

$2\times C_{12}^{2}\times C_{11}^{*}\times S_{2233}\times S_{3322} + 2\times C_{12}^{2}\times C_{12}^{*}\times S_{2222}\times S_{3333} - 2\times C_{12}^{2}\times C_{12}^{*}\times S_{2233}\times S_{3322} +$

$C_{11}^{3}\times S_{1111}\times S_{2222}\times S_{3333} - C_{11}^{3}\times S_{1111}\times S_{2233}\times S_{3322} - C_{11}^{3}\times S_{1122}\times S_{2211}\times S_{3333} + C_{11}^{3}\times S_{1122}\times S_{2233}\times S_{3311} +$

$C_{11}^{3}\times S_{1133}\times S_{2211}\times S_{3322} - C_{11}^{3}\times S_{1133}\times S_{2222}\times S_{3311} + 2\times C_{12}^{3}\times S_{1111}\times S_{2222}\times S_{3333} -$

$2\times C_{12}^{3}\times S_{1111}\times S_{2233}\times S_{3322} - 2\times C_{12}^{3}\times S_{1122}\times S_{2211}\times S_{3333} + 2\times C_{12}^{3}\times S_{1122}\times S_{2233}\times S_{3311} +$

$2\times C_{12}^{3}\times S_{1133}\times S_{2211}\times S_{3322} - 2\times C_{12}^{3}\times S_{1133}\times S_{2222}\times S_{3311} - 3\times C_{11}\times C_{12}^{2}\times S_{1111}\times S_{2222}\times S_{3333} +$

$3\times C_{11}\times C_{12}^{2}\times S_{1111}\times S_{2233}\times S_{3322} + 3\times C_{11}\times C_{12}^{2}\times S_{1122}\times S_{2211}\times S_{3333} - 3\times C_{11}\times C_{12}^{2}\times S_{1122}\times S_{2233}\times S_{3311} -$

$3\times C_{11}\times C_{12}^{2}\times S_{1133}\times S_{2211}\times S_{3322} + 3\times C_{11}\times C_{12}^{2}\times S_{1133}\times S_{2222}\times S_{3311} + C_{11}\times C_{11}^{*2}\times S_{1111}\times S_{2222}\times S_{3333} -$

$C_{11}\times C_{11}^{*2}\times S_{1111}\times S_{2233}\times S_{3322} - C_{11}\times C_{11}^{*2}\times S_{1122}\times S_{2211}\times S_{3333} + C_{11}\times C_{11}^{*2}\times S_{1122}\times S_{2233}\times S_{3311} +$

$C_{11}\times C_{11}^{*2}\times S_{1133}\times S_{2211}\times S_{3322} - C_{11}\times C_{11}^{*2}\times S_{1133}\times S_{2222}\times S_{3311} - 2\times C_{11}^{2}\times C_{11}^{*}\times S_{1111}\times S_{2222}\times S_{3333} +$

$2\times C_{11}^{2}\times C_{11}^{*}\times S_{1111}\times S_{2233}\times S_{3322} + 2\times C_{11}^{2}\times C_{11}^{*}\times S_{1122}\times S_{2211}\times S_{3333} - 2\times C_{11}^{2}\times C_{11}^{*}\times S_{1122}\times S_{2233}\times S_{3311} -$

$2\times C_{11}^{2}\times C_{11}^{*}\times S_{1133}\times S_{2211}\times S_{3322} + 2\times C_{11}^{2}\times C_{11}^{*}\times S_{1133}\times S_{2222}\times S_{3311} + C_{11}\times C_{12}^{*2}\times S_{1111}\times S_{2222}\times S_{3333} -$

$C_{11}\times C_{12}^{*2}\times S_{1111}\times S_{2233}\times S_{3322} - C_{11}\times C_{12}^{*2}\times S_{1122}\times S_{2211}\times S_{3333} + C_{11}\times C_{12}^{*2}\times S_{1122}\times S_{2233}\times S_{3311} +$

$C_{11}\times C_{12}^{*2}\times S_{1133}\times S_{2211}\times S_{3322} - C_{11}\times C_{12}^{*2}\times S_{1133}\times S_{2222}\times S_{3311} + 2\times C_{12}\times C_{11}^{*2}\times S_{1111}\times S_{2222}\times S_{3333} -$

$2\times C_{12}\times C_{11}^{*2}\times S_{1111}\times S_{2233}\times S_{3322} - 2\times C_{12}\times C_{11}^{*2}\times S_{1122}\times S_{2211}\times S_{3333} + 2\times C_{12}\times C_{11}^{*2}\times S_{1122}\times S_{2233}\times S_{3311}$

$+ 2\times C_{12}\times C_{11}^{*2}\times S_{1133}\times S_{2211}\times S_{3322} - 2\times C_{12}\times C_{11}^{*2}\times S_{1133}\times S_{2222}\times S_{3311} +$

$2\times C_{11}^{2}\times C_{12}^{*}\times S_{1111}\times S_{2222}\times S_{3333} - 2\times C_{11}^{2}\times C_{12}^{*}\times S_{1111}\times S_{2233}\times S_{3322} - 2\times C_{11}^{2}\times C_{12}^{*}\times S_{1122}\times S_{2211}\times S_{3333} +$

$2\times C_{11}^{2}\times C_{12}^{*}\times S_{1122}\times S_{2233}\times S_{3311} + 2\times C_{11}^{2}\times C_{12}^{*}\times S_{1133}\times S_{2211}\times S_{3322} - 2\times C_{11}^{2}\times C_{12}^{*}\times S_{1133}\times S_{2222}\times S_{3311}$

$+ 4\times C_{12}^{2}\times C_{11}^{*}\times S_{1111}\times S_{2222}\times S_{3333} - 4\times C_{12}^{2}\times C_{11}^{*}\times S_{1111}\times S_{2233}\times S_{3322} - 4\times C_{12}^{2}\times C_{11}^{*}\times S_{1122}\times S_{2211}\times S_{3333}$

$+ 4\times C_{12}^{2}\times C_{11}^{*}\times S_{1122}\times S_{2233}\times S_{3311} + 4\times C_{12}^{2}\times C_{11}^{*}\times S_{1133}\times S_{2211}\times S_{3322} -$

$4\times C_{12}^{2}\times C_{11}^{*}\times S_{1133}\times S_{2222}\times S_{3311} + 2\times C_{12}\times C_{12}^{*2}\times S_{1111}\times S_{2222}\times S_{3333} - 2\times C_{12}\times C_{12}^{*2}\times S_{1111}\times S_{2233}\times S_{3322} -$

$2\times C_{12}\times C_{12}^{*2}\times S_{1122}\times S_{2211}\times S_{3333} + 2\times C_{12}\times C_{12}^{*2}\times S_{1122}\times S_{2233}\times S_{3311} + 2\times C_{12}\times C_{12}^{*2}\times S_{1133}\times S_{2211}\times S_{3322}$

$- 2\times C_{12}\times C_{12}^{*2}\times S_{1133}\times S_{2222}\times S_{3311} - 4\times C_{12}^{2}\times C_{12}^{*}\times S_{1111}\times S_{2222}\times S_{3333} + 4\times C_{12}^{2}\times C_{12}^{*}\times S_{1111}\times S_{2233}\times S_{3322}$

$+ 4\times C_{12}^{2}\times C_{12}^{*}\times S_{1122}\times S_{2211}\times S_{3333} - 4\times C_{12}^{2}\times C_{12}^{*}\times S_{1122}\times S_{2233}\times S_{3311} - 4\times C_{12}^{2}\times C_{12}^{*}\times S_{1133}\times S_{2211}\times S_{3322}$

$+ 4\times C_{12}^{2}\times C_{12}^{*}\times S_{1133}\times S_{2222}\times S_{3311} + 2\times C_{11}\times C_{12}\times C_{11}^{*}\times S_{1111}\times S_{2222} - 2\times C_{11}\times C_{12}\times C_{11}^{*}\times S_{1122}\times S_{2211} -$

$2\times C_{11}\times C_{12}\times C_{12}^{*}\times S_{1111}\times S_{2222} + 2\times C_{11}\times C_{12}\times C_{12}^{*}\times S_{1122}\times S_{2211} - C_{11}\times C_{12}\times C_{11}^{*}\times S_{1111}\times S_{2233} +$

$C_{11}\times C_{12}\times C_{11}^{*}\times S_{1133}\times S_{2211} + C_{11}\times C_{12}\times C_{12}^{*}\times S_{1111}\times S_{2233} - C_{11}\times C_{12}\times C_{12}^{*}\times S_{1133}\times S_{2211} -$

$C_{11}\times C_{12}\times C_{11}^{*}\times S_{1122}\times S_{2233} + C_{11}\times C_{12}\times C_{11}^{*}\times S_{1133}\times S_{2222} + C_{11}\times C_{12}\times C_{12}^{*}\times S_{1122}\times S_{2233} -$

$C_{11}\times C_{12}\times C_{12}^{*}\times S_{1133}\times S_{2222} + 2\times C_{12}\times C_{11}^{*}\times C_{12}^{*}\times S_{1111}\times S_{2222} - 2\times C_{12}\times C_{11}^{*}\times C_{12}^{*}\times S_{1122}\times S_{2211} -$

$2\times C_{12}\times C_{11}^{*}\times C_{12}^{*}\times S_{1111}\times S_{2233} + 2\times C_{12}\times C_{11}^{*}\times C_{12}^{*}\times S_{1133}\times S_{2211} + 2\times C_{11}\times C_{11}^{*}\times C_{12}^{*}\times S_{1122}\times S_{2233} -$

$2\times C_{11}\times C_{11}^{*}\times C_{12}^{*}\times S_{1133}\times S_{2222} - C_{11}\times C_{12}\times C_{11}^{*}\times S_{1111}\times S_{3322} + C_{11}\times C_{12}\times C_{11}^{*}\times S_{1122}\times S_{3311} +$

$C_{11}\times C_{12}\times C_{12}^{*}\times S_{1111}\times S_{3322} - C_{11}\times C_{12}\times C_{12}^{*}\times S_{1122}\times S_{3311} + 2\times C_{11}\times C_{12}\times C_{11}^{*}\times S_{1111}\times S_{3333} -$

$2\times C_{11}\times C_{12}\times C_{11}^{*}\times S_{1133}\times S_{3311} - 2\times C_{11}\times C_{12}\times C_{12}^{*}\times S_{1111}\times S_{3333} + 2\times C_{11}\times C_{12}\times C_{12}^{*}\times S_{1133}\times S_{3311} +$

$C_{11}\times C_{12}\times C_{11}^{*}\times S_{1122}\times S_{3333} - C_{11}\times C_{12}\times C_{11}^{*}\times S_{1133}\times S_{3322} - C_{11}\times C_{12}\times C_{12}^{*}\times S_{1122}\times S_{3333} +$

$C_{11}\times C_{12}\times C_{12}^{*}\times S_{1133}\times S_{3322} - 2\times C_{12}\times C_{11}^{*}\times C_{12}^{*}\times S_{1111}\times S_{3322} + 2\times C_{12}\times C_{11}^{*}\times C_{12}^{*}\times S_{1122}\times S_{3311} +$

$$2\times C_{12}\times C_{11}^{*}\times C_{12}^{*}\times S_{1111}\times S_{3333} - 2\times C_{12}\times C_{11}^{*}\times C_{12}^{*}\times S_{1133}\times S_{3311} - 2\times C_{11}\times C_{11}^{*}\times C_{12}^{*}\times S_{1122}\times S_{3333} +$$

$$2\times C_{11}\times C_{11}^{*}\times C_{12}^{*}\times S_{1133}\times S_{3322} + C_{11}\times C_{12}\times C_{11}^{*}\times S_{2211}\times S_{3322} - C_{11}\times C_{12}\times C_{11}^{*}\times S_{2222}\times S_{3311} -$$

$$C_{11}\times C_{12}\times C_{12}^{*}\times S_{2211}\times S_{3322} + C_{11}\times C_{12}\times C_{12}^{*}\times S_{2222}\times S_{3311} - C_{11}\times C_{12}\times C_{11}^{*}\times S_{2211}\times S_{3333} +$$

$$C_{11}\times C_{12}\times C_{11}^{*}\times S_{2233}\times S_{3311} + C_{11}\times C_{12}\times C_{12}^{*}\times S_{2211}\times S_{3333} - C_{11}\times C_{12}\times C_{12}^{*}\times S_{2233}\times S_{3311} +$$

$$2\times C_{12}\times C_{11}^{*}\times C_{12}^{*}\times S_{2211}\times S_{3322} - 2\times C_{12}\times C_{11}^{*}\times C_{12}^{*}\times S_{2222}\times S_{3311} - 2\times C_{12}\times C_{11}^{*}\times C_{12}^{*}\times S_{2211}\times S_{3333} +$$

$$2\times C_{12}\times C_{11}^{*}\times C_{12}^{*}\times S_{2233}\times S_{3311} + 2\times C_{11}\times C_{11}^{*}\times C_{12}^{*}\times S_{2222}\times S_{3333} - 2\times C_{11}\times C_{11}^{*}\times C_{12}^{*}\times S_{2233}\times S_{3322} -$$

$$2\times C_{11}\times C_{12}\times C_{11}^{*}\times S_{1111}\times S_{2222}\times S_{3333} + 2\times C_{11}\times C_{12}\times C_{11}^{*}\times S_{1111}\times S_{2233}\times S_{3322} +$$

$$2\times C_{11}\times C_{12}\times C_{11}^{*}\times S_{1122}\times S_{2211}\times S_{3333} - 2\times C_{11}\times C_{12}\times C_{11}^{*}\times S_{1122}\times S_{2233}\times S_{3311} -$$

$$2\times C_{11}\times C_{12}\times C_{11}^{*}\times S_{1133}\times S_{2211}\times S_{3322} + 2\times C_{11}\times C_{12}\times C_{11}^{*}\times S_{1133}\times S_{2222}\times S_{3311} +$$

$$2\times C_{11}\times C_{12}\times C_{12}^{*}\times S_{1111}\times S_{2222}\times S_{3333} - 2\times C_{11}\times C_{12}\times C_{12}^{*}\times S_{1111}\times S_{2233}\times S_{3322} -$$

$$2\times C_{11}\times C_{12}\times C_{12}^{*}\times S_{1122}\times S_{2211}\times S_{3333} + 2\times C_{11}\times C_{12}\times C_{12}^{*}\times S_{1122}\times S_{2233}\times S_{3311} +$$

$$2\times C_{11}\times C_{12}\times C_{12}^{*}\times S_{1133}\times S_{2211}\times S_{3322} - 2\times C_{11}\times C_{12}\times C_{12}^{*}\times S_{1133}\times S_{2222}\times S_{3311} -$$

$$2\times C_{11}\times C_{11}^{*}\times C_{12}^{*}\times S_{1111}\times S_{2222}\times S_{3333} + 2\times C_{11}\times C_{11}^{*}\times C_{12}^{*}\times S_{1111}\times S_{2233}\times S_{3322} +$$

$$2\times C_{11}\times C_{11}^{*}\times C_{12}^{*}\times S_{1122}\times S_{2211}\times S_{3333} - 2\times C_{11}\times C_{11}^{*}\times C_{12}^{*}\times S_{1122}\times S_{2233}\times S_{3311} -$$

$$2\times C_{11}\times C_{11}^{*}\times C_{12}^{*}\times S_{1133}\times S_{2211}\times S_{3322} + 2\times C_{11}\times C_{11}^{*}\times C_{12}^{*}\times S_{1133}\times S_{2222}\times S_{3311} -$$

$$4\times C_{12}\times C_{11}^{*}\times C_{12}^{*}\times S_{1111}\times S_{2222}\times S_{3333} + 4\times C_{12}\times C_{11}^{*}\times C_{12}^{*}\times S_{1111}\times S_{2233}\times S_{3322} +$$

$$4\times C_{12}\times C_{11}^{*}\times C_{12}^{*}\times S_{1122}\times S_{2211}\times S_{3333} - 4\times C_{12}\times C_{11}^{*}\times C_{12}^{*}\times S_{1122}\times S_{2233}\times S_{3311} -$$

$$4\times C_{12}\times C_{11}^{*}\times C_{12}^{*}\times S_{1133}\times S_{2211}\times S_{3322} + 4\times C_{12}\times C_{11}^{*}\times C_{12}^{*}\times S_{1133}\times S_{2222}\times S_{3311}))/(3\times C_{11}\times C_{12}^{2} +$$

$$C_{11}^{3}\times S_{1111} + 2\times C_{12}^{3}\times S_{1111} + C_{11}^{3}\times S_{2222} + 2\times C_{12}^{3}\times S_{2222} + C_{11}^{3}\times S_{3333} + 2\times C_{12}^{3}\times S_{3333} - C_{11}^{3} - 2\times C_{12}^{3} -$$

$$3\times C_{11}\times C_{12}^{2}\times S_{1111} - C_{11}^{2}\times C_{11}^{*}\times S_{1111} + C_{12}^{2}\times C_{11}^{*}\times S_{1111} - 2\times C_{12}^{2}\times C_{12}^{*}\times S_{1111} - C_{11}^{2}\times C_{12}^{*}\times S_{1122} -$$

$$C_{12}^{2}\times C_{11}^{*}\times S_{1122} - C_{11}^{2}\times C_{12}^{*}\times S_{1133} - C_{12}^{2}\times C_{11}^{*}\times S_{1133} - 3\times C_{11}\times C_{12}^{2}\times S_{2222} - C_{11}^{2}\times C_{12}^{*}\times S_{2211} -$$

$$C_{12}^{2}\times C_{11}^{*}\times S_{2211} - C_{11}^{2}\times C_{11}^{*}\times S_{2222} + C_{12}^{2}\times C_{11}^{*}\times S_{2222} - 2\times C_{12}^{2}\times C_{12}^{*}\times S_{2222} - C_{11}^{2}\times C_{12}^{*}\times S_{2233} -$$

$$C_{12}^{2}\times C_{11}^{*}\times S_{2233} - 3\times C_{11}\times C_{12}^{2}\times S_{3333} - C_{11}^{2}\times C_{12}^{*}\times S_{3311} - C_{12}^{2}\times C_{11}^{*}\times S_{3311} - C_{11}^{2}\times C_{12}^{*}\times S_{3322} -$$

$$C_{12}^{2}\times C_{11}^{*}\times S_{3322} - C_{11}^{2}\times C_{11}^{*}\times S_{3333} + C_{12}^{2}\times C_{11}^{*}\times S_{3333} - 2\times C_{12}^{2}\times C_{12}^{*}\times S_{3333} - C_{11}^{3}\times S_{1111}\times S_{2222} +$$

$$C_{11}^{3}\times S_{1122}\times S_{2211} - 2\times C_{12}^{3}\times S_{1111}\times S_{2222} + 2\times C_{12}^{3}\times S_{1122}\times S_{2211} - C_{11}^{3}\times S_{1111}\times S_{3333} + C_{11}^{3}\times S_{1133}\times S_{3311} -$$

$$2\times C_{12}^{3}\times S_{1111}\times S_{3333} + 2\times C_{12}^{3}\times S_{1133}\times S_{3311} - C_{11}^{3}\times S_{2222}\times S_{3333} + C_{11}^{3}\times S_{2233}\times S_{3322} - 2\times C_{12}^{3}\times S_{2222}\times S_{3333}$$

$+ 2\times C_{12}^{3}\times S_{2233}\times S_{3322} + 2\times C_{11}\times C_{12}\times C_{12}^{*}\times S_{1111} + C_{11}\times C_{12}\times C_{11}^{*}\times S_{1122} + C_{11}\times C_{12}\times C_{12}^{*}\times S_{1122} +$

$C_{11}\times C_{12}\times C_{11}^{*}\times S_{1133} + C_{11}\times C_{12}\times C_{12}^{*}\times S_{1133} + C_{11}\times C_{12}\times C_{11}^{*}\times S_{2211} + C_{11}\times C_{12}\times C_{12}^{*}\times S_{2211} +$

$2\times C_{11}\times C_{12}\times C_{12}^{*}\times S_{2222} + C_{11}\times C_{12}\times C_{11}^{*}\times S_{2233} + C_{11}\times C_{12}\times C_{12}^{*}\times S_{2233} + C_{11}\times C_{12}\times C_{11}^{*}\times S_{3311} +$

$C_{11}\times C_{12}\times C_{12}^{*}\times S_{3311} + C_{11}\times C_{12}\times C_{11}^{*}\times S_{3322} + C_{11}\times C_{12}\times C_{12}^{*}\times S_{3322} + 2\times C_{11}\times C_{12}\times C_{12}^{*}\times S_{3333} +$

$3\times C_{11}\times C_{12}^{2}\times S_{1111}\times S_{2222} - 3\times C_{11}\times C_{12}^{2}\times S_{1122}\times S_{2211} - C_{11}\times C_{11}^{*2}\times S_{1111}\times S_{2222} + C_{11}\times C_{11}^{*2}\times S_{1122}\times S_{2211}$

$+ 2\times C_{11}^{2}\times C_{11}^{*}\times S_{1111}\times S_{2222} - 2\times C_{11}^{2}\times C_{11}^{*}\times S_{1122}\times S_{2211} + C_{11}\times C_{12}^{*2}\times S_{1111}\times S_{2222} -$

$C_{11}\times C_{12}^{*2}\times S_{1122}\times S_{2211} - 2\times C_{12}^{2}\times C_{11}^{*}\times S_{1111}\times S_{2222} + 2\times C_{12}^{2}\times C_{11}^{*}\times S_{1122}\times S_{2211} -$

$2\times C_{12}\times C_{12}^{*2}\times S_{1111}\times S_{2222} + 2\times C_{12}\times C_{12}^{*2}\times S_{1122}\times S_{2211} + 4\times C_{12}^{2}\times C_{12}^{*}\times S_{1111}\times S_{2222} -$

$4\times C_{12}^{2}\times C_{12}^{*}\times S_{1122}\times S_{2211} + C_{11}\times C_{12}^{*2}\times S_{1111}\times S_{2233} - C_{11}\times C_{12}^{*2}\times S_{1133}\times S_{2211} + C_{12}\times C_{11}^{*2}\times S_{1111}\times S_{2233}$

$- C_{12}\times C_{11}^{*2}\times S_{1133}\times S_{2211} + C_{11}^{2}\times C_{12}^{*}\times S_{1111}\times S_{2233} - C_{11}^{2}\times C_{12}^{*}\times S_{1133}\times S_{2211} + C_{12}^{2}\times C_{11}^{*}\times S_{1111}\times S_{2233} -$

$C_{12}^{2}\times C_{11}^{*}\times S_{1133}\times S_{2211} - C_{11}\times C_{12}^{*2}\times S_{1122}\times S_{2233} + C_{11}\times C_{12}^{*2}\times S_{1133}\times S_{2222} - C_{12}\times C_{11}^{*2}\times S_{1122}\times S_{2233} +$

$C_{12}\times C_{11}^{*2}\times S_{1133}\times S_{2222} - C_{11}^{2}\times C_{12}^{*}\times S_{1122}\times S_{2233} + C_{11}^{2}\times C_{12}^{*}\times S_{1133}\times S_{2222} - C_{12}^{2}\times C_{11}^{*}\times S_{1122}\times S_{2233} +$

$C_{12}^{2}\times C_{11}^{*}\times S_{1133}\times S_{2222} + 3\times C_{11}\times C_{12}^{2}\times S_{1111}\times S_{3333} - 3\times C_{11}\times C_{12}^{2}\times S_{1133}\times S_{3311} + C_{11}\times C_{12}^{*2}\times S_{1111}\times S_{3322}$

$- C_{11}\times C_{12}^{*2}\times S_{1122}\times S_{3311} + C_{12}\times C_{11}^{*2}\times S_{1111}\times S_{3322} - C_{12}\times C_{11}^{*2}\times S_{1122}\times S_{3311} + C_{11}^{2}\times C_{12}^{*}\times S_{1111}\times S_{3322} -$

$C_{11}^{2}\times C_{12}^{*}\times S_{1122}\times S_{3311} + C_{12}^{2}\times C_{11}^{*}\times S_{1111}\times S_{3322} - C_{12}^{2}\times C_{11}^{*}\times S_{1122}\times S_{3311} - C_{11}\times C_{11}^{*2}\times S_{1111}\times S_{3333} +$

$C_{11}\times C_{11}^{*2}\times S_{1133}\times S_{3311} + 2\times C_{11}^{2}\times C_{11}^{*}\times S_{1111}\times S_{3333} - 2\times C_{11}^{2}\times C_{11}^{*}\times S_{1133}\times S_{3311} +$

$C_{11}\times C_{12}^{*2}\times S_{1111}\times S_{3333} - C_{11}\times C_{12}^{*2}\times S_{1133}\times S_{3311} - 2\times C_{12}^{2}\times C_{11}^{*}\times S_{1111}\times S_{3333} +$

$2\times C_{12}^{2}\times C_{11}^{*}\times S_{1133}\times S_{3311} - 2\times C_{12}\times C_{12}^{*2}\times S_{1111}\times S_{3333} + 2\times C_{12}\times C_{12}^{*2}\times S_{1133}\times S_{3311} +$

$4\times C_{12}^{2}\times C_{12}^{*}\times S_{1111}\times S_{3333} - 4\times C_{12}^{2}\times C_{12}^{*}\times S_{1133}\times S_{3311} + C_{11}\times C_{12}^{*2}\times S_{1122}\times S_{3333} -$

$C_{11}\times C_{12}^{*2}\times S_{1133}\times S_{3322} + C_{12}\times C_{11}^{*2}\times S_{1122}\times S_{3333} - C_{12}\times C_{11}^{*2}\times S_{1133}\times S_{3322} + C_{11}^{2}\times C_{12}^{*}\times S_{1122}\times S_{3333} -$

$C_{11}^{2}\times C_{12}^{*}\times S_{1133}\times S_{3322} + C_{12}^{2}\times C_{11}^{*}\times S_{1122}\times S_{3333} - C_{12}^{2}\times C_{11}^{*}\times S_{1133}\times S_{3322} + 3\times C_{11}\times C_{12}^{2}\times S_{2222}\times S_{3333} -$

$3\times C_{11}\times C_{12}^{2}\times S_{2233}\times S_{3322} - C_{11}\times C_{12}^{*2}\times S_{2211}\times S_{3322} + C_{11}\times C_{12}^{*2}\times S_{2222}\times S_{3311} - C_{12}\times C_{11}^{*2}\times S_{2211}\times S_{3322} +$

$C_{12}\times C_{11}^{*2}\times S_{2222}\times S_{3311} - C_{11}^{2}\times C_{12}^{*}\times S_{2211}\times S_{3322} + C_{11}^{2}\times C_{12}^{*}\times S_{2222}\times S_{3311} - C_{12}^{2}\times C_{11}^{*}\times S_{2211}\times S_{3322} +$

$C_{12}^{2}\times C_{11}^{*}\times S_{2222}\times S_{3311} + C_{11}\times C_{12}^{*2}\times S_{2211}\times S_{3333} - C_{11}\times C_{12}^{*2}\times S_{2233}\times S_{3311} + C_{12}\times C_{11}^{*2}\times S_{2211}\times S_{3333} -$

$C_{12}\times C_{11}^{*2}\times S_{2233}\times S_{3311} + C_{11}^{2}\times C_{12}^{*}\times S_{2211}\times S_{3333} - C_{11}^{2}\times C_{12}^{*}\times S_{2233}\times S_{3311} + C_{12}^{2}\times C_{11}^{*}\times S_{2211}\times S_{3333} -$

$C_{12}^{2}\times C_{11}^{*}\times S_{2233}\times S_{3311} - C_{11}\times C_{11}^{*2}\times S_{2222}\times S_{3333} + C_{11}\times C_{11}^{*2}\times S_{2233}\times S_{3322} + 2\times C_{11}^{2}\times C_{11}^{*}\times S_{2222}\times S_{3333}$

$$- 2\times C_{11}^{2}\times C_{11}^{*}\times S_{2233}\times S_{3322} + C_{11}\times C_{12}^{*2}\times S_{2222}\times S_{3333} - C_{11}\times C_{12}^{*2}\times S_{2233}\times S_{3322} -$$

$$2\times C_{12}^{2}\times C_{11}^{*}\times S_{2222}\times S_{3333} + 2\times C_{12}^{2}\times C_{11}^{*}\times S_{2233}\times S_{3322} - 2\times C_{12}\times C_{12}^{*2}\times S_{2222}\times S_{3333} +$$

$$2\times C_{12}\times C_{12}^{*2}\times S_{2233}\times S_{3322} + 4\times C_{12}^{2}\times C_{12}^{*}\times S_{2222}\times S_{3333} - 4\times C_{12}^{2}\times C_{12}^{*}\times S_{2233}\times S_{3322} +$$

$$C_{11}^{3}\times S_{1111}\times S_{2222}\times S_{3333} - C_{11}^{3}\times S_{1111}\times S_{2233}\times S_{3322} - C_{11}^{3}\times S_{1122}\times S_{2211}\times S_{3333} + C_{11}^{3}\times S_{1122}\times S_{2233}\times S_{3311} +$$

$$C_{11}^{3}\times S_{1133}\times S_{2211}\times S_{3322} - C_{11}^{3}\times S_{1133}\times S_{2222}\times S_{3311} + 2\times C_{12}^{3}\times S_{1111}\times S_{2222}\times S_{3333} -$$

$$2\times C_{12}^{3}\times S_{1111}\times S_{2233}\times S_{3322} - 2\times C_{12}^{3}\times S_{1122}\times S_{2211}\times S_{3333} + 2\times C_{12}^{3}\times S_{1122}\times S_{2233}\times S_{3311} +$$

$$2\times C_{12}^{3}\times S_{1133}\times S_{2211}\times S_{3322} - 2\times C_{12}^{3}\times S_{1133}\times S_{2222}\times S_{3311} - C_{11}^{*3}\times S_{1111}\times S_{2222}\times S_{3333} +$$

$$C_{11}^{*3}\times S_{1111}\times S_{2233}\times S_{3322} + C_{11}^{*3}\times S_{1122}\times S_{2211}\times S_{3333} - C_{11}^{*3}\times S_{1122}\times S_{2233}\times S_{3311} -$$

$$C_{11}^{*3}\times S_{1133}\times S_{2211}\times S_{3322} + C_{11}^{*3}\times S_{1133}\times S_{2222}\times S_{3311} - 2\times C_{12}^{*3}\times S_{1111}\times S_{2222}\times S_{3333} +$$

$$2\times C_{12}^{*3}\times S_{1111}\times S_{2233}\times S_{3322} + 2\times C_{12}^{*3}\times S_{1122}\times S_{2211}\times S_{3333} - 2\times C_{12}^{*3}\times S_{1122}\times S_{2233}\times S_{3311} -$$

$$2\times C_{12}^{*3}\times S_{1133}\times S_{2211}\times S_{3322} + 2\times C_{12}^{*3}\times S_{1133}\times S_{2222}\times S_{3311} - 3\times C_{11}\times C_{12}^{2}\times S_{1111}\times S_{2222}\times S_{3333} +$$

$$3\times C_{11}\times C_{12}^{2}\times S_{1111}\times S_{2233}\times S_{3322} + 3\times C_{11}\times C_{12}^{2}\times S_{1122}\times S_{2211}\times S_{3333} - 3\times C_{11}\times C_{12}^{2}\times S_{1122}\times S_{2233}\times S_{3311} -$$

$$3\times C_{11}\times C_{12}^{2}\times S_{1133}\times S_{2211}\times S_{3322} + 3\times C_{11}\times C_{12}^{2}\times S_{1133}\times S_{2222}\times S_{3311} + 3\times C_{11}\times C_{11}^{*2}\times S_{1111}\times S_{2222}\times S_{3333} -$$

$$3\times C_{11}\times C_{11}^{*2}\times S_{1111}\times S_{2233}\times S_{3322} - 3\times C_{11}\times C_{11}^{*2}\times S_{1122}\times S_{2211}\times S_{3333} + 3\times C_{11}\times C_{11}^{*2}\times S_{1122}\times S_{2233}\times S_{3311}$$

$$+ 3\times C_{11}\times C_{11}^{*2}\times S_{1133}\times S_{2211}\times S_{3322} - 3\times C_{11}\times C_{11}^{*2}\times S_{1133}\times S_{2222}\times S_{3311} - 3\times C_{11}^{2}\times C_{11}^{*}\times S_{1111}\times S_{2222}\times S_{3333}$$

$$+ 3\times C_{11}^{2}\times C_{11}^{*}\times S_{1111}\times S_{2233}\times S_{3322} + 3\times C_{11}^{2}\times C_{11}^{*}\times S_{1122}\times S_{2211}\times S_{3333} -$$

$$3\times C_{11}^{2}\times C_{11}^{*}\times S_{1122}\times S_{2233}\times S_{3311} - 3\times C_{11}^{2}\times C_{11}^{*}\times S_{1133}\times S_{2211}\times S_{3322} + 3\times C_{11}^{2}\times C_{11}^{*}\times S_{1133}\times S_{2222}\times S_{3311} -$$

$$3\times C_{11}\times C_{12}^{*2}\times S_{1111}\times S_{2222}\times S_{3333} + 3\times C_{11}\times C_{12}^{*2}\times S_{1111}\times S_{2233}\times S_{3322} + 3\times C_{11}\times C_{12}^{*2}\times S_{1122}\times S_{2211}\times S_{3333}$$

$$- 3\times C_{11}\times C_{12}^{*2}\times S_{1122}\times S_{2233}\times S_{3311} - 3\times C_{11}\times C_{12}^{*2}\times S_{1133}\times S_{2211}\times S_{3322} + 3\times C_{11}\times C_{12}^{*2}\times S_{1133}\times S_{2222}\times S_{3311}$$

$$+ 3\times C_{12}^{2}\times C_{11}^{*}\times S_{1111}\times S_{2222}\times S_{3333} - 3\times C_{12}^{2}\times C_{11}^{*}\times S_{1111}\times S_{2233}\times S_{3322} - 3\times C_{12}^{2}\times C_{11}^{*}\times S_{1122}\times S_{2211}\times S_{3333}$$

$$+ 3\times C_{12}^{2}\times C_{11}^{*}\times S_{1122}\times S_{2233}\times S_{3311} + 3\times C_{12}^{2}\times C_{11}^{*}\times S_{1133}\times S_{2211}\times S_{3322} -$$

$$3\times C_{12}^{2}\times C_{11}^{*}\times S_{1133}\times S_{2222}\times S_{3311} + 6\times C_{12}\times C_{12}^{*2}\times S_{1111}\times S_{2222}\times S_{3333} - 6\times C_{12}\times C_{12}^{*2}\times S_{1111}\times S_{2233}\times S_{3322} -$$

$$6\times C_{12}\times C_{12}^{*2}\times S_{1122}\times S_{2211}\times S_{3333} + 6\times C_{12}\times C_{12}^{*2}\times S_{1122}\times S_{2233}\times S_{3311} + 6\times C_{12}\times C_{12}^{*2}\times S_{1133}\times S_{2211}\times S_{3322}$$

$$- 6\times C_{12}\times C_{12}^{*2}\times S_{1133}\times S_{2222}\times S_{3311} - 6\times C_{12}^{2}\times C_{12}^{*}\times S_{1111}\times S_{2222}\times S_{3333} + 6\times C_{12}^{2}\times C_{12}^{*}\times S_{1111}\times S_{2233}\times S_{3322}$$

$$+ 6\times C_{12}^{2}\times C_{12}^{*}\times S_{1122}\times S_{2211}\times S_{3333} - 6\times C_{12}^{2}\times C_{12}^{*}\times S_{1122}\times S_{2233}\times S_{3311} - 6\times C_{12}^{2}\times C_{12}^{*}\times S_{1133}\times S_{2211}\times S_{3322}$$

$$+ 6\times C_{12}^{2}\times C_{12}^{*}\times S_{1133}\times S_{2222}\times S_{3311} + 3\times C_{11}^{*}\times C_{12}^{*2}\times S_{1111}\times S_{2222}\times S_{3333} -$$

$3\times C_{11}^{*}\times C_{12}^{*2}\times S_{1111}\times S_{2233}\times S_{3322} - 3\times C_{11}^{*}\times C_{12}^{*2}\times S_{1122}\times S_{2211}\times S_{3333} +$

$3\times C_{11}^{*}\times C_{12}^{*2}\times S_{1122}\times S_{2233}\times S_{3311} + 3\times C_{11}^{*}\times C_{12}^{*2}\times S_{1133}\times S_{2211}\times S_{3322} -$

$3\times C_{11}^{*}\times C_{12}^{*2}\times S_{1133}\times S_{2222}\times S_{3311} - 4\times C_{11}\times C_{12}\times C_{12}^{*}\times S_{1111}\times S_{2222} + 4\times C_{11}\times C_{12}\times C_{12}^{*}\times S_{1122}\times S_{2211} -$

$C_{11}\times C_{12}\times C_{11}^{*}\times S_{1111}\times S_{2233} + C_{11}\times C_{12}\times C_{11}^{*}\times S_{1133}\times S_{2211} - C_{11}\times C_{12}\times C_{12}^{*}\times S_{1111}\times S_{2233} +$

$C_{11}\times C_{12}\times C_{12}^{*}\times S_{1133}\times S_{2211} + C_{11}\times C_{12}\times C_{11}^{*}\times S_{1122}\times S_{2233} - C_{11}\times C_{12}\times C_{11}^{*}\times S_{1133}\times S_{2222} +$

$C_{11}\times C_{12}\times C_{12}^{*}\times S_{1122}\times S_{2233} - C_{11}\times C_{12}\times C_{12}^{*}\times S_{1133}\times S_{2222} + 2\times C_{12}\times C_{11}^{*}\times C_{12}^{*}\times S_{1111}\times S_{2222} -$

$2\times C_{12}\times C_{11}^{*}\times C_{12}^{*}\times S_{1122}\times S_{2211} - C_{11}\times C_{11}^{*}\times C_{12}^{*}\times S_{1111}\times S_{2233} + C_{11}\times C_{11}^{*}\times C_{12}^{*}\times S_{1133}\times S_{2211} -$

$C_{12}\times C_{11}^{*}\times C_{12}^{*}\times S_{1111}\times S_{2233} + C_{12}\times C_{11}^{*}\times C_{12}^{*}\times S_{1133}\times S_{2211} + C_{11}\times C_{11}^{*}\times C_{12}^{*}\times S_{1122}\times S_{2233} -$

$C_{11}\times C_{11}^{*}\times C_{12}^{*}\times S_{1133}\times S_{2222} + C_{12}\times C_{11}^{*}\times C_{12}^{*}\times S_{1122}\times S_{2233} - C_{12}\times C_{11}^{*}\times C_{12}^{*}\times S_{1133}\times S_{2222} -$

$C_{11}\times C_{12}\times C_{11}^{*}\times S_{1111}\times S_{3322} + C_{11}\times C_{12}\times C_{11}^{*}\times S_{1122}\times S_{3311} - C_{11}\times C_{12}\times C_{12}^{*}\times S_{1111}\times S_{3322} +$

$C_{11}\times C_{12}\times C_{12}^{*}\times S_{1122}\times S_{3311} - 4\times C_{11}\times C_{12}\times C_{12}^{*}\times S_{1111}\times S_{3333} + 4\times C_{11}\times C_{12}\times C_{12}^{*}\times S_{1133}\times S_{3311} -$

$C_{11}\times C_{12}\times C_{11}^{*}\times S_{1122}\times S_{3333} + C_{11}\times C_{12}\times C_{11}^{*}\times S_{1133}\times S_{3322} - C_{11}\times C_{12}\times C_{12}^{*}\times S_{1122}\times S_{3333} +$

$C_{11}\times C_{12}\times C_{12}^{*}\times S_{1133}\times S_{3322} - C_{11}\times C_{11}^{*}\times C_{12}^{*}\times S_{1111}\times S_{3322} + C_{11}\times C_{11}^{*}\times C_{12}^{*}\times S_{1122}\times S_{3311} -$

$C_{12}\times C_{11}^{*}\times C_{12}^{*}\times S_{1111}\times S_{3322} + C_{12}\times C_{11}^{*}\times C_{12}^{*}\times S_{1122}\times S_{3311} + 2\times C_{12}\times C_{11}^{*}\times C_{12}^{*}\times S_{1111}\times S_{3333} -$

$2\times C_{12}\times C_{11}^{*}\times C_{12}^{*}\times S_{1133}\times S_{3311} - C_{11}\times C_{11}^{*}\times C_{12}^{*}\times S_{1122}\times S_{3333} + C_{11}\times C_{11}^{*}\times C_{12}^{*}\times S_{1133}\times S_{3322} -$

$C_{12}\times C_{11}^{*}\times C_{12}^{*}\times S_{1122}\times S_{3333} + C_{12}\times C_{11}^{*}\times C_{12}^{*}\times S_{1133}\times S_{3322} + C_{11}\times C_{12}\times C_{11}^{*}\times S_{2211}\times S_{3322} -$

$C_{11}\times C_{12}\times C_{11}^{*}\times S_{2222}\times S_{3311} + C_{11}\times C_{12}\times C_{12}^{*}\times S_{2211}\times S_{3322} - C_{11}\times C_{12}\times C_{12}^{*}\times S_{2222}\times S_{3311} -$

$C_{11}\times C_{12}\times C_{11}^{*}\times S_{2211}\times S_{3333} + C_{11}\times C_{12}\times C_{11}^{*}\times S_{2233}\times S_{3311} - C_{11}\times C_{12}\times C_{12}^{*}\times S_{2211}\times S_{3333} +$

$C_{11}\times C_{12}\times C_{12}^{*}\times S_{2233}\times S_{3311} - 4\times C_{11}\times C_{12}\times C_{12}^{*}\times S_{2222}\times S_{3333} + 4\times C_{11}\times C_{12}\times C_{12}^{*}\times S_{2233}\times S_{3322} +$

$C_{11}\times C_{11}^{*}\times C_{12}^{*}\times S_{2211}\times S_{3322} - C_{11}\times C_{11}^{*}\times C_{12}^{*}\times S_{2222}\times S_{3311} + C_{12}\times C_{11}^{*}\times C_{12}^{*}\times S_{2211}\times S_{3322} -$

$C_{12}\times C_{11}^{*}\times C_{12}^{*}\times S_{2222}\times S_{3311} - C_{11}\times C_{11}^{*}\times C_{12}^{*}\times S_{2211}\times S_{3333} + C_{11}\times C_{11}^{*}\times C_{12}^{*}\times S_{2233}\times S_{3311} -$

$C_{12}\times C_{11}^{*}\times C_{12}^{*}\times S_{2211}\times S_{3333} + C_{12}\times C_{11}^{*}\times C_{12}^{*}\times S_{2233}\times S_{3311} + 2\times C_{12}\times C_{11}^{*}\times C_{12}^{*}\times S_{2222}\times S_{3333} -$

$2\times C_{12}\times C_{11}^{*}\times C_{12}^{*}\times S_{2233}\times S_{3322} + 6\times C_{11}\times C_{12}\times C_{12}^{*}\times S_{1111}\times S_{2222}\times S_{3333} -$

$6\times C_{11}\times C_{12}\times C_{12}^{*}\times S_{1111}\times S_{2233}\times S_{3322} - 6\times C_{11}\times C_{12}\times C_{12}^{*}\times S_{1122}\times S_{2211}\times S_{3333} +$

$6\times C_{11}\times C_{12}\times C_{12}^{*}\times S_{1122}\times S_{2233}\times S_{3311} + 6\times C_{11}\times C_{12}\times C_{12}^{*}\times S_{1133}\times S_{2211}\times S_{3322} -$

$6\times C_{11}\times C_{12}\times C_{12}^{*}\times S_{1133}\times S_{2222}\times S_{3311} - 6\times C_{12}\times C_{11}^{*}\times C_{12}^{*}\times S_{1111}\times S_{2222}\times S_{3333} +$

$6\times C_{12}\times C_{11}^{*}\times C_{12}^{*}\times S_{1111}\times S_{2233}\times S_{3322} + 6\times C_{12}\times C_{11}^{*}\times C_{12}^{*}\times S_{1122}\times S_{2211}\times S_{3333} -$

$6\times C_{12}\times C_{11}^{*}\times C_{12}^{*}\times S_{1122}\times S_{2233}\times S_{3311} - 6\times C_{12}\times C_{11}^{*}\times C_{12}^{*}\times S_{1133}\times S_{2211}\times S_{3322} +$

$6\times C_{12}\times C_{11}^{*}\times C_{12}^{*}\times S_{1133}\times S_{2222}\times S_{3311})$

$$\sigma_{22} = -(\varepsilon \times (C_{11}^{*} + 2 \times C_{12}^{*}) \times (3 \times C_{11} \times C_{12}^{2} + C_{11}^{3} \times S_{1111} + 2 \times C_{12}^{3} \times S_{1111} + C_{11}^{3} \times S_{2222} + 2 \times C_{12}^{3} \times S_{2222} + C_{11}^{3} \times S_{3333} + 2 \times C_{12}^{3} \times S_{3333} - C_{11}^{3} - 2 \times C_{12}^{3} - 3 \times C_{11} \times C_{12}^{2} \times S_{1111} - C_{11}^{2} \times C_{11}^{*} \times S_{1111} + C_{11}^{2} \times C_{12}^{*} \times S_{1111} + C_{12}^{2} \times C_{11}^{*} \times S_{1111} - C_{12}^{2} \times C_{12}^{*} \times S_{1111} - C_{12}^{2} \times C_{11}^{*} \times S_{1122} + C_{12}^{2} \times C_{12}^{*} \times S_{1122} - C_{12}^{2} \times C_{11}^{*} \times S_{1133} + C_{12}^{2} \times C_{12}^{*} \times S_{1133} - 3 \times C_{11} \times C_{12}^{2} \times S_{2222} + C_{11}^{2} \times C_{11}^{*} \times S_{2211} - C_{11}^{2} \times C_{12}^{*} \times S_{2211} + 2 \times C_{12}^{2} \times C_{11}^{*} \times S_{2222} - 2 \times C_{12}^{2} \times C_{12}^{*} \times S_{2222} + C_{11}^{2} \times C_{11}^{*} \times S_{2233} - C_{11}^{2} \times C_{12}^{*} \times S_{2233} - 3 \times C_{11} \times C_{12}^{2} \times S_{3333} - C_{12}^{2} \times C_{11}^{*} \times S_{3311} + C_{12}^{2} \times C_{12}^{*} \times S_{3311} - C_{12}^{2} \times C_{11}^{*} \times S_{3322} + C_{12}^{2} \times C_{12}^{*} \times S_{3322} - C_{11}^{2} \times C_{11}^{*} \times S_{3333} + C_{11}^{2} \times C_{12}^{*} \times S_{3333} + C_{12}^{2} \times C_{11}^{*} \times S_{3333} - C_{12}^{2} \times C_{12}^{*} \times S_{3333} - C_{11}^{3} \times S_{1111} \times S_{2222} + C_{11}^{3} \times S_{1122} \times S_{2211} - 2 \times C_{12}^{3} \times S_{1111} \times S_{2222} + 2 \times C_{12}^{3} \times S_{1122} \times S_{2211} - C_{11}^{3} \times S_{1111} \times S_{3333} + C_{11}^{3} \times S_{1133} \times S_{3311} - 2 \times C_{12}^{3} \times S_{1111} \times S_{3333} + 2 \times C_{12}^{3} \times S_{1133} \times S_{3311} - C_{11}^{3} \times S_{2222} \times S_{3333} + C_{11}^{3} \times S_{2233} \times S_{3322} - 2 \times C_{12}^{3} \times S_{2222} \times S_{3333} + 2 \times C_{12}^{3} \times S_{2233} \times S_{3322} + C_{11} \times C_{12} \times C_{11}^{*} \times S_{1122} - C_{11} \times C_{12} \times C_{12}^{*} \times S_{1122} + C_{11} \times C_{12} \times C_{11}^{*} \times S_{1133} - C_{11} \times C_{12} \times C_{12}^{*} \times S_{1133} - C_{11} \times C_{12} \times C_{11}^{*} \times S_{2211} + C_{11} \times C_{12} \times C_{12}^{*} \times S_{2211} - 2 \times C_{11} \times C_{12} \times C_{11}^{*} \times S_{2222} + 2 \times C_{11} \times C_{12} \times C_{12}^{*} \times S_{2222} - C_{11} \times C_{12} \times C_{11}^{*} \times S_{2233} + C_{11} \times C_{12} \times C_{12}^{*} \times S_{2233} + C_{11} \times C_{12} \times C_{11}^{*} \times S_{3311} - C_{11} \times C_{12} \times C_{12}^{*} \times S_{3311} + C_{11} \times C_{12} \times C_{11}^{*} \times S_{3322} - C_{11} \times C_{12} \times C_{12}^{*} \times S_{3322} + 3 \times C_{11} \times C_{12}^{2} \times S_{1111} \times S_{2222} - 3 \times C_{11} \times C_{12}^{2} \times S_{1122} \times S_{2211} + C_{11}^{2} \times C_{11}^{*} \times S_{1111} \times S_{2222} - C_{11}^{2} \times C_{11}^{*} \times S_{1122} \times S_{2211} - C_{12} \times C_{11}^{*2} \times S_{1111} \times S_{2222} + C_{12} \times C_{11}^{*2} \times S_{1122} \times S_{2211} - C_{11}^{2} \times C_{12}^{*} \times S_{1111} \times S_{2222} + C_{11}^{2} \times C_{12}^{*} \times S_{1122} \times S_{2211} - 3 \times C_{12}^{2} \times C_{11}^{*} \times S_{1111} \times S_{2222} + 3 \times C_{12}^{2} \times C_{11}^{*} \times S_{1122} \times S_{2211} - C_{12} \times C_{12}^{*2} \times S_{1111} \times S_{2222} + C_{12} \times C_{12}^{*2} \times S_{1122} \times S_{2211} + 3 \times C_{12}^{2} \times C_{12}^{*} \times S_{1111} \times S_{2222} - 3 \times C_{12}^{2} \times C_{12}^{*} \times S_{1122} \times S_{2211} + C_{11} \times C_{11}^{*2} \times S_{1111} \times S_{2233} - C_{11} \times C_{11}^{*2} \times S_{1133} \times S_{2211} - C_{11}^{2} \times C_{11}^{*} \times S_{1111} \times S_{2233} + C_{11}^{2} \times C_{11}^{*} \times S_{1133} \times S_{2211} + C_{11} \times C_{12}^{*2} \times S_{1111} \times S_{2233} - C_{11} \times C_{12}^{*2} \times S_{1133} \times S_{2211} + C_{11}^{2} \times C_{12}^{*} \times S_{1111} \times S_{2233} - C_{11}^{2} \times C_{12}^{*} \times S_{1133} \times S_{2211} - C_{12} \times C_{11}^{*2} \times S_{1122} \times S_{2233} + C_{12} \times C_{11}^{*2} \times S_{1133} \times S_{2222} - C_{12}^{2} \times C_{11}^{*} \times S_{1122} \times S_{2233} + C_{12}^{2} \times C_{11}^{*} \times S_{1133} \times S_{2222} - C_{12} \times C_{12}^{*2} \times S_{1122} \times S_{2233} + C_{12} \times C_{12}^{*2} \times S_{1133} \times S_{2222} + C_{12}^{2} \times C_{12}^{*} \times S_{1122} \times S_{2233} - C_{12}^{2} \times C_{12}^{*} \times S_{1133} \times S_{2222} + 3 \times C_{11} \times C_{12}^{2} \times S_{1111} \times S_{3333} - 3 \times C_{11} \times C_{12}^{2} \times S_{1133} \times S_{3311} + C_{12} \times C_{11}^{*2} \times S_{1111} \times S_{3322} - C_{12} \times C_{11}^{*2} \times S_{1122} \times S_{3311} + C_{12}^{2} \times C_{11}^{*} \times S_{1111} \times S_{3322} - C_{12}^{2} \times C_{11}^{*} \times S_{1122} \times S_{3311} + C_{12} \times C_{12}^{*2} \times S_{1111} \times S_{3322} - C_{12} \times C_{12}^{*2} \times S_{1122} \times S_{3311} - C_{12}^{2} \times C_{12}^{*} \times S_{1111} \times S_{3322} + C_{12}^{2} \times C_{12}^{*} \times S_{1122} \times S_{3311} - C_{11} \times C_{11}^{*2} \times S_{1111} \times S_{3333} + C_{11} \times C_{11}^{*2} \times S_{1133} \times S_{3311} + 2 \times C_{11}^{2} \times C_{11}^{*} \times S_{1111} \times S_{3333} - 2 \times C_{11}^{2} \times C_{11}^{*} \times S_{1133} \times S_{3311} - C_{11} \times C_{12}^{*2} \times S_{1111} \times S_{3333} + C_{11} \times C_{12}^{*2} \times S_{1133} \times S_{3311} -$$

$2\times C_{11}^{2}\times C_{12}^{*}\times S_{1111}\times S_{3333} + 2\times C_{11}^{2}\times C_{12}^{*}\times S_{1133}\times S_{3311} - 2\times C_{12}^{2}\times C_{11}^{*}\times S_{1111}\times S_{3333} +$

$2\times C_{12}^{2}\times C_{11}^{*}\times S_{1133}\times S_{3311} + 2\times C_{12}^{2}\times C_{12}^{*}\times S_{1111}\times S_{3333} - 2\times C_{12}^{2}\times C_{12}^{*}\times S_{1133}\times S_{3311} +$

$C_{12}\times C_{11}^{*2}\times S_{1122}\times S_{3333} - C_{12}\times C_{11}^{*2}\times S_{1133}\times S_{3322} + C_{12}^{2}\times C_{11}^{*}\times S_{1122}\times S_{3333} - C_{12}^{2}\times C_{11}^{*}\times S_{1133}\times S_{3322} +$

$C_{12}\times C_{12}^{*2}\times S_{1122}\times S_{3333} - C_{12}\times C_{12}^{*2}\times S_{1133}\times S_{3322} - C_{12}^{2}\times C_{12}^{*}\times S_{1122}\times S_{3333} + C_{12}^{2}\times C_{12}^{*}\times S_{1133}\times S_{3322} +$

$3\times C_{11}\times C_{12}^{2}\times S_{2222}\times S_{3333} - 3\times C_{11}\times C_{12}^{2}\times S_{2233}\times S_{3322} - C_{12}\times C_{11}^{*2}\times S_{2211}\times S_{3322} + C_{12}\times C_{11}^{*2}\times S_{2222}\times S_{3311}$

$- C_{12}^{2}\times C_{11}^{*}\times S_{2211}\times S_{3322} + C_{12}^{2}\times C_{11}^{*}\times S_{2222}\times S_{3311} - C_{12}\times C_{12}^{*2}\times S_{2211}\times S_{3322} + C_{12}\times C_{12}^{*2}\times S_{2222}\times S_{3311}$

$+ C_{12}^{2}\times C_{12}^{*}\times S_{2211}\times S_{3322} - C_{12}^{2}\times C_{12}^{*}\times S_{2222}\times S_{3311} + C_{11}\times C_{11}^{*2}\times S_{2211}\times S_{3333} - C_{11}\times C_{11}^{*2}\times S_{2233}\times S_{3311} -$

$C_{11}^{2}\times C_{11}^{*}\times S_{2211}\times S_{3333} + C_{11}^{2}\times C_{11}^{*}\times S_{2233}\times S_{3311} + C_{11}\times C_{12}^{*2}\times S_{2211}\times S_{3333} - C_{11}\times C_{12}^{*2}\times S_{2233}\times S_{3311} +$

$C_{11}^{2}\times C_{12}^{*}\times S_{2211}\times S_{3333} - C_{11}^{2}\times C_{12}^{*}\times S_{2233}\times S_{3311} + C_{11}^{2}\times C_{11}^{*}\times S_{2222}\times S_{3333} - C_{11}^{2}\times C_{11}^{*}\times S_{2233}\times S_{3322} -$

$C_{12}\times C_{11}^{*2}\times S_{2222}\times S_{3333} + C_{12}\times C_{11}^{*2}\times S_{2233}\times S_{3322} - C_{11}^{2}\times C_{12}^{*}\times S_{2222}\times S_{3333} + C_{11}^{2}\times C_{12}^{*}\times S_{2233}\times S_{3322} -$

$3\times C_{12}^{2}\times C_{11}^{*}\times S_{2222}\times S_{3333} + 3\times C_{12}^{2}\times C_{11}^{*}\times S_{2233}\times S_{3322} - C_{12}\times C_{12}^{*2}\times S_{2222}\times S_{3333} +$

$C_{12}\times C_{12}^{*2}\times S_{2233}\times S_{3322} + 3\times C_{12}^{2}\times C_{12}^{*}\times S_{2222}\times S_{3333} - 3\times C_{12}^{2}\times C_{12}^{*}\times S_{2233}\times S_{3322} +$

$C_{11}^{3}\times S_{1111}\times S_{2222}\times S_{3333} - C_{11}^{3}\times S_{1111}\times S_{2233}\times S_{3322} - C_{11}^{3}\times S_{1122}\times S_{2211}\times S_{3333} + C_{11}^{3}\times S_{1122}\times S_{2233}\times S_{3311} +$

$C_{11}^{3}\times S_{1133}\times S_{2211}\times S_{3322} - C_{11}^{3}\times S_{1133}\times S_{2222}\times S_{3311} + 2\times C_{12}^{3}\times S_{1111}\times S_{2222}\times S_{3333} -$

$2\times C_{12}^{3}\times S_{1111}\times S_{2233}\times S_{3322} - 2\times C_{12}^{3}\times S_{1122}\times S_{2211}\times S_{3333} + 2\times C_{12}^{3}\times S_{1122}\times S_{2233}\times S_{3311} +$

$2\times C_{12}^{3}\times S_{1133}\times S_{2211}\times S_{3322} - 2\times C_{12}^{3}\times S_{1133}\times S_{2222}\times S_{3311} - 3\times C_{11}\times C_{12}^{2}\times S_{1111}\times S_{2222}\times S_{3333} +$

$3\times C_{11}\times C_{12}^{2}\times S_{1111}\times S_{2233}\times S_{3322} + 3\times C_{11}\times C_{12}^{2}\times S_{1122}\times S_{2211}\times S_{3333} - 3\times C_{11}\times C_{12}^{2}\times S_{1122}\times S_{2233}\times S_{3311} -$

$3\times C_{11}\times C_{12}^{2}\times S_{1133}\times S_{2211}\times S_{3322} + 3\times C_{11}\times C_{12}^{2}\times S_{1133}\times S_{2222}\times S_{3311} + C_{11}\times C_{11}^{*2}\times S_{1111}\times S_{2222}\times S_{3333} -$

$C_{11}\times C_{11}^{*2}\times S_{1111}\times S_{2233}\times S_{3322} - C_{11}\times C_{11}^{*2}\times S_{1122}\times S_{2211}\times S_{3333} + C_{11}\times C_{11}^{*2}\times S_{1122}\times S_{2233}\times S_{3311} +$

$C_{11}\times C_{11}^{*2}\times S_{1133}\times S_{2211}\times S_{3322} - C_{11}\times C_{11}^{*2}\times S_{1133}\times S_{2222}\times S_{3311} - 2\times C_{11}^{2}\times C_{11}^{*}\times S_{1111}\times S_{2222}\times S_{3333} +$

$2\times C_{11}^{2}\times C_{11}^{*}\times S_{1111}\times S_{2233}\times S_{3322} + 2\times C_{11}^{2}\times C_{11}^{*}\times S_{1122}\times S_{2211}\times S_{3333} - 2\times C_{11}^{2}\times C_{11}^{*}\times S_{1122}\times S_{2233}\times S_{3311} -$

$2\times C_{11}^{2}\times C_{11}^{*}\times S_{1133}\times S_{2211}\times S_{3322} + 2\times C_{11}^{2}\times C_{11}^{*}\times S_{1133}\times S_{2222}\times S_{3311} + C_{11}\times C_{12}^{*2}\times S_{1111}\times S_{2222}\times S_{3333} -$

$C_{11}\times C_{12}^{*2}\times S_{1111}\times S_{2233}\times S_{3322} - C_{11}\times C_{12}^{*2}\times S_{1122}\times S_{2211}\times S_{3333} + C_{11}\times C_{12}^{*2}\times S_{1122}\times S_{2233}\times S_{3311} +$

$C_{11}\times C_{12}^{*2}\times S_{1133}\times S_{2211}\times S_{3322} - C_{11}\times C_{12}^{*2}\times S_{1133}\times S_{2222}\times S_{3311} + 2\times C_{12}\times C_{11}^{*2}\times S_{1111}\times S_{2222}\times S_{3333} -$

$2\times C_{12}\times C_{11}^{*2}\times S_{1111}\times S_{2233}\times S_{3322} - 2\times C_{12}\times C_{11}^{*2}\times S_{1122}\times S_{2211}\times S_{3333} + 2\times C_{12}\times C_{11}^{*2}\times S_{1122}\times S_{2233}\times S_{3311}$

$+ 2\times C_{12}\times C_{11}^{*2}\times S_{1133}\times S_{2211}\times S_{3322} - 2\times C_{12}\times C_{11}^{*2}\times S_{1133}\times S_{2222}\times S_{3311} +$

$2\times C_{11}^2\times C_{12}^*\times S_{1111}\times S_{2222}\times S_{3333} - 2\times C_{11}^2\times C_{12}^*\times S_{1111}\times S_{2233}\times S_{3322} - 2\times C_{11}^2\times C_{12}^*\times S_{1122}\times S_{2211}\times S_{3333} +$

$2\times C_{11}^2\times C_{12}^*\times S_{1122}\times S_{2233}\times S_{3311} + 2\times C_{11}^2\times C_{12}^*\times S_{1133}\times S_{2211}\times S_{3322} - 2\times C_{11}^2\times C_{12}^*\times S_{1133}\times S_{2222}\times S_{3311}$

$+ 4\times C_{12}^2\times C_{11}^*\times S_{1111}\times S_{2222}\times S_{3333} - 4\times C_{12}^2\times C_{11}^*\times S_{1111}\times S_{2233}\times S_{3322} - 4\times C_{12}^2\times C_{11}^*\times S_{1122}\times S_{2211}\times S_{3333}$

$+ 4\times C_{12}^2\times C_{11}^*\times S_{1122}\times S_{2233}\times S_{3311} + 4\times C_{12}^2\times C_{11}^*\times S_{1133}\times S_{2211}\times S_{3322} -$

$4\times C_{12}^2\times C_{11}^*\times S_{1133}\times S_{2222}\times S_{3311} + 2\times C_{12}\times C_{12}^{*2}\times S_{1111}\times S_{2222}\times S_{3333} - 2\times C_{12}\times C_{12}^{*2}\times S_{1111}\times S_{2233}\times S_{3322} -$

$2\times C_{12}\times C_{12}^{*2}\times S_{1122}\times S_{2211}\times S_{3333} + 2\times C_{12}\times C_{12}^{*2}\times S_{1122}\times S_{2233}\times S_{3311} + 2\times C_{12}\times C_{12}^{*2}\times S_{1133}\times S_{2211}\times S_{3322}$

$- 2\times C_{12}\times C_{12}^{*2}\times S_{1133}\times S_{2222}\times S_{3311} - 4\times C_{12}^2\times C_{12}^*\times S_{1111}\times S_{2222}\times S_{3333} + 4\times C_{12}^2\times C_{12}^*\times S_{1111}\times S_{2233}\times S_{3322}$

$+ 4\times C_{12}^2\times C_{12}^*\times S_{1122}\times S_{2211}\times S_{3333} - 4\times C_{12}^2\times C_{12}^*\times S_{1122}\times S_{2233}\times S_{3311} - 4\times C_{12}^2\times C_{12}^*\times S_{1133}\times S_{2211}\times S_{3322}$

$+ 4\times C_{12}^2\times C_{12}^*\times S_{1133}\times S_{2222}\times S_{3311} + 2\times C_{11}\times C_{12}\times C_{11}^*\times S_{1111}\times S_{2222} - 2\times C_{11}\times C_{12}\times C_{11}^*\times S_{1122}\times S_{2211} -$

$2\times C_{11}\times C_{12}\times C_{12}^*\times S_{1111}\times S_{2222} + 2\times C_{11}\times C_{12}\times C_{12}^*\times S_{1122}\times S_{2211} + C_{11}\times C_{12}\times C_{11}^*\times S_{1111}\times S_{2233} -$

$C_{11}\times C_{12}\times C_{11}^*\times S_{1133}\times S_{2211} - C_{11}\times C_{12}\times C_{12}^*\times S_{1111}\times S_{2233} + C_{11}\times C_{12}\times C_{12}^*\times S_{1133}\times S_{2211} +$

$C_{11}\times C_{12}\times C_{11}^*\times S_{1122}\times S_{2233} - C_{11}\times C_{12}\times C_{11}^*\times S_{1133}\times S_{2222} - C_{11}\times C_{12}\times C_{12}^*\times S_{1122}\times S_{2233} +$

$C_{11}\times C_{12}\times C_{12}^*\times S_{1133}\times S_{2222} + 2\times C_{12}\times C_{11}^*\times C_{12}^*\times S_{1111}\times S_{2222} - 2\times C_{12}\times C_{11}^*\times C_{12}^*\times S_{1122}\times S_{2211} -$

$2\times C_{11}\times C_{11}^*\times C_{12}^*\times S_{1111}\times S_{2233} + 2\times C_{11}\times C_{11}^*\times C_{12}^*\times S_{1133}\times S_{2211} + 2\times C_{12}\times C_{11}^*\times C_{12}^*\times S_{1122}\times S_{2233} -$

$2\times C_{12}\times C_{11}^*\times C_{12}^*\times S_{1133}\times S_{2222} - C_{11}\times C_{12}\times C_{11}^*\times S_{1111}\times S_{3322} + C_{11}\times C_{12}\times C_{11}^*\times S_{1122}\times S_{3311} +$

$C_{11}\times C_{12}\times C_{12}^*\times S_{1111}\times S_{3322} - C_{11}\times C_{12}\times C_{12}^*\times S_{1122}\times S_{3311} - C_{11}\times C_{12}\times C_{11}^*\times S_{1122}\times S_{3333} +$

$C_{11}\times C_{12}\times C_{11}^*\times S_{1133}\times S_{3322} + C_{11}\times C_{12}\times C_{12}^*\times S_{1122}\times S_{3333} - C_{11}\times C_{12}\times C_{12}^*\times S_{1133}\times S_{3322} -$

$2\times C_{12}\times C_{11}^*\times C_{12}^*\times S_{1111}\times S_{3322} + 2\times C_{12}\times C_{11}^*\times C_{12}^*\times S_{1122}\times S_{3311} + 2\times C_{11}\times C_{11}^*\times C_{12}^*\times S_{1111}\times S_{3333} -$

$2\times C_{11}\times C_{11}^*\times C_{12}^*\times S_{1133}\times S_{3311} - 2\times C_{12}\times C_{11}^*\times C_{12}^*\times S_{1122}\times S_{3333} + 2\times C_{12}\times C_{11}^*\times C_{12}^*\times S_{1133}\times S_{3322} +$

$C_{11}\times C_{12}\times C_{11}^*\times S_{2211}\times S_{3322} - C_{11}\times C_{12}\times C_{11}^*\times S_{2222}\times S_{3311} - C_{11}\times C_{12}\times C_{12}^*\times S_{2211}\times S_{3322} +$

$C_{11}\times C_{12}\times C_{12}^*\times S_{2222}\times S_{3311} + C_{11}\times C_{12}\times C_{11}^*\times S_{2211}\times S_{3333} - C_{11}\times C_{12}\times C_{11}^*\times S_{2233}\times S_{3311} -$

$C_{11}\times C_{12}\times C_{12}^*\times S_{2211}\times S_{3333} + C_{11}\times C_{12}\times C_{12}^*\times S_{2233}\times S_{3311} + 2\times C_{11}\times C_{12}\times C_{11}^*\times S_{2222}\times S_{3333} -$

$2\times C_{11}\times C_{12}\times C_{11}^*\times S_{2233}\times S_{3322} - 2\times C_{11}\times C_{12}\times C_{12}^*\times S_{2222}\times S_{3333} + 2\times C_{11}\times C_{12}\times C_{12}^*\times S_{2233}\times S_{3322} +$

$2\times C_{12}\times C_{11}^*\times C_{12}^*\times S_{2211}\times S_{3322} - 2\times C_{12}\times C_{11}^*\times C_{12}^*\times S_{2222}\times S_{3311} - 2\times C_{11}\times C_{11}^*\times C_{12}^*\times S_{2211}\times S_{3333} +$

$2\times C_{11}\times C_{11}^*\times C_{12}^*\times S_{2233}\times S_{3311} + 2\times C_{12}\times C_{11}^*\times C_{12}^*\times S_{2222}\times S_{3333} - 2\times C_{12}\times C_{11}^*\times C_{12}^*\times S_{2233}\times S_{3322} -$

$2\times C_{11}\times C_{12}\times C_{11}^*\times S_{1111}\times S_{2222}\times S_{3333} + 2\times C_{11}\times C_{12}\times C_{11}^*\times S_{1111}\times S_{2233}\times S_{3322} +$

$2\times C_{11}\times C_{12}\times C_{11}^{*}\times S_{1122}\times S_{2211}\times S_{3333} - 2\times C_{11}\times C_{12}\times C_{11}^{*}\times S_{1122}\times S_{2233}\times S_{3311} -$

$2\times C_{11}\times C_{12}\times C_{11}^{*}\times S_{1133}\times S_{2211}\times S_{3322} + 2\times C_{11}\times C_{12}\times C_{11}^{*}\times S_{1133}\times S_{2222}\times S_{3311} +$

$2\times C_{11}\times C_{12}\times C_{12}^{*}\times S_{1111}\times S_{2222}\times S_{3333} - 2\times C_{11}\times C_{12}\times C_{12}^{*}\times S_{1111}\times S_{2233}\times S_{3322} -$

$2\times C_{11}\times C_{12}\times C_{12}^{*}\times S_{1122}\times S_{2211}\times S_{3333} + 2\times C_{11}\times C_{12}\times C_{12}^{*}\times S_{1122}\times S_{2233}\times S_{3311} +$

$2\times C_{11}\times C_{12}\times C_{12}^{*}\times S_{1133}\times S_{2211}\times S_{3322} - 2\times C_{11}\times C_{12}\times C_{12}^{*}\times S_{1133}\times S_{2222}\times S_{3311} -$

$2\times C_{11}\times C_{11}^{*}\times C_{12}^{*}\times S_{1111}\times S_{2222}\times S_{3333} + 2\times C_{11}\times C_{11}^{*}\times C_{12}^{*}\times S_{1111}\times S_{2233}\times S_{3322} +$

$2\times C_{11}\times C_{11}^{*}\times C_{12}^{*}\times S_{1122}\times S_{2211}\times S_{3333} - 2\times C_{11}\times C_{11}^{*}\times C_{12}^{*}\times S_{1122}\times S_{2233}\times S_{3311} -$

$2\times C_{11}\times C_{11}^{*}\times C_{12}^{*}\times S_{1133}\times S_{2211}\times S_{3322} + 2\times C_{11}\times C_{11}^{*}\times C_{12}^{*}\times S_{1133}\times S_{2222}\times S_{3311} -$

$4\times C_{12}\times C_{11}^{*}\times C_{12}^{*}\times S_{1111}\times S_{2222}\times S_{3333} + 4\times C_{12}\times C_{11}^{*}\times C_{12}^{*}\times S_{1111}\times S_{2233}\times S_{3322} +$

$4\times C_{12}\times C_{11}^{*}\times C_{12}^{*}\times S_{1122}\times S_{2211}\times S_{3333} - 4\times C_{12}\times C_{11}^{*}\times C_{12}^{*}\times S_{1122}\times S_{2233}\times S_{3311} -$

$4\times C_{12}\times C_{11}^{*}\times C_{12}^{*}\times S_{1133}\times S_{2211}\times S_{3322} + 4\times C_{12}\times C_{11}^{*}\times C_{12}^{*}\times S_{1133}\times S_{2222}\times S_{3311}))/(3\times C_{11}\times C_{12}^{2} +$

$C_{11}^{3}\times S_{1111} + 2\times C_{12}^{3}\times S_{1111} + C_{11}^{3}\times S_{2222} + 2\times C_{12}^{3}\times S_{2222} + C_{11}^{3}\times S_{3333} + 2\times C_{12}^{3}\times S_{3333} - C_{11}^{3} - 2\times C_{12}^{3} -$

$3\times C_{11}\times C_{12}^{2}\times S_{1111} - C_{11}^{2}\times C_{11}^{*}\times S_{1111} + C_{12}^{2}\times C_{11}^{*}\times S_{1111} - 2\times C_{12}^{2}\times C_{12}^{*}\times S_{1111} - C_{11}^{2}\times C_{12}^{*}\times S_{1122} -$

$C_{12}^{2}\times C_{11}^{*}\times S_{1122} - C_{11}^{2}\times C_{12}^{*}\times S_{1133} - C_{12}^{2}\times C_{11}^{*}\times S_{1133} - 3\times C_{11}\times C_{12}^{2}\times S_{2222} - C_{11}^{2}\times C_{12}^{*}\times S_{2211} -$

$C_{12}^{2}\times C_{11}^{*}\times S_{2211} - C_{11}^{2}\times C_{11}^{*}\times S_{2222} + C_{12}^{2}\times C_{11}^{*}\times S_{2222} - 2\times C_{12}^{2}\times C_{12}^{*}\times S_{2222} - C_{11}^{2}\times C_{12}^{*}\times S_{2233} -$

$C_{12}^{2}\times C_{11}^{*}\times S_{2233} - 3\times C_{11}\times C_{12}^{2}\times S_{3333} - C_{11}^{2}\times C_{12}^{*}\times S_{3311} - C_{12}^{2}\times C_{11}^{*}\times S_{3311} - C_{11}^{2}\times C_{12}^{*}\times S_{3322} -$

$C_{12}^{2}\times C_{11}^{*}\times S_{3322} - C_{11}^{2}\times C_{11}^{*}\times S_{3333} + C_{12}^{2}\times C_{11}^{*}\times S_{3333} - 2\times C_{12}^{2}\times C_{12}^{*}\times S_{3333} - C_{11}^{3}\times S_{1111}\times S_{2222} +$

$C_{11}^{3}\times S_{1122}\times S_{2211} - 2\times C_{12}^{3}\times S_{1111}\times S_{2222} + 2\times C_{12}^{3}\times S_{1122}\times S_{2211} - C_{11}^{3}\times S_{1111}\times S_{3333} + C_{11}^{3}\times S_{1133}\times S_{3311} -$

$2\times C_{12}^{3}\times S_{1111}\times S_{3333} + 2\times C_{12}^{3}\times S_{1133}\times S_{3311} - C_{11}^{3}\times S_{2222}\times S_{3333} + C_{11}^{3}\times S_{2233}\times S_{3322} - 2\times C_{12}^{3}\times S_{2222}\times S_{3333}$

$+ 2\times C_{12}^{3}\times S_{2233}\times S_{3322} + 2\times C_{11}\times C_{12}\times C_{12}^{*}\times S_{1111} + C_{11}\times C_{12}\times C_{11}^{*}\times S_{1122} + C_{11}\times C_{12}\times C_{12}^{*}\times S_{1122} +$

$C_{11}\times C_{12}\times C_{11}^{*}\times S_{1133} + C_{11}\times C_{12}\times C_{12}^{*}\times S_{1133} + C_{11}\times C_{12}\times C_{11}^{*}\times S_{2211} + C_{11}\times C_{12}\times C_{12}^{*}\times S_{2211} +$

$2\times C_{11}\times C_{12}\times C_{12}^{*}\times S_{2222} + C_{11}\times C_{12}\times C_{11}^{*}\times S_{2233} + C_{11}\times C_{12}\times C_{12}^{*}\times S_{2233} + C_{11}\times C_{12}\times C_{11}^{*}\times S_{3311} +$

$C_{11}\times C_{12}\times C_{12}^{*}\times S_{3311} + C_{11}\times C_{12}\times C_{11}^{*}\times S_{3322} + C_{11}\times C_{12}\times C_{12}^{*}\times S_{3322} + 2\times C_{11}\times C_{12}\times C_{12}^{*}\times S_{3333} +$

$3\times C_{11}\times C_{12}^{2}\times S_{1111}\times S_{2222} - 3\times C_{11}\times C_{12}^{2}\times S_{1122}\times S_{2211} - C_{11}\times C_{11}^{*2}\times S_{1111}\times S_{2222} + C_{11}\times C_{11}^{*2}\times S_{1122}\times S_{2211}$

$+ 2\times C_{11}^{2}\times C_{11}^{*}\times S_{1111}\times S_{2222} - 2\times C_{11}^{2}\times C_{11}^{*}\times S_{1122}\times S_{2211} + C_{11}\times C_{12}^{*2}\times S_{1111}\times S_{2222} -$

$C_{11}\times C_{12}^{*2}\times S_{1122}\times S_{2211} - 2\times C_{12}^{2}\times C_{11}^{*}\times S_{1111}\times S_{2222} + 2\times C_{12}^{2}\times C_{11}^{*}\times S_{1122}\times S_{2211} -$

$2\times C_{12}\times C_{12}^{*2}\times S_{1111}\times S_{2222} + 2\times C_{12}\times C_{12}^{*2}\times S_{1122}\times S_{2211} + 4\times C_{12}^{2}\times C_{12}^{*}\times S_{1111}\times S_{2222} -$

$4\times C_{12}^{2}\times C_{12}^{*}\times S_{1122}\times S_{2211} + C_{11}\times C_{12}^{*2}\times S_{1111}\times S_{2233} - C_{11}\times C_{12}^{*2}\times S_{1133}\times S_{2211} + C_{12}\times C_{11}^{*2}\times S_{1111}\times S_{2233}$

$- C_{12}\times C_{11}^{*2}\times S_{1133}\times S_{2211} + C_{11}^{2}\times C_{12}^{*}\times S_{1111}\times S_{2233} - C_{11}^{2}\times C_{12}^{*}\times S_{1133}\times S_{2211} + C_{12}^{2}\times C_{11}^{*}\times S_{1111}\times S_{2233} -$

$C_{12}^{2}\times C_{11}^{*}\times S_{1133}\times S_{2211} - C_{11}\times C_{12}^{*2}\times S_{1122}\times S_{2233} + C_{11}\times C_{12}^{*2}\times S_{1133}\times S_{2222} - C_{12}\times C_{11}^{*2}\times S_{1122}\times S_{2233} +$

$C_{12}\times C_{11}^{*2}\times S_{1133}\times S_{2222} - C_{11}^{2}\times C_{12}^{*}\times S_{1122}\times S_{2233} + C_{11}^{2}\times C_{12}^{*}\times S_{1133}\times S_{2222} - C_{12}^{2}\times C_{11}^{*}\times S_{1122}\times S_{2233} +$

$C_{12}^{2}\times C_{11}^{*}\times S_{1133}\times S_{2222} + 3\times C_{11}\times C_{12}^{2}\times S_{1111}\times S_{3333} - 3\times C_{11}\times C_{12}^{2}\times S_{1133}\times S_{3311} + C_{11}\times C_{12}^{*2}\times S_{1111}\times S_{3322}$

$- C_{11}\times C_{12}^{*2}\times S_{1122}\times S_{3311} + C_{12}\times C_{11}^{*2}\times S_{1111}\times S_{3322} - C_{12}\times C_{11}^{*2}\times S_{1122}\times S_{3311} + C_{11}^{2}\times C_{12}^{*}\times S_{1111}\times S_{3322} -$

$C_{11}^{2}\times C_{12}^{*}\times S_{1122}\times S_{3311} + C_{12}^{2}\times C_{11}^{*}\times S_{1111}\times S_{3322} - C_{12}^{2}\times C_{11}^{*}\times S_{1122}\times S_{3311} - C_{11}\times C_{11}^{*2}\times S_{1111}\times S_{3333} +$

$C_{11}\times C_{11}^{*2}\times S_{1133}\times S_{3311} + 2\times C_{11}^{2}\times C_{11}^{*}\times S_{1111}\times S_{3333} - 2\times C_{11}^{2}\times C_{11}^{*}\times S_{1133}\times S_{3311} +$

$C_{11}\times C_{12}^{*2}\times S_{1111}\times S_{3333} - C_{11}\times C_{12}^{*2}\times S_{1133}\times S_{3311} - 2\times C_{12}^{2}\times C_{11}^{*}\times S_{1111}\times S_{3333} +$

$2\times C_{12}^{2}\times C_{11}^{*}\times S_{1133}\times S_{3311} - 2\times C_{12}\times C_{12}^{*2}\times S_{1111}\times S_{3333} + 2\times C_{12}\times C_{12}^{*2}\times S_{1133}\times S_{3311} +$

$4\times C_{12}^{2}\times C_{12}^{*}\times S_{1111}\times S_{3333} - 4\times C_{12}^{2}\times C_{12}^{*}\times S_{1133}\times S_{3311} + C_{11}\times C_{12}^{*2}\times S_{1122}\times S_{3333} -$

$C_{11}\times C_{12}^{*2}\times S_{1133}\times S_{3322} + C_{12}\times C_{11}^{*2}\times S_{1122}\times S_{3333} - C_{12}\times C_{11}^{*2}\times S_{1133}\times S_{3322} + C_{11}^{2}\times C_{12}^{*}\times S_{1122}\times S_{3333} -$

$C_{11}^{2}\times C_{12}^{*}\times S_{1133}\times S_{3322} + C_{12}^{2}\times C_{11}^{*}\times S_{1122}\times S_{3333} - C_{12}^{2}\times C_{11}^{*}\times S_{1133}\times S_{3322} + 3\times C_{11}\times C_{12}^{2}\times S_{2222}\times S_{3333} -$

$3\times C_{11}\times C_{12}^{2}\times S_{2233}\times S_{3322} - C_{11}\times C_{12}^{*2}\times S_{2211}\times S_{3322} + C_{11}\times C_{12}^{*2}\times S_{2222}\times S_{3311} - C_{12}\times C_{11}^{*2}\times S_{2211}\times S_{3322} +$

$C_{12}\times C_{11}^{*2}\times S_{2222}\times S_{3311} - C_{11}^{2}\times C_{12}^{*}\times S_{2211}\times S_{3322} + C_{11}^{2}\times C_{12}^{*}\times S_{2222}\times S_{3311} - C_{12}^{2}\times C_{11}^{*}\times S_{2211}\times S_{3322} +$

$C_{12}^{2}\times C_{11}^{*}\times S_{2222}\times S_{3311} + C_{11}\times C_{12}^{*2}\times S_{2211}\times S_{3333} - C_{11}\times C_{12}^{*2}\times S_{2233}\times S_{3311} + C_{12}\times C_{11}^{*2}\times S_{2211}\times S_{3333} -$

$C_{12}\times C_{11}^{*2}\times S_{2233}\times S_{3311} + C_{11}^{2}\times C_{12}^{*}\times S_{2211}\times S_{3333} - C_{11}^{2}\times C_{12}^{*}\times S_{2233}\times S_{3311} + C_{12}^{2}\times C_{11}^{*}\times S_{2211}\times S_{3333} -$

$C_{12}^{2}\times C_{11}^{*}\times S_{2233}\times S_{3311} - C_{11}\times C_{11}^{*2}\times S_{2222}\times S_{3333} + C_{11}\times C_{11}^{*2}\times S_{2233}\times S_{3322} + 2\times C_{11}^{2}\times C_{11}^{*}\times S_{2222}\times S_{3333}$

$- 2\times C_{11}^{2}\times C_{11}^{*}\times S_{2233}\times S_{3322} + C_{11}\times C_{12}^{*2}\times S_{2222}\times S_{3333} - C_{11}\times C_{12}^{*2}\times S_{2233}\times S_{3322} -$

$2\times C_{12}^{2}\times C_{11}^{*}\times S_{2222}\times S_{3333} + 2\times C_{12}^{2}\times C_{11}^{*}\times S_{2233}\times S_{3322} - 2\times C_{12}\times C_{12}^{*2}\times S_{2222}\times S_{3333} +$

$2\times C_{12}\times C_{12}^{*2}\times S_{2233}\times S_{3322} + 4\times C_{12}^{2}\times C_{12}^{*}\times S_{2222}\times S_{3333} - 4\times C_{12}^{2}\times C_{12}^{*}\times S_{2233}\times S_{3322} +$

$C_{11}^{3}\times S_{1111}\times S_{2222}\times S_{3333} - C_{11}^{3}\times S_{1111}\times S_{2233}\times S_{3322} - C_{11}^{3}\times S_{1122}\times S_{2211}\times S_{3333} + C_{11}^{3}\times S_{1122}\times S_{2233}\times S_{3311} +$

$C_{11}^{3}\times S_{1133}\times S_{2211}\times S_{3322} - C_{11}^{3}\times S_{1133}\times S_{2222}\times S_{3311} + 2\times C_{12}^{3}\times S_{1111}\times S_{2222}\times S_{3333} -$

$2\times C_{12}^{3}\times S_{1111}\times S_{2233}\times S_{3322} - 2\times C_{12}^{3}\times S_{1122}\times S_{2211}\times S_{3333} + 2\times C_{12}^{3}\times S_{1122}\times S_{2233}\times S_{3311} +$

$2\times C_{12}^{3}\times S_{1133}\times S_{2211}\times S_{3322} - 2\times C_{12}^{3}\times S_{1133}\times S_{2222}\times S_{3311} - C_{11}^{*3}\times S_{1111}\times S_{2222}\times S_{3333} +$

$C_{11}{}^{*3}\times S_{1111}\times S_{2233}\times S_{3322} + C_{11}{}^{*3}\times S_{1122}\times S_{2211}\times S_{3333} - C_{11}{}^{*3}\times S_{1122}\times S_{2233}\times S_{3311} -$

$C_{11}{}^{*3}\times S_{1133}\times S_{2211}\times S_{3322} + C_{11}{}^{*3}\times S_{1133}\times S_{2222}\times S_{3311} - 2\times C_{12}{}^{*3}\times S_{1111}\times S_{2222}\times S_{3333} +$

$2\times C_{12}{}^{*3}\times S_{1111}\times S_{2233}\times S_{3322} + 2\times C_{12}{}^{*3}\times S_{1122}\times S_{2211}\times S_{3333} - 2\times C_{12}{}^{*3}\times S_{1122}\times S_{2233}\times S_{3311} -$

$2\times C_{12}{}^{*3}\times S_{1133}\times S_{2211}\times S_{3322} + 2\times C_{12}{}^{*3}\times S_{1133}\times S_{2222}\times S_{3311} - 3\times C_{11}\times C_{12}{}^{2}\times S_{1111}\times S_{2222}\times S_{3333} +$

$3\times C_{11}\times C_{12}{}^{2}\times S_{1111}\times S_{2233}\times S_{3322} + 3\times C_{11}\times C_{12}{}^{2}\times S_{1122}\times S_{2211}\times S_{3333} - 3\times C_{11}\times C_{12}{}^{2}\times S_{1122}\times S_{2233}\times S_{3311} -$

$3\times C_{11}\times C_{12}{}^{2}\times S_{1133}\times S_{2211}\times S_{3322} + 3\times C_{11}\times C_{12}{}^{2}\times S_{1133}\times S_{2222}\times S_{3311} + 3\times C_{11}\times C_{11}{}^{*2}\times S_{1111}\times S_{2222}\times S_{3333} -$

$3\times C_{11}\times C_{11}{}^{*2}\times S_{1111}\times S_{2233}\times S_{3322} - 3\times C_{11}\times C_{11}{}^{*2}\times S_{1122}\times S_{2211}\times S_{3333} + 3\times C_{11}\times C_{11}{}^{*2}\times S_{1122}\times S_{2233}\times S_{3311}$

$+ 3\times C_{11}\times C_{11}{}^{*2}\times S_{1133}\times S_{2211}\times S_{3322} - 3\times C_{11}\times C_{11}{}^{*2}\times S_{1133}\times S_{2222}\times S_{3311} - 3\times C_{11}{}^{2}\times C_{11}{}^{*}\times S_{1111}\times S_{2222}\times S_{3333}$

$+ 3\times C_{11}{}^{2}\times C_{11}{}^{*}\times S_{1111}\times S_{2233}\times S_{3322} + 3\times C_{11}{}^{2}\times C_{11}{}^{*}\times S_{1122}\times S_{2211}\times S_{3333} -$

$3\times C_{11}{}^{2}\times C_{11}{}^{*}\times S_{1122}\times S_{2233}\times S_{3311} - 3\times C_{11}{}^{2}\times C_{11}{}^{*}\times S_{1133}\times S_{2211}\times S_{3322} + 3\times C_{11}{}^{2}\times C_{11}{}^{*}\times S_{1133}\times S_{2222}\times S_{3311} -$

$3\times C_{11}\times C_{12}{}^{*2}\times S_{1111}\times S_{2222}\times S_{3333} + 3\times C_{11}\times C_{12}{}^{*2}\times S_{1111}\times S_{2233}\times S_{3322} + 3\times C_{11}\times C_{12}{}^{*2}\times S_{1122}\times S_{2211}\times S_{3333}$

$- 3\times C_{11}\times C_{12}{}^{*2}\times S_{1122}\times S_{2233}\times S_{3311} - 3\times C_{11}\times C_{12}{}^{*2}\times S_{1133}\times S_{2211}\times S_{3322} + 3\times C_{11}\times C_{12}{}^{*2}\times S_{1133}\times S_{2222}\times S_{3311}$

$+ 3\times C_{12}{}^{2}\times C_{11}{}^{*}\times S_{1111}\times S_{2222}\times S_{3333} - 3\times C_{12}{}^{2}\times C_{11}{}^{*}\times S_{1111}\times S_{2233}\times S_{3322} - 3\times C_{12}{}^{2}\times C_{11}{}^{*}\times S_{1122}\times S_{2211}\times S_{3333}$

$+ 3\times C_{12}{}^{2}\times C_{11}{}^{*}\times S_{1122}\times S_{2233}\times S_{3311} + 3\times C_{12}{}^{2}\times C_{11}{}^{*}\times S_{1133}\times S_{2211}\times S_{3322} -$

$3\times C_{12}{}^{2}\times C_{11}{}^{*}\times S_{1133}\times S_{2222}\times S_{3311} + 6\times C_{12}\times C_{12}{}^{*2}\times S_{1111}\times S_{2222}\times S_{3333} - 6\times C_{12}\times C_{12}{}^{*2}\times S_{1111}\times S_{2233}\times S_{3322} -$

$6\times C_{12}\times C_{12}{}^{*2}\times S_{1122}\times S_{2211}\times S_{3333} + 6\times C_{12}\times C_{12}{}^{*2}\times S_{1122}\times S_{2233}\times S_{3311} + 6\times C_{12}\times C_{12}{}^{*2}\times S_{1133}\times S_{2211}\times S_{3322}$

$- 6\times C_{12}\times C_{12}{}^{*2}\times S_{1133}\times S_{2222}\times S_{3311} - 6\times C_{12}{}^{2}\times C_{12}{}^{*}\times S_{1111}\times S_{2222}\times S_{3333} + 6\times C_{12}{}^{2}\times C_{12}{}^{*}\times S_{1111}\times S_{2233}\times S_{3322}$

$+ 6\times C_{12}{}^{2}\times C_{12}{}^{*}\times S_{1122}\times S_{2211}\times S_{3333} - 6\times C_{12}{}^{2}\times C_{12}{}^{*}\times S_{1122}\times S_{2233}\times S_{3311} - 6\times C_{12}{}^{2}\times C_{12}{}^{*}\times S_{1133}\times S_{2211}\times S_{3322}$

$+ 6\times C_{12}{}^{2}\times C_{12}{}^{*}\times S_{1133}\times S_{2222}\times S_{3311} + 3\times C_{11}{}^{*}\times C_{12}{}^{*2}\times S_{1111}\times S_{2222}\times S_{3333} -$

$3\times C_{11}{}^{*}\times C_{12}{}^{*2}\times S_{1111}\times S_{2233}\times S_{3322} - 3\times C_{11}{}^{*}\times C_{12}{}^{*2}\times S_{1122}\times S_{2211}\times S_{3333} +$

$3\times C_{11}{}^{*}\times C_{12}{}^{*2}\times S_{1122}\times S_{2233}\times S_{3311} + 3\times C_{11}{}^{*}\times C_{12}{}^{*2}\times S_{1133}\times S_{2211}\times S_{3322} -$

$3\times C_{11}{}^{*}\times C_{12}{}^{*2}\times S_{1133}\times S_{2222}\times S_{3311} - 4\times C_{11}\times C_{12}\times C_{12}{}^{*}\times S_{1111}\times S_{2222} + 4\times C_{11}\times C_{12}\times C_{12}{}^{*}\times S_{1122}\times S_{2211} -$

$C_{11}\times C_{12}\times C_{11}{}^{*}\times S_{1111}\times S_{2233} + C_{11}\times C_{12}\times C_{11}{}^{*}\times S_{1133}\times S_{2211} - C_{11}\times C_{12}\times C_{12}{}^{*}\times S_{1111}\times S_{2233} +$

$C_{11}\times C_{12}\times C_{12}{}^{*}\times S_{1133}\times S_{2211} + C_{11}\times C_{12}\times C_{11}{}^{*}\times S_{1122}\times S_{2233} - C_{11}\times C_{12}\times C_{11}{}^{*}\times S_{1133}\times S_{2222} +$

$C_{11}\times C_{12}\times C_{12}{}^{*}\times S_{1122}\times S_{2233} - C_{11}\times C_{12}\times C_{12}{}^{*}\times S_{1133}\times S_{2222} + 2\times C_{12}\times C_{11}{}^{*}\times C_{12}{}^{*}\times S_{1111}\times S_{2222} -$

$2\times C_{12}\times C_{11}{}^{*}\times C_{12}{}^{*}\times S_{1122}\times S_{2211} - C_{11}\times C_{11}{}^{*}\times C_{12}{}^{*}\times S_{1111}\times S_{2233} + C_{11}\times C_{11}{}^{*}\times C_{12}{}^{*}\times S_{1133}\times S_{2211} -$

$C_{12}\times C_{11}^{*}\times C_{12}^{*}\times S_{1111}\times S_{2233} + C_{12}\times C_{11}^{*}\times C_{12}^{*}\times S_{1133}\times S_{2211} + C_{11}\times C_{11}^{*}\times C_{12}^{*}\times S_{1122}\times S_{2233} -$

$C_{11}\times C_{11}^{*}\times C_{12}^{*}\times S_{1133}\times S_{2222} + C_{12}\times C_{11}^{*}\times C_{12}^{*}\times S_{1122}\times S_{2233} - C_{12}\times C_{11}^{*}\times C_{12}^{*}\times S_{1133}\times S_{2222} -$

$C_{11}\times C_{12}\times C_{11}^{*}\times S_{1111}\times S_{3322} + C_{11}\times C_{12}\times C_{11}^{*}\times S_{1122}\times S_{3311} - C_{11}\times C_{12}\times C_{12}^{*}\times S_{1111}\times S_{3322} +$

$C_{11}\times C_{12}\times C_{12}^{*}\times S_{1122}\times S_{3311} - 4\times C_{11}\times C_{12}\times C_{12}^{*}\times S_{1111}\times S_{3333} + 4\times C_{11}\times C_{12}\times C_{12}^{*}\times S_{1133}\times S_{3311} -$

$C_{11}\times C_{12}\times C_{11}^{*}\times S_{1122}\times S_{3333} + C_{11}\times C_{12}\times C_{11}^{*}\times S_{1133}\times S_{3322} - C_{11}\times C_{12}\times C_{12}^{*}\times S_{1122}\times S_{3333} +$

$C_{11}\times C_{12}\times C_{12}^{*}\times S_{1133}\times S_{3322} - C_{11}\times C_{11}^{*}\times C_{12}^{*}\times S_{1111}\times S_{3322} + C_{11}\times C_{11}^{*}\times C_{12}^{*}\times S_{1122}\times S_{3311} -$

$C_{12}\times C_{11}^{*}\times C_{12}^{*}\times S_{1111}\times S_{3322} + C_{12}\times C_{11}^{*}\times C_{12}^{*}\times S_{1122}\times S_{3311} + 2\times C_{12}\times C_{11}^{*}\times C_{12}^{*}\times S_{1111}\times S_{3333} -$

$2\times C_{12}\times C_{11}^{*}\times C_{12}^{*}\times S_{1133}\times S_{3311} - C_{11}\times C_{11}^{*}\times C_{12}^{*}\times S_{1122}\times S_{3333} + C_{11}\times C_{11}^{*}\times C_{12}^{*}\times S_{1133}\times S_{3322} -$

$C_{12}\times C_{11}^{*}\times C_{12}^{*}\times S_{1122}\times S_{3333} + C_{12}\times C_{11}^{*}\times C_{12}^{*}\times S_{1133}\times S_{3322} + C_{11}\times C_{12}\times C_{11}^{*}\times S_{2211}\times S_{3322} -$

$C_{11}\times C_{12}\times C_{11}^{*}\times S_{2222}\times S_{3311} + C_{11}\times C_{12}\times C_{12}^{*}\times S_{2211}\times S_{3322} - C_{11}\times C_{12}\times C_{12}^{*}\times S_{2222}\times S_{3311} -$

$C_{11}\times C_{12}\times C_{11}^{*}\times S_{2211}\times S_{3333} + C_{11}\times C_{12}\times C_{11}^{*}\times S_{2233}\times S_{3311} - C_{11}\times C_{12}\times C_{12}^{*}\times S_{2211}\times S_{3333} +$

$C_{11}\times C_{12}\times C_{12}^{*}\times S_{2233}\times S_{3311} - 4\times C_{11}\times C_{12}\times C_{12}^{*}\times S_{2222}\times S_{3333} + 4\times C_{11}\times C_{12}\times C_{12}^{*}\times S_{2233}\times S_{3322} +$

$C_{11}\times C_{11}^{*}\times C_{12}^{*}\times S_{2211}\times S_{3322} - C_{11}\times C_{11}^{*}\times C_{12}^{*}\times S_{2222}\times S_{3311} + C_{12}\times C_{11}^{*}\times C_{12}^{*}\times S_{2211}\times S_{3322} -$

$C_{12}\times C_{11}^{*}\times C_{12}^{*}\times S_{2222}\times S_{3311} - C_{11}\times C_{11}^{*}\times C_{12}^{*}\times S_{2211}\times S_{3333} + C_{11}\times C_{11}^{*}\times C_{12}^{*}\times S_{2233}\times S_{3311} -$

$C_{12}\times C_{11}^{*}\times C_{12}^{*}\times S_{2211}\times S_{3333} + C_{12}\times C_{11}^{*}\times C_{12}^{*}\times S_{2233}\times S_{3311} + 2\times C_{12}\times C_{11}^{*}\times C_{12}^{*}\times S_{2222}\times S_{3333} -$

$2\times C_{12}\times C_{11}^{*}\times C_{12}^{*}\times S_{2233}\times S_{3322} + 6\times C_{11}\times C_{12}\times C_{12}^{*}\times S_{1111}\times S_{2222}\times S_{3333} -$

$6\times C_{11}\times C_{12}\times C_{12}^{*}\times S_{1111}\times S_{2233}\times S_{3322} - 6\times C_{11}\times C_{12}\times C_{12}^{*}\times S_{1122}\times S_{2211}\times S_{3333} +$

$6\times C_{11}\times C_{12}\times C_{12}^{*}\times S_{1122}\times S_{2233}\times S_{3311} + 6\times C_{11}\times C_{12}\times C_{12}^{*}\times S_{1133}\times S_{2211}\times S_{3322} -$

$6\times C_{11}\times C_{12}\times C_{12}^{*}\times S_{1133}\times S_{2222}\times S_{3311} - 6\times C_{12}\times C_{11}^{*}\times C_{12}^{*}\times S_{1111}\times S_{2222}\times S_{3333} +$

$6\times C_{12}\times C_{11}^{*}\times C_{12}^{*}\times S_{1111}\times S_{2233}\times S_{3322} + 6\times C_{12}\times C_{11}^{*}\times C_{12}^{*}\times S_{1122}\times S_{2211}\times S_{3333} -$

$6\times C_{12}\times C_{11}^{*}\times C_{12}^{*}\times S_{1122}\times S_{2233}\times S_{3311} - 6\times C_{12}\times C_{11}^{*}\times C_{12}^{*}\times S_{1133}\times S_{2211}\times S_{3322} +$

$6\times C_{12}\times C_{11}^{*}\times C_{12}^{*}\times S_{1133}\times S_{2222}\times S_{3311})$

$$\sigma_{33} = -(\varepsilon\times(C_{11}^{*} + 2\times C_{12}^{*})\times(3\times C_{11}\times C_{12}^{2} + C_{11}^{3}\times S_{1111} + 2\times C_{12}^{3}\times S_{1111} + C_{11}^{3}\times S_{2222} + 2\times C_{12}^{3}\times S_{2222} + C_{11}^{3}\times S_{3333} + 2\times C_{12}^{3}\times S_{3333} - C_{11}^{3} - 2\times C_{12}^{3} - 3\times C_{11}\times C_{12}^{2}\times S_{1111} - C_{11}^{2}\times C_{11}^{*}\times S_{1111} + C_{11}^{2}\times C_{12}^{*}\times S_{1111} + C_{12}^{2}\times C_{11}^{*}\times S_{1111} - C_{12}^{2}\times C_{12}^{*}\times S_{1111} - C_{12}^{2}\times C_{11}^{*}\times S_{1122} + C_{12}^{2}\times C_{12}^{*}\times S_{1122} - C_{12}^{2}\times C_{11}^{*}\times S_{1133} + C_{12}^{2}\times C_{12}^{*}\times S_{1133} - 3\times C_{11}\times C_{12}^{2}\times S_{2222} - C_{12}^{2}\times C_{11}^{*}\times S_{2211} + C_{12}^{2}\times C_{12}^{*}\times S_{2211} - C_{11}^{2}\times C_{11}^{*}\times S_{2222} + C_{11}^{2}\times C_{12}^{*}\times S_{2222} + C_{12}^{2}\times C_{11}^{*}\times S_{2222} - C_{12}^{2}\times C_{12}^{*}\times S_{2222} - C_{12}^{2}\times C_{11}^{*}\times S_{2233} + C_{12}^{2}\times C_{12}^{*}\times S_{2233} - 3\times C_{11}\times C_{12}^{2}\times S_{3333} + C_{11}^{2}\times C_{11}^{*}\times S_{3311} - C_{11}^{2}\times C_{12}^{*}\times S_{3311} + C_{11}^{2}\times C_{11}^{*}\times S_{3322} - C_{11}^{2}\times C_{12}^{*}\times S_{3322} + 2\times C_{12}^{2}\times C_{11}^{*}\times S_{3333} - 2\times C_{12}^{2}\times C_{12}^{*}\times S_{3333} - C_{11}^{3}\times S_{1111}\times S_{2222} + C_{11}^{3}\times S_{1122}\times S_{2211} - 2\times C_{12}^{3}\times S_{1111}\times S_{2222} + 2\times C_{12}^{3}\times S_{1122}\times S_{2211} - C_{11}^{3}\times S_{1111}\times S_{3333} + C_{11}^{3}\times S_{1133}\times S_{3311} - 2\times C_{12}^{3}\times S_{1111}\times S_{3333} + 2\times C_{12}^{3}\times S_{1133}\times S_{3311} - C_{11}^{3}\times S_{2222}\times S_{3333} + C_{11}^{3}\times S_{2233}\times S_{3322} - 2\times C_{12}^{3}\times S_{2222}\times S_{3333} + 2\times C_{12}^{3}\times S_{2233}\times S_{3322} + C_{11}\times C_{12}\times C_{11}^{*}\times S_{1122} - C_{11}\times C_{12}\times C_{12}^{*}\times S_{1122} + C_{11}\times C_{12}\times C_{11}^{*}\times S_{1133} - C_{11}\times C_{12}\times C_{12}^{*}\times S_{1133} + C_{11}\times C_{12}\times C_{11}^{*}\times S_{2211} - C_{11}\times C_{12}\times C_{12}^{*}\times S_{2211} + C_{11}\times C_{12}\times C_{11}^{*}\times S_{2233} - C_{11}\times C_{12}\times C_{12}^{*}\times S_{2233} - C_{11}\times C_{12}\times C_{11}^{*}\times S_{3311} + C_{11}\times C_{12}\times C_{12}^{*}\times S_{3311} - C_{11}\times C_{12}\times C_{11}^{*}\times S_{3322} + C_{11}\times C_{12}\times C_{12}^{*}\times S_{3322} - 2\times C_{11}\times C_{12}\times C_{11}^{*}\times S_{3333} + 2\times C_{11}\times C_{12}\times C_{12}^{*}\times S_{3333} + 3\times C_{11}\times C_{12}^{2}\times S_{1111}\times S_{2222} - 3\times C_{11}\times C_{12}^{2}\times S_{1122}\times S_{2211} - C_{11}\times C_{11}^{*2}\times S_{1111}\times S_{2222} + C_{11}\times C_{11}^{*2}\times S_{1122}\times S_{2211} + 2\times C_{11}^{2}\times C_{11}^{*}\times S_{1111}\times S_{2222} - 2\times C_{11}^{2}\times C_{11}^{*}\times S_{1122}\times S_{2211} - C_{11}\times C_{12}^{*2}\times S_{1111}\times S_{2222} + C_{11}\times C_{12}^{*2}\times S_{1122}\times S_{2211} - 2\times C_{11}^{2}\times C_{12}^{*}\times S_{1111}\times S_{2222} + 2\times C_{11}^{2}\times C_{12}^{*}\times S_{1122}\times S_{2211} - 2\times C_{12}^{2}\times C_{11}^{*}\times S_{1111}\times S_{2222} + 2\times C_{12}^{2}\times C_{11}^{*}\times S_{1122}\times S_{2211} + 2\times C_{12}^{2}\times C_{12}^{*}\times S_{1111}\times S_{2222} - 2\times C_{12}^{2}\times C_{12}^{*}\times S_{1122}\times S_{2211} + C_{12}\times C_{11}^{*2}\times S_{1111}\times S_{2233} - C_{12}\times C_{11}^{*2}\times S_{1133}\times S_{2211} + C_{12}^{2}\times C_{11}^{*}\times S_{1111}\times S_{2233} - C_{12}^{2}\times C_{11}^{*}\times S_{1133}\times S_{2211} + C_{12}\times C_{12}^{*2}\times S_{1111}\times S_{2233} - C_{12}\times C_{12}^{*2}\times S_{1133}\times S_{2211} - C_{12}^{2}\times C_{12}^{*}\times S_{1111}\times S_{2233} + C_{12}^{2}\times C_{12}^{*}\times S_{1133}\times S_{2211} - C_{12}\times C_{11}^{*2}\times S_{1122}\times S_{2233} + C_{12}\times C_{11}^{*2}\times S_{1133}\times S_{2222} - C_{12}^{2}\times C_{11}^{*}\times S_{1122}\times S_{2233} + C_{12}^{2}\times C_{11}^{*}\times S_{1133}\times S_{2222} - C_{12}\times C_{12}^{*2}\times S_{1122}\times S_{2233} + C_{12}\times C_{12}^{*2}\times S_{1133}\times S_{2222} + C_{12}^{2}\times C_{12}^{*}\times S_{1122}\times S_{2233} - C_{12}^{2}\times C_{12}^{*}\times S_{1133}\times S_{2222} + 3\times C_{11}\times C_{12}^{2}\times S_{1111}\times S_{3333} - 3\times C_{11}\times C_{12}^{2}\times S_{1133}\times S_{3311} + C_{11}\times C_{11}^{*2}\times S_{1111}\times S_{3322} - C_{11}\times C_{11}^{*2}\times S_{1122}\times S_{3311} - C_{11}^{2}\times C_{11}^{*}\times S_{1111}\times S_{3322} + C_{11}^{2}\times C_{11}^{*}\times S_{1122}\times S_{3311} + C_{11}\times C_{12}^{*2}\times S_{1111}\times S_{3322} - C_{11}\times C_{12}^{*2}\times S_{1122}\times S_{3311} + C_{11}^{2}\times C_{12}^{*}\times S_{1111}\times S_{3322} - C_{11}^{2}\times C_{12}^{*}\times S_{1122}\times S_{3311} + C_{11}^{2}\times C_{11}^{*}\times S_{1111}\times S_{3333} - C_{11}^{2}\times C_{11}^{*}\times S_{1133}\times S_{3311} - C_{12}\times C_{11}^{*2}\times S_{1111}\times S_{3333} + C_{12}\times C_{11}^{*2}\times S_{1133}\times S_{3311} - C_{11}^{2}\times C_{12}^{*}\times S_{1111}\times S_{3333} +$$

$C_{11}^2 \times C_{12}^* \times S_{1133} \times S_{3311} - 3 \times C_{12}^2 \times C_{11}^* \times S_{1111} \times S_{3333} + 3 \times C_{12}^2 \times C_{11}^* \times S_{1133} \times S_{3311} -$

$C_{12} \times C_{12}^{*2} \times S_{1111} \times S_{3333} + C_{12} \times C_{12}^{*2} \times S_{1133} \times S_{3311} + 3 \times C_{12}^2 \times C_{12}^* \times S_{1111} \times S_{3333} -$

$3 \times C_{12}^2 \times C_{12}^* \times S_{1133} \times S_{3311} + C_{12} \times C_{11}^{*2} \times S_{1122} \times S_{3333} - C_{12} \times C_{11}^{*2} \times S_{1133} \times S_{3322} + C_{12}^2 \times C_{11}^* \times S_{1122} \times S_{3333}$

$- C_{12}^2 \times C_{11}^* \times S_{1133} \times S_{3322} + C_{12} \times C_{12}^{*2} \times S_{1122} \times S_{3333} - C_{12} \times C_{12}^{*2} \times S_{1133} \times S_{3322} - C_{12}^2 \times C_{12}^* \times S_{1122} \times S_{3333} +$

$C_{12}^2 \times C_{12}^* \times S_{1133} \times S_{3322} + 3 \times C_{11} \times C_{12}^2 \times S_{2222} \times S_{3333} - 3 \times C_{11} \times C_{12}^2 \times S_{2233} \times S_{3322} - C_{11} \times C_{11}^{*2} \times S_{2211} \times S_{3322}$

$+ C_{11} \times C_{11}^{*2} \times S_{2222} \times S_{3311} + C_{11}^2 \times C_{11}^* \times S_{2211} \times S_{3322} - C_{11}^2 \times C_{11}^* \times S_{2222} \times S_{3311} - C_{11} \times C_{12}^{*2} \times S_{2211} \times S_{3322}$

$+ C_{11} \times C_{12}^{*2} \times S_{2222} \times S_{3311} - C_{11}^2 \times C_{12}^* \times S_{2211} \times S_{3322} + C_{11}^2 \times C_{12}^* \times S_{2222} \times S_{3311} + C_{12} \times C_{11}^{*2} \times S_{2211} \times S_{3333}$

$- C_{12} \times C_{11}^{*2} \times S_{2233} \times S_{3311} + C_{12}^2 \times C_{11}^* \times S_{2211} \times S_{3333} - C_{12}^2 \times C_{11}^* \times S_{2233} \times S_{3311} + C_{12} \times C_{12}^{*2} \times S_{2211} \times S_{3333} -$

$C_{12} \times C_{12}^{*2} \times S_{2233} \times S_{3311} - C_{12}^2 \times C_{12}^* \times S_{2211} \times S_{3333} + C_{12}^2 \times C_{12}^* \times S_{2233} \times S_{3311} + C_{11}^2 \times C_{11}^* \times S_{2222} \times S_{3333} -$

$C_{11}^2 \times C_{11}^* \times S_{2233} \times S_{3322} - C_{12} \times C_{11}^{*2} \times S_{2222} \times S_{3333} + C_{12} \times C_{11}^{*2} \times S_{2233} \times S_{3322} - C_{11}^2 \times C_{12}^* \times S_{2222} \times S_{3333} +$

$C_{11}^2 \times C_{12}^* \times S_{2233} \times S_{3322} - 3 \times C_{12}^2 \times C_{11}^* \times S_{2222} \times S_{3333} + 3 \times C_{12}^2 \times C_{11}^* \times S_{2233} \times S_{3322} -$

$C_{12} \times C_{12}^{*2} \times S_{2222} \times S_{3333} + C_{12} \times C_{12}^{*2} \times S_{2233} \times S_{3322} + 3 \times C_{12}^2 \times C_{12}^* \times S_{2222} \times S_{3333} -$

$3 \times C_{12}^2 \times C_{12}^* \times S_{2233} \times S_{3322} + C_{11}^3 \times S_{1111} \times S_{2222} \times S_{3333} - C_{11}^3 \times S_{1111} \times S_{2233} \times S_{3322} - C_{11}^3 \times S_{1122} \times S_{2211} \times S_{3333}$

$+ C_{11}^3 \times S_{1122} \times S_{2233} \times S_{3311} + C_{11}^3 \times S_{1133} \times S_{2211} \times S_{3322} - C_{11}^3 \times S_{1133} \times S_{2222} \times S_{3311} +$

$2 \times C_{12}^3 \times S_{1111} \times S_{2222} \times S_{3333} - 2 \times C_{12}^3 \times S_{1111} \times S_{2233} \times S_{3322} - 2 \times C_{12}^3 \times S_{1122} \times S_{2211} \times S_{3333} +$

$2 \times C_{12}^3 \times S_{1122} \times S_{2233} \times S_{3311} + 2 \times C_{12}^3 \times S_{1133} \times S_{2211} \times S_{3322} - 2 \times C_{12}^3 \times S_{1133} \times S_{2222} \times S_{3311} -$

$3 \times C_{11} \times C_{12}^2 \times S_{1111} \times S_{2222} \times S_{3333} + 3 \times C_{11} \times C_{12}^2 \times S_{1111} \times S_{2233} \times S_{3322} + 3 \times C_{11} \times C_{12}^2 \times S_{1122} \times S_{2211} \times S_{3333} -$

$3 \times C_{11} \times C_{12}^2 \times S_{1122} \times S_{2233} \times S_{3311} - 3 \times C_{11} \times C_{12}^2 \times S_{1133} \times S_{2211} \times S_{3322} + 3 \times C_{11} \times C_{12}^2 \times S_{1133} \times S_{2222} \times S_{3311} +$

$C_{11} \times C_{11}^{*2} \times S_{1111} \times S_{2222} \times S_{3333} - C_{11} \times C_{11}^{*2} \times S_{1111} \times S_{2233} \times S_{3322} - C_{11} \times C_{11}^{*2} \times S_{1122} \times S_{2211} \times S_{3333} +$

$C_{11} \times C_{11}^{*2} \times S_{1122} \times S_{2233} \times S_{3311} + C_{11} \times C_{11}^{*2} \times S_{1133} \times S_{2211} \times S_{3322} - C_{11} \times C_{11}^{*2} \times S_{1133} \times S_{2222} \times S_{3311} -$

$2 \times C_{11}^2 \times C_{11}^* \times S_{1111} \times S_{2222} \times S_{3333} + 2 \times C_{11}^2 \times C_{11}^* \times S_{1111} \times S_{2233} \times S_{3322} + 2 \times C_{11}^2 \times C_{11}^* \times S_{1122} \times S_{2211} \times S_{3333}$

$- 2 \times C_{11}^2 \times C_{11}^* \times S_{1122} \times S_{2233} \times S_{3311} - 2 \times C_{11}^2 \times C_{11}^* \times S_{1133} \times S_{2211} \times S_{3322} + 2 \times C_{11}^2 \times C_{11}^* \times S_{1133} \times S_{2222} \times S_{3311}$

$+ C_{11} \times C_{12}^{*2} \times S_{1111} \times S_{2222} \times S_{3333} - C_{11} \times C_{12}^{*2} \times S_{1111} \times S_{2233} \times S_{3322} - C_{11} \times C_{12}^{*2} \times S_{1122} \times S_{2211} \times S_{3333} +$

$C_{11} \times C_{12}^{*2} \times S_{1122} \times S_{2233} \times S_{3311} + C_{11} \times C_{12}^{*2} \times S_{1133} \times S_{2211} \times S_{3322} - C_{11} \times C_{12}^{*2} \times S_{1133} \times S_{2222} \times S_{3311} +$

$2 \times C_{12} \times C_{11}^{*2} \times S_{1111} \times S_{2222} \times S_{3333} - 2 \times C_{12} \times C_{11}^{*2} \times S_{1111} \times S_{2233} \times S_{3322} - 2 \times C_{12} \times C_{11}^{*2} \times S_{1122} \times S_{2211} \times S_{3333} +$

$2 \times C_{12} \times C_{11}^{*2} \times S_{1122} \times S_{2233} \times S_{3311} + 2 \times C_{12} \times C_{11}^{*2} \times S_{1133} \times S_{2211} \times S_{3322} - 2 \times C_{12} \times C_{11}^{*2} \times S_{1133} \times S_{2222} \times S_{3311}$

$$+ 2\times C_{11}^{2}\times C_{12}^{*}\times S_{1111}\times S_{2222}\times S_{3333} - 2\times C_{11}^{2}\times C_{12}^{*}\times S_{1111}\times S_{2233}\times S_{3322} - 2\times C_{11}^{2}\times C_{12}^{*}\times S_{1122}\times S_{2211}\times S_{3333}$$

$$+ 2\times C_{11}^{2}\times C_{12}^{*}\times S_{1122}\times S_{2233}\times S_{3311} + 2\times C_{11}^{2}\times C_{12}^{*}\times S_{1133}\times S_{2211}\times S_{3322} -$$

$$2\times C_{11}^{2}\times C_{12}^{*}\times S_{1133}\times S_{2222}\times S_{3311} + 4\times C_{12}^{2}\times C_{11}^{*}\times S_{1111}\times S_{2222}\times S_{3333} - 4\times C_{12}^{2}\times C_{11}^{*}\times S_{1111}\times S_{2233}\times S_{3322} -$$

$$4\times C_{12}^{2}\times C_{11}^{*}\times S_{1122}\times S_{2211}\times S_{3333} + 4\times C_{12}^{2}\times C_{11}^{*}\times S_{1122}\times S_{2233}\times S_{3311} + 4\times C_{12}^{2}\times C_{11}^{*}\times S_{1133}\times S_{2211}\times S_{3322}$$

$$- 4\times C_{12}^{2}\times C_{11}^{*}\times S_{1133}\times S_{2222}\times S_{3311} + 2\times C_{12}\times C_{12}^{*2}\times S_{1111}\times S_{2222}\times S_{3333} - 2\times C_{12}\times C_{12}^{*2}\times S_{1111}\times S_{2233}\times S_{3322}$$

$$- 2\times C_{12}\times C_{12}^{*2}\times S_{1122}\times S_{2211}\times S_{3333} + 2\times C_{12}\times C_{12}^{*2}\times S_{1122}\times S_{2233}\times S_{3311} +$$

$$2\times C_{12}\times C_{12}^{*2}\times S_{1133}\times S_{2211}\times S_{3322} - 2\times C_{12}\times C_{12}^{*2}\times S_{1133}\times S_{2222}\times S_{3311} - 4\times C_{12}^{2}\times C_{12}^{*}\times S_{1111}\times S_{2222}\times S_{3333} +$$

$$4\times C_{12}^{2}\times C_{12}^{*}\times S_{1111}\times S_{2233}\times S_{3322} + 4\times C_{12}^{2}\times C_{12}^{*}\times S_{1122}\times S_{2211}\times S_{3333} - 4\times C_{12}^{2}\times C_{12}^{*}\times S_{1122}\times S_{2233}\times S_{3311} -$$

$$4\times C_{12}^{2}\times C_{12}^{*}\times S_{1133}\times S_{2211}\times S_{3322} + 4\times C_{12}^{2}\times C_{12}^{*}\times S_{1133}\times S_{2222}\times S_{3311} - C_{11}\times C_{12}\times C_{11}^{*}\times S_{1111}\times S_{2233} +$$

$$C_{11}\times C_{12}\times C_{11}^{*}\times S_{1133}\times S_{2211} + C_{11}\times C_{12}\times C_{12}^{*}\times S_{1111}\times S_{2233} - C_{11}\times C_{12}\times C_{12}^{*}\times S_{1133}\times S_{2211} +$$

$$C_{11}\times C_{12}\times C_{11}^{*}\times S_{1122}\times S_{2233} - C_{11}\times C_{12}\times C_{11}^{*}\times S_{1133}\times S_{2222} - C_{11}\times C_{12}\times C_{12}^{*}\times S_{1122}\times S_{2233} +$$

$$C_{11}\times C_{12}\times C_{12}^{*}\times S_{1133}\times S_{2222} + 2\times C_{11}\times C_{11}^{*}\times C_{12}^{*}\times S_{1111}\times S_{2222} - 2\times C_{11}\times C_{11}^{*}\times C_{12}^{*}\times S_{1122}\times S_{2211} -$$

$$2\times C_{12}\times C_{11}^{*}\times C_{12}^{*}\times S_{1111}\times S_{2233} + 2\times C_{12}\times C_{11}^{*}\times C_{12}^{*}\times S_{1133}\times S_{2211} + 2\times C_{12}\times C_{11}^{*}\times C_{12}^{*}\times S_{1122}\times S_{2233} -$$

$$2\times C_{12}\times C_{11}^{*}\times C_{12}^{*}\times S_{1133}\times S_{2222} + C_{11}\times C_{12}\times C_{11}^{*}\times S_{1111}\times S_{3322} - C_{11}\times C_{12}\times C_{11}^{*}\times S_{1122}\times S_{3311} -$$

$$C_{11}\times C_{12}\times C_{12}^{*}\times S_{1111}\times S_{3322} + C_{11}\times C_{12}\times C_{12}^{*}\times S_{1122}\times S_{3311} + 2\times C_{11}\times C_{12}\times C_{11}^{*}\times S_{1111}\times S_{3333} -$$

$$2\times C_{11}\times C_{12}\times C_{11}^{*}\times S_{1133}\times S_{3311} - 2\times C_{11}\times C_{12}\times C_{12}^{*}\times S_{1111}\times S_{3333} + 2\times C_{11}\times C_{12}\times C_{12}^{*}\times S_{1133}\times S_{3311} -$$

$$C_{11}\times C_{12}\times C_{11}^{*}\times S_{1122}\times S_{3333} + C_{11}\times C_{12}\times C_{11}^{*}\times S_{1133}\times S_{3322} + C_{11}\times C_{12}\times C_{12}^{*}\times S_{1122}\times S_{3333} -$$

$$C_{11}\times C_{12}\times C_{12}^{*}\times S_{1133}\times S_{3322} - 2\times C_{11}\times C_{11}^{*}\times C_{12}^{*}\times S_{1111}\times S_{3322} + 2\times C_{11}\times C_{11}^{*}\times C_{12}^{*}\times S_{1122}\times S_{3311} +$$

$$2\times C_{12}\times C_{11}^{*}\times C_{12}^{*}\times S_{1111}\times S_{3333} - 2\times C_{12}\times C_{11}^{*}\times C_{12}^{*}\times S_{1133}\times S_{3311} - 2\times C_{12}\times C_{11}^{*}\times C_{12}^{*}\times S_{1122}\times S_{3333} +$$

$$2\times C_{12}\times C_{11}^{*}\times C_{12}^{*}\times S_{1133}\times S_{3322} - C_{11}\times C_{12}\times C_{11}^{*}\times S_{2211}\times S_{3322} + C_{11}\times C_{12}\times C_{11}^{*}\times S_{2222}\times S_{3311} +$$

$$C_{11}\times C_{12}\times C_{12}^{*}\times S_{2211}\times S_{3322} - C_{11}\times C_{12}\times C_{12}^{*}\times S_{2222}\times S_{3311} - C_{11}\times C_{12}\times C_{11}^{*}\times S_{2211}\times S_{3333} +$$

$$C_{11}\times C_{12}\times C_{11}^{*}\times S_{2233}\times S_{3311} + C_{11}\times C_{12}\times C_{12}^{*}\times S_{2211}\times S_{3333} - C_{11}\times C_{12}\times C_{12}^{*}\times S_{2233}\times S_{3311} +$$

$$2\times C_{11}\times C_{12}\times C_{11}^{*}\times S_{2222}\times S_{3333} - 2\times C_{11}\times C_{12}\times C_{11}^{*}\times S_{2233}\times S_{3322} - 2\times C_{11}\times C_{12}\times C_{12}^{*}\times S_{2222}\times S_{3333} +$$

$$2\times C_{11}\times C_{12}\times C_{12}^{*}\times S_{2233}\times S_{3322} + 2\times C_{11}\times C_{11}^{*}\times C_{12}^{*}\times S_{2211}\times S_{3322} - 2\times C_{11}\times C_{11}^{*}\times C_{12}^{*}\times S_{2222}\times S_{3311} -$$

$$2\times C_{12}\times C_{11}^{*}\times C_{12}^{*}\times S_{2211}\times S_{3333} + 2\times C_{12}\times C_{11}^{*}\times C_{12}^{*}\times S_{2233}\times S_{3311} + 2\times C_{12}\times C_{11}^{*}\times C_{12}^{*}\times S_{2222}\times S_{3333} -$$

$$2\times C_{12}\times C_{11}^{*}\times C_{12}^{*}\times S_{2233}\times S_{3322} - 2\times C_{11}\times C_{12}\times C_{11}^{*}\times S_{1111}\times S_{2222}\times S_{3333} +$$

$$2\times C_{11}\times C_{12}\times C_{11}^{*}\times S_{1111}\times S_{2233}\times S_{3322} + 2\times C_{11}\times C_{12}\times C_{11}^{*}\times S_{1122}\times S_{2211}\times S_{3333} -$$

$$2\times C_{11}\times C_{12}\times C_{11}^{*}\times S_{1122}\times S_{2233}\times S_{3311} - 2\times C_{11}\times C_{12}\times C_{11}^{*}\times S_{1133}\times S_{2211}\times S_{3322} +$$

$$2\times C_{11}\times C_{12}\times C_{11}^{*}\times S_{1133}\times S_{2222}\times S_{3311} + 2\times C_{11}\times C_{12}\times C_{12}^{*}\times S_{1111}\times S_{2222}\times S_{3333} -$$

$$2\times C_{11}\times C_{12}\times C_{12}^{*}\times S_{1111}\times S_{2233}\times S_{3322} - 2\times C_{11}\times C_{12}\times C_{12}^{*}\times S_{1122}\times S_{2211}\times S_{3333} +$$

$$2\times C_{11}\times C_{12}\times C_{12}^{*}\times S_{1122}\times S_{2233}\times S_{3311} + 2\times C_{11}\times C_{12}\times C_{12}^{*}\times S_{1133}\times S_{2211}\times S_{3322} -$$

$$2\times C_{11}\times C_{12}\times C_{12}^{*}\times S_{1133}\times S_{2222}\times S_{3311} - 2\times C_{11}\times C_{11}^{*}\times C_{12}^{*}\times S_{1111}\times S_{2222}\times S_{3333} +$$

$$2\times C_{11}\times C_{11}^{*}\times C_{12}^{*}\times S_{1111}\times S_{2233}\times S_{3322} + 2\times C_{11}\times C_{11}^{*}\times C_{12}^{*}\times S_{1122}\times S_{2211}\times S_{3333} -$$

$$2\times C_{11}\times C_{11}^{*}\times C_{12}^{*}\times S_{1122}\times S_{2233}\times S_{3311} - 2\times C_{11}\times C_{11}^{*}\times C_{12}^{*}\times S_{1133}\times S_{2211}\times S_{3322} +$$

$$2\times C_{11}\times C_{11}^{*}\times C_{12}^{*}\times S_{1133}\times S_{2222}\times S_{3311} - 4\times C_{12}\times C_{11}^{*}\times C_{12}^{*}\times S_{1111}\times S_{2222}\times S_{3333} +$$

$$4\times C_{12}\times C_{11}^{*}\times C_{12}^{*}\times S_{1111}\times S_{2233}\times S_{3322} + 4\times C_{12}\times C_{11}^{*}\times C_{12}^{*}\times S_{1122}\times S_{2211}\times S_{3333} -$$

$$4\times C_{12}\times C_{11}^{*}\times C_{12}^{*}\times S_{1122}\times S_{2233}\times S_{3311} - 4\times C_{12}\times C_{11}^{*}\times C_{12}^{*}\times S_{1133}\times S_{2211}\times S_{3322} +$$

$$4\times C_{12}\times C_{11}^{*}\times C_{12}^{*}\times S_{1133}\times S_{2222}\times S_{3311}))/(3\times C_{11}\times C_{12}^{2} + C_{11}^{3}\times S_{1111} + 2\times C_{12}^{3}\times S_{1111} + C_{11}^{3}\times S_{2222} +$$

$$2\times C_{12}^{3}\times S_{2222} + C_{11}^{3}\times S_{3333} + 2\times C_{12}^{3}\times S_{3333} - C_{11}^{3} - 2\times C_{12}^{3} - 3\times C_{11}\times C_{12}^{2}\times S_{1111} - C_{11}^{2}\times C_{11}^{*}\times S_{1111} +$$

$$C_{12}^{2}\times C_{11}^{*}\times S_{1111} - 2\times C_{12}^{2}\times C_{12}^{*}\times S_{1111} - C_{11}^{2}\times C_{12}^{*}\times S_{1122} - C_{12}^{2}\times C_{11}^{*}\times S_{1122} - C_{11}^{2}\times C_{12}^{*}\times S_{1133} -$$

$$C_{12}^{2}\times C_{11}^{*}\times S_{1133} - 3\times C_{11}\times C_{12}^{2}\times S_{2222} - C_{11}^{2}\times C_{12}^{*}\times S_{2211} - C_{12}^{2}\times C_{11}^{*}\times S_{2211} - C_{11}^{2}\times C_{11}^{*}\times S_{2222} +$$

$$C_{12}^{2}\times C_{11}^{*}\times S_{2222} - 2\times C_{12}^{2}\times C_{12}^{*}\times S_{2222} - C_{11}^{2}\times C_{12}^{*}\times S_{2233} - C_{12}^{2}\times C_{11}^{*}\times S_{2233} - 3\times C_{11}\times C_{12}^{2}\times S_{3333} -$$

$$C_{11}^{2}\times C_{12}^{*}\times S_{3311} - C_{12}^{2}\times C_{11}^{*}\times S_{3311} - C_{11}^{2}\times C_{12}^{*}\times S_{3322} - C_{12}^{2}\times C_{11}^{*}\times S_{3322} - C_{11}^{2}\times C_{11}^{*}\times S_{3333} +$$

$$C_{12}^{2}\times C_{11}^{*}\times S_{3333} - 2\times C_{12}^{2}\times C_{12}^{*}\times S_{3333} - C_{11}^{3}\times S_{1111}\times S_{2222} + C_{11}^{3}\times S_{1122}\times S_{2211} - 2\times C_{12}^{3}\times S_{1111}\times S_{2222} +$$

$$2\times C_{12}^{3}\times S_{1122}\times S_{2211} - C_{11}^{3}\times S_{1111}\times S_{3333} + C_{11}^{3}\times S_{1133}\times S_{3311} - 2\times C_{12}^{3}\times S_{1111}\times S_{3333} + 2\times C_{12}^{3}\times S_{1133}\times S_{3311}$$

$$- C_{11}^{3}\times S_{2222}\times S_{3333} + C_{11}^{3}\times S_{2233}\times S_{3322} - 2\times C_{12}^{3}\times S_{2222}\times S_{3333} + 2\times C_{12}^{3}\times S_{2233}\times S_{3322} +$$

$$2\times C_{11}\times C_{12}\times C_{12}^{*}\times S_{1111} + C_{11}\times C_{12}\times C_{11}^{*}\times S_{1122} + C_{11}\times C_{12}\times C_{12}^{*}\times S_{1122} + C_{11}\times C_{12}\times C_{11}^{*}\times S_{1133} +$$

$$C_{11}\times C_{12}\times C_{12}^{*}\times S_{1133} + C_{11}\times C_{12}\times C_{11}^{*}\times S_{2211} + C_{11}\times C_{12}\times C_{12}^{*}\times S_{2211} + 2\times C_{11}\times C_{12}\times C_{12}^{*}\times S_{2222} +$$

$$C_{11}\times C_{12}\times C_{11}^{*}\times S_{2233} + C_{11}\times C_{12}\times C_{12}^{*}\times S_{2233} + C_{11}\times C_{12}\times C_{11}^{*}\times S_{3311} + C_{11}\times C_{12}\times C_{12}^{*}\times S_{3311} +$$

$$C_{11}\times C_{12}\times C_{11}^{*}\times S_{3322} + C_{11}\times C_{12}\times C_{12}^{*}\times S_{3322} + 2\times C_{11}\times C_{12}\times C_{12}^{*}\times S_{3333} + 3\times C_{11}\times C_{12}^{2}\times S_{1111}\times S_{2222} -$$

$$3\times C_{11}\times C_{12}^{2}\times S_{1122}\times S_{2211} - C_{11}\times C_{11}^{*2}\times S_{1111}\times S_{2222} + C_{11}\times C_{11}^{*2}\times S_{1122}\times S_{2211} +$$

$$2\times C_{11}^{2}\times C_{11}^{*}\times S_{1111}\times S_{2222} - 2\times C_{11}^{2}\times C_{11}^{*}\times S_{1122}\times S_{2211} + C_{11}\times C_{12}^{*2}\times S_{1111}\times S_{2222} -$$

$C_{11}\times C_{12}{}^{*2}\times S_{1122}\times S_{2211} - 2\times C_{12}{}^{2}\times C_{11}{}^{*}\times S_{1111}\times S_{2222} + 2\times C_{12}{}^{2}\times C_{11}{}^{*}\times S_{1122}\times S_{2211} -$

$2\times C_{12}\times C_{12}{}^{*2}\times S_{1111}\times S_{2222} + 2\times C_{12}\times C_{12}{}^{*2}\times S_{1122}\times S_{2211} + 4\times C_{12}{}^{2}\times C_{12}{}^{*}\times S_{1111}\times S_{2222} -$

$4\times C_{12}{}^{2}\times C_{12}{}^{*}\times S_{1122}\times S_{2211} + C_{11}\times C_{12}{}^{*2}\times S_{1111}\times S_{2233} - C_{11}\times C_{12}{}^{*2}\times S_{1133}\times S_{2211} + C_{12}\times C_{11}{}^{*2}\times S_{1111}\times S_{2233}$

$- C_{12}\times C_{11}{}^{*2}\times S_{1133}\times S_{2211} + C_{11}{}^{2}\times C_{12}{}^{*}\times S_{1111}\times S_{2233} - C_{11}{}^{2}\times C_{12}{}^{*}\times S_{1133}\times S_{2211} + C_{12}{}^{2}\times C_{11}{}^{*}\times S_{1111}\times S_{2233} -$

$C_{12}{}^{2}\times C_{11}{}^{*}\times S_{1133}\times S_{2211} - C_{11}\times C_{12}{}^{*2}\times S_{1122}\times S_{2233} + C_{11}\times C_{12}{}^{*2}\times S_{1133}\times S_{2222} - C_{12}\times C_{11}{}^{*2}\times S_{1122}\times S_{2233} +$

$C_{12}\times C_{11}{}^{*2}\times S_{1133}\times S_{2222} - C_{11}{}^{2}\times C_{12}{}^{*}\times S_{1122}\times S_{2233} + C_{11}{}^{2}\times C_{12}{}^{*}\times S_{1133}\times S_{2222} - C_{12}{}^{2}\times C_{11}{}^{*}\times S_{1122}\times S_{2233} +$

$C_{12}{}^{2}\times C_{11}{}^{*}\times S_{1133}\times S_{2222} + 3\times C_{11}\times C_{12}{}^{2}\times S_{1111}\times S_{3333} - 3\times C_{11}\times C_{12}{}^{2}\times S_{1133}\times S_{3311} + C_{11}\times C_{12}{}^{*2}\times S_{1111}\times S_{3322}$

$- C_{11}\times C_{12}{}^{*2}\times S_{1122}\times S_{3311} + C_{12}\times C_{11}{}^{*2}\times S_{1111}\times S_{3322} - C_{12}\times C_{11}{}^{*2}\times S_{1122}\times S_{3311} + C_{11}{}^{2}\times C_{12}{}^{*}\times S_{1111}\times S_{3322} -$

$C_{11}{}^{2}\times C_{12}{}^{*}\times S_{1122}\times S_{3311} + C_{12}{}^{2}\times C_{11}{}^{*}\times S_{1111}\times S_{3322} - C_{12}{}^{2}\times C_{11}{}^{*}\times S_{1122}\times S_{3311} - C_{11}\times C_{11}{}^{*2}\times S_{1111}\times S_{3333} +$

$C_{11}\times C_{11}{}^{*2}\times S_{1133}\times S_{3311} + 2\times C_{11}{}^{2}\times C_{11}{}^{*}\times S_{1111}\times S_{3333} - 2\times C_{11}{}^{2}\times C_{11}{}^{*}\times S_{1133}\times S_{3311} +$

$C_{11}\times C_{12}{}^{*2}\times S_{1111}\times S_{3333} - C_{11}\times C_{12}{}^{*2}\times S_{1133}\times S_{3311} - 2\times C_{12}{}^{2}\times C_{11}{}^{*}\times S_{1111}\times S_{3333} +$

$2\times C_{12}{}^{2}\times C_{11}{}^{*}\times S_{1133}\times S_{3311} - 2\times C_{12}\times C_{12}{}^{*2}\times S_{1111}\times S_{3333} + 2\times C_{12}\times C_{12}{}^{*2}\times S_{1133}\times S_{3311} +$

$4\times C_{12}{}^{2}\times C_{12}{}^{*}\times S_{1111}\times S_{3333} - 4\times C_{12}{}^{2}\times C_{12}{}^{*}\times S_{1133}\times S_{3311} + C_{11}\times C_{12}{}^{*2}\times S_{1122}\times S_{3333} -$

$C_{11}\times C_{12}{}^{*2}\times S_{1133}\times S_{3322} + C_{12}\times C_{11}{}^{*2}\times S_{1122}\times S_{3333} - C_{12}\times C_{11}{}^{*2}\times S_{1133}\times S_{3322} + C_{11}{}^{2}\times C_{12}{}^{*}\times S_{1122}\times S_{3333} -$

$C_{11}{}^{2}\times C_{12}{}^{*}\times S_{1133}\times S_{3322} + C_{12}{}^{2}\times C_{11}{}^{*}\times S_{1122}\times S_{3333} - C_{12}{}^{2}\times C_{11}{}^{*}\times S_{1133}\times S_{3322} + 3\times C_{11}\times C_{12}{}^{2}\times S_{2222}\times S_{3333} -$

$3\times C_{11}\times C_{12}{}^{2}\times S_{2233}\times S_{3322} - C_{11}\times C_{12}{}^{*2}\times S_{2211}\times S_{3322} + C_{11}\times C_{12}{}^{*2}\times S_{2222}\times S_{3311} - C_{12}\times C_{11}{}^{*2}\times S_{2211}\times S_{3322} +$

$C_{12}\times C_{11}{}^{*2}\times S_{2222}\times S_{3311} - C_{11}{}^{2}\times C_{12}{}^{*}\times S_{2211}\times S_{3322} + C_{11}{}^{2}\times C_{12}{}^{*}\times S_{2222}\times S_{3311} - C_{12}{}^{2}\times C_{11}{}^{*}\times S_{2211}\times S_{3322} +$

$C_{12}{}^{2}\times C_{11}{}^{*}\times S_{2222}\times S_{3311} + C_{11}\times C_{12}{}^{*2}\times S_{2211}\times S_{3333} - C_{11}\times C_{12}{}^{*2}\times S_{2233}\times S_{3311} + C_{12}\times C_{11}{}^{*2}\times S_{2211}\times S_{3333} -$

$C_{12}\times C_{11}{}^{*2}\times S_{2233}\times S_{3311} + C_{11}{}^{2}\times C_{12}{}^{*}\times S_{2211}\times S_{3333} - C_{11}{}^{2}\times C_{12}{}^{*}\times S_{2233}\times S_{3311} + C_{12}{}^{2}\times C_{11}{}^{*}\times S_{2211}\times S_{3333} -$

$C_{12}{}^{2}\times C_{11}{}^{*}\times S_{2233}\times S_{3311} - C_{11}\times C_{11}{}^{*2}\times S_{2222}\times S_{3333} + C_{11}\times C_{11}{}^{*2}\times S_{2233}\times S_{3322} + 2\times C_{11}{}^{2}\times C_{11}{}^{*}\times S_{2222}\times S_{3333}$

$- 2\times C_{11}{}^{2}\times C_{11}{}^{*}\times S_{2233}\times S_{3322} + C_{11}\times C_{12}{}^{*2}\times S_{2222}\times S_{3333} - C_{11}\times C_{12}{}^{*2}\times S_{2233}\times S_{3322} -$

$2\times C_{12}{}^{2}\times C_{11}{}^{*}\times S_{2222}\times S_{3333} + 2\times C_{12}{}^{2}\times C_{11}{}^{*}\times S_{2233}\times S_{3322} - 2\times C_{12}\times C_{12}{}^{*2}\times S_{2222}\times S_{3333} +$

$2\times C_{12}\times C_{12}{}^{*2}\times S_{2233}\times S_{3322} + 4\times C_{12}{}^{2}\times C_{12}{}^{*}\times S_{2222}\times S_{3333} - 4\times C_{12}{}^{2}\times C_{12}{}^{*}\times S_{2233}\times S_{3322} +$

$C_{11}{}^{3}\times S_{1111}\times S_{2222}\times S_{3333} - C_{11}{}^{3}\times S_{1111}\times S_{2233}\times S_{3322} - C_{11}{}^{3}\times S_{1122}\times S_{2211}\times S_{3333} + C_{11}{}^{3}\times S_{1122}\times S_{2233}\times S_{3311} +$

$C_{11}{}^{3}\times S_{1133}\times S_{2211}\times S_{3322} - C_{11}{}^{3}\times S_{1133}\times S_{2222}\times S_{3311} + 2\times C_{12}{}^{3}\times S_{1111}\times S_{2222}\times S_{3333} -$

$2\times C_{12}{}^{3}\times S_{1111}\times S_{2233}\times S_{3322} - 2\times C_{12}{}^{3}\times S_{1122}\times S_{2211}\times S_{3333} + 2\times C_{12}{}^{3}\times S_{1122}\times S_{2233}\times S_{3311} +$

$2\times C_{12}^{3}\times S_{1133}\times S_{2211}\times S_{3322} - 2\times C_{12}^{3}\times S_{1133}\times S_{2222}\times S_{3311} - C_{11}^{*3}\times S_{1111}\times S_{2222}\times S_{3333} +$

$C_{11}^{*3}\times S_{1111}\times S_{2233}\times S_{3322} + C_{11}^{*3}\times S_{1122}\times S_{2211}\times S_{3333} - C_{11}^{*3}\times S_{1122}\times S_{2233}\times S_{3311} -$

$C_{11}^{*3}\times S_{1133}\times S_{2211}\times S_{3322} + C_{11}^{*3}\times S_{1133}\times S_{2222}\times S_{3311} - 2\times C_{12}^{*3}\times S_{1111}\times S_{2222}\times S_{3333} +$

$2\times C_{12}^{*3}\times S_{1111}\times S_{2233}\times S_{3322} + 2\times C_{12}^{*3}\times S_{1122}\times S_{2211}\times S_{3333} - 2\times C_{12}^{*3}\times S_{1122}\times S_{2233}\times S_{3311} -$

$2\times C_{12}^{*3}\times S_{1133}\times S_{2211}\times S_{3322} + 2\times C_{12}^{*3}\times S_{1133}\times S_{2222}\times S_{3311} - 3\times C_{11}\times C_{12}^{2}\times S_{1111}\times S_{2222}\times S_{3333} +$

$3\times C_{11}\times C_{12}^{2}\times S_{1111}\times S_{2233}\times S_{3322} + 3\times C_{11}\times C_{12}^{2}\times S_{1122}\times S_{2211}\times S_{3333} - 3\times C_{11}\times C_{12}^{2}\times S_{1122}\times S_{2233}\times S_{3311} -$

$3\times C_{11}\times C_{12}^{2}\times S_{1133}\times S_{2211}\times S_{3322} + 3\times C_{11}\times C_{12}^{2}\times S_{1133}\times S_{2222}\times S_{3311} + 3\times C_{11}\times C_{11}^{*2}\times S_{1111}\times S_{2222}\times S_{3333} -$

$3\times C_{11}\times C_{11}^{*2}\times S_{1111}\times S_{2233}\times S_{3322} - 3\times C_{11}\times C_{11}^{*2}\times S_{1122}\times S_{2211}\times S_{3333} + 3\times C_{11}\times C_{11}^{*2}\times S_{1122}\times S_{2233}\times S_{3311}$

$+ 3\times C_{11}\times C_{11}^{*2}\times S_{1133}\times S_{2211}\times S_{3322} - 3\times C_{11}\times C_{11}^{*2}\times S_{1133}\times S_{2222}\times S_{3311} - 3\times C_{11}^{2}\times C_{11}^{*}\times S_{1111}\times S_{2222}\times S_{3333}$

$+ 3\times C_{11}^{2}\times C_{11}^{*}\times S_{1111}\times S_{2233}\times S_{3322} + 3\times C_{11}^{2}\times C_{11}^{*}\times S_{1122}\times S_{2211}\times S_{3333} -$

$3\times C_{11}^{2}\times C_{11}^{*}\times S_{1122}\times S_{2233}\times S_{3311} - 3\times C_{11}^{2}\times C_{11}^{*}\times S_{1133}\times S_{2211}\times S_{3322} + 3\times C_{11}^{2}\times C_{11}^{*}\times S_{1133}\times S_{2222}\times S_{3311} -$

$3\times C_{11}\times C_{12}^{*2}\times S_{1111}\times S_{2222}\times S_{3333} + 3\times C_{11}\times C_{12}^{*2}\times S_{1111}\times S_{2233}\times S_{3322} + 3\times C_{11}\times C_{12}^{*2}\times S_{1122}\times S_{2211}\times S_{3333}$

$- 3\times C_{11}\times C_{12}^{*2}\times S_{1122}\times S_{2233}\times S_{3311} - 3\times C_{11}\times C_{12}^{*2}\times S_{1133}\times S_{2211}\times S_{3322} + 3\times C_{11}\times C_{12}^{*2}\times S_{1133}\times S_{2222}\times S_{3311}$

$+ 3\times C_{12}^{2}\times C_{11}^{*}\times S_{1111}\times S_{2222}\times S_{3333} - 3\times C_{12}^{2}\times C_{11}^{*}\times S_{1111}\times S_{2233}\times S_{3322} - 3\times C_{12}^{2}\times C_{11}^{*}\times S_{1122}\times S_{2211}\times S_{3333}$

$+ 3\times C_{12}^{2}\times C_{11}^{*}\times S_{1122}\times S_{2233}\times S_{3311} + 3\times C_{12}^{2}\times C_{11}^{*}\times S_{1133}\times S_{2211}\times S_{3322} -$

$3\times C_{12}^{2}\times C_{11}^{*}\times S_{1133}\times S_{2222}\times S_{3311} + 6\times C_{12}\times C_{12}^{*2}\times S_{1111}\times S_{2222}\times S_{3333} - 6\times C_{12}\times C_{12}^{*2}\times S_{1111}\times S_{2233}\times S_{3322} -$

$6\times C_{12}\times C_{12}^{*2}\times S_{1122}\times S_{2211}\times S_{3333} + 6\times C_{12}\times C_{12}^{*2}\times S_{1122}\times S_{2233}\times S_{3311} + 6\times C_{12}\times C_{12}^{*2}\times S_{1133}\times S_{2211}\times S_{3322}$

$- 6\times C_{12}\times C_{12}^{*2}\times S_{1133}\times S_{2222}\times S_{3311} - 6\times C_{12}^{2}\times C_{12}^{*}\times S_{1111}\times S_{2222}\times S_{3333} + 6\times C_{12}^{2}\times C_{12}^{*}\times S_{1111}\times S_{2233}\times S_{3322}$

$+ 6\times C_{12}^{2}\times C_{12}^{*}\times S_{1122}\times S_{2211}\times S_{3333} - 6\times C_{12}^{2}\times C_{12}^{*}\times S_{1122}\times S_{2233}\times S_{3311} - 6\times C_{12}^{2}\times C_{12}^{*}\times S_{1133}\times S_{2211}\times S_{3322}$

$+ 6\times C_{12}^{2}\times C_{12}^{*}\times S_{1133}\times S_{2222}\times S_{3311} + 3\times C_{11}^{*}\times C_{12}^{*2}\times S_{1111}\times S_{2222}\times S_{3333} -$

$3\times C_{11}^{*}\times C_{12}^{*2}\times S_{1111}\times S_{2233}\times S_{3322} - 3\times C_{11}^{*}\times C_{12}^{*2}\times S_{1122}\times S_{2211}\times S_{3333} +$

$3\times C_{11}^{*}\times C_{12}^{*2}\times S_{1122}\times S_{2233}\times S_{3311} + 3\times C_{11}^{*}\times C_{12}^{*2}\times S_{1133}\times S_{2211}\times S_{3322} -$

$3\times C_{11}^{*}\times C_{12}^{*2}\times S_{1133}\times S_{2222}\times S_{3311} - 4\times C_{11}\times C_{12}\times C_{12}^{*}\times S_{1111}\times S_{2222} + 4\times C_{11}\times C_{12}\times C_{12}^{*}\times S_{1122}\times S_{2211} -$

$C_{11}\times C_{12}\times C_{11}^{*}\times S_{1111}\times S_{2233} + C_{11}\times C_{12}\times C_{11}^{*}\times S_{1133}\times S_{2211} - C_{11}\times C_{12}\times C_{12}^{*}\times S_{1111}\times S_{2233} +$

$C_{11}\times C_{12}\times C_{12}^{*}\times S_{1133}\times S_{2211} + C_{11}\times C_{12}\times C_{11}^{*}\times S_{1122}\times S_{2233} - C_{11}\times C_{12}\times C_{11}^{*}\times S_{1133}\times S_{2222} +$

$C_{11}\times C_{12}\times C_{12}^{*}\times S_{1122}\times S_{2233} - C_{11}\times C_{12}\times C_{12}^{*}\times S_{1133}\times S_{2222} + 2\times C_{12}\times C_{11}^{*}\times C_{12}^{*}\times S_{1111}\times S_{2222} -$

$2\times C_{12}\times C_{11}^{*}\times C_{12}^{*}\times S_{1122}\times S_{2211} - C_{11}\times C_{11}^{*}\times C_{12}^{*}\times S_{1111}\times S_{2233} + C_{11}\times C_{11}^{*}\times C_{12}^{*}\times S_{1133}\times S_{2211} -$

$C_{12}\times C_{11}^{*}\times C_{12}^{*}\times S_{1111}\times S_{2233} + C_{12}\times C_{11}^{*}\times C_{12}^{*}\times S_{1133}\times S_{2211} + C_{11}\times C_{11}^{*}\times C_{12}^{*}\times S_{1122}\times S_{2233} -$

$C_{11}\times C_{11}^{*}\times C_{12}^{*}\times S_{1133}\times S_{2222} + C_{12}\times C_{11}^{*}\times C_{12}^{*}\times S_{1122}\times S_{2233} - C_{12}\times C_{11}^{*}\times C_{12}^{*}\times S_{1133}\times S_{2222} -$

$C_{11}\times C_{12}\times C_{11}^{*}\times S_{1111}\times S_{3322} + C_{11}\times C_{12}\times C_{11}^{*}\times S_{1122}\times S_{3311} - C_{11}\times C_{12}\times C_{12}^{*}\times S_{1111}\times S_{3322} +$

$C_{11}\times C_{12}\times C_{12}^{*}\times S_{1122}\times S_{3311} - 4\times C_{11}\times C_{12}\times C_{12}^{*}\times S_{1111}\times S_{3333} + 4\times C_{11}\times C_{12}\times C_{12}^{*}\times S_{1133}\times S_{3311} -$

$C_{11}\times C_{12}\times C_{11}^{*}\times S_{1122}\times S_{3333} + C_{11}\times C_{12}\times C_{11}^{*}\times S_{1133}\times S_{3322} - C_{11}\times C_{12}\times C_{12}^{*}\times S_{1122}\times S_{3333} +$

$C_{11}\times C_{12}\times C_{12}^{*}\times S_{1133}\times S_{3322} - C_{11}\times C_{11}^{*}\times C_{12}^{*}\times S_{1111}\times S_{3322} + C_{11}\times C_{11}^{*}\times C_{12}^{*}\times S_{1122}\times S_{3311} -$

$C_{12}\times C_{11}^{*}\times C_{12}^{*}\times S_{1111}\times S_{3322} + C_{12}\times C_{11}^{*}\times C_{12}^{*}\times S_{1122}\times S_{3311} + 2\times C_{12}\times C_{11}^{*}\times C_{12}^{*}\times S_{1111}\times S_{3333} -$

$2\times C_{12}\times C_{11}^{*}\times C_{12}^{*}\times S_{1133}\times S_{3311} - C_{11}\times C_{11}^{*}\times C_{12}^{*}\times S_{1122}\times S_{3333} + C_{11}\times C_{11}^{*}\times C_{12}^{*}\times S_{1133}\times S_{3322} -$

$C_{12}\times C_{11}^{*}\times C_{12}^{*}\times S_{1122}\times S_{3333} + C_{12}\times C_{11}^{*}\times C_{12}^{*}\times S_{1133}\times S_{3322} + C_{11}\times C_{12}\times C_{11}^{*}\times S_{2211}\times S_{3322} -$

$C_{11}\times C_{12}\times C_{11}^{*}\times S_{2222}\times S_{3311} + C_{11}\times C_{12}\times C_{12}^{*}\times S_{2211}\times S_{3322} - C_{11}\times C_{12}\times C_{12}^{*}\times S_{2222}\times S_{3311} -$

$C_{11}\times C_{12}\times C_{11}^{*}\times S_{2211}\times S_{3333} + C_{11}\times C_{12}\times C_{11}^{*}\times S_{2233}\times S_{3311} - C_{11}\times C_{12}\times C_{12}^{*}\times S_{2211}\times S_{3333} +$

$C_{11}\times C_{12}\times C_{12}^{*}\times S_{2233}\times S_{3311} - 4\times C_{11}\times C_{12}\times C_{12}^{*}\times S_{2222}\times S_{3333} + 4\times C_{11}\times C_{12}\times C_{12}^{*}\times S_{2233}\times S_{3322} +$

$C_{11}\times C_{11}^{*}\times C_{12}^{*}\times S_{2211}\times S_{3322} - C_{11}\times C_{11}^{*}\times C_{12}^{*}\times S_{2222}\times S_{3311} + C_{12}\times C_{11}^{*}\times C_{12}^{*}\times S_{2211}\times S_{3322} -$

$C_{12}\times C_{11}^{*}\times C_{12}^{*}\times S_{2222}\times S_{3311} - C_{11}\times C_{11}^{*}\times C_{12}^{*}\times S_{2211}\times S_{3333} + C_{11}\times C_{11}^{*}\times C_{12}^{*}\times S_{2233}\times S_{3311} -$

$C_{12}\times C_{11}^{*}\times C_{12}^{*}\times S_{2211}\times S_{3333} + C_{12}\times C_{11}^{*}\times C_{12}^{*}\times S_{2233}\times S_{3311} + 2\times C_{12}\times C_{11}^{*}\times C_{12}^{*}\times S_{2222}\times S_{3333} -$

$2\times C_{12}\times C_{11}^{*}\times C_{12}^{*}\times S_{2233}\times S_{3322} + 6\times C_{11}\times C_{12}\times C_{12}^{*}\times S_{1111}\times S_{2222}\times S_{3333} -$

$6\times C_{11}\times C_{12}\times C_{12}^{*}\times S_{1111}\times S_{2233}\times S_{3322} - 6\times C_{11}\times C_{12}\times C_{12}^{*}\times S_{1122}\times S_{2211}\times S_{3333} +$

$6\times C_{11}\times C_{12}\times C_{12}^{*}\times S_{1122}\times S_{2233}\times S_{3311} + 6\times C_{11}\times C_{12}\times C_{12}^{*}\times S_{1133}\times S_{2211}\times S_{3322} -$

$6\times C_{11}\times C_{12}\times C_{12}^{*}\times S_{1133}\times S_{2222}\times S_{3311} - 6\times C_{12}\times C_{11}^{*}\times C_{12}^{*}\times S_{1111}\times S_{2222}\times S_{3333} +$

$6\times C_{12}\times C_{11}^{*}\times C_{12}^{*}\times S_{1111}\times S_{2233}\times S_{3322} + 6\times C_{12}\times C_{11}^{*}\times C_{12}^{*}\times S_{1122}\times S_{2211}\times S_{3333} -$

$6\times C_{12}\times C_{11}^{*}\times C_{12}^{*}\times S_{1122}\times S_{2233}\times S_{3311} - 6\times C_{12}\times C_{11}^{*}\times C_{12}^{*}\times S_{1133}\times S_{2211}\times S_{3322} +$

$6\times C_{12}\times C_{11}^{*}\times C_{12}^{*}\times S_{1133}\times S_{2222}\times S_{3311})$

Appendix B

The closed form expression of the strain energy per unit volume (ω^{coh}) for a coherent anisotropic inhomogeneity (without shear stress) in an anisotropic matrix is given below. In the expression, ε denotes the lattice mismatch between the inhomogeneity and the matrix, S_{ijkl} is referred to as the Eshelby tensor and C_{ij}^{*} and C_{ij} denote the elastic constants of the inhomogeneity and matrix respectively.

ω^{coh} = (ε^2×(C_{11} + 2×C_{12})×(C_{11}* + 2×C_{12}*)×(3×C_{11}^2×S_{1111} + 3×C_{12}^2×S_{1111} + 3×C_{11}^2×S_{2222} + 3×C_{12}^2×S_{2222} + 3×C_{11}^2×S_{3333} + 3×C_{12}^2×S_{3333} - 3×C_{11}^2 - 3×C_{12}^2 + 6×C_{11}×C_{12} - 6×C_{11}×C_{12}×S_{1111} - 2×C_{11}×C_{11}*×S_{1111} + 2×C_{11}×C_{12}*×S_{1111} + 2×C_{12}×C_{11}*×S_{1111} - 2×C_{12}×C_{12}*×S_{1111} + C_{11}×C_{11}*×S_{1122} - C_{11}×C_{12}*×S_{1122} - C_{12}×C_{11}*×S_{1122} + C_{12}×C_{12}*×S_{1122} + C_{11}×C_{11}*×S_{1133} - C_{11}×C_{12}*×S_{1133} - C_{12}×C_{11}*×S_{1133} + C_{12}×C_{12}*×S_{1133} - 6×C_{11}×C_{12}×S_{2222} + C_{11}×C_{11}*×S_{2211} - C_{11}×C_{12}*×S_{2211} - C_{12}×C_{11}*×S_{2211} + C_{12}×C_{12}*×S_{2211} - 2×C_{11}×C_{11}*×S_{2222} + 2×C_{11}×C_{12}*×S_{2222} + 2×C_{12}×C_{11}*×S_{2222} - 2×C_{12}×C_{12}*×S_{2222} + C_{11}×C_{11}*×S_{2233} - C_{11}×C_{12}*×S_{2233} - C_{12}×C_{11}*×S_{2233} + C_{12}×C_{12}*×S_{2233} - 6×C_{11}×C_{12}×S_{3333} + C_{11}×C_{11}*×S_{3311} - C_{11}×C_{12}*×S_{3311} - C_{12}×C_{11}*×S_{3311} + C_{12}×C_{12}*×S_{3311} + C_{11}×C_{11}*×S_{3322} - C_{11}×C_{12}*×S_{3322} - C_{12}×C_{11}*×S_{3322} + C_{12}×C_{12}*×S_{3322} - 2×C_{11}×C_{11}*×S_{3333} + 2×C_{11}×C_{12}*×S_{3333} + 2×C_{12}×C_{11}*×S_{3333} - 2×C_{12}×C_{12}*×S_{3333} - 3×C_{11}^2×S_{1111}×S_{2222} + 3×C_{11}^2×S_{1122}×S_{2211} - 3×C_{12}^2×S_{1111}×S_{2222} + 3×C_{12}^2×S_{1122}×S_{2211} - C_{11}*^{2}×S_{1111}×S_{2222} + C_{11}*^{2}×S_{1122}×S_{2211} - C_{12}*^{2}×S_{1111}×S_{2222} + C_{12}*^{2}×S_{1122}×S_{2211} + C_{11}*^{2}×S_{1111}×S_{2233} - C_{11}*^{2}×S_{1133}×S_{2211} + C_{12}*^{2}×S_{1111}×S_{2233} - C_{12}*^{2}×S_{1133}×S_{2211} - C_{11}*^{2}×S_{1122}×S_{2233} + C_{11}*^{2}×S_{1133}×S_{2222} - C_{12}*^{2}×S_{1122}×S_{2233} + C_{12}*^{2}×S_{1133}×S_{2222} - 3×C_{11}^2×S_{1111}×S_{3333} + 3×C_{11}^2×S_{1133}×S_{3311} - 3×C_{12}^2×S_{1111}×S_{3333} + 3×C_{12}^2×S_{1133}×S_{3311} + C_{11}*^{2}×S_{1111}×S_{3322} - C_{11}*^{2}×S_{1122}×S_{3311} + C_{12}*^{2}×S_{1111}×S_{3322} - C_{12}*^{2}×S_{1122}×S_{3311} - C_{11}*^{2}×S_{1111}×S_{3333} + C_{11}*^{2}×S_{1133}×S_{3311} - C_{12}*^{2}×S_{1111}×S_{3333} + C_{12}*^{2}×S_{1133}×S_{3311} + C_{11}*^{2}×S_{1122}×S_{3333} - C_{11}*^{2}×S_{1133}×S_{3322} + C_{12}*^{2}×S_{1122}×S_{3333} - C_{12}*^{2}×S_{1133}×S_{3322} - 3×C_{11}^2×S_{2222}×S_{3333} +

$3\times C_{11}^{2}\times S_{2233}\times S_{3322} - 3\times C_{12}^{2}\times S_{2222}\times S_{3333} + 3\times C_{12}^{2}\times S_{2233}\times S_{3322} - C_{11}^{*2}\times S_{2211}\times S_{3322} +$

$C_{11}^{*2}\times S_{2222}\times S_{3311} - C_{12}^{*2}\times S_{2211}\times S_{3322} + C_{12}^{*2}\times S_{2222}\times S_{3311} + C_{11}^{*2}\times S_{2211}\times S_{3333} - C_{11}^{*2}\times S_{2233}\times S_{3311} +$

$C_{12}^{*2}\times S_{2211}\times S_{3333} - C_{12}^{*2}\times S_{2233}\times S_{3311} - C_{11}^{*2}\times S_{2222}\times S_{3333} + C_{11}^{*2}\times S_{2233}\times S_{3322} - C_{12}^{*2}\times S_{2222}\times S_{3333} +$

$C_{12}^{*2}\times S_{2233}\times S_{3322} + 6\times C_{11}\times C_{12}\times S_{1111}\times S_{2222} - 6\times C_{11}\times C_{12}\times S_{1122}\times S_{2211} + 4\times C_{11}\times C_{11}^{*}\times S_{1111}\times S_{2222} -$

$4\times C_{11}\times C_{11}^{*}\times S_{1122}\times S_{2211} - 4\times C_{11}\times C_{12}^{*}\times S_{1111}\times S_{2222} + 4\times C_{11}\times C_{12}^{*}\times S_{1122}\times S_{2211} -$

$4\times C_{12}\times C_{11}^{*}\times S_{1111}\times S_{2222} + 4\times C_{12}\times C_{11}^{*}\times S_{1122}\times S_{2211} + 4\times C_{12}\times C_{12}^{*}\times S_{1111}\times S_{2222} -$

$4\times C_{12}\times C_{12}^{*}\times S_{1122}\times S_{2211} - C_{11}\times C_{11}^{*}\times S_{1111}\times S_{2233} + C_{11}\times C_{11}^{*}\times S_{1133}\times S_{2211} + C_{11}\times C_{12}^{*}\times S_{1111}\times S_{2233} -$

$C_{11}\times C_{12}^{*}\times S_{1133}\times S_{2211} + C_{12}\times C_{11}^{*}\times S_{1111}\times S_{2233} - C_{12}\times C_{11}^{*}\times S_{1133}\times S_{2211} - C_{12}\times C_{12}^{*}\times S_{1111}\times S_{2233} +$

$C_{12}\times C_{12}^{*}\times S_{1133}\times S_{2211} + C_{11}\times C_{11}^{*}\times S_{1122}\times S_{2233} - C_{11}\times C_{11}^{*}\times S_{1133}\times S_{2222} - C_{11}\times C_{12}^{*}\times S_{1122}\times S_{2233} +$

$C_{11}\times C_{12}^{*}\times S_{1133}\times S_{2222} - C_{12}\times C_{11}^{*}\times S_{1122}\times S_{2233} + C_{12}\times C_{11}^{*}\times S_{1133}\times S_{2222} + C_{12}\times C_{12}^{*}\times S_{1122}\times S_{2233} -$

$C_{12}\times C_{12}^{*}\times S_{1133}\times S_{2222} + 2\times C_{11}^{*}\times C_{12}^{*}\times S_{1111}\times S_{2222} - 2\times C_{11}^{*}\times C_{12}^{*}\times S_{1122}\times S_{2211} -$

$2\times C_{11}^{*}\times C_{12}^{*}\times S_{1111}\times S_{2233} + 2\times C_{11}^{*}\times C_{12}^{*}\times S_{1133}\times S_{2211} + 2\times C_{11}^{*}\times C_{12}^{*}\times S_{1122}\times S_{2233} -$

$2\times C_{11}^{*}\times C_{12}^{*}\times S_{1133}\times S_{2222} + 6\times C_{11}\times C_{12}\times S_{1111}\times S_{3333} - 6\times C_{11}\times C_{12}\times S_{1133}\times S_{3311} - C_{11}\times C_{11}^{*}\times S_{1111}\times S_{3322}$

$+ C_{11}\times C_{11}^{*}\times S_{1122}\times S_{3311} + C_{11}\times C_{12}^{*}\times S_{1111}\times S_{3322} - C_{11}\times C_{12}^{*}\times S_{1122}\times S_{3311} + C_{12}\times C_{11}^{*}\times S_{1111}\times S_{3322} -$

$C_{12}\times C_{11}^{*}\times S_{1122}\times S_{3311} - C_{12}\times C_{12}^{*}\times S_{1111}\times S_{3322} + C_{12}\times C_{12}^{*}\times S_{1122}\times S_{3311} + 4\times C_{11}\times C_{11}^{*}\times S_{1111}\times S_{3333} -$

$4\times C_{11}\times C_{11}^{*}\times S_{1133}\times S_{3311} - 4\times C_{11}\times C_{12}^{*}\times S_{1111}\times S_{3333} + 4\times C_{11}\times C_{12}^{*}\times S_{1133}\times S_{3311} -$

$4\times C_{12}\times C_{11}^{*}\times S_{1111}\times S_{3333} + 4\times C_{12}\times C_{11}^{*}\times S_{1133}\times S_{3311} + 4\times C_{12}\times C_{12}^{*}\times S_{1111}\times S_{3333} -$

$4\times C_{12}\times C_{12}^{*}\times S_{1133}\times S_{3311} - C_{11}\times C_{11}^{*}\times S_{1122}\times S_{3333} + C_{11}\times C_{11}^{*}\times S_{1133}\times S_{3322} + C_{11}\times C_{12}^{*}\times S_{1122}\times S_{3333} -$

$C_{11}\times C_{12}^{*}\times S_{1133}\times S_{3322} + C_{12}\times C_{11}^{*}\times S_{1122}\times S_{3333} - C_{12}\times C_{11}^{*}\times S_{1133}\times S_{3322} - C_{12}\times C_{12}^{*}\times S_{1122}\times S_{3333} +$

$C_{12}\times C_{12}^{*}\times S_{1133}\times S_{3322} - 2\times C_{11}^{*}\times C_{12}^{*}\times S_{1111}\times S_{3322} + 2\times C_{11}^{*}\times C_{12}^{*}\times S_{1122}\times S_{3311} +$

$2\times C_{11}^{*}\times C_{12}^{*}\times S_{1111}\times S_{3333} - 2\times C_{11}^{*}\times C_{12}^{*}\times S_{1133}\times S_{3311} - 2\times C_{11}^{*}\times C_{12}^{*}\times S_{1122}\times S_{3333} +$

$2\times C_{11}^{*}\times C_{12}^{*}\times S_{1133}\times S_{3322} + 6\times C_{11}\times C_{12}\times S_{2222}\times S_{3333} - 6\times C_{11}\times C_{12}\times S_{2233}\times S_{3322} +$

$C_{11}\times C_{11}^{*}\times S_{2211}\times S_{3322} - C_{11}\times C_{11}^{*}\times S_{2222}\times S_{3311} - C_{11}\times C_{12}^{*}\times S_{2211}\times S_{3322} + C_{11}\times C_{12}^{*}\times S_{2222}\times S_{3311} -$

$C_{12}\times C_{11}^{*}\times S_{2211}\times S_{3322} + C_{12}\times C_{11}^{*}\times S_{2222}\times S_{3311} + C_{12}\times C_{12}^{*}\times S_{2211}\times S_{3322} - C_{12}\times C_{12}^{*}\times S_{2222}\times S_{3311} -$

$C_{11}\times C_{11}^{*}\times S_{2211}\times S_{3333} + C_{11}\times C_{11}^{*}\times S_{2233}\times S_{3311} + C_{11}\times C_{12}^{*}\times S_{2211}\times S_{3333} - C_{11}\times C_{12}^{*}\times S_{2233}\times S_{3311} +$

$C_{12}\times C_{11}^{*}\times S_{2211}\times S_{3333} - C_{12}\times C_{11}^{*}\times S_{2233}\times S_{3311} - C_{12}\times C_{12}^{*}\times S_{2211}\times S_{3333} + C_{12}\times C_{12}^{*}\times S_{2233}\times S_{3311} +$

$4\times C_{11}\times C_{11}^{*}\times S_{2222}\times S_{3333} - 4\times C_{11}\times C_{11}^{*}\times S_{2233}\times S_{3322} - 4\times C_{11}\times C_{12}^{*}\times S_{2222}\times S_{3333} +$

$4\times C_{11}\times C_{12}^{*}\times S_{2233}\times S_{3322} - 4\times C_{12}\times C_{11}^{*}\times S_{2222}\times S_{3333} + 4\times C_{12}\times C_{11}^{*}\times S_{2233}\times S_{3322} +$

$4\times C_{12}\times C_{12}^{*}\times S_{2222}\times S_{3333} - 4\times C_{12}\times C_{12}^{*}\times S_{2233}\times S_{3322} + 2\times C_{11}^{*}\times C_{12}^{*}\times S_{2211}\times S_{3322} -$

$2\times C_{11}^{*}\times C_{12}^{*}\times S_{2222}\times S_{3311} - 2\times C_{11}^{*}\times C_{12}^{*}\times S_{2211}\times S_{3333} + 2\times C_{11}^{*}\times C_{12}^{*}\times S_{2233}\times S_{3311} +$

$2\times C_{11}^{*}\times C_{12}^{*}\times S_{2222}\times S_{3333} - 2\times C_{11}^{*}\times C_{12}^{*}\times S_{2233}\times S_{3322} + 3\times C_{11}^{2}\times S_{1111}\times S_{2222}\times S_{3333} -$

$3\times C_{11}^{2}\times S_{1111}\times S_{2233}\times S_{3322} - 3\times C_{11}^{2}\times S_{1122}\times S_{2211}\times S_{3333} + 3\times C_{11}^{2}\times S_{1122}\times S_{2233}\times S_{3311} +$

$3\times C_{11}^{2}\times S_{1133}\times S_{2211}\times S_{3322} - 3\times C_{11}^{2}\times S_{1133}\times S_{2222}\times S_{3311} + 3\times C_{12}^{2}\times S_{1111}\times S_{2222}\times S_{3333} -$

$3\times C_{12}^{2}\times S_{1111}\times S_{2233}\times S_{3322} - 3\times C_{12}^{2}\times S_{1122}\times S_{2211}\times S_{3333} + 3\times C_{12}^{2}\times S_{1122}\times S_{2233}\times S_{3311} +$

$3\times C_{12}^{2}\times S_{1133}\times S_{2211}\times S_{3322} - 3\times C_{12}^{2}\times S_{1133}\times S_{2222}\times S_{3311} + 3\times C_{11}^{*2}\times S_{1111}\times S_{2222}\times S_{3333} -$

$3\times C_{11}^{*2}\times S_{1111}\times S_{2233}\times S_{3322} - 3\times C_{11}^{*2}\times S_{1122}\times S_{2211}\times S_{3333} + 3\times C_{11}^{*2}\times S_{1122}\times S_{2233}\times S_{3311} +$

$3\times C_{11}^{*2}\times S_{1133}\times S_{2211}\times S_{3322} - 3\times C_{11}^{*2}\times S_{1133}\times S_{2222}\times S_{3311} + 3\times C_{12}^{*2}\times S_{1111}\times S_{2222}\times S_{3333} -$

$3\times C_{12}^{*2}\times S_{1111}\times S_{2233}\times S_{3322} - 3\times C_{12}^{*2}\times S_{1122}\times S_{2211}\times S_{3333} + 3\times C_{12}^{*2}\times S_{1122}\times S_{2233}\times S_{3311} +$

$3\times C_{12}^{*2}\times S_{1133}\times S_{2211}\times S_{3322} - 3\times C_{12}^{*2}\times S_{1133}\times S_{2222}\times S_{3311} - 6\times C_{11}\times C_{12}\times S_{1111}\times S_{2222}\times S_{3333} +$

$6\times C_{11}\times C_{12}\times S_{1111}\times S_{2233}\times S_{3322} + 6\times C_{11}\times C_{12}\times S_{1122}\times S_{2211}\times S_{3333} - 6\times C_{11}\times C_{12}\times S_{1122}\times S_{2233}\times S_{3311} -$

$6\times C_{11}\times C_{12}\times S_{1133}\times S_{2211}\times S_{3322} + 6\times C_{11}\times C_{12}\times S_{1133}\times S_{2222}\times S_{3311} - 6\times C_{11}\times C_{11}^{*}\times S_{1111}\times S_{2222}\times S_{3333} +$

$6\times C_{11}\times C_{11}^{*}\times S_{1111}\times S_{2233}\times S_{3322} + 6\times C_{11}\times C_{11}^{*}\times S_{1122}\times S_{2211}\times S_{3333} - 6\times C_{11}\times C_{11}^{*}\times S_{1122}\times S_{2233}\times S_{3311} -$

$6\times C_{11}\times C_{11}^{*}\times S_{1133}\times S_{2211}\times S_{3322} + 6\times C_{11}\times C_{11}^{*}\times S_{1133}\times S_{2222}\times S_{3311} + 6\times C_{11}\times C_{12}^{*}\times S_{1111}\times S_{2222}\times S_{3333} -$

$6\times C_{11}\times C_{12}^{*}\times S_{1111}\times S_{2233}\times S_{3322} - 6\times C_{11}\times C_{12}^{*}\times S_{1122}\times S_{2211}\times S_{3333} + 6\times C_{11}\times C_{12}^{*}\times S_{1122}\times S_{2233}\times S_{3311} +$

$6\times C_{11}\times C_{12}^{*}\times S_{1133}\times S_{2211}\times S_{3322} - 6\times C_{11}\times C_{12}^{*}\times S_{1133}\times S_{2222}\times S_{3311} + 6\times C_{12}\times C_{11}^{*}\times S_{1111}\times S_{2222}\times S_{3333} -$

$6\times C_{12}\times C_{11}^{*}\times S_{1111}\times S_{2233}\times S_{3322} - 6\times C_{12}\times C_{11}^{*}\times S_{1122}\times S_{2211}\times S_{3333} + 6\times C_{12}\times C_{11}^{*}\times S_{1122}\times S_{2233}\times S_{3311} +$

$6\times C_{12}\times C_{11}^{*}\times S_{1133}\times S_{2211}\times S_{3322} - 6\times C_{12}\times C_{11}^{*}\times S_{1133}\times S_{2222}\times S_{3311} - 6\times C_{12}\times C_{12}^{*}\times S_{1111}\times S_{2222}\times S_{3333} +$

$6\times C_{12}\times C_{12}^{*}\times S_{1111}\times S_{2233}\times S_{3322} + 6\times C_{12}\times C_{12}^{*}\times S_{1122}\times S_{2211}\times S_{3333} - 6\times C_{12}\times C_{12}^{*}\times S_{1122}\times S_{2233}\times S_{3311} -$

$6\times C_{12}\times C_{12}^{*}\times S_{1133}\times S_{2211}\times S_{3322} + 6\times C_{12}\times C_{12}^{*}\times S_{1133}\times S_{2222}\times S_{3311} - 6\times C_{11}^{*}\times C_{12}^{*}\times S_{1111}\times S_{2222}\times S_{3333} +$

$6\times C_{11}^{*}\times C_{12}^{*}\times S_{1111}\times S_{2233}\times S_{3322} + 6\times C_{11}^{*}\times C_{12}^{*}\times S_{1122}\times S_{2211}\times S_{3333} - 6\times C_{11}^{*}\times C_{12}^{*}\times S_{1122}\times S_{2233}\times S_{3311}$

$- 6\times C_{11}^{*}\times C_{12}^{*}\times S_{1133}\times S_{2211}\times S_{3322} + 6\times C_{11}^{*}\times C_{12}^{*}\times S_{1133}\times S_{2222}\times S_{3311}))/(2\times(3\times C_{11}\times C_{12}^{2} + C_{11}^{3}\times S_{1111}$

$+ 2\times C_{12}^{3}\times S_{1111} + C_{11}^{3}\times S_{2222} + 2\times C_{12}^{3}\times S_{2222} + C_{11}^{3}\times S_{3333} + 2\times C_{12}^{3}\times S_{3333} - C_{11}^{3} - 2\times C_{12}^{3} -$

$3\times C_{11}\times C_{12}^2\times S_{1111} - C_{11}^2\times C_{11}^*\times S_{1111} + C_{12}^2\times C_{11}^*\times S_{1111} - 2\times C_{12}^2\times C_{12}^*\times S_{1111} - C_{11}^2\times C_{12}^*\times S_{1122} -$

$C_{12}^2\times C_{11}^*\times S_{1122} - C_{11}^2\times C_{12}^*\times S_{1133} - C_{12}^2\times C_{11}^*\times S_{1133} - 3\times C_{11}\times C_{12}^2\times S_{2222} - C_{11}^2\times C_{12}^*\times S_{2211} -$

$C_{12}^2\times C_{11}^*\times S_{2211} - C_{11}^2\times C_{11}^*\times S_{2222} + C_{12}^2\times C_{11}^*\times S_{2222} - 2\times C_{12}^2\times C_{12}^*\times S_{2222} - C_{11}^2\times C_{12}^*\times S_{2233} -$

$C_{12}^2\times C_{11}^*\times S_{2233} - 3\times C_{11}\times C_{12}^2\times S_{3333} - C_{11}^2\times C_{12}^*\times S_{3311} - C_{12}^2\times C_{11}^*\times S_{3311} - C_{11}^2\times C_{12}^*\times S_{3322} -$

$C_{12}^2\times C_{11}^*\times S_{3322} - C_{11}^2\times C_{11}^*\times S_{3333} + C_{12}^2\times C_{11}^*\times S_{3333} - 2\times C_{12}^2\times C_{12}^*\times S_{3333} - C_{11}^3\times S_{1111}\times S_{2222} +$

$C_{11}^3\times S_{1122}\times S_{2211} - 2\times C_{12}^3\times S_{1111}\times S_{2222} + 2\times C_{12}^3\times S_{1122}\times S_{2211} - C_{11}^3\times S_{1111}\times S_{3333} + C_{11}^3\times S_{1133}\times S_{3311} -$

$2\times C_{12}^3\times S_{1111}\times S_{3333} + 2\times C_{12}^3\times S_{1133}\times S_{3311} - C_{11}^3\times S_{2222}\times S_{3333} + C_{11}^3\times S_{2233}\times S_{3322} - 2\times C_{12}^3\times S_{2222}\times S_{3333}$

$+ 2\times C_{12}^3\times S_{2233}\times S_{3322} + 2\times C_{11}\times C_{12}\times C_{12}^*\times S_{1111} + C_{11}\times C_{12}\times C_{11}^*\times S_{1122} + C_{11}\times C_{12}\times C_{12}^*\times S_{1122} +$

$C_{11}\times C_{12}\times C_{11}^*\times S_{1133} + C_{11}\times C_{12}\times C_{12}^*\times S_{1133} + C_{11}\times C_{12}\times C_{11}^*\times S_{2211} + C_{11}\times C_{12}\times C_{12}^*\times S_{2211} +$

$2\times C_{11}\times C_{12}\times C_{12}^*\times S_{2222} + C_{11}\times C_{12}\times C_{11}^*\times S_{2233} + C_{11}\times C_{12}\times C_{12}^*\times S_{2233} + C_{11}\times C_{12}\times C_{11}^*\times S_{3311} +$

$C_{11}\times C_{12}\times C_{12}^*\times S_{3311} + C_{11}\times C_{12}\times C_{11}^*\times S_{3322} + C_{11}\times C_{12}\times C_{12}^*\times S_{3322} + 2\times C_{11}\times C_{12}\times C_{12}^*\times S_{3333} +$

$3\times C_{11}\times C_{12}^2\times S_{1111}\times S_{2222} - 3\times C_{11}\times C_{12}^2\times S_{1122}\times S_{2211} - C_{11}\times C_{11}^{*2}\times S_{1111}\times S_{2222} + C_{11}\times C_{11}^{*2}\times S_{1122}\times S_{2211}$

$+ 2\times C_{11}^2\times C_{11}^*\times S_{1111}\times S_{2222} - 2\times C_{11}^2\times C_{11}^*\times S_{1122}\times S_{2211} + C_{11}\times C_{12}^{*2}\times S_{1111}\times S_{2222} -$

$C_{11}\times C_{12}^{*2}\times S_{1122}\times S_{2211} - 2\times C_{12}^2\times C_{11}^*\times S_{1111}\times S_{2222} + 2\times C_{12}^2\times C_{11}^*\times S_{1122}\times S_{2211} -$

$2\times C_{12}\times C_{12}^{*2}\times S_{1111}\times S_{2222} + 2\times C_{12}\times C_{12}^{*2}\times S_{1122}\times S_{2211} + 4\times C_{12}^2\times C_{12}^*\times S_{1111}\times S_{2222} -$

$4\times C_{12}^2\times C_{12}^*\times S_{1122}\times S_{2211} + C_{11}\times C_{12}^{*2}\times S_{1111}\times S_{2233} - C_{11}\times C_{12}^{*2}\times S_{1133}\times S_{2211} + C_{12}\times C_{11}^{*2}\times S_{1111}\times S_{2233}$

$- C_{12}\times C_{11}^{*2}\times S_{1133}\times S_{2211} + C_{11}^2\times C_{12}^*\times S_{1111}\times S_{2233} - C_{11}^2\times C_{12}^*\times S_{1133}\times S_{2211} + C_{12}^2\times C_{11}^*\times S_{1111}\times S_{2233} -$

$C_{12}^2\times C_{11}^*\times S_{1133}\times S_{2211} - C_{11}\times C_{12}^{*2}\times S_{1122}\times S_{2233} + C_{11}\times C_{12}^{*2}\times S_{1133}\times S_{2222} - C_{12}\times C_{11}^{*2}\times S_{1122}\times S_{2233} +$

$C_{12}\times C_{11}^{*2}\times S_{1133}\times S_{2222} - C_{11}^2\times C_{12}^*\times S_{1122}\times S_{2233} + C_{11}^2\times C_{12}^*\times S_{1133}\times S_{2222} - C_{12}^2\times C_{11}^*\times S_{1122}\times S_{2233} +$

$C_{12}^2\times C_{11}^*\times S_{1133}\times S_{2222} + 3\times C_{11}\times C_{12}^2\times S_{1111}\times S_{3333} - 3\times C_{11}\times C_{12}^2\times S_{1133}\times S_{3311} + C_{11}\times C_{12}^{*2}\times S_{1111}\times S_{3322}$

$- C_{11}\times C_{12}^{*2}\times S_{1122}\times S_{3311} + C_{12}\times C_{11}^{*2}\times S_{1111}\times S_{3322} - C_{12}\times C_{11}^{*2}\times S_{1122}\times S_{3311} + C_{11}^2\times C_{12}^*\times S_{1111}\times S_{3322} -$

$C_{11}^2\times C_{12}^*\times S_{1122}\times S_{3311} + C_{12}^2\times C_{11}^*\times S_{1111}\times S_{3322} - C_{12}^2\times C_{11}^*\times S_{1122}\times S_{3311} - C_{11}\times C_{11}^{*2}\times S_{1111}\times S_{3333} +$

$C_{11}\times C_{11}^{*2}\times S_{1133}\times S_{3311} + 2\times C_{11}^2\times C_{11}^*\times S_{1111}\times S_{3333} - 2\times C_{11}^2\times C_{11}^*\times S_{1133}\times S_{3311} +$

$C_{11}\times C_{12}^{*2}\times S_{1111}\times S_{3333} - C_{11}\times C_{12}^{*2}\times S_{1133}\times S_{3311} - 2\times C_{12}^2\times C_{11}^*\times S_{1111}\times S_{3333} +$

$2\times C_{12}^2\times C_{11}^*\times S_{1133}\times S_{3311} - 2\times C_{12}\times C_{12}^{*2}\times S_{1111}\times S_{3333} + 2\times C_{12}\times C_{12}^{*2}\times S_{1133}\times S_{3311} +$

$4\times C_{12}^2\times C_{12}^*\times S_{1111}\times S_{3333} - 4\times C_{12}^2\times C_{12}^*\times S_{1133}\times S_{3311} + C_{11}\times C_{12}^{*2}\times S_{1122}\times S_{3333} -$

$C_{11}\times C_{12}{}^{*2}\times S_{1133}\times S_{3322} + C_{12}\times C_{11}{}^{*2}\times S_{1122}\times S_{3333} - C_{12}\times C_{11}{}^{*2}\times S_{1133}\times S_{3322} + C_{11}{}^{2}\times C_{12}{}^{*}\times S_{1122}\times S_{3333} -$

$C_{11}{}^{2}\times C_{12}{}^{*}\times S_{1133}\times S_{3322} + C_{12}{}^{2}\times C_{11}{}^{*}\times S_{1122}\times S_{3333} - C_{12}{}^{2}\times C_{11}{}^{*}\times S_{1133}\times S_{3322} + 3\times C_{11}\times C_{12}{}^{2}\times S_{2222}\times S_{3333} -$

$3\times C_{11}\times C_{12}{}^{2}\times S_{2233}\times S_{3322} - C_{11}\times C_{12}{}^{*2}\times S_{2211}\times S_{3322} + C_{11}\times C_{12}{}^{*2}\times S_{2222}\times S_{3311} - C_{12}\times C_{11}{}^{*2}\times S_{2211}\times S_{3322} +$

$C_{12}\times C_{11}{}^{*2}\times S_{2222}\times S_{3311} - C_{11}{}^{2}\times C_{12}{}^{*}\times S_{2211}\times S_{3322} + C_{11}{}^{2}\times C_{12}{}^{*}\times S_{2222}\times S_{3311} - C_{12}{}^{2}\times C_{11}{}^{*}\times S_{2211}\times S_{3322} +$

$C_{12}{}^{2}\times C_{11}{}^{*}\times S_{2222}\times S_{3311} + C_{11}\times C_{12}{}^{*2}\times S_{2211}\times S_{3333} - C_{11}\times C_{12}{}^{*2}\times S_{2233}\times S_{3311} + C_{12}\times C_{11}{}^{*2}\times S_{2211}\times S_{3333} -$

$C_{12}\times C_{11}{}^{*2}\times S_{2233}\times S_{3311} + C_{11}{}^{2}\times C_{12}{}^{*}\times S_{2211}\times S_{3333} - C_{11}{}^{2}\times C_{12}{}^{*}\times S_{2233}\times S_{3311} + C_{12}{}^{2}\times C_{11}{}^{*}\times S_{2211}\times S_{3333} -$

$C_{12}{}^{2}\times C_{11}{}^{*}\times S_{2233}\times S_{3311} - C_{11}\times C_{11}{}^{*2}\times S_{2222}\times S_{3333} + C_{11}\times C_{11}{}^{*2}\times S_{2233}\times S_{3322} + 2\times C_{11}{}^{2}\times C_{11}{}^{*}\times S_{2222}\times S_{3333}$

$- 2\times C_{11}{}^{2}\times C_{11}{}^{*}\times S_{2233}\times S_{3322} + C_{11}\times C_{12}{}^{*2}\times S_{2222}\times S_{3333} - C_{11}\times C_{12}{}^{*2}\times S_{2233}\times S_{3322} -$

$2\times C_{12}{}^{2}\times C_{11}{}^{*}\times S_{2222}\times S_{3333} + 2\times C_{12}{}^{2}\times C_{11}{}^{*}\times S_{2233}\times S_{3322} - 2\times C_{12}\times C_{12}{}^{*2}\times S_{2222}\times S_{3333} +$

$2\times C_{12}\times C_{12}{}^{*2}\times S_{2233}\times S_{3322} + 4\times C_{12}{}^{2}\times C_{12}{}^{*}\times S_{2222}\times S_{3333} - 4\times C_{12}{}^{2}\times C_{12}{}^{*}\times S_{2233}\times S_{3322} +$

$C_{11}{}^{3}\times S_{1111}\times S_{2222}\times S_{3333} - C_{11}{}^{3}\times S_{1111}\times S_{2233}\times S_{3322} - C_{11}{}^{3}\times S_{1122}\times S_{2211}\times S_{3333} + C_{11}{}^{3}\times S_{1122}\times S_{2233}\times S_{3311} +$

$C_{11}{}^{3}\times S_{1133}\times S_{2211}\times S_{3322} - C_{11}{}^{3}\times S_{1133}\times S_{2222}\times S_{3311} + 2\times C_{12}{}^{3}\times S_{1111}\times S_{2222}\times S_{3333} -$

$2\times C_{12}{}^{3}\times S_{1111}\times S_{2233}\times S_{3322} - 2\times C_{12}{}^{3}\times S_{1122}\times S_{2211}\times S_{3333} + 2\times C_{12}{}^{3}\times S_{1122}\times S_{2233}\times S_{3311} +$

$2\times C_{12}{}^{3}\times S_{1133}\times S_{2211}\times S_{3322} - 2\times C_{12}{}^{3}\times S_{1133}\times S_{2222}\times S_{3311} - C_{11}{}^{*3}\times S_{1111}\times S_{2222}\times S_{3333} +$

$C_{11}{}^{*3}\times S_{1111}\times S_{2233}\times S_{3322} + C_{11}{}^{*3}\times S_{1122}\times S_{2211}\times S_{3333} - C_{11}{}^{*3}\times S_{1122}\times S_{2233}\times S_{3311} -$

$C_{11}{}^{*3}\times S_{1133}\times S_{2211}\times S_{3322} + C_{11}{}^{*3}\times S_{1133}\times S_{2222}\times S_{3311} - 2\times C_{12}{}^{*3}\times S_{1111}\times S_{2222}\times S_{3333} +$

$2\times C_{12}{}^{*3}\times S_{1111}\times S_{2233}\times S_{3322} + 2\times C_{12}{}^{*3}\times S_{1122}\times S_{2211}\times S_{3333} - 2\times C_{12}{}^{*3}\times S_{1122}\times S_{2233}\times S_{3311} -$

$2\times C_{12}{}^{*3}\times S_{1133}\times S_{2211}\times S_{3322} + 2\times C_{12}{}^{*3}\times S_{1133}\times S_{2222}\times S_{3311} - 3\times C_{11}\times C_{12}{}^{2}\times S_{1111}\times S_{2222}\times S_{3333} +$

$3\times C_{11}\times C_{12}{}^{2}\times S_{1111}\times S_{2233}\times S_{3322} + 3\times C_{11}\times C_{12}{}^{2}\times S_{1122}\times S_{2211}\times S_{3333} - 3\times C_{11}\times C_{12}{}^{2}\times S_{1122}\times S_{2233}\times S_{3311} -$

$3\times C_{11}\times C_{12}{}^{2}\times S_{1133}\times S_{2211}\times S_{3322} + 3\times C_{11}\times C_{12}{}^{2}\times S_{1133}\times S_{2222}\times S_{3311} + 3\times C_{11}\times C_{11}{}^{*2}\times S_{1111}\times S_{2222}\times S_{3333} -$

$3\times C_{11}\times C_{11}{}^{*2}\times S_{1111}\times S_{2233}\times S_{3322} - 3\times C_{11}\times C_{11}{}^{*2}\times S_{1122}\times S_{2211}\times S_{3333} + 3\times C_{11}\times C_{11}{}^{*2}\times S_{1122}\times S_{2233}\times S_{3311}$

$+ 3\times C_{11}\times C_{11}{}^{*2}\times S_{1133}\times S_{2211}\times S_{3322} - 3\times C_{11}\times C_{11}{}^{*2}\times S_{1133}\times S_{2222}\times S_{3311} - 3\times C_{11}{}^{2}\times C_{11}{}^{*}\times S_{1111}\times S_{2222}\times S_{3333}$

$+ 3\times C_{11}{}^{2}\times C_{11}{}^{*}\times S_{1111}\times S_{2233}\times S_{3322} + 3\times C_{11}{}^{2}\times C_{11}{}^{*}\times S_{1122}\times S_{2211}\times S_{3333} -$

$3\times C_{11}{}^{2}\times C_{11}{}^{*}\times S_{1122}\times S_{2233}\times S_{3311} - 3\times C_{11}{}^{2}\times C_{11}{}^{*}\times S_{1133}\times S_{2211}\times S_{3322} + 3\times C_{11}{}^{2}\times C_{11}{}^{*}\times S_{1133}\times S_{2222}\times S_{3311} -$

$3\times C_{11}\times C_{12}{}^{*2}\times S_{1111}\times S_{2222}\times S_{3333} + 3\times C_{11}\times C_{12}{}^{*2}\times S_{1111}\times S_{2233}\times S_{3322} + 3\times C_{11}\times C_{12}{}^{*2}\times S_{1122}\times S_{2211}\times S_{3333}$

$- 3\times C_{11}\times C_{12}{}^{*2}\times S_{1122}\times S_{2233}\times S_{3311} - 3\times C_{11}\times C_{12}{}^{*2}\times S_{1133}\times S_{2211}\times S_{3322} + 3\times C_{11}\times C_{12}{}^{*2}\times S_{1133}\times S_{2222}\times S_{3311}$

$$+ 3\times C_{12}^{2}\times C_{11}^{*}\times S_{1111}\times S_{2222}\times S_{3333} - 3\times C_{12}^{2}\times C_{11}^{*}\times S_{1111}\times S_{2233}\times S_{3322} - 3\times C_{12}^{2}\times C_{11}^{*}\times S_{1122}\times S_{2211}\times S_{3333}$$

$$+ 3\times C_{12}^{2}\times C_{11}^{*}\times S_{1122}\times S_{2233}\times S_{3311} + 3\times C_{12}^{2}\times C_{11}^{*}\times S_{1133}\times S_{2211}\times S_{3322} -$$

$$3\times C_{12}^{2}\times C_{11}^{*}\times S_{1133}\times S_{2222}\times S_{3311} + 6\times C_{12}\times C_{12}^{*2}\times S_{1111}\times S_{2222}\times S_{3333} - 6\times C_{12}\times C_{12}^{*2}\times S_{1111}\times S_{2233}\times S_{3322} -$$

$$6\times C_{12}\times C_{12}^{*2}\times S_{1122}\times S_{2211}\times S_{3333} + 6\times C_{12}\times C_{12}^{*2}\times S_{1122}\times S_{2233}\times S_{3311} + 6\times C_{12}\times C_{12}^{*2}\times S_{1133}\times S_{2211}\times S_{3322}$$

$$- 6\times C_{12}\times C_{12}^{*2}\times S_{1133}\times S_{2222}\times S_{3311} - 6\times C_{12}^{2}\times C_{12}^{*}\times S_{1111}\times S_{2222}\times S_{3333} + 6\times C_{12}^{2}\times C_{12}^{*}\times S_{1111}\times S_{2233}\times S_{3322}$$

$$+ 6\times C_{12}^{2}\times C_{12}^{*}\times S_{1122}\times S_{2211}\times S_{3333} - 6\times C_{12}^{2}\times C_{12}^{*}\times S_{1122}\times S_{2233}\times S_{3311} - 6\times C_{12}^{2}\times C_{12}^{*}\times S_{1133}\times S_{2211}\times S_{3322}$$

$$+ 6\times C_{12}^{2}\times C_{12}^{*}\times S_{1133}\times S_{2222}\times S_{3311} + 3\times C_{11}^{*}\times C_{12}^{*2}\times S_{1111}\times S_{2222}\times S_{3333} -$$

$$3\times C_{11}^{*}\times C_{12}^{*2}\times S_{1111}\times S_{2233}\times S_{3322} - 3\times C_{11}^{*}\times C_{12}^{*2}\times S_{1122}\times S_{2211}\times S_{3333} +$$

$$3\times C_{11}^{*}\times C_{12}^{*2}\times S_{1122}\times S_{2233}\times S_{3311} + 3\times C_{11}^{*}\times C_{12}^{*2}\times S_{1133}\times S_{2211}\times S_{3322} -$$

$$3\times C_{11}^{*}\times C_{12}^{*2}\times S_{1133}\times S_{2222}\times S_{3311} - 4\times C_{11}\times C_{12}\times C_{12}^{*}\times S_{1111}\times S_{2222} + 4\times C_{11}\times C_{12}\times C_{12}^{*}\times S_{1122}\times S_{2211} -$$

$$C_{11}\times C_{12}\times C_{11}^{*}\times S_{1111}\times S_{2233} + C_{11}\times C_{12}\times C_{11}^{*}\times S_{1133}\times S_{2211} - C_{11}\times C_{12}\times C_{12}^{*}\times S_{1111}\times S_{2233} +$$

$$C_{11}\times C_{12}\times C_{12}^{*}\times S_{1133}\times S_{2211} + C_{11}\times C_{12}\times C_{11}^{*}\times S_{1122}\times S_{2233} - C_{11}\times C_{12}\times C_{11}^{*}\times S_{1133}\times S_{2222} +$$

$$C_{11}\times C_{12}\times C_{12}^{*}\times S_{1122}\times S_{2233} - C_{11}\times C_{12}\times C_{12}^{*}\times S_{1133}\times S_{2222} + 2\times C_{12}\times C_{11}^{*}\times C_{12}^{*}\times S_{1111}\times S_{2222} -$$

$$2\times C_{12}\times C_{11}^{*}\times C_{12}^{*}\times S_{1122}\times S_{2211} - C_{11}\times C_{11}^{*}\times C_{12}^{*}\times S_{1111}\times S_{2233} + C_{11}\times C_{11}^{*}\times C_{12}^{*}\times S_{1133}\times S_{2211} -$$

$$C_{12}\times C_{11}^{*}\times C_{12}^{*}\times S_{1111}\times S_{2233} + C_{12}\times C_{11}^{*}\times C_{12}^{*}\times S_{1133}\times S_{2211} + C_{11}\times C_{11}^{*}\times C_{12}^{*}\times S_{1122}\times S_{2233} -$$

$$C_{11}\times C_{11}^{*}\times C_{12}^{*}\times S_{1133}\times S_{2222} + C_{12}\times C_{11}^{*}\times C_{12}^{*}\times S_{1122}\times S_{2233} - C_{12}\times C_{11}^{*}\times C_{12}^{*}\times S_{1133}\times S_{2222} -$$

$$C_{11}\times C_{12}\times C_{11}^{*}\times S_{1111}\times S_{3322} + C_{11}\times C_{12}\times C_{11}^{*}\times S_{1122}\times S_{3311} - C_{11}\times C_{12}\times C_{12}^{*}\times S_{1111}\times S_{3322} +$$

$$C_{11}\times C_{12}\times C_{12}^{*}\times S_{1122}\times S_{3311} - 4\times C_{11}\times C_{12}\times C_{12}^{*}\times S_{1111}\times S_{3333} + 4\times C_{11}\times C_{12}\times C_{12}^{*}\times S_{1133}\times S_{3311} -$$

$$C_{11}\times C_{12}\times C_{11}^{*}\times S_{1122}\times S_{3333} + C_{11}\times C_{12}\times C_{11}^{*}\times S_{1133}\times S_{3322} - C_{11}\times C_{12}\times C_{12}^{*}\times S_{1122}\times S_{3333} +$$

$$C_{11}\times C_{12}\times C_{12}^{*}\times S_{1133}\times S_{3322} - C_{11}\times C_{11}^{*}\times C_{12}^{*}\times S_{1111}\times S_{3322} + C_{11}\times C_{11}^{*}\times C_{12}^{*}\times S_{1122}\times S_{3311} -$$

$$C_{12}\times C_{11}^{*}\times C_{12}^{*}\times S_{1111}\times S_{3322} + C_{12}\times C_{11}^{*}\times C_{12}^{*}\times S_{1122}\times S_{3311} + 2\times C_{12}\times C_{11}^{*}\times C_{12}^{*}\times S_{1111}\times S_{3333} -$$

$$2\times C_{12}\times C_{11}^{*}\times C_{12}^{*}\times S_{1133}\times S_{3311} - C_{11}\times C_{11}^{*}\times C_{12}^{*}\times S_{1122}\times S_{3333} + C_{11}\times C_{11}^{*}\times C_{12}^{*}\times S_{1133}\times S_{3322} -$$

$$C_{12}\times C_{11}^{*}\times C_{12}^{*}\times S_{1122}\times S_{3333} + C_{12}\times C_{11}^{*}\times C_{12}^{*}\times S_{1133}\times S_{3322} + C_{11}\times C_{12}\times C_{11}^{*}\times S_{2211}\times S_{3322} -$$

$$C_{11}\times C_{12}\times C_{11}^{*}\times S_{2222}\times S_{3311} + C_{11}\times C_{12}\times C_{12}^{*}\times S_{2211}\times S_{3322} - C_{11}\times C_{12}\times C_{12}^{*}\times S_{2222}\times S_{3311} -$$

$$C_{11}\times C_{12}\times C_{11}^{*}\times S_{2211}\times S_{3333} + C_{11}\times C_{12}\times C_{11}^{*}\times S_{2233}\times S_{3311} - C_{11}\times C_{12}\times C_{12}^{*}\times S_{2211}\times S_{3333} +$$

$$C_{11}\times C_{12}\times C_{12}^{*}\times S_{2233}\times S_{3311} - 4\times C_{11}\times C_{12}\times C_{12}^{*}\times S_{2222}\times S_{3333} + 4\times C_{11}\times C_{12}\times C_{12}^{*}\times S_{2233}\times S_{3322} +$$

$C_{11}\times C_{11}^{*}\times C_{12}^{*}\times S_{2211}\times S_{3322} - C_{11}\times C_{11}^{*}\times C_{12}^{*}\times S_{2222}\times S_{3311} + C_{12}\times C_{11}^{*}\times C_{12}^{*}\times S_{2211}\times S_{3322} -$

$C_{12}\times C_{11}^{*}\times C_{12}^{*}\times S_{2222}\times S_{3311} - C_{11}\times C_{11}^{*}\times C_{12}^{*}\times S_{2211}\times S_{3333} + C_{11}\times C_{11}^{*}\times C_{12}^{*}\times S_{2233}\times S_{3311} -$

$C_{12}\times C_{11}^{*}\times C_{12}^{*}\times S_{2211}\times S_{3333} + C_{12}\times C_{11}^{*}\times C_{12}^{*}\times S_{2233}\times S_{3311} + 2\times C_{12}\times C_{11}^{*}\times C_{12}^{*}\times S_{2222}\times S_{3333} -$

$2\times C_{12}\times C_{11}^{*}\times C_{12}^{*}\times S_{2233}\times S_{3322} + 6\times C_{11}\times C_{12}\times C_{12}^{*}\times S_{1111}\times S_{2222}\times S_{3333} -$

$6\times C_{11}\times C_{12}\times C_{12}^{*}\times S_{1111}\times S_{2233}\times S_{3322} - 6\times C_{11}\times C_{12}\times C_{12}^{*}\times S_{1122}\times S_{2211}\times S_{3333} +$

$6\times C_{11}\times C_{12}\times C_{12}^{*}\times S_{1122}\times S_{2233}\times S_{3311} + 6\times C_{11}\times C_{12}\times C_{12}^{*}\times S_{1133}\times S_{2211}\times S_{3322} -$

$6\times C_{11}\times C_{12}\times C_{12}^{*}\times S_{1133}\times S_{2222}\times S_{3311} - 6\times C_{12}\times C_{11}^{*}\times C_{12}^{*}\times S_{1111}\times S_{2222}\times S_{3333} +$

$6\times C_{12}\times C_{11}^{*}\times C_{12}^{*}\times S_{1111}\times S_{2233}\times S_{3322} + 6\times C_{12}\times C_{11}^{*}\times C_{12}^{*}\times S_{1122}\times S_{2211}\times S_{3333} -$

$6\times C_{12}\times C_{11}^{*}\times C_{12}^{*}\times S_{1122}\times S_{2233}\times S_{3311} - 6\times C_{12}\times C_{11}^{*}\times C_{12}^{*}\times S_{1133}\times S_{2211}\times S_{3322} +$

$6\times C_{12}\times C_{11}^{*}\times C_{12}^{*}\times S_{1133}\times S_{2222}\times S_{3311}))$

Appendix C

A B-spline function is a powerful tool that is commonly used in various 3D computer-aided design packages[127]. By using the B-spline function, a curve or a surface can be constructed by using various control points. The control points can be treated as "magnets" that attract the curve or surface to them, which allows localized control of the function shape by moving the individual control points without influencing the overall shape of the function. An examples of two B-spline curves (curve 1: red, curve 2: blue) constructed by 6 control points are shown in Figure 6.1. The overall shapes of two curves are essentially the same except at around $x = 5$ where the control point for curve 2 is lower.

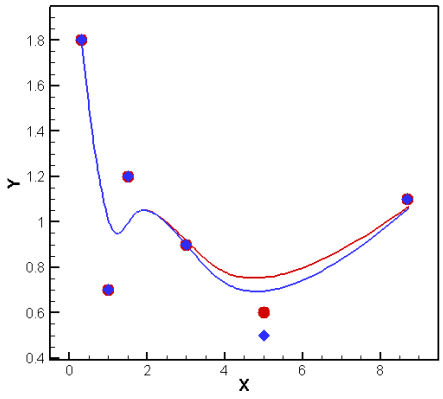

Figure 6.1: Schematic of B-spline curves and its control points. Red-curve 1 and Blue-curve 2.

The B-spline function is a linear combination of control points and basis functions. The basis function is a piecewise polynomial function. The places where the pieces meet are known as knots. The coordinates of 3D B-spline surface (constructed by $n \times m$ control points) in a Cartesian coordinates can be calculated by:

$$x_{Bspline} = \sum_{i=0}^{n}\sum_{j=0}^{m} \Phi_{i,3}(u)\Phi_{j,3}(u)C_{i,j}^{ctrl(x)} \quad , \tag{28}$$

$$y_{Bspline} = \sum_{i=0}^{n}\sum_{j=0}^{m} \Phi_{i,3}(u)\Phi_{j,3}(u)C_{i,j}^{ctrl(y)} \quad , \tag{29}$$

$$z_{Bspline} = \sum_{i=0}^{n}\sum_{j=0}^{m} \Phi_{i,3}(u)\Phi_{j,3}(u)C_{i,j}^{ctrl(z)} \quad , \tag{30}$$

where *i* and *j* represents the grid of the control points (*i* for *x* coordinates and *j* for *y* coordinates) , $C_{i,j}^{ctrl(\varphi)}, (\varphi = x, y, z)$ are the (*x*,*y*,*z*) coordinates of the control points and $\Phi_{j,3}$ is the basis function defined on an interval $u_i < u < u_{i+1}$ (u_i are the knots):

$$\Phi_{i,0} = \begin{cases} 1 & u_i < u < u_{i+1} \\ 0 & else \end{cases} \quad , \tag{31}$$

$$\Phi_{i,d} = \frac{u - u_i}{u_{i+p} - u_i}\Phi_{i,d-1}(u) + \frac{u_{i+p+1} - u}{u_{i+p+1} - u_{i+1}}\Phi_{i+1,d-1}(u) . \tag{32}$$

Shown in Figure 6.2 is an example of a 3D B-spline surface energy that reproduces the general features of the “P1” interface energy model discussed in Chapter 4 using 10 parameters.

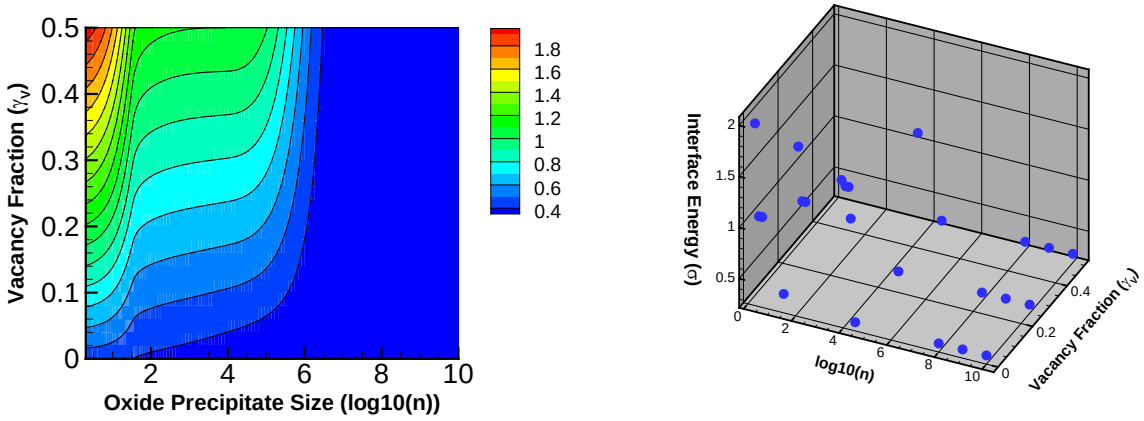

(a) (b)

Figure 6.2: (a) 2D contour plot of the surface energy as a function of vacancy fraction (γ_V) and log scale cluster size (n). (b) Control points.

BIBLIOGRAPHY

1 (http://www.semi.org/en/node/54591).

2 (http://www.icinsights.com/data/articles/documents/761.pdf).

3 G. Fisher, M. R. Seacrist, and R. W. Standley, Proceedings of the IEEE **100,** 1454 (2012).

4 J. Vanhellemont, O. De Gryse, and P. Clauws, physica status solidi (a) **203,** 2341 (2006).

5 J. Vanhellemont, E. Dornberger, J. Esfandyari, G. Kissinger, M.-A. Trauwaert, H. Bender, D. Gräf, U. Lambert, and W. von Ammon, in *Defects in as-grown silicon and their evolution during heat treatments*, 1997 (Trans Tech Publ), p. 341.

6 F. Ponce, T. Yamashita, and S. Hahn, Applied physics letters **43,** 1051 (1983).

7 P. Roksnoer and M. Van den Boom, Journal of Crystal Growth **53,** 563 (1981).

8 J. Ryuta, E. Morita, T. Tanaka, and Y. Shimanuki, Japanese journal of applied physics **31,** L293 (1992).

9 J.-G. Park, G.-S. Lee, K.-D. Kwack, and J.-M. Park, Japanese Journal of Applied Physics **39,** 197 (2000).

10 E. Dornberger, D. Temmler, and W. Von Ammon, Journal of The Electrochemical Society **149,** G226 (2002).

11 T. Tan, E. Gardner, and W. Tice, Applied Physics Letters **30,** 175 (1977).

12 K. Sumino and I. Yonenaga, Semiconductors and semimetals **42,** 449 (1994).

13 A. Borghesi, B. Pivac, A. Sassella, and A. Stella, Journal of Applied Physics **77,** 4169 (1995).

14 K. F. Kelton, R. Falster, D. Gambaro, M. Olmo, M. Cornara, and P. F. Wei, Journal of Applied Physics **85,** 8097 (1999).

15 R. J. Falster and V. V. Voronkov, in *Rapid Thermal Processing and the Control of Oxygen Precipitation Behaviour in Silicon Wafers*, 2008 (Trans Tech Publ), p. 45.

16 W. Zulehner, G. Harbeke, and M. Schulz, in *Springer Series in Material Science*; *Vol. 13* (Springer-Verlag Berlin-Heidelberg, 1989), p. 127.

17 S. A. Campbell, *The science and engineering of microelectronic fabrication* (Oxford University Press, USA, 1996).

18 W. Bergholz, Semiconductors and Semimetals **42,** 513 (1994).

19 M. Akatsuka, M. Okui, N. Morimoto, and K. Sueoka, Japanese Journal of Applied Physics **40,** 3055 (2001).

20 J. Vanhellemont, Applied Physics Letters **68,** 3413 (1996).

21 J. Vanhellemont and C. Claeys, Journal of Applied Physics **62,** 3960 (1987).

22 N. Inoue, J. Osaka, and K. Wada, Journal of The Electrochemical Society **129,** 2780 (1982).

23 M. Schrems, in *Simulation of Oxygen Precipitation and Denuded Zone Formation during Thermal Anneals*, 1993 (Trans Tech Publ), p. 231.

24 K. Sueoka, N. Ikeda, T. Yamamoto, and S. Kobayashi, Journal of applied physics **74,** 5437 (1993).

25 J. Vanhellemont, Journal of applied physics **78,** 4297 (1995).

[26] J. Esfandyari, C. Schmeiser, S. Senkader, G. Hobler, and B. Murphy, Journal of the Electrochemical Society **143,** 995 (1996).
[27] S. Senkader, G. Hobler, and C. Schmeiser, Applied Physics Letters **69,** 2202 (1996).
[28] B. G. Ko and K. D. Kwack, Journal of Applied Physics **85,** 2100 (1999).
[29] V. V. Voronkov and R. Falster, Journal of the Electrochemical Society **149,** G167 (2002).
[30] Z. Wang, Thesis, Massachusetts Institute of Technology, 2002.
[31] K. Sueoka, M. Akatsuka, M. Okui, and H. Katahama, Journal of The Electrochemical Society **150,** G469 (2003).
[32] J. Vanhellemont, O. De Gryse, and P. Clauws, Applied Physics Letters **86,** 221903 (2005).
[33] J. Tersoff, Physical Review B **39,** 5566 (1989).
[34] C. Y. Chuang, Q. M. Li, D. Leonhardt, S. M. Han, and T. Sinno, Surface Science **609,** 221 (2013).
[35] J. Tersoff, Physical review letters **56,** 632 (1986).
[36] J. Tersoff, Physical Review B **38,** 9902 (1988).
[37] S. Munetoh, T. Motooka, K. Moriguchi, and A. Shintani, Computational Materials Science **39,** 334 (2007).
[38] B. M. Lee, T. Motooka, and S. Munetoh, Journal of Physics: Condensed Matter **20,** 055205 (2008).
[39] V. Dragoi, E. Pabo, J. Burggraf, and G. Mittendorfer, Microsystem Technologies-Micro-and Nanosystems-Information Storage and Processing Systems **18,** 1065 (2012).
[40] T. Plach, V. Dragoi, F. Murauer, and K. Hingerl, ECS Transactions **16,** 549 (2008).
[41] T. Plach, K. Hingerl, S. Tollabimazraehno, G. Hesser, V. Dragoi, and M. Wimplinger, Journal of Applied Physics **113** (2013).
[42] K. Schjolberg-Henriksen, S. Moe, M. M. V. Taklo, P. Storas, and J. H. Ulvensoen, Sensors and Actuators a-Physical **142,** 413 (2008).
[43] T. Suni, K. Henttinen, I. Suni, and J. Makinen, Journal of the Electrochemical Society **149,** G348 (2002).
[44] Q. Y. Tong, U. Gösele, and Electrochemical Society., *Semiconductor wafer bonding : science and technology* (John Wiley, New York, 1999).
[45] W. P. Maszara, G. Goetz, A. Caviglia, and J. B. Mckitterick, Journal of Applied Physics **64,** 4943 (1988).
[46] Y. Tu and J. Tersoff, Physical Review Letters **84,** 4393 (2000).
[47] F. Wooten, K. Winer, and D. Weaire, Physical Review Letters **54,** 1392 (1985).
[48] G. Hadjisavvas, I. N. Remediakis, and P. C. Kelires, Physical Review B **74** (2006).
[49] L. Kong and L. J. Lewis, Physical Review B **77** (2008).
[50] P. Kroll and H. J. Schulte, Physica Status Solidi B-Basic Solid State Physics **243,** R47 (2006).
[51] F. Djurabekova and K. Nordlund, Physical Review B **77** (2008).
[52] T. Watanabe, D. Yamasaki, K. Tatsumura, and I. Ohdomari, Applied Surface Science **234,** 207 (2004).

[53] H. Ohta and S. Hamaguchi, Journal of Chemical Physics **115,** 6679 (2001).
[54] S. Munetoh, T. Motooka, K. Moriguchi, and A. Shintani, Computational Materials Science **39,** 334 (2007).
[55] B. M. Lee, T. Motooka, and S. Munetoh, Journal of Physics-Condensed Matter **20** (2008).
[56] V. V. Voronkov and R. Falster, Journal of Applied Physics **91,** 5802 (2002).
[57] S. Messoloras, R. Newman, R. Stewart, and J. Tucker, Semiconductor Science and Technology **2,** 14 (1987).
[58] P. F. Wei, K. F. Kelton, and R. Falster, Journal of Applied Physics **88,** 5062 (2000).
[59] B. C. Trzynadlowski and S. T. Dunham, Journal of Applied Physics **114** (2013).
[60] R. Swaroop, W. Lin, N. Kim, M. Bullis, A. Rice, E. Castel, M. Crist, and L. Shive, Journal of the Electrochemical Society **133,** C445 (1986).
[61] H. Chiou and L. Shive, VLSI Sci. Technol **429** (1985).
[62] S. Senkader, J. Esfandyari, and G. Hobler, Journal of Applied Physics **78,** 6469 (1995).
[63] T. Sinno and R. A. Brown, Journal of the Electrochemical Society **146,** 2300 (1999).
[64] D. Kashchiev, *Nucleation* (Butterworth-Heinemann, 2000).
[65] J. L. Katz and H. Wiedersich, The Journal of Chemical Physics **55,** 1414 (1971).
[66] S. S. Kapur, M. Prasad, J. C. Crocker, and T. Sinno, Physical Review B **72,** 014119 (2005).
[67] J. Dai, W. Seider, and T. Sinno, Molecular Simulation **32,** 305 (2006).
[68] J. K. Lee and W. C. Johnson, Acta Metallurgica **26,** 541 (1978).
[69] J. Eshelby, in *The elastic field outside an ellipsoidal inclusion*, 1959 (The Royal Society), p. 561.
[70] J. D. Eshelby, in *The determination of the elastic field of an ellipsoidal inclusion, and related problems*, 1957 (The Royal Society), p. 376.
[71] J. D. Eshelby, *Elastic inclusions and inhomogeneities*, Vol. 2 (North-Holland Publishing Company, Amsterdam, 1961).
[72] T. A. Frewen, (2004).
[73] T. Mori, Thesis, Massachusetts Institute of Technology, 2000.
[74] J. Chang and G. Cooper, Journal of Computational Physics **6,** 1 (1970).
[75] E. Dornberger, Thesis, Université catholique de Louvain, 1997.
[76] G. Kissinger, D. Kot, J. Dabrowski, V. Akhmetov, A. Sattler, and W. Von Ammon, ECS Transactions **16,** 97 (2008).
[77] G. Kissinger, T. Müller, A. Sattler, W. Häckl, P. Krottenthalerc, T. Grabolla, H. Richter, and W. von Ammon, Materials Science in Semiconductor Processing **9,** 236 (2006).
[78] J. Nicolai, N. Burle, C. Serafino, and B. Pichaud, Journal of Crystal Growth **372,** 138 (2013).
[79] J. Mikkelsen, in *The diffusivity and solubility of oxygen in silicon*, 1985 (Cambridge Univ Press), p. 19.
[80] S. Senkader, P. Wilshaw, and R. Falster, Journal of Applied Physics **89,** 4803 (2001).
[81] K. Yasutake, M. Umeno, and H. Kawabe, physica status solidi (a) **83,** 207 (1984).

[82] M. Hopcroft, W. D. Nix, and T. W. Kenny, Microelectromechanical Systems, Journal of **19,** 229 (2010).
[83] G. Kissinger, J. Dabrowski, D. Kot, V. Akhmetov, A. Sattler, and W. von Ammon, Journal of The Electrochemical Society **158,** H343 (2011).
[84] G. Kissinger, J. Dabrowski, T. Sinno, Y. Yang, D. Kot, and A. Sattler, Journal of Crystal Growth (2016).
[85] B. M. Adams, W. Bohnhoff, K. Dalbey, J. Eddy, M. Eldred, D. Gay, K. Haskell, P. D. Hough, and L. Swiler, Sandia National Laboratories, Tech. Rep. SAND2010-2183 (2009).
[86] R. Storn and K. Price, Journal of global optimization **11,** 341 (1997).
[87] F. Biscani, D. Izzo, and C. H. Yam, arXiv preprint arXiv:1004.3824 (2010).
[88] D. R. Askeland, P. P. Fulay, and W. J. Wright, *The Science and Engineering of Materials, SI Edition* (CL-Engineering, 2011).
[89] A. G. Cullis, D. J. Robbins, S. J. Barnett, and A. J. Pidduck, Journal of Vacuum Science & Technology A **12,** 1924 (1994).
[90] D. J. Eaglesham and M. Cerullo, Physical Review Letters **64,** 1943 (1990).
[91] M. L. Lee, E. A. Fitzgerald, M. T. Bulsara, M. T. Currie, and A. Lochtefeld, Journal of Applied Physics **97,** 011101 (2005).
[92] Y. H. Xie, D. Monroe, E. A. Fitzgerald, P. J. Silverman, F. A. Thiel, and G. P. Watson, Applied Physics Letters **63,** 2263 (1993).
[93] E. A. Fitzgerald, Annual Review of Materials Science **25,** 417 (1995).
[94] P. Mooney, Materials Science and Engineering: R: Reports **17,** 105 (1996).
[95] A. Bourret, J. Thibault-Desseaux, and D. N. Seidman, Journal of Applied Physics **55,** 825 (1984).
[96] T. Mura, *Micromechanics of defects in solids*, Vol. 3 (Springer Science & Business Media, 2012).
[97] J. K. Lee, D. Barnett, and H. Aaronson, Metallurgical Transactions A **8,** 963 (1977).
[98] R. J. Asaro and D. M. Barnett, Journal of the Mechanics and Physics of Solids **23,** 77 (1975).
[99] R. W. Balluffi, S. Allen, and W. C. Carter, *Kinetics of materials* (John Wiley & Sons, 2005).
[100] M. Jaswon and R. Bhargava, in *Two-dimensional elastic inclusion problems*, 1961 (Cambridge Univ Press), p. 669.
[101] X. Jin, Z. Wang, Q. Zhou, L. M. Keer, and Q. Wang, Journal of Elasticity **114,** 1 (2014).
[102] Z. Hashin, Journal of the Mechanics and Physics of Solids **50,** 2509 (2002).
[103] H. Duan, J.-x. Wang, Z. Huang, and Y. Zhong, in *Stress fields of a spheroidal inhomogeneity with an interphase in an infinite medium under remote loadings*, 2005 (The Royal Society), p. 1055.
[104] S. Li, X. Zeng, B. Ren, J. Qian, J. Zhang, and A. K. Jha, Computer Methods in Applied Mechanics and Engineering **229,** 87 (2012).
[105] M. P. Lutz and R. W. Zimmerman, International Journal of Solids and Structures **42,** 429 (2005).
[106] I. Sevostianov and M. Kachanov, International Journal of Solids and Structures **44,** 1304 (2007).

[107] J. W. Christian, *The theory of transformations in metals and alloys* (Newnes, 2002).
[108] S. Plimpton, Journal of computational physics **117,** 1 (1995).
[109] A. P. Thompson, S. J. Plimpton, and W. Mattson, The Journal of chemical physics **131,** 154107 (2009).
[110] J. A. Zimmerman, R. E. Jones, and J. A. Templeton, Journal of Computational Physics **229,** 2364 (2010).
[111] C. Rycroft, Lawrence Berkeley National Laboratory (2009).
[112] P. Kelires, Applied surface science **102,** 12 (1996).
[113] P. N. Keating, Physical Review **145,** 637 (1966).
[114] J. Ju and L. Sun, Journal of Applied Mechanics **66,** 570 (1999).
[115] F. Nabarro, in *The strains produced by precipitation in alloys*, 1940 (The Royal Society), p. 519.
[116] M. Volmer and A. Weber, Z. phys. Chem **119,** 277 (1926).
[117] R. Becker and W. Döring, Annalen der Physik **416,** 719 (1935).
[118] M. Beck, A. Van de Walle, and M. Asta, Physical Review B **70,** 205337 (2004).
[119] T. Hoang, A. Arsenlis, H. Lee-Voigt, D. Chrzan, and B. Wirth, Modelling and Simulation in Materials Science and Engineering **19,** 085001 (2011).
[120] L. Sun, *Micromechanics and overall elastoplasticity of discontinuously reinforced metal-matrix composites* (1998).
[121] W. Skiff, H. Tsai, and R. Carpenter, MRS Online Proceedings Library Archive **59** (1985).
[122] O. D. Gryse, P. Clauws, J. Van Landuyt, O. Lebedev, C. Claeys, E. Simoen, and J. Vanhellemont, Journal of applied physics **91,** 2493 (2002).
[123] M. Meduňa, O. Caha, and J. Buršík, Journal of Crystal Growth **348,** 53 (2012).
[124] J. Nicolai, N. Burle, and B. Pichaud, Journal of Crystal Growth **363,** 93 (2013).
[125] G. Kissinger, M. Schubert, D. Kot, and T. Grabolla, ECS Journal of Solid State Science and Technology **6,** N54 (2017).
[126] D. Kot, G. Kissinger, M. Schubert, and A. Sattler, ECS Journal of Solid State Science and Technology **6,** N17 (2017).
[127] L. Piegl and W. Tiller, *The NURBS book* (Springer Science & Business Media, 2012).

Reprints and Permission

All of the reprinted tables are republished with permission of publishers of the Ref.20, 21, from Ref.20, 21; permission conveyed through Copyright Clearance Center, Inc.

All of the reprinted figures are republished with permission of publishers of the Ref.3-6, 14, 15, 18, 22, 23, 26, 28, 39-43, 45, 56, 58, 59, 62, from Ref 3-6, 14, 15, 18, 22, 23, 26, 28, 39-43, 45, 56, 58, 59, 62; permission conveyed through Copyright Clearance Center, Inc.

Figures taken from Ref.30 are republished with the permission of MIT.

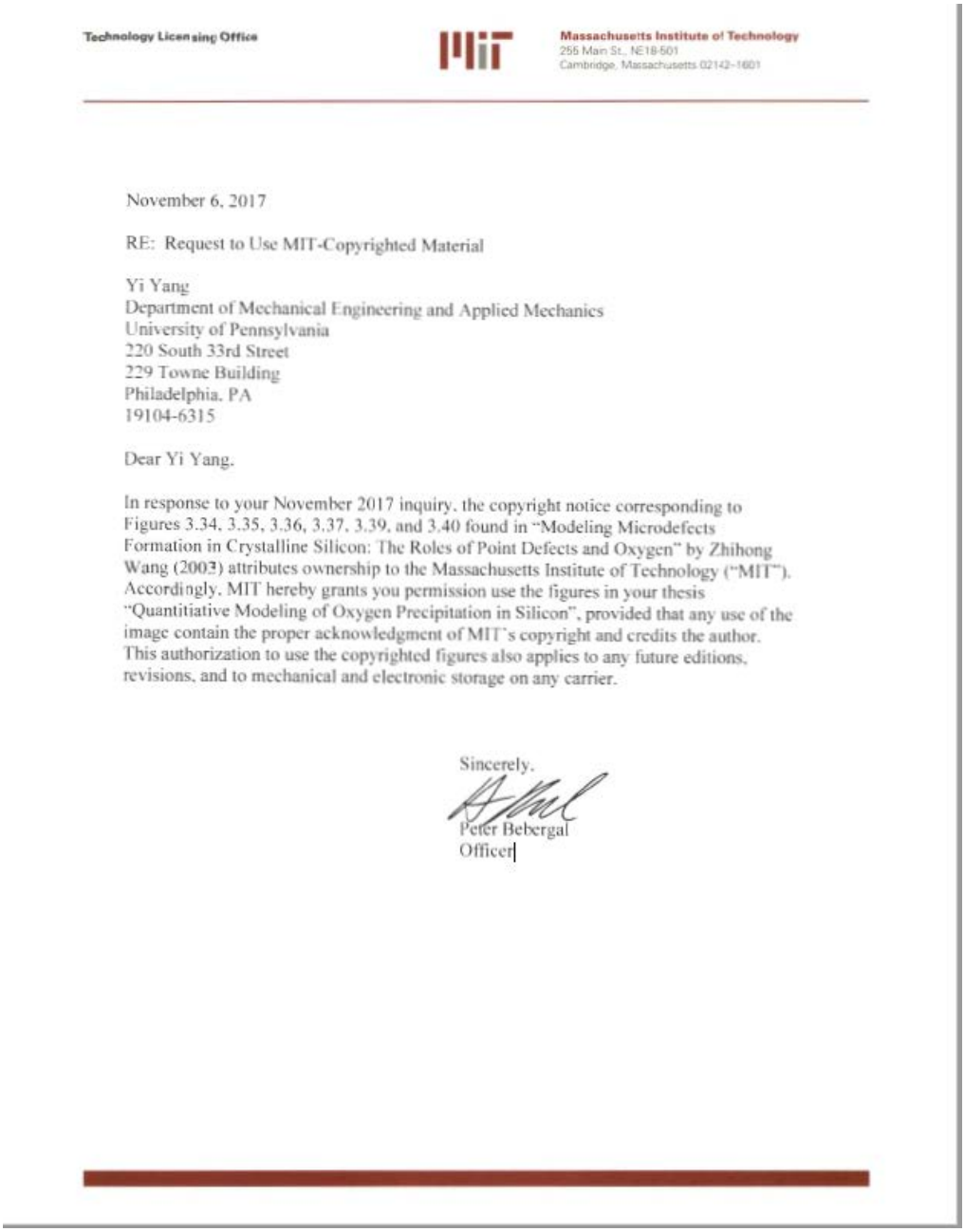

Technology Licensing Office

Massachusetts Institute of Technology
255 Main St., NE18-501
Cambridge, Massachusetts 02142-1601

November 6, 2017

RE: Request to Use MIT-Copyrighted Material

Yi Yang
Department of Mechanical Engineering and Applied Mechanics
University of Pennsylvania
220 South 33rd Street
229 Towne Building
Philadelphia, PA
19104-6315

Dear Yi Yang,

In response to your November 2017 inquiry, the copyright notice corresponding to Figures 3.34, 3.35, 3.36, 3.37, 3.39, and 3.40 found in "Modeling Microdefects Formation in Crystalline Silicon: The Roles of Point Defects and Oxygen" by Zhihong Wang (2003) attributes ownership to the Massachusetts Institute of Technology ("MIT"). Accordingly, MIT hereby grants you permission use the figures in your thesis "Quantitiative Modeling of Oxygen Precipitation in Silicon", provided that any use of the image contain the proper acknowledgment of MIT's copyright and credits the author. This authorization to use the copyrighted figures also applies to any future editions, revisions, and to mechanical and electronic storage on any carrier.

Sincerely,

Peter Bebergal
Officer